THE ISOTHERMAL PYROLYSIS OF n-BUTANE IN A LAMINAR FLOW REACTOR

A Thesis Submitted for the Degree of

Doctor of Philosophy of the

University of London

by

Patrick William Leaney

Department of Chemical Engineering and Chemical Technology

Imperial College of Science and Technology

London, S.W.7.

January, 1982

A B S T R A C T

A study has been carried out on the global and mechanistic free radical kinetics of the pyrolysis of n-butane in the temperature range 646 - 736^{o}C. The experimental procedure was characterised by the objective to minimise any extraneous design complications such as heat and mass transfer limitations which might obscure the kinetics of the true pyrolysis reaction. Data were collected in a laminar flow vertical pilot scale Inconel 600 reactor (1.5m x 0.0525m I.D.), approximately 1m of which was situated in an insulated furnace with five independently controlled heating zones. Consequently an isothermal gas zone in the lower region of the reactor, $\sim$ 30 cm was reproducibly apparent. A mechanism situated at the base of the reactor enabled probes to be inserted into the reactor space so that detailed axial and radial composition and temperature profiles were obtained within the isothermal section.

A detailed design analysis revealed that insignificant errors were introduced by the sampling sequence along the reactor centreline. Accordingly sets of experiments were performed at constant throughput rates (Re $\sim$ 80 - 160) for different isothermal gas temperatures leading to conversions between 10 - 80% for a feed composition of 5 - 10 mole % butane in nitrogen at 1.48 bar a (7 psig). The chromatographic analysis of composition measured all the major products of the pyrolysis and most of the minor products so that a detailed analysis could be made on the pyrolysis product distribution.

The study revealed that the global kinetics of the n-butane decomposition rate was well fitted as a first order rate expression with a single activation energy of 212 KJ/mole which was independent of the conversion

upto values as high as 75%. This suggests inhibitive properties of the n-butane products do not become a major influence on the decomposition rate and overall order of reaction until conversions greater than this. Furthermore, a mixed heterogeneous-homogeneous nature for the n-butane pyrolysis was observed, caused by the catalytic nature of the Inconel. Quantification of the heterogeneous contribution was however not fully established.

The free radical mechanistics was modelled by a 98 elementary rate step model proposed by Edelson and Allara (1980). Using rate data compiled independently from any pyrolysis experiments good agreement between experimental and predicted results was obtained for the product distribution as a function of n-butane conversion. Predicted decomposition rates were lower than those observed, but agreement was possible by adjustment of initiation rate data well within the recognised bounds of uncertainty, whilst still remaining consistent with the experimental product distribution.

A C K N O W L E D G E M E N T S

I would like to extend my gratitude to my supervisor, Dr. L. Kershenbaum, for his exuberant support, beneficial criticisms and genuine encouragement during the cause of developing this research.

In addition, the work accomplished for me by the technicians in the Department is most commendable and has been greatly appreciated. In particular, I would like to mention Terry Stephenson, Alan Barnes, Bob King whose comments on the construction of the probe were most helpful, and Austin Harrup whose anachronic wit served to brighten up even the most doleful days. Likewise the talents of the Electronics Workshop and Analytical Services have not passed unnoticed especially those of Dick Wood and Ian Drummond whose efforts merit special thanks.

A warm mention to my typists Miranda and Joyce for their time and effort and to the librarians Peggy and Caroline for their assistance when needed.

Last and most certainly least, a thank-you to three great friends of mine, Ron Newman, Velisa Vesovic and Peggy Browett for not excessively annoying and distracting me, thus making the completion of this study possible.

Science is nothing but trained and organized common sense, differing from the latter only as a veteran may differ from a raw recruit: and its methods differ from those of common sense only as far as the guardsman's cut and thrust differ from the manner in which a savage wields his club.

T.H. Huxley

(1825 - 1895)

To my parents and Christine, my fiancée

"Never pain to tell thy love,
Love that never told can be;
For the gentle wind does move
Silently, invisibly."

William Blake
(1757 - 1827)

L I S T O F C O N T E N T S

A P P E N D I C E S

LIST OF TABLES

L I S T O F F I G U R E S

Page

C H A P T E R 1

INTRODUCTION

The thermal decomposition or pyrolysis of butane has been extensively studied over the past fifty years, since the major products include simple olefins used as raw material in the petrochemical industry. Most work has sought to determine the product distribution over a range of different operating conditions and to express the gross behaviour using overall global kinetic expressions. Despite the significant amount of work done on butane pyrolysis it still poses many challenging problems. There is wide discrepancy and contradiction in reported literature between various workers both in terms of product distributions and regarding apparent activation energies for the overall reaction, in many cases under reportedly similar experimental operating conditions. Recent work has attempted to correlate the conflicting data in terms of more complex kinetic models which more closely reflect the chemical steps in these reactions.

The major premise for this work is the belief that conflicting data reported by various workers may well have been caused in part by improperly defined experimental conditions which had not been well-characterised by the reactor modelling procedure used when interpreting the resulting data. Under these circumstances, it becomes futile to attempt to correlate the contradictions merely by complicating the kinetic models used to simulate the data.

Generally a reactor is modelled to be plug flow with a non-isothermal axial temperature profile and only the effluent composition is measured in any single run. The effect of residence time on conversion and the

product distribution is obtained by altering the feed rate and composition to the reactor and noting the relevant changes at the reactor exit. In an ideal homogeneous isothermal plug flow reactor, this is a perfectly acceptable method of collecting kinetic data. In reality, however, for complex reaction kinetics in a non-isothermal reactor where there is an uncertain velocity profile and possible wall effects, this approach seems to be fraught with possible gross error.

The unmeasured gas temperature profile, whether in the radial or axial direction, will certainly be a function of Reynolds number. Since each run has associated with it a different flowrate and hence Reynolds number, the heat transfer characteristics will introduce a variable error from run to run, giving rise to possible obscurity in the kinetic steps. Similarly, mass transfer effects between the wall and non-ideal radial and axial mixing will also tend to vary, further biassing the kinetics. Thus, equating reactor wall temperature to the gas temperature in a tubular flow reactor, rather than actually measuring it, is especially difficult to justify.

Furthermore, the use of non-isothermal data increases further the problems of obtaining well-defined kinetic parameters. Uncertainties with the heating and quenching zones of the process stream are only partly removed by assuming non-isothermal profiles, or utilizing concepts of equivalent volumes and temperatures. The necessary simultaneous estimation of frequency factor and activation energy from non-isothermal data gives lower confidence in the final results, because of the known high correlation between parameter estimates.

Accordingly, experiments should be carried out such as to eliminate, at worst to measure and minimise, the effects that heat transfer, mass transfer and non-isothermality may have in extracting experimental kine-

tic data for pyrolytic reactions. The uncertainties present in the original data would then become more consistent with appropriately complex kinetic modelling techniques. To achieve this required the construction of a well-instrumented, large-scale, pilot plant for which gas measurements could be made within the reactor space, with a small but known disturbance to the flow pattern and a small but known error in the axial position of the measurement. Probes could be inserted which could travel through the reactor space, both radially and axially measuring point composition and temperature. The ability to establish and experimentally illustrate an isothermal region somewhere within the reactor yields a complete set of information fron one run on conversion versus residence time for a well-characterised constant set of operating conditions.

The objectives of this work have now clearly been determined. The primary objective is to establish the global parameters for butane decomposition and to compare the experimental product distribution using the data from this reactor with predicted values using a well-constructed and consistent radical mechanism. To accomplish this required a certain amount of preparatory work and justification. The specific experiments in this study were performed in the laminar flow regime (Re $\sim$ 150). On this basis, efficient temperature and sampling probes were designed to ensure that measurements from the reactor space were representative of a well-determined sampling position within the reactor. However, the special care taken to obtain reliable experimental data becomes meaningless if not accompanied by a stringent analysis of the mathematical model intended for interpreting the data. Subsequently, a rigorous procedure was undertaken to establish under what operating conditions the radial dispersion model could be replaced by the simpler plug flow model for esti-

mation of the global rate constant, to characterise the gross behaviour of the homogeneous butane decomposition.

In this way a complete study can be completed for the pyrolysis characteristics of butane, using a procedure which adds much confidence to the modelling techniques employed and to the experimental data collected, and thus to the final results.

CHAPTER 2

LITERATURE REVIEW

The interpretation of experimentally observed pyrolysis kinetics of small paraffinic hydrocarbon molecules has been the subject of much investigation. The need to understand the kinetics is vital to provide information for the production of simple olefins such as ethylene and propylene, essential feedstock for the petrochemical industry. In spite of improved analytical methods and better appreciation of the physical factors which affect the pyrolysis, reliable basic data still remains lacking. In the following review this situation is discussed and highlighted and remedial cures suggested to reduce the amount of contradictory data prevalent in literature. Attention will be drawn to the progress which has developed into analysing the pyrolysis mechanism, the mathematical modelling and the shortcomings associated with this, and the parameters which play a key rôle. Particularly, effects of such variables as reactor material, reaction time, temperature, pressure and surface/volume (S/V) ratios will be discussed and the discrepancies and contradictions noted. In this way, reconciliations for work performed in this study will become evident.

Early Work on Pyrolysis

Early workers in the field of pyrolysis sought primarily to determine product distributions over a wide range of operating conditions or overall global kinetic expressions to predict the gross behaviour of the total process. Up to about 1925, most work was concerned with pyrolysis characteristics of ethane and methane and a review is given by Williams-Gardner (1925). Over the next decade several authors (Pease, 1928;

Frey and Smith, 1928; Hurd and Spence, 1929) had indicated that the thermal dissociation of the paraffin hydrocarbons, except methane, were well modelled as homogeneous first-order reactions yielding as primary products, mono-olefins and either a lower paraffin or hydrogen. Pease and Durgan (1930) investigated butane pyrolysis in the temperature range 600 - 650°C and confirmed first-order homogeneous kinetics. They concluded not more than 1% of the reaction appeared to be heterogeneous and that even this effect may have been due to better heat transfer created by packing the glass reactor. Paul and Marek (1934) investigated the primary thermal dissociation of butane over the temperature range 530 - 625°C in two reactors fabricated from copper and fused silica and determined an overall activation energy for butane disappearance of 73.9 kcal/mole, substantially higher than that reported by Pease and Durgan (1930) of 65.0 kcal/mole, while Steacie and Puddington (1938) determined an activation energy of 58.7 kcal/mole. Paul and Marek (1934) also concluded the pyrolysis to be totally homogeneous with no effect on the reaction from changes in reactor S/V ratios, reactor surface or dilution with nitrogen.

Product distributions were also studied at this time but were hampered by the severe lack of good analytical systems. However, the early work on butane (Hurd and Spence, 1929; Pease and Durgan, 1930; Cambron, 1932) indicated the main cause of its pyrolysis to be represented by the molecular reactions

$$C_4H_{10} \rightarrow C_3H_6 + CH_4$$

$$C_4H_{10} \rightarrow C_2H_4 + C_2H_6$$

Free Radical Reactions

In 1931, Ebrey and Engelder, and especially Rice, proposed the idea which has been generally accepted as being the major contributory process in

hydrocarbon decompositions (Laidler, 1965). It was suggested that the pyrolysis proceeded via production and reactions of free radicals, created by break-up of specific molecular species. Rice's proposed radical mechanism appeared to account for the improbable but experimentally observed presence of methane and ethylene among the primary products of propane pyrolysis (Frey and Smith, 1928).

Any proposed mechanism must satisfy and remain consistent with experimental measurements of the overall pyrolysis rates, overall activation energies and any observed radical concentrations, and Rice and Herzfield (1934) showed that free radical mechanisms could be devised which were not inconsistent with experimental data.

The general free radical mechanism can be subdivided into five elementary reaction types:

Initiation is the only way in which the free radicals originate (Steacie, 1954). Initiation reactions involve normally C-C bond rupture because it is weaker than the C-H bond. Typically for butane the initiations reactions would be given by

$$C_4H_{10} \rightarrow 2C_2H_5\cdot$$

$$C_4H_{10} \rightarrow CH_3\cdot + 1\text{-}C_3H_7\cdot$$

Abstraction reactions are metathetical reactions in which a radical reacts with a stable molecule to produce a different molecule and a different radical. Most commonly it is the hydrogen atom which is transferred and the definition is frequently retermed H-transfer reactions, e.g.

$$C_4H_{10} + CH_3\cdot \rightarrow 1\text{-}C_4H_9\cdot + CH_4$$

Decomposition reactions are of considerable importance in the mechanism since they are the principal generators of the olefins detected in the

product composition. Decomposition occurs when a radical decomposes to form a molecule of lower or equal carbon number and a smaller radical

$$C_2H_5^{\cdot} \rightarrow C_2H_4 + H^{\cdot}$$

Addition reactions are the reverse of decomposition where a radical combines with an unsaturated hydrocarbon to give a radical of equal or higher carbon number than the unsaturated hydrocarbon, e.g.

$$C_2H_4 + CH_3^{\cdot} \rightarrow 1\text{-}C_3H_7^{\cdot}$$

The two types of Termination when two radicals interact and disappear from the system with the formation of stable molecular species are termed recombination and disproportionation. Disproportionation is the bimolecular reaction where two molecular species are created, at least one being unsaturated, by transfer of a hydrogen atom, e.g.

$$C_2H_5^{\cdot} + C_2H_5^{\cdot} \rightarrow C_2H_4 + C_2H_6$$

Recombination occurs when only one molecular species is formed, e.g.

$$C_2H_5^{\cdot} + C_2H_5^{\cdot} \rightarrow C_4H_{10}$$

Abstraction and decomposition are known as chain propagating steps (Steacie, 1954) and the radicals which are regenerated in such reactions, carriers. Additions reactions are not strictly chain propagating since there is no regeneration of radicals merely radical transformation.

Goldfinger, Letort and Niclause (1948) showed the order of the overall reaction for disappearance of the reacting hydrocarbon is dependent on the initiation and termination steps assumed in the radical mechanism. They defined a β radical as one which was involved in a bimolecular propagating step, such as abstraction and a μ radical as one which propagated

the chain by a unimolecular step such as decomposition and their results are summarised below:

First-Order Initiation e.g. $R_1R_2 \rightarrow R_1^{\cdot} + R_2^{\cdot}$	Second-Order Initiation e.g. $2R_1R_2 \rightarrow R_1R_1 + 2R_2^{\cdot}$	Overall order
Termination	Termination	
-	ββ	2
ββ	βμ	3/2
βμ	μμ	1
μμ	-	½

This method provides a direct way of determining possible termination steps once the overall order of reaction and the initiation steps have been determined. In most cases, however, experimentally determined orders tend to be non-integer whence no information can be gained from this idea. Torok and Sandler (1969) criticised this approach since it neglected the treatment of the homogeneous reaction phenomena frequently encountered in chain reactions such as some radicals, e.g. $C_2H_5^{\cdot}$ acting both as β and μ radicals. They proposed a method to evaluate the predominant chain termination step providing the chain propagation mechanism was well understood.

In the wake of these ideas it was determined that free radicals could be detected in certain pyrolysis reactions. Much of the work was accomplished by Rice and coworkers (Rice, Johnston and Evering, 1932; Rice and Johnston, 1934; Evering, 1939) and particularly for butane was confirmed by Hurd and Azarlosa (1951).

More Recent Studies on Pyrolysis

The early work on pyrolysis of the light hydrocarbons drew attention to the sensitivity of the mechanism to many parameters which needed special consideration; reactor S/V ratios, catalytic effects, temperature,

duration of reaction, pressure, dilution effects, trace impurities in the feed gas and the effect of secondary products on the product distribution.

Since then, modifications and improvements in the experimental and analytical procedure have enabled more reliable data to be collected giving greater confidence in the conclusions drawn about the pyrolysis characteristics. In spite of this, contradiction and disagreements still remain in literature concerning values of activation energies, pre-exponential factors, overall orders of reaction, radical mechanisms and rate data for many individual free radical reactions.

Most recent studies on butane pyrolysis have been carried out in the temperature range 450 - 600^{o}C, where reaction is slow enough that much information could be gathered about the primary reaction scheme. This compares with the industrially important range 700 - 950^{o}C. In agreement with earlier work, the principal primary products of butane pyrolysis have been estabished as methane, propylene, ethane and ethylene. Purnell and Quinn (1962) carried out an extensive investigation into the product distribution in the temperature range 420 - 530^{o}C and showed that a Rice-type free radical mechanism gave an excellent quantitative account of the reactions occurring. They determined that yields of methane and propylene were virtually identical but that considerable differences between yields of ethane and ethylene were common. They showed that discrepancy was due to dehydrogenation of ethane, a secondary reaction giving hydrogen and excess ethylene in approximately equal amounts. Sandler and Chung (1961) observed similar phenomena in the temperature range 700 - 900^{o}C but concluded that the discrepancy could be accounted for by a primary reaction stoichiometrically represented as

$$C_4H_{10} \rightarrow 2C_2H_4 + H_2$$

At conversions greater than 10% Purnell and Quinn (1962) reported small quantities of secondary products, 1-butene, cis-2-butene, trans-2-butene, 1,3 butadiene and 1-pentane. Sundaram and Froment (1978a) reported that acetylene was also present as a secondary product in very small quantities. It has been observed by most authors that the propylene yield passes through a peak at higher conversion before dropping towards zero at near total conversion.

Frey and Hepp (1953) studied the pyrolysis of propane and butane under elevated pressure and found the decomposition rates to be substantially higher than at normal pressures, with lower yields of olefins.

Sensitization and Inhibition of the Decomposition Rate

Establishing the activity of radicals during butane pyrolysis was achieved by introducing substances which were known to readily combine with free radicals. Echols and Pease (1936), Steacie and Folkins (1939), and Stubbs and Hinshelwood (1950) to name but a few, all noticed that introduction of nitric oxide had a pronounced inhibitory effect on the butane pyrolysis rate. An interesting feature of the inhibition was that the decomposition rate appeared to be lowered to a limiting value as more and more nitric oxide was added. Stubbs and Hinshelwood (1950) reported that the residual rate corresponded to a residual molecular reaction scheme, unaffected by introduction of more radical inhibiting substance.

Laidler, Sagert and coworkers (Wojciechowski and Laidler, 1960; Laidler and Wojciechowski, 1961; Laidler, Sagert and Wojciechowski, 1962) reported, however, evidence which claimed the residual rate was still caused by radical reactions but of much smaller chain length than in the uninhibited decomposition.

Rice and Polly (1938), Blakemore et al. (1973), Illés et al. (1979), and many others, have reported the interesting feature that propylene, a product from butane pyrolysis, also acts as a radical inhibitor.

Hill (1977) observed that introduction of bromides and sulphides modified the decomposition rate so that higher yields of propylene were attained. Maizus et al. (1949) and Appleby et al. (1953) showed that decomposition of butane is highly sensitized by the presence of oxygen, for instance, 0.5% oxygen increased the decomposition rate 100 fold. Presumably this is because of the generation of other radicals. Note that the feedstock of many of the earlier workers were noticeably contaminated with oxygen, up to 1% (e.g. Pease and Durgan, 1930).

Blakemore et al. (1973) showed that trace quantities of oxygen (above 10 ppm to 800 ppm) had a marked effect on the product distribution at very low conversions, less than 1%, with yields of the butenes much more prominent. Albright (1978) suggested that the presence of trace oxygen must change the composition of the inner surface whether or not the reactor material is catalytically active.

Wall Effects

There have been several attempts to determine the rôle of heterogeneous reactions for the light paraffinic hydrocarbons. The exact rôle of the surface remains unknown, although there is a growing trend in literature to suggest that the majority of the pyrolysis is homogeneous. Investigations have shown that surface effects can be sensitive to the type of reactor material, the kind of pretreatment, if any, of its surface and the reactor S/V ratio. Some authors have suggested that the wall, if active, affects only the initiation and termination steps of the pyrolysis (Voevodsky, 1959; Poltorak et al., 1959; Sagert and Laidler, 1963).

King, Sandler and Chung (1959) investigated butane pyrolysis through flow reactors constructed of different materials, vycor glass, stainless steel and chromium iron in the temperature range 730 - 800^{o}C. They showed that carbon was not deposited on chromium-plated stainless steel whereas untreated stainless steel had a far more active surface with profuse carbon laydown. Crynes and Albright (1969) investigated propane pyrolysis in the temperature range 600 - 750^{o}C in tubular flow reactors constructed from stainless steel, low carbon steel or nickel and discovered that when pretreated with oxygen, hydrogen bromide or steam, stainless steel was very effective in promoting secondary reactions, whereas hydrogen sulphide and other sulphide treatments removed the surface effects by forming a protective metal sulphide film. Decrease in surface activity due to sulphide treatment was also noted by Dunkleman and Albright (1976) for ethane pyrolysis.

Blakemore et al. (1973) observed that at low conversions of butane pyrolysis in the temperature range 530 - 600^{o}C, results from their gold microreactor were comparable to earlier work for quartz, ceramic and stainless steel vessels. Purnell and Quinn (1961) pretreated a pyrex reactor in seven different ways and determined that heterogeneous termination processes may be important in vessels coated with carbon or potassium chloride. Powers and Corcoran (1974) in the temperature range 515 - 605^{o}C, found the rate of reaction of butane decomposition to be independent of reactor pretreatment with nitric acid and/or oxygen in a gold reactor only after an initial period of conditioning. During the conditioning process, sufficient chain terminations probably occur at the surface causing the rate of pyrolysis to be slower and production of carbon to be higher.

A number of workers have also studied the effects of changing the S/V ratios but to date, the exact extent of this effect has not been confirmed.

Pratt and Rogers (1979) have carried out extensive testing on ethane, propane and butane pyrolysis using the so-called "wall-less" reactor developed by Taylor and coworkers (1969). They effectively showed that underestimating the effect of the wall did not seriously undermine the knowledge accumulated by more conventional studies, and thus the pyrolysis of ethane, propane or butane was not seriously affected by any heterogeneous reaction on the vessel walls.

Voevodsky (1959) presented evidence that a tenfold increase in S/V reduced the rate of propane pyrolysis at 610^{o}C in a quartz reactor. Laidler et al. (1962) substantiated this by observing a reduction of 35% in the reaction rate for propane at 580^{o}C also in a quartz reactor. Dunkleman and Albright (1976) indicated that significant differences for ethane pyrolysis between laboratory-scale products and commercial units may be due to S/V effects.

Purnell and Quinn (1961) studied the effect of variation of S/V ratio for pyrex glass at 527^{o}C on butane pyrolysis up to 9% conversion and determined that reaction rates remained reproducible throughout the series of experiments. Sagert and Laidler (1963) studied butane pyrolysis at 520 - 590^{o}C in a quartz reactor and concluded the reaction to be largely homogeneous although increase in the S/V ratio by a factor of eleven did decrease the reaction rate. They proposed that free surface sites abstracted hydrogen atoms from the butane molecule in a manner similar to nitric oxide and aided recombination of ethyl radicals.

Martin et al. (1964), Niclause et al. (1967), Leathard and Purnell (1968), and more recently, Blakemore et al. (1973) have all shown that influence of trace quantities of undetectable oxygen act as either an inhibitor at large S/V ratios, or as an accelerator at low S/V ratios.

Global Kinetics

There has been a proliferate amount of work done on the global kinetics of the pyrolysis of light saturated hydrocarbons. In particular, work has centred about evaluation of pre-exponential factors, activation energies and order of reaction with respect to the parent hydrocarbon and their variation, if any, with variation in conversion and temperature. Controversy still exists over the overall order of reaction for butane pyrolysis although for propane pyrolysis it has generally been accepted as one. Buekens and Froment (1968) have reported an order of 1 for propane, although they found the order varied with conversion and/or temperature. Variation of the rate constant with conversion was allowed by introducing a hyperbolic function with an inhibition coefficient which related the rate constant at a given conversion to the rate constant at zero conversion. Murata and Saito (1975) observed similar characteristics for butane by assuming it was first-order at 700^{o}C.

A tendency in literature suggests at low temperatures (500 - 600^{o}C) the order for butane pyrolysis is 3/2, steadily decreasing towards 1 as the reaction temperature increases. Froment et al. (1977) found the order to be 1 in the temperature range 650 - 850^{o}C, whilst Sagert and Laidler (1963) and Blakemore et al. (1973) determined an order of 3/2 between 520 - 590^{o}C. Illés and Szalai (1979) observed the same trend but reported that an order of 3/2 existed at temperatures as high as 700^{o}C which steadily decreased thereafter on increasing the reaction temperature. Illés (1969) had earlier observed that in the range 600 - 820^{o}C the overall decomposition rate could not be described by a simple first-order kinetic relationship.

Kupparman and Larson (1962) reported an order of one between 480 - 570^{o}C, in direct contrast to the findings of Sagert and Laidler (1963) while

Fritz et al. (1977) reported an overall order of 3/2 between 900 - 1200°C in shock tube pyrolysis of butane. Wang et al. (1963) found an order of between 1 and 2 for the overall disappearance of butane in the range 460 - 560°C.

Perhaps the most surprising range of reported data for butane has been for values of the activation energy and pre-exponential factor for the overall disappearance of butane. Values of the activation energy range from 40 kcal/mole (King et al., 1959) to 73.9 kcal/mole (Paul and Marek, 1934). This suggests that there is something more fundamentally wrong than relating this variation in order and activation energy totally to spurious effects created by heterogeneous activity at the reactor wall. In the past, most data has been collected either in a static reactor (e.g. Purnell and Quinn, 1962; Sagert and Laidler, 1963), or a continuous tubular flow reactor (e.g. Sandler and Chung, 1962; Blakemore et al., 1973). The resulting non-isothermality of data from tubular flow reactors has called for techniques to reduce the data to equivalent isothermal data before calculation of the activation energy is possible. The most common procedure is the concept of effective volume introduced by Watson (1947) and used, for example, by Buekens and Froment (1968). The effective volume is defined as that volume which when operating isothermally at a reference temperature and pressure, gives the same conversion as the actual reactor volume. Eisenberg and Bliss (1966) used a similar concept except evaluated on effective temperature with a reference volume equal to that of the actual reactor.

Sandler and Chung (1961) have highlighted the dangers of determining activation energies under static conditions, effectively demonstrating the different heat transfer limitations in tubular reactors which lead to large radial temperature differentials resulting from the endothermic

nature of the reaction. Calderbank (1954) has even suggested that measurements of reaction rates from externally heated tubular reactors used for hydrocarbon pyrolysis are in reality measurements of heat transfer, especially at high temperature, since this is the limiting process rather than the reaction kinetics.

These ideas might explain the general discrepancy between parameters estimated from static and continuous flow reactors but fails to fully reconcile the vast range of activation energies still evident from data collected in tubular flow reactors.

Free Radical Mechanisms

The desire to accurately predict overall order of reaction, activation energy of the decomposition reaction, and the resulting product distribution, has produced much development of the mechanistic kinetics which represent the actual free radical mechanism. Most have been based largely on the Rice-Herzfield mechanisms (Rice and Herzfield, 1934) and the generally accepted mechanism for the primary stage of butane decomposition is that given by Pacey and Purnell (1972a):

$$C_4H_{10} \rightarrow 2C_2H_5^{\cdot}$$

$$C_4H_{10} \rightarrow CH_3^{\cdot} + C_3H_7^{\cdot}$$

$$CH_3^{\cdot} + C_4H_{10} \rightarrow CH_4 + C_4H_9^{\cdot}$$

$$C_2H_5^{\cdot} + C_4H_{10} \rightarrow C_2H_6 + C_4H_9^{\cdot}$$

$$H^{\cdot} + C_4H_{10} \rightarrow H_2 + C_4H_9^{\cdot}$$

$$C_4H_9^{\cdot} \rightarrow C_3H_6 + CH_3^{\cdot}$$

$$C_4H_9^{\cdot} \rightarrow C_2H_4 + C_2H_5^{\cdot}$$

$$C_2H_5^{\cdot} \rightarrow C_2H_4 + H^{\cdot}$$

$$2C_2H_5^{\cdot} \rightarrow C_4H_{10}$$

$$2C_2H_5^{\cdot} \rightarrow C_2H_4 + C_2H_6$$

Often there has been disagreement among workers as to the significance of various proposed critical reaction steps and many different general mechanisms have been suggested for ethane, propane and butane under varying conditions of temperature and pressure. Even to date, there is no satisfactory mechanism universally recognised as being acceptable for any of them.

The major problems associated with deriving quantitative mechanisms have stemmed from the following (Allara and Edelson, 1975):

(i) The large number of coupled reactions which simultaneously occur create significant difficulties in the quantitative measurement of individual reaction steps.

(ii) The mechanistic simplifications, inevitably invoked to make the kinetic problems mathematically tractable.

(iii) The secondary effects of reactions involving primary product molecules.

Attempts to model the butane mechanistics have resulted in radical schemes ranging in size from 18 (Wang et al., 1963) up to 500 (Allara and Edelson, 1975).

Assuming the reactions to be elementary in an ideal plug flow reactor, continuity equations for N species, either molecular or radical, can be mathematically derived as N simultaneous coupled and non-linear ordinary differential equations (Sundaram and Froment, 1978a). The coupling and non-linearity precludes analytical solutions and the equation set is solved numerically. Radical concentrations are much lower than those of the molecular species and the large range of rate constants (e.g. 10^{-3} sec^{-1} for initiation, 10^{10} sec^{-1} for decomposition) mean that to maintain numerical stability with classical integration methods, an

extremely small step size is necessary, and the equations are commonly classed "stiff".

Two different approaches to this problem are available in literature. Integration of the equations as they stand is possible using more modern integration methods (Seinfeld et al., 1970; Gear, 1971; Sena and Kershenbaum, 1975; Aiken and Lapidus, 1975). By far the most efficient and popular method is the one proposed by Gear (1971) which can be used for any degree of stiffness and allows for any degree of accuracy with moderate computer time. The second approach is a simplification which overcomes the "stiffness" by assuming radical concentrations to be very quickly established and much smaller than the molecular concentrations. The Steady State Approximation for pyrolytic systems was first proposed by Snow (1966) in the kinetic modelling of ethane pyrolysis. Since the radical species are known to be destroyed and produced extremely quickly, the use of steady state assumes the differentials for the radical species to be much smaller than the terms which make up the differentials and are thus approximated to be zero. In this way, the "stiffness" is removed and the system is reduced to a set of ordinary differential equations for the molecular species, plus a set of algebraic equations for the radical species. Now classical methods can be used to integrate the equations with simultaneous solution of the algebraic equations at each integration point, to determine the radical concentrations.

Surprisingly enough, there has been little work done on comparing the relative merits and dismerits of either approach. Some authors have criticised the use of the steady state approximation (Allara and Edelson, 1975; Sundaram and Froment, 1978a), particularly in the early stages of reaction when the radical concentrations are being established. However, several authors have endorsed its use (Wang et al., 1963; Dente

et al., 1979), while some have used it without even commenting on its validity (Pacey and Purnell, 1972b; Illés and Szalai, 1979).

Sundaram and Froment (1978b) have recently questioned the accuracy of the steady state assumption by comparing profiles from the various modifications of this approach to the solution from Gear's method using equivalent models and rate data for pyrolysis of ethane. They concluded that inaccuracies incurred using this simplification were no longer compatible with the contemporary standard of pyrolytic reactor design.

One of the problems with free radical mechanisms is the enormous amount of free radical kinetic rate data required. Some workers (Allara and Edelson, 1975) have chosen to use rate parameters as determined from theoretical prediction or from independent fundamental studies, normally determined at temperatures significantly lower, 20 - 450^{o}C, than the recognised temperature range under which industrial pyrolysis proceeds, 700 - 950^{o}C.

As a result of the great uncertainties and errors which many of the parameters have associated with them (Allara and Shaw, 1980), other workers (Herriot et al., 1972; Sundaram and Froment, 1978a) have used some as adjustable constants in their model to minimise deviation from experimental results. Sundaram and Froment (1978a) used the equivalent reactor volume concept to reduce their initially non-isothermal data to isothermality before fitting their reaction model by trial and error adjustment of some of the model parameters. When reapplying the adjusted model to the original non-isothermal data, discrepancies between experimental and predicted product distributions were as great as 100%.

Both approaches have been criticised. Edelson and Allara (1973) objected most strongly to the publication of parameters derived from trial and error as rate constants, a term implying a fundamental property of the

reactions. They pointed out the ever-increasing proliferation of misleading rate constants in literature resulting from this type of approach. In a later publication (Allara and Edelson, 1975) they advocated the use of fundamentally predicted or measured rate data as being more readily acceptable when using a free radical model. In addition, they believed that the model itself must be fundamentally generated until it can be established which reactions are unimportant and do not partake in the development of the product distribution. By applying these ideas, good agreement was predicted between models for propane, butane and n-pentane and experimental data from literature in the range 400 - 560^{o}C.

More recently, Edelson and Allara (1980) supplemented this work by introducing a sensitivity analysis on each rate expression in their proposed models for propane and butane decomposition. The analysis revealed that errors in the overall pyrolysis rates were sensitive to a combination of initiation, H-abstraction, radical decomposition and recombination reactions. Updating of the accepted rate data for butane pyrolysis proved a poorer fit for the rate of disappearance than earlier reported (Allara and Edelson, 1975). The reactions of largest effect on the rate for butane are abstraction, initiation and decomposition reactions. Since the major uncertainties lie in the rate data for these reactions, the need for more experimental work to obtain better rate parameters is clearly apparent.

Sundaram et al. (1978a) have pointed out the disadvantage of using data from literature for high temperature pyrolysis since the majority of reported studies are limited to low temperatures and pressures. Experimentally, it is found that Arrhenius parameters are generally constant over only a small temperature range $\sim$100^{o}C although it is not uncommon to have little variation over larger ranges $\sim$500^{o}C (Benson, 1968).

Pacey and Purnell (1972a) report that Arrhenius plots for alkyl radical-alkane metathetical reactions are in fact strongly curved, especially those involving hydrogen atoms. They reported considerable discrepancy between Arrhenius parameters measured at 674^{o}C and those obtained at lower temperatures for metathetical reactions involving butane. Interestingly enough, the same authors reported excellent agreement between a proposed radical mechanism using low temperature rate data for butane pyrolysis in a flow reactor at 600 - 720^{o}C (1972b).

Molecular Reaction Schemes

Mainly because of the difficulties associated with the free radical mechanism, there is an increasing tendency to favour modelling the pyrolysis using a simpler set of coupled pseudo-molecular reactions, chosen to reflect the free radical reaction steps. Thus the reaction set contains much fewer kinetic parameters which can now be simultaneously estimated using non-linear parameter estimation with experimental data from integral reactors. Some molecular schemes for pyrolysis of ethane and propane (Murata and Saito, 1975; Van Damme et al., 1975) had so many pseudo-kinetic parameters that these too had also been obtained by trial and error. Such an approach is clearly unsatisfactory.

The basis for the development of the reaction schemes is the product distributions. Molecular models for butane pyrolysis have been proposed by Andrews and Pollock (1959) and Shah (1967) and were utilised principally for purposes of industrial reactor tube design.

More recently, Sundaram and Froment (1977) used this idea to model most of the light paraffins including butane and was found to give quite satisfactory results. In extending their models for single components to multicomponent mixtures, they determined that satisfactory fits were also obtained without any adjustment to the rate data.

Present Study

The purpose of this study is to illustrate the inadequate attention paid to the quality of the experimental data used when modelling either global or mechanistic kinetics of the pyrolysis of light paraffins. Whilst it is accepted that the reactions have complex mechanisms which cannot be described by simple models, it appears that some of the "abnormal" behaviour, especially for global parameters under reported similar conditions may, in part, be due to improper defining of experimental conditions.

Previously most experimental work has revolved around designing reactors where plug flow for radial temperature and composition is approached. Many workers have assumed this valid enough to use ideal plug flow to model the data obtained without substantiating the assumption by measurements within the reactor. The method of altering the throughput rate to vary residence time and hence conversion in the reactor, commonly practiced to obtain typically required kinetic data at the reactor exit, can thus lead to effects which obscure the true kinetic steps. Only in an ideal plug flow will change in flowrate unaffect the heat and mass transfer effects prevalent, especially at and near the reactor wall. It is proposed that in reality this procedure to collect data has introduced a variable error due to poor justification for use of plug flow which would undoubtedly bias the observed kinetics and might explain some of the reported abnormal and conflicting behaviour. For example, Buekens and Froment (1968) used this approach to collect data, assuming plug flow in a reactor where the average Reynolds number was 100, clearly below the fully-turbulent range given by Re > 10,000 (e.g. Massey, 1970). There does, however, appear to be an increasing awareness of the changes associated with this experimental technique, typified by a

very recent paper by Hautman et al. (1981). The global kinetics for propane decomposition were studied in a cylindrical quartz turbulent flow reactor in the range 1110 - 1235 K and atmospheric pressure using a water-cooled sampling probe which withdrew samples from the centreline of the reactor.

Furthermore, use of a non-isothermal reactor increases the difficulty of obtaining well-defined kinetic parameters. Uncertainties associated with the heating and quenching zones are only partially redressed by using the equivalent volume or temperature concept.

Under these conditions, it seems rather futile to use a complex free radical model in an attempt to simulate the available experimental data. Edelson and Allara (1980) pointed out that by making no mathematical assumptions and by considering nearly all possible reactions to occur, discrepancies between computation and experiment can be narrowed to errors in rate constant assignments and/or incorrect assumptions that the data were free from various experimental complications such as wall effects. By eliminating lack of confidence in the experimental design, more emphasis can be placed on establishing the exact rôle of inaccurate rate data in modelling the free radical process during pyrolysis.

While it is recognised that parameters derived by model fitting serve a useful purpose describing a set of experimental data, they must not be granted the status of true rate constants. Thus, it is believed that the set of rate constants should be developed in a self-consistent manner using fundamental experimental data, thermochemistry, theory and structural analogy independent of the pyrolysis data.

Accordingly, this study was carried out to try and eliminate, or at least minimise, the effect of heat transfer, mass transfer, partial mixing, and non-isothermal profiles in the cause of collecting information on the pyrolysis of butane.

C H A P T E R 3

EXPERIMENTAL APPARATUS AND PROBE DESIGN

3.1 Introduction

For any experimental system a number of assumptions are unavoidably inherent when a specific theoretical model is applied for interpretation of experimental data. The fundamental objective of the design procedure was to build a reactor system by which the data required could be collected under conditions with errors well-analysed, understood, and where necessary, accounted for. In this study the reactor was designed principally to attain an isothermal gas region located within a section of the reactor space. In this way kinetic data could be handled in a more straightforward manner, without loss in accuracy, than if the data were non-isothermal.

Immediately this imposes a number of restrictions which must be scrutinised to ensure the proposed model remains consistent with the data. It is vital, for example, to show experimentally that an isothermal region has indeed been attained and that because of error introduced by the sampling process, the reactor position for any gas samples removed from within this region can be confidently defined with an acceptable degree of uncertainty.

Furthermore, because of the time scale of measurements, it would be necessary that no drifting of experimental conditions was detected and that fluctuations of such factors as feed flowrate, feed composition and temperature zones were kept to a minimum, thoughout the period of data collection. Only then could the data be assumed to be isothermal. In this Chapter, a description of the experimental system is followed by the design of the temperature and composition probes which ensured overall efficient sampling.

3.2 Experimental Apparatus

The are four principal parts to the experimental equipment:

(a) Reactor feed gas supply and flow metering system;

(b) Reactor and Furnace Assembly;

(c) Electrical measurement and control;

(d) Analytical System.

Plate 1 shows the general features of the experimental system and Fig. 3.1 represents a schematic line diagram of parts (a), (b) and (d). The majority of design for the reactor tube, furnace, electrical measurement and control was performed by Beshty (1978) in his work on the homogeneous pyrolysis of propane. The detailed design features are not presented here but can be located in his thesis.

Figure 3.2 shows the main dimensions of the reactor-furnace assembly. Located within the furnace are situated five independently-controlled electrical heaters, fabricated from SWG Kanthol A-1 wire. Axial wall temperature profiles were measured using 19 Pt/Pt 13% Rh thermocouples, diameter 0.375 mm, embedded into the reactor tube wall axially 5 cm apart, 5 of which are used as measurement for the temperature controllers. Controllers 1 - 4 are three-term, whereas controller 5 is an on-off with a constant voltage supply of 100 volts. The output signals from controllers 1 - 4 trigger a bank of thyristors which become conductive at a certain point in the voltage cycle.

The reactor tube is fabricated from schedule 40 inconel 600, 6.03 cm outer diameter, 5.25 cm inner diameter. This is located in the furnace, fixed at the furnace base and centred with a bellows configuration at the top of the furnace to allow for thermal expansion whilst heating the reactor tube. The furnace consists of a grooved recrystallised alumina tube, 1 m long, 7.5 cm outer diameter, 6.5 cm bore with grooves, 4 turns per cm, 1.33 mm wide, 1.5 mm deep into which the heating element

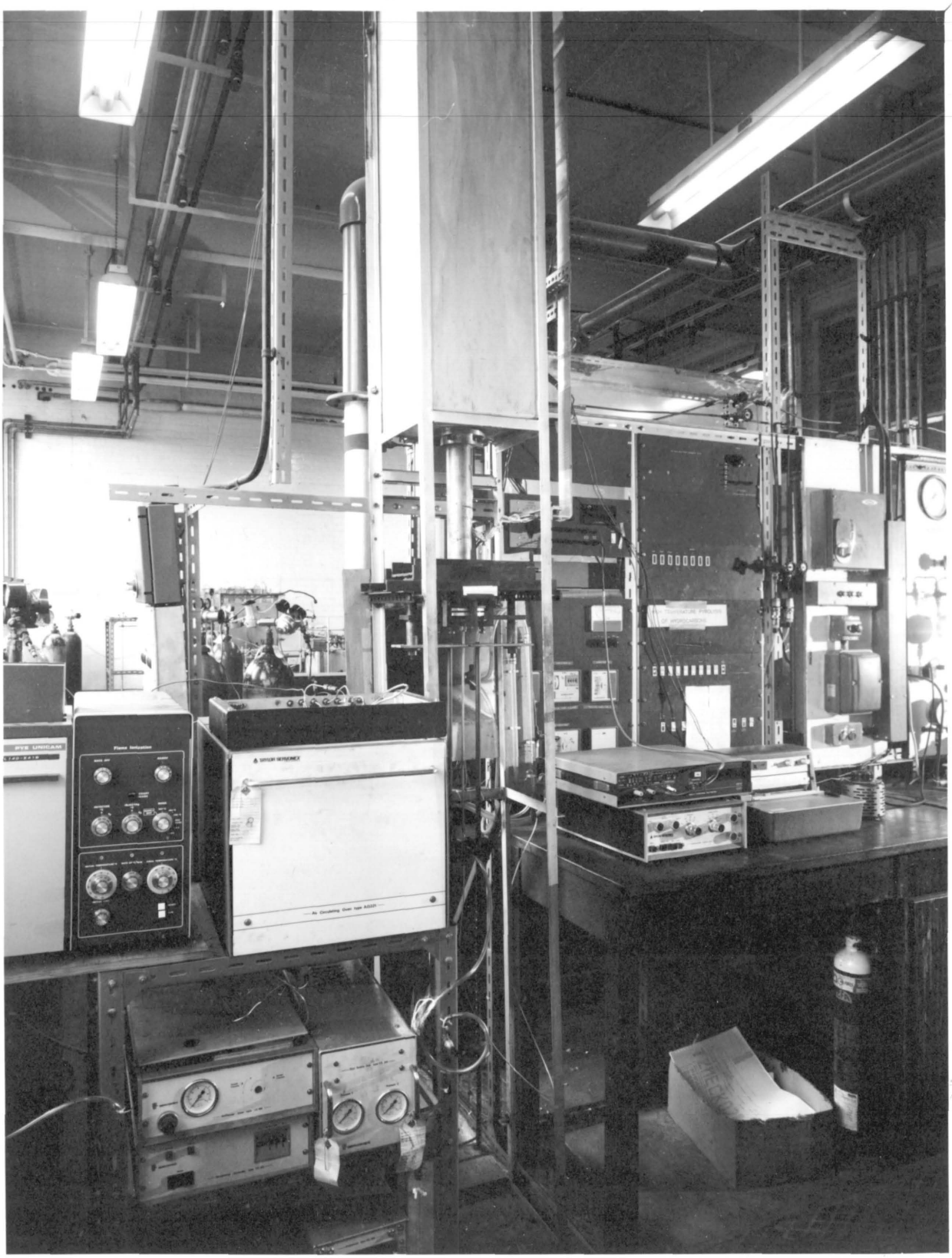

PLATE 1: General Features of the Experimental Apparatus

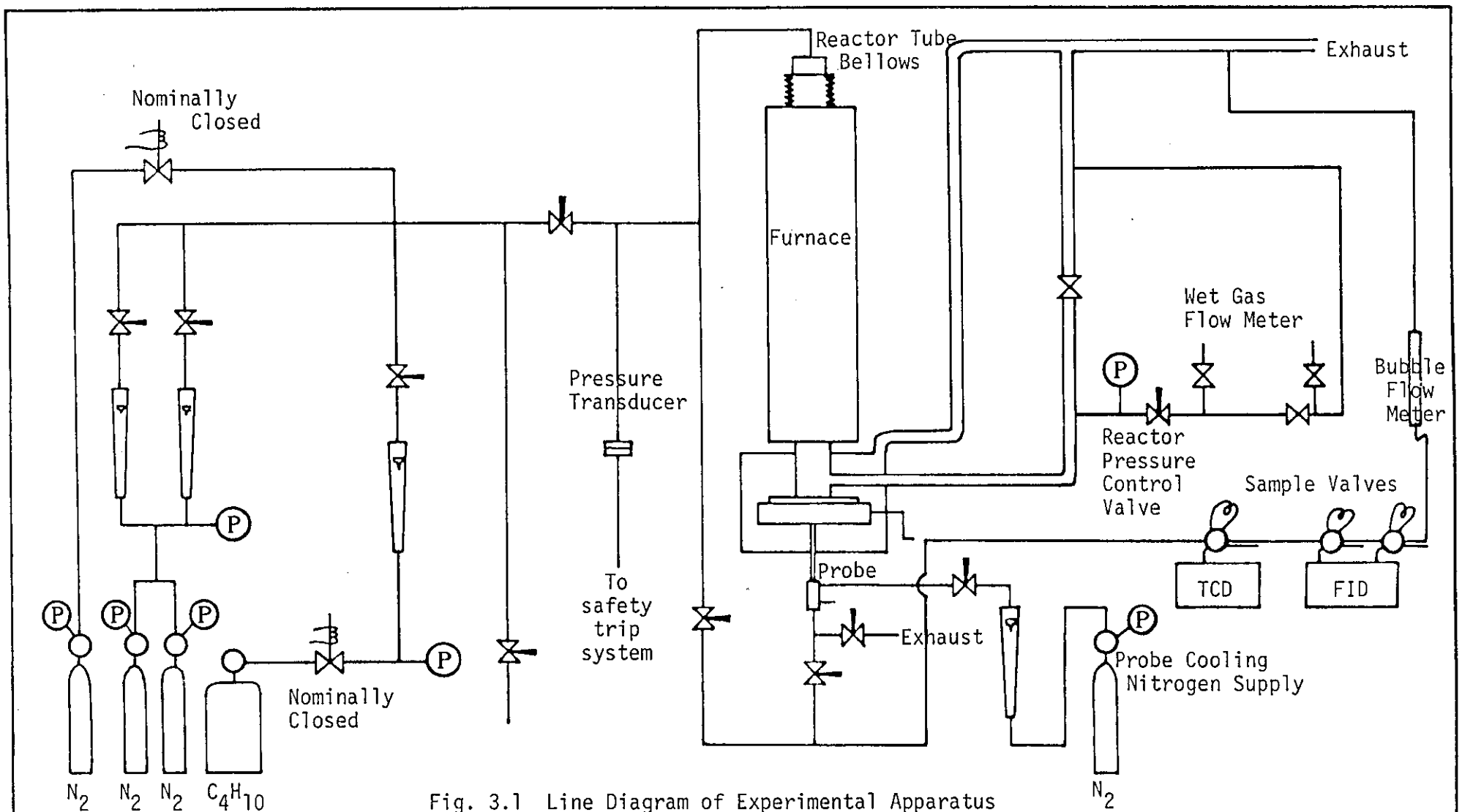

Fig. 3.1 Line Diagram of Experimental Apparatus

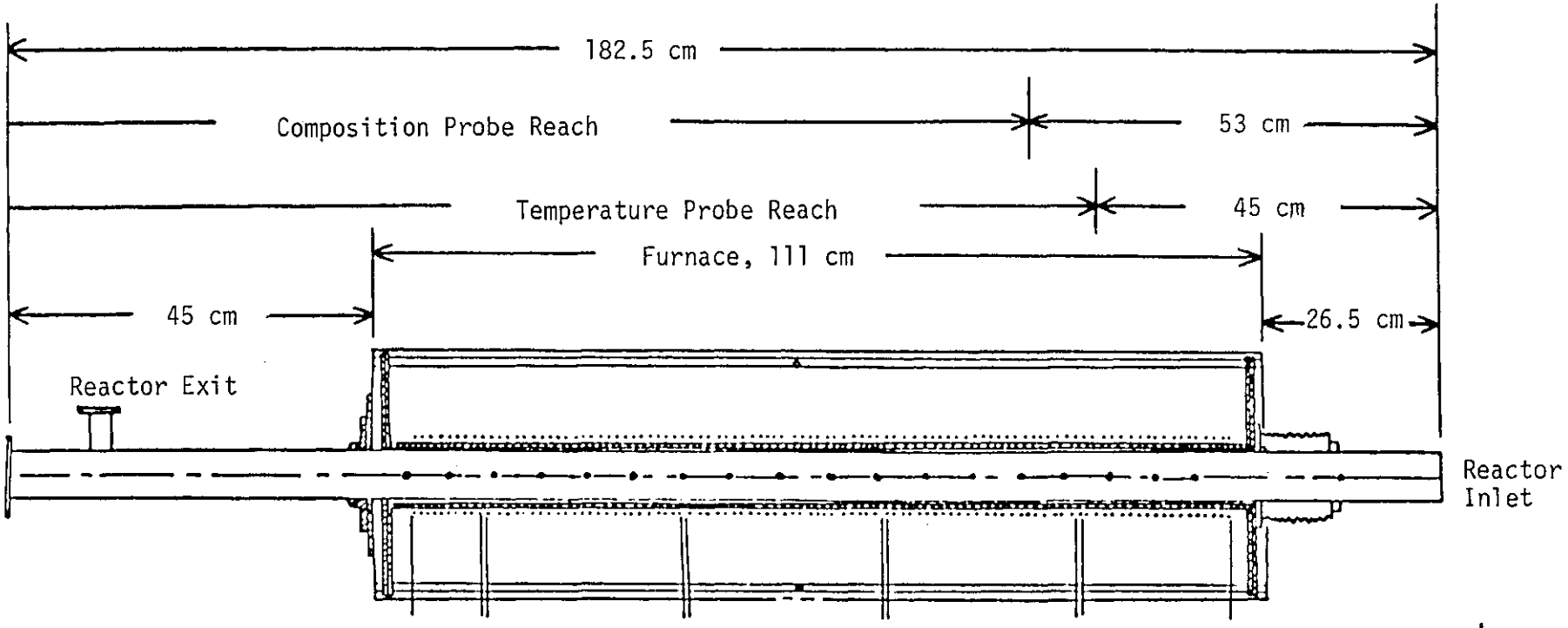

5	4	3	2	1	Heater No.
8	23.9	23.4	22.9	19.2	Lenght, cm
9	26.2	25.5	24.8	21.0	Resistance, Ω
31	94	92	91	76	No. of Turns

Fig. 3.2 The Reactor-Furnace Assembly

was laid. This is insulated by Kaowool fibres designed to achieve a safe furnace outer casing temperature of 60 - 70^{o}C. The insulation is wrapped around the furnace and held in place by a stainless steel frame, 25.5 cm square and 1.5 m high allowing 1.5 cm clearance between insulant surface and the furnace outer casing.

At the base of the reactor is situated a probe support mechanism which facilitated use of probes to measure temperature and composition at any radial and axial position within the reactor space.

3.3 Flow Gas Supply and Metering System

Feed gas during this study comprised two distinct composition mixtures and two distinct volumetric flowrates. The feed composition was chosen nominally to be either 5 or 10% (mole/mole) butane in nitrogen. Feed flowrates were nominally measured as either 100 cc/sec or 200 cc/sec at atmospheric pressure and room temperature, taken to be 290 K. The butane feed supply was C.P. grade, approximately 99.4% w/w pure with typical impurities, 0.3% w/w isobutane, 0.2% w/w isopentane and 0.1% w/w n-pentane. The nitrogen was 99.9% w/w pure with impurities 0.1% w/w argon, 10 ppm oxygen and 8 ppm moisture.

Both gases were metered separately before intimate mixing along the feed line leading to the reactor. Both rotameters were calibrated at a pressure of 10 psig which meant selection of the reactor operating pressure was a free variable in the design features of the composition sampling probe. Pressure drop through the valves upstream of the flow rotameters also smoothed out any back pressure fluctuations due to disturbances upstream of the metering point, resulting in better flow metering control. The assumption of an ideal gas mixture enabled evaluation of the flowrate into the reactor, that is, the sum of the individual flowrates. At the pressures used in this study, this assumption incurred almost no error.

The feed line was ¼" (0.635 cm) low pressure copper tubing introduced tangentially into the reactor. This provided additional mixing of reactants and eliminated any possibility of streaming effects which can occur when the feed is introduced axially (Batten, 1970).

The composition of the feed was measured by gas chromatographic analysis using a standard mixture of known composition (see Section 3.4). Reactor pressure was controlled by a manual valve, situated in the exhaust line from the reactor. A by-pass facility enabled flow measurement of the outlet gases using a wet gas meter but this was thought an inaccurate method of obtaining the overall flow, mainly because of the uncertainty of the effluent gas temperature.

3.4 The Analytical System

The samples withdrawn from the reactor by the composition probe were analysed using two chromatographs. A Pye Unicam gas chromatograph with a flame ionisation detector (FID) measured the majority of the hydrocarbons whilst a Taylor Servomex oven, type A0221, with a thermal conductivity detector (TCD) measured the non-ionisable molecular components of the sample. The analytical system was capable of separating and measuring CH_4, C_2H_4, C_2H_6, C_3H_6, C_4H_{10}, 1-C_4H_8, trans-2-C_4H_8, cis-2-C_4H_8 1,3 C_4H_6, C_3H_8, H_2 and N_2. Only acetylene was unmeasurable. In the past, very few authors have even detected the presence of acetylene. Typical chromatograms are given in Figs. 3.3a and 3.3b and column details and operating conditions are given in Table 3.1. Because of the regular gaussian-type shapes of the peaks, peak heights rather than areas were used for data processing.

Calibration of the chromatographs was obtained by preparing standard mixtures based on the assumption that partial pressures were directly

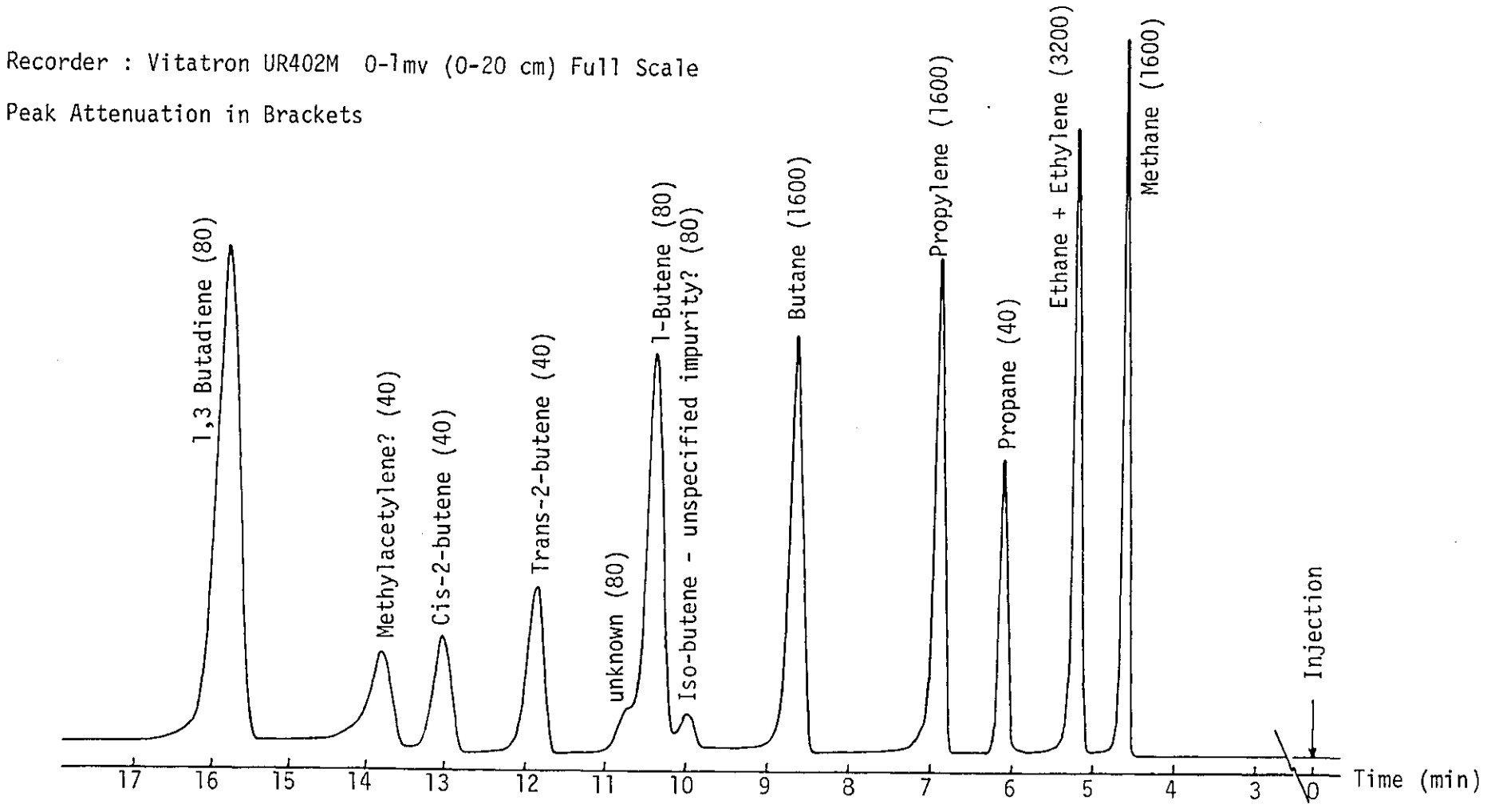

Fig. 3.3a Chromatogram for Sebaconitrile Column

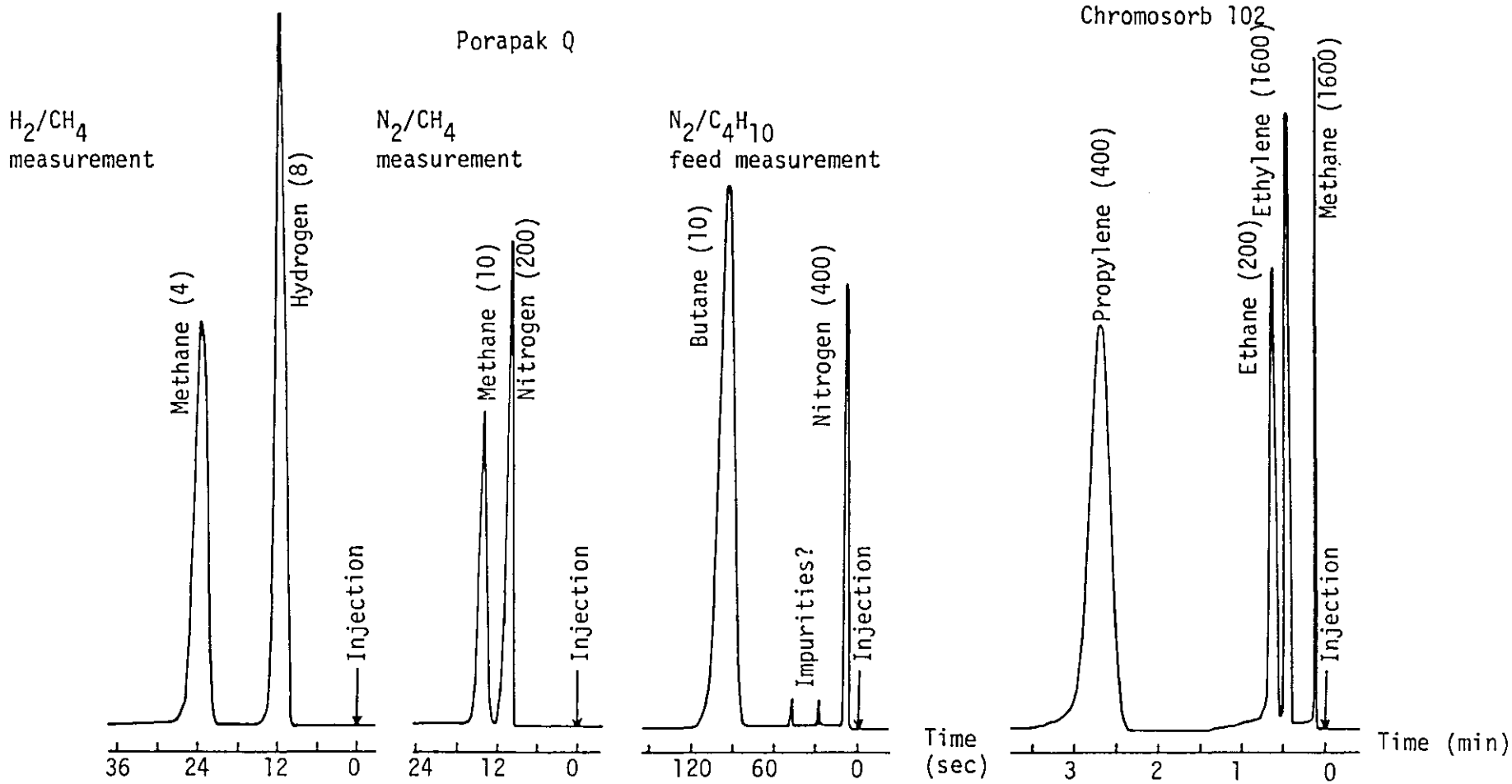

Fig. 3.3b Typical Chromatograms for Chromosorb 102 and Porapak Q columns

TABLE 3.1

Details of Chromatographic Analysis

Chromatograph	Column	Sample Loop Size (cm^3)	Operating Conditions	Components Measured
Pye Unicam FID	9 m x ⅛" OD 17% Sebaconitrile /Chromosorb PAW 70/80	∿0.03	Oven temperature = 50°C; Pressure drop = 50 psi; Flowrate through column = 1.0 l/hr; Carrier gas = nitrogen; Detector head temperature = 100°C; Injector temperature = 100°C; Air/hydrogen ratio = 3.	CH_4, C_3H_8, C_3H_6 C_4H_{10}, 1-C_4H_8 trans-2-C_4H_8, cis-2-C_4H_6, 1,3 C_4H_6
Pye Unicam FID	2 m x ⅛" OD* Chromosorb 102 80/100 mesh size	∿0.03	Oven temperature = 50°C; Pressure drop = 50 psi; Flowrate through column = 5.7 l/hr; Carrier gas = nitrogen.	C_2H_4, C_2H_6, C_3H_6
Taylor Servomex AO 221 oven + Bridge control unit type GC197 + Micro-Katharometer MK.158	2 m x ⅛" OD Porapak Q	2.0	Oven temperature = 30°C; Pressure drop = 15 psi; Flowrate through column = 2.9 l/hr (Reference column flowrate = 1.8 l/hr); Carrier gas = nitrogen; Bridge sensitivity = 4.5 v; Detector head temperature = 100°C.	H_2, CH_4
As above	2 m x ⅛" OD Porapak Q	2.0	Oven temperature = 150°C; Pressure drop = 20 psi; Flowrate through column = 4.7 l/hr (Reference column flowrate = 2.9 l/hr); Carrier gas = hydrogen; Bridge sensitivity = 6.5 v; Detector head temperature = 100°C.	C_4H_{10}, N_2
As above	2 m x ⅛" OD Porapak Q	2.0	Oven temperature = 30°C; Pressure drop = 20 psi; Flowrate through column = 8.1 l/hr (Reference column flowrate = 5.2 l/hr); Carrier gas = hydrogen; Bridge sensitivity = 6.5 v; Detector head temperature = 100°C.	CH_4, N_2

* Chromosorb 102 column in reference position for sebaconitrile column

proportional to the individual gas flowrates. Details of the calibration and analytical procedure are available in Appendices I and II. Long elution times from the columns in the FID chromatograph meant one complete measurement took about 40 minutes. The major delay was the elution of C_4H_{10} from the chromosorb 102 column. This restricted the number of measurements per experimental run to one per axial position in the reactor.

3.5 Error Analysis of the Composition Measurement

To test for possible drift in the experimental conditions during the period of a run, autocovariance functions (e.g. see Papoulis, 1965) were estimated for the feed noise (nitrogen/butane) and for the butane/methane noise at 700°C, 7 psig and conversion, $\phi \approx 32\%$, and are shown in Figs. 3.4a and 3.4b. The plots show a satisfactory lack of correlation between samples throughout the sampling period $\sim$ 6 hours. A drift in the experimental conditions would have been reflected in these plots, see Appendix III.

The limited number of composition readings which could be taken during one experimental run introduced an immediate source of possible gross error within the process of collecting data. The inability to state with confidence that one reading is sufficient for an accurate composition measurement would virtually invalidate the use of any kinetic data collected from the apparatus. Since the sampling analysis is non-linear with respect to the possible component peak errors, evaluation of the composition errors is not straightforward. By estimating the variation in ratios between component peak heights some idea of error incurred from one sample measurement alone can be obtained.

Table 3.2 gives results for an analysis of accuracy on the six major components for measurement at low and high conversion of the butane feed. Ratio statistics were determined by a series of measurements

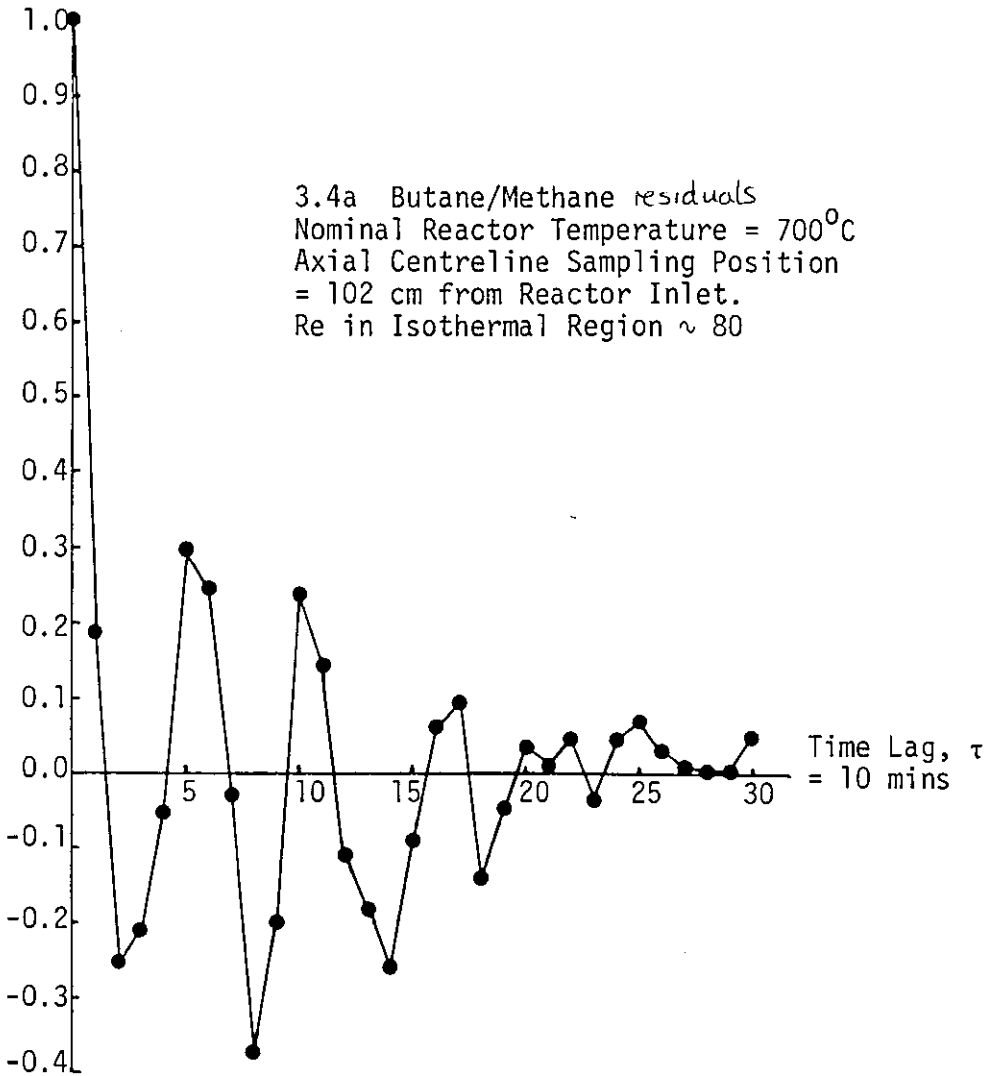

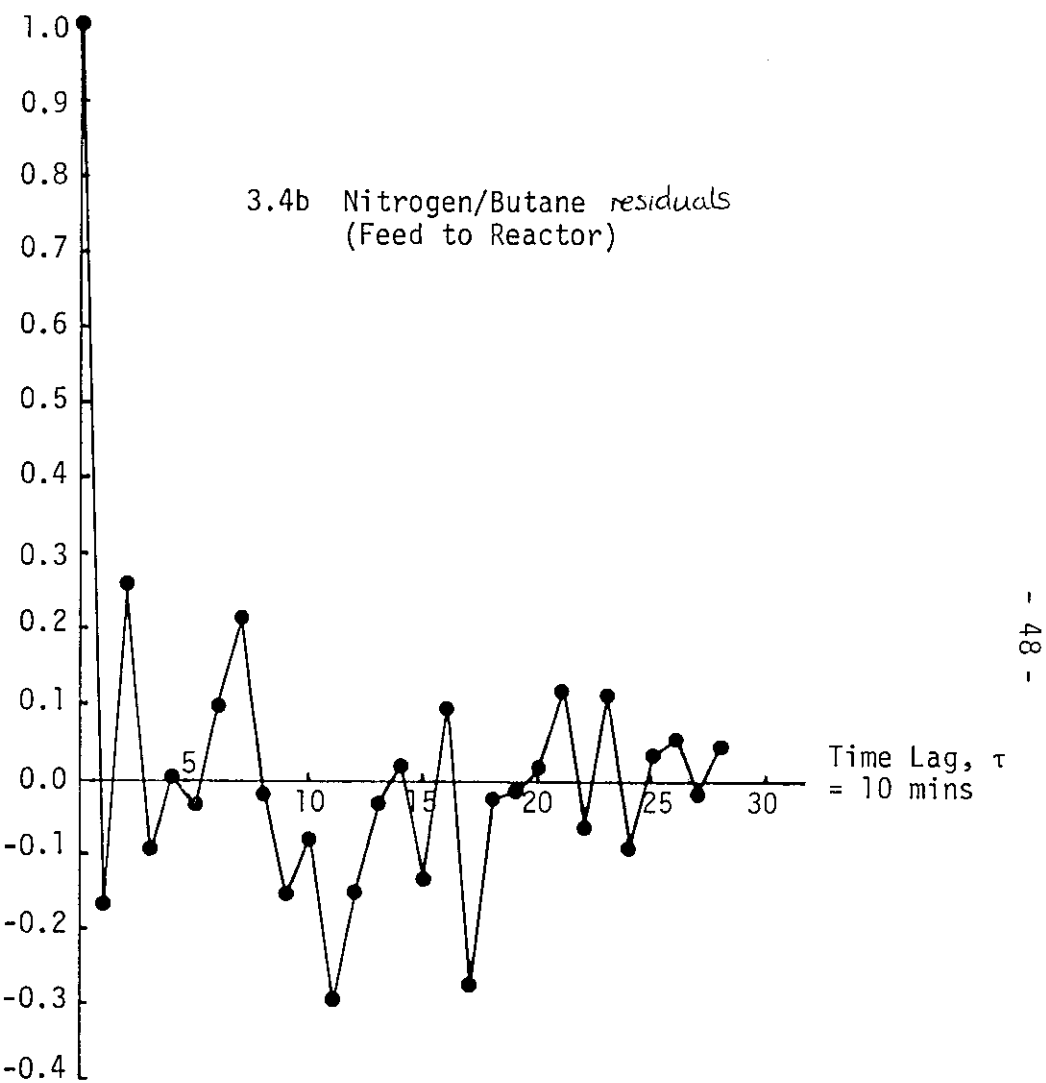

Fig. 3.4 Autocovariance Functions

TABLE 3.2

Error Analysis for Composition Measurement

	$\frac{C_4H_{10}}{C_3H_6}$	$\frac{CH_4}{C_3H_6}$	$\frac{C_2H_4}{C_3H_6}$	$\frac{C_2H_6}{C_3H_6}$	$\frac{H_2}{CH_4}$	Resulting Change in Composition (%)					
	Normalised 95% Confidence Limits of Sample Mean					LOW CONVERSION, $\phi \sim 26\%$					
	±5.2%	±4.1%	±2.0%	±5.8%	±3.7%	CH_4	C_3H_6	C_4H_{10}	C_2H_6	C_2H_6	H_2
Error Test 1	4.0	-3.0	1.0	-2.0	2.5	-4.8	-1.8	2.0	-0.8	-3.9	-2.4
Error Test 2	-4.0	4.0	-1.0	-2.0	-2.0	5.9	1.9	-2.2	0.9	-0.3	3.8
Error Test 3	2.0	-1.0	-2.0	2.5	-1.0	-1.7	-0.7	1.3	-2.7	1.7	-2.7
						HIGH CONVERSION, $\phi \sim 72\%$					
Error Test 1	4.0	-3.0	1.0	-2.0	2.5	-2.8	0.2	4.2	1.2	1.9	-0.4
Error Test 2	-4.0	4.0	-1.0	-2.0	-2.0	-1.3	2.8	-1.4	1.7	0.7	-3.3
Error Test 3	2.0	-1.0	-2.0	2.5	-1.0	-0.3	0.8	2.8	-1.3	3.2	-1.3

under identical conditions from the same sampling point in the reactor. Subjecting the measured composition to errors in the component ratios gave an idea of the resulting composition errors. From the Table it appears most compositions are accurate to within ±5% relative to the measured value. It is noted that this error also incorporates the sampling and process disturbances within the reactor during the sampling. Since this accumulated error appears to have a reasonably small confidence range the high frequency process noise will also be of a small nature.

Variation in feed composition was of the order ±6% relative (95% confidence interval), as determined by a series of feed composition measurements. This agrees with the idea of small process disturbance proposed by the sampling analysis, moreover because most of the variation is due to chromatographic error. Doubling the available length of tubing for mixing between the two feed components decreased only marginally (± 5.2% relative) the scatter of the measurement variation (see Appendix III).

There is no doubt that several measurements rather than one from each axial sampling point is more desirable, and this could have been obtained with one more gas chromatograph. The analysis has shown quite categorically, however, that one measurement is quite adequate to represent the composition of process gas at the point from where the sample is being withdrawn.

3.6 Design of the Probes

One of the design features of the reactor configuration was the mechanism through which probes could be inserted to measure, in situ, the gas temperature and composition. A simultaneous record of velocity, temperature and composition from one probe would have been highly desirable,

but Beshty (1978) has shown the enormous design limitations this would have presented. Emphasis was placed on designing separate probes for measurement of temperature and composition. The low axial gas velocities used in this system meant no adequate velocity probe could be designed.

For both the temperature and composition probes a number of errors are incurred during measurement. Specifically for temperature measurements, corrections due to convection, radiation and conduction are necessary. The errors of gas sampling are more complex and a simplified mathematical model was used to estimate the errors and assist in the final design of the probe.

There is strong motivation to sample axial composition profiles from just one radial position, most conveniently the centreline. Then complexity of data collection is reduced considerably. Design, therefore, of the measuring probes was based on sampling from the centreline.

3.7 The Temperature Probe

The most direct method of temperature measurement is by thermocouple. Then the principal errors would be the increase in recorded temperature due to radiation effects from the reactor tube wall. Disturbance to the thermal field and gas flow around the probe tip would be insignificant providing the diameter of the probe was small compared to the reactor diameter.

A minerally-insulated nickel chromium/nickel aluminium thermocouple with a 3 mm O.D. outer inconel sheath was supplied by Stanton Redcroft Ltd. where the couple tip was shielded, but electrically insulated, by the sheath for physical protection. The probe was supported by an outer tube, $\frac{1}{4}$" O.D., constructed from seamless 321 stainless steel which ended

a significant distance, 10 cm, from the probe tip to avoid thermal disturbance. The probe was capable of being inserted 135 cm into the reactor through the mechanism at the base of the reactor.

There are numerous reviews in literature (e.g. Bradley and Matthews, 1968) covering the problem of radiation from the tube wall but deal mainly with thermocouples exposed to the gas flow, although the heat transfer principles here remain unchanged. An energy balance around the tip shows the true gas temperature, T_g, to be expressed by

$$T_g = T_s - \frac{\varepsilon \sigma_c T_w^4}{h} (1 - (T_s/T_w)^4) \qquad (3.1)$$

where: T_s is the indicated thermocouple temperature (K)

T_w is the wall temperature (K)

ε is the emissivity of inconel

σ_c is the Stefan's constant = 5.75×10^{-8} ($W/m^2 K^4$)

h is the heat transfer coefficient between the thermocouple tip and process gas ($W/m^2 K$)

The conduction term is considered zero since the temperature gradient along the probe near the probe tip is zero, principally because of the high external thermal conductivity, small thermal capacitance of the probe tip and the large portion of probe immersed within the furnace. Typical calculations and derivation of equation (3.1) are given in Appendix IV.

3.8 Temperature Zones in the Reactor

The design feature to attain an isothermal gas region was verified conclusively using the temperature probe. Beshty's intensive measurements revealed an isothermal region, axially and radially, within a section of the reactor. These results were reproduced during this study and Figs. 3.5a and 3.5b show a typical axial and radial profile within the isothermal region.

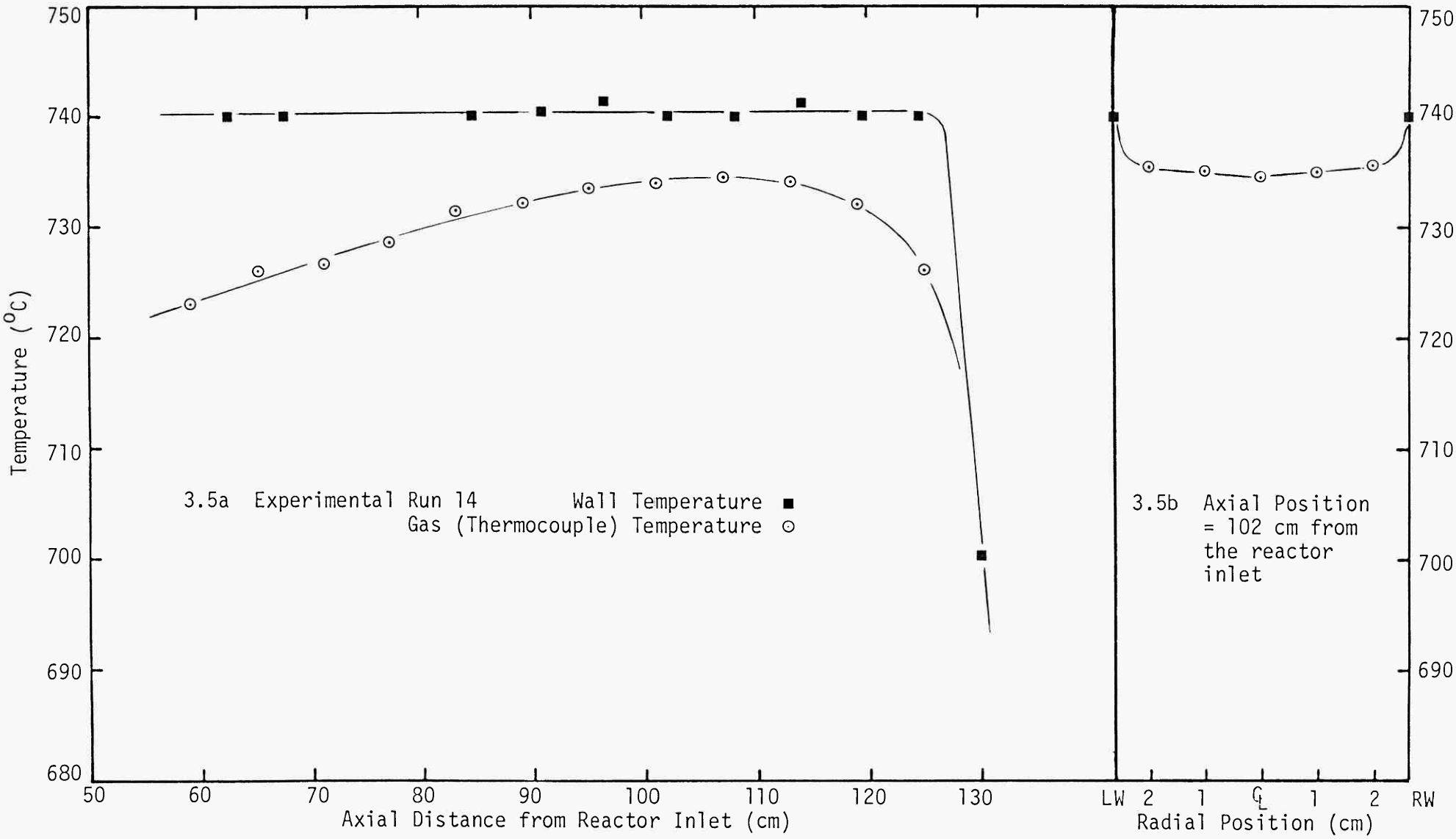

Fig. 3.5 Typical Axial and Radial Measured Temperature Profiles

Preliminary experiments showed isothermal gas regions to be of length $\sim$ 36 cm, in which measured temperatures varied normally by less than $4^{o}C$. Continuous centreline gas measurements throughout the time of a typical run showed local temperature variation to be less than $\pm 1^{o}C$. This correlates well with the results for drifting in composition during the period of an experimental run.

3.9 The Gas Sampling Probe

It was important during sampling that a representative gas sample could be withdrawn from the reactor with a known disturbance. With so many degrees of freedom on the design variables, e.g. reactor pressure, probe material and probe dimensions, emphasis was placed not on optimising the sampling procedure, but on designing a probe which gave an error much smaller than any other inherent errors in the sampling analysis, notably the composition measurement error.

Preliminary investigation showed basically three sources of potential major disturbance: aerodynamic effects exist because the presence of the probe disturbs the aerodynamic flow at and around the probe tip. Distortion introduced by the sample withdrawal has been discussed by Rosen (1954) using a disc sink model. The theoretical analysis revealed an expression for the fractional flow distortion, f, that is the ratio of radial velocity of the fluid elements to the nominal gas velocity, u_{∞}, as a function of the distance perpendicular to the sink and the sampling rate, α'

$$\alpha' = \frac{Q}{\pi r_c^2 u_{\infty}} \qquad (3.2)$$

where: Q is the volumetric sampling flowrate

r_c is the radius of the probe capillary

Secondly, the probe represents a heat sink which would disturb the flow and temperature fields especially near the probe tip. The degree of

thermal effect depends primarily upon the design features of the probe. Finally, there is reaction occurring in the capillary since the surface of the capillary represents an interference with the sample through its heterogeneous catalytic effect, negligible before the gas enters the probe. In addition, insufficient cooling of the sample would mean continuation of homogeneous reaction even after the gas has been sampled, an error which must not be overlooked. In fact, quenching of the reaction mixture is the most important single requirement if the probe is to obtain a meaningful sample.

3.10 Established Sampling Techniques

Most work done on gas sampling has been associated with flames (Fristrom and Westenberg, 1965). Two of the common techniques were re-examined with a view to their effectiveness in sampling from this reactor system.

Isokinetic Sampling occurs when the gas is removed without any increase in its velocity thus ensuring no aerodynamic disturbance to the flow field apart from the actual presence of the probe. Quenching is achieved by use of a coolant, normally water, when sampling from flames. This method proved totally unacceptable because the low axial velocities in this study ($\sim$ 0.2 m/s) would demand a very efficient cooling system, which quenched the sample immediately upon entering the probe capillary. Such a probe would prove difficult to design without introducing serious thermal effects on the surrounding flow field.

Aerodynamic Sampling requires the use of a critical flow probe where efficient sampling depends on maintaining supersonic flow downstream of a converging-diverging nozzle situated at the capillary tip. In this way pressure and temperature profiles along the sample line continue to drop and the sample composition effectively freezes. The main principal behind the quenching is the decrease in sensible heat energy, hence the gas temperature, to accommodate the corresponding increase in sample gas kinetic energy.

Preliminary calculations showed no possibility of maintaining supersonic flow downstream of the nozzle for typical L/D ratios necessary for the probe design (Shapiro, 1954). An enthalpy balance around the nozzle showed subsonic flow would not achieve the necessary cooling to quench the sample. For example, a capillary velocity of 40 m/sec would drop the sample temperature by only $1^{o}C$. At these velocities to ensure small aerodynamic disturbance, a very small capillary diameter would be necessary ($\sim$ 0.2 mm). The problems associated with such an idea, e.g. available pressure drop, insufficient quenching, clearly showed the idea of aerodynamic sampling alone to be inadequate.

3.11 Construction of the Test Probes

The investigation showed that individually, neither technique could provide a design readily acceptable for sampling from this system and a compromise design was necessary. For a fixed sample flowrate reducing the sample capillary diameter reduces the residence time and hence any chemical reaction of the fluid elements within the probe, with or without a cooling medium. The pressure drop through the capillary could provide a control on the sampling flowrate and hence the corresponding aerodynamic disturbance. Subsequent construction of several probes was therefore based around trying to minimise the inner capillary diameter whilst being capable of withdrawing samples over a typical experimental time period without blockage due to carbon buildup. The results are summarised in Table 3.3 and details of the probe construction are given in Fig. 3.6.

The minimum I.D. for the capillary without danger of blockage during sampling due to carbon laydown appeared to be $\sim$0.6 mm. The carbon is produced mainly by the heterogeneous catalytic effect of the capillary wall. Construction of a nozzle in probe I clearly demonstrated the impossibility of using such a design due to immediate blockage of the

TABLE 3.3

Construction and Testing of the Gas Sampling Probe

	d_{1*} (mm)	d_2 (mm)	d_3 (mm)	d_4 (mm)	d_5 (mm)	d_6 (mm)	Probe Length (cm)	Material of Construction	Reactor Conditions	Details
PROBE I	0.38	0.80	3.50	4.00	5.33	6.35	139.2	321 (Seamless) Stainless Steel	Wall temperature = 700°C. Reactor pressure = 7 psig	Converging-diverging nozzle ~0.2 mm diameter constructed at probe tip. Repeated blockage of capillary after ~2 minutes operation.
PROBE II	0.38	0.80	3.50	4.00	5.33	6.35	139.2	321 (Seamless) Stainless Steel	Feed composition = 10% molar butane in nitrogen	No nozzle. Repeated blockage of capillary after 2-3 hours operation.
PROBE III	0.55	1.02	2.69	3.51	4.52	6.35	139.2	321 (Seamless) Stainless Steel	Feed flowrate (1 atm, 300 K) = 100 cm^3/sec (Re ~ 80). Centreline sampling position = 102 cm from reactor inlet	No blockage after maximum period of test ~6 hours. Test repeatable.

* For nomenclature, see Fig. 3.6.

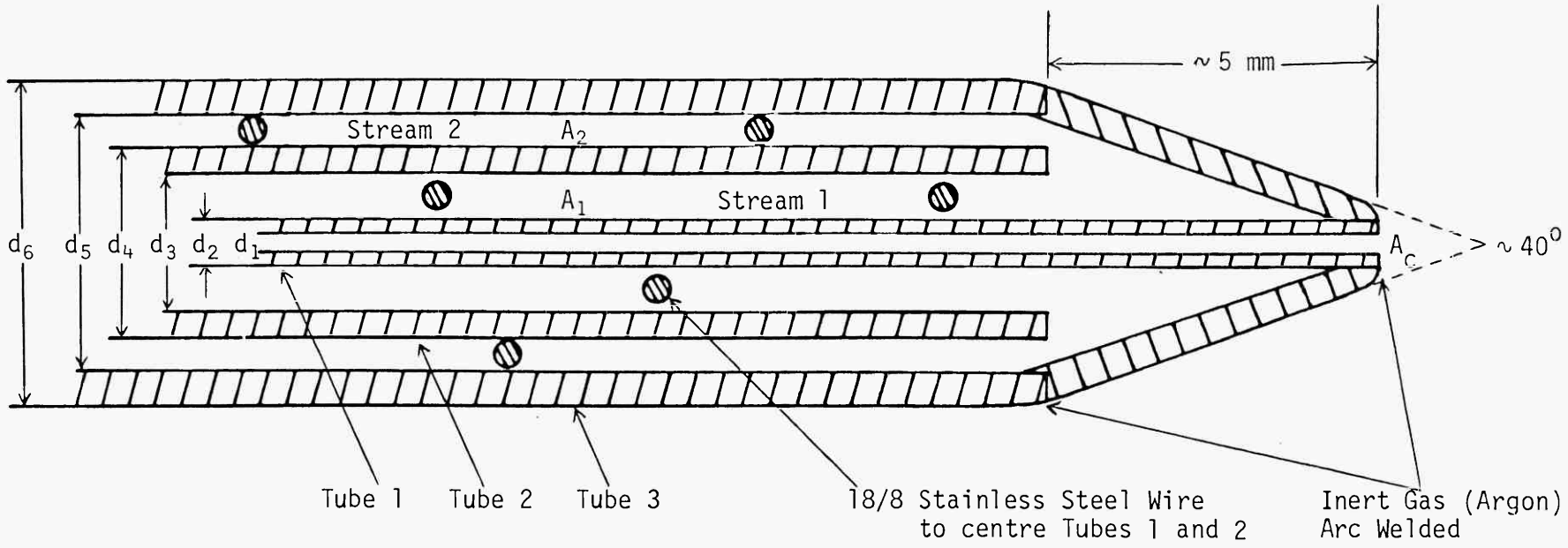

Fig. 3.6 Design and Construction of the Test Probes

capillary. The enhanced laydown appears to correlate well with the results from Beshty (1978) who discovered local turbulence creates greater opportunity for heterogeneous reaction because of increased mass transfer near the wall.

Inner capillaries constructed of less catalytically active materials were considered. Such material as quartz, known to have little catalytic activity, was discounted because of its fragility and hence unsuitability for probes of this length.

3.12 Modelling the Sampling Probe

Details were confirmed after developing a model to describe the probe's behaviour when the capillary was surrounded by a stream of nitrogen gas coolant.

One of the advantages of using a gas rather than a liquid, such as water, is immediately apparent. Since gases are not restricted by a temperature limitation and because the mass flowrate and hence thermal capacitance of the coolant is proportionately much smaller than for a liquid, the thermal effect of cooling on the temperature field around the probe tip can be considerably reduced. A second, perhaps less obvious, advantage is the larger heat transfer between gas sample and coolant than between coolant and reactor system. The typical correlation for flow conditions in the probe (Shah and London, 1978) clearly shows the near hyperbolic relationship between heat transfer coefficient, h, and diameter, D

$$h = 3.6568 \frac{K}{D} \left\{ 1 + \frac{1.227K^2}{G^2 C_p D} \right\} \qquad (3.3)$$

where: C_p is the specific heat capacity (J/kg K)

G is the mass velocity (kg/m^2 s)

K is the thermal conductivity (W/mK)

A series of mass, energy and momentum balances on the probe (see Fig. 3.6) lead to seven ordinary differential equations constituting a two-point boundary value problem, solvable by simultaneous estimation of three of the model variables. Instabilities frequently encountered with use of the "shooting method" (e.g. Carnahan et al., 1969) and the simplicity of the model led to a simplification to the equations such that sequential iteration could be used to solve the model equations. The series of assumptions discussed in Appendix V led to the following differential balances.

Energy

$$\frac{dT_1}{d\ell} = \frac{h_{02}\pi d_3 A_1 (T_1 - T_2)}{G_1 C_p}$$

$$\frac{dT_2}{d\ell} = \frac{h_{01}\pi d_5 A_2 (T_p - T_2)}{G_2 C_p} + \frac{h_{02}\pi d_3 A_2 (T_1 - T_2)}{G_2 C_p}$$

$$\frac{dT_c}{d\ell} = \frac{h_{03}\pi d_1 A_c (T_1 - T_c)}{G_c C_p}$$

Momentum

$$\frac{dP_1}{d\ell} = \frac{G_1^2 C_{f\pi}(d_3+d_2)}{2\rho_1 A_1} \qquad (3.4)$$

$$\frac{dP_2}{d\ell} = \frac{-G_2^2 C_{f\pi}(d_5+d_4)}{2\rho_2 A_2}$$

$$\frac{dP_c}{d\ell} = \frac{-2C_f G_c^2}{\rho_c d_1}$$

Mass

$$\frac{dF_c}{d\ell} = -k_b C_b A_c$$

where: h_0 denotes overall heat transfer coefficient. Individual coefficients were calculated using eqn. (3.3) with the hydraulic diameter substituted for the diameter when relevant

F_c is the flowrate of butane through the capillary

C_f is the friction factor

ρ is the density

Boundary Conditions @ $\ell = 0$ (Probe Tip) $T_1 = T_2$, $P_1 = P_2$

@ $\ell = L_p$ (Probe End) $P_c = P_2 = 1$ atm, $T_1 = 300$ K

The model generates a temperature profile to which the sample elements are subjected as they pass down the capillary from the reactor space. In this way the amount of reaction which occurs within the capillary can be estimated.

3.13 Sampling Errors in the Model

One of the difficulties was the characterisation of each disturbance such that each error could be directly compared. Individual studies showed that the thermal effect, even with a cooling medium, was much smaller than the other two effects. The study revealed that thermal influences due to cooling were propagated upstream of the probe tip so little as to be virtually undetectable. For example, at a nominal gas temperature of 700^{o}C, a temperature difference between the coolant gas and unaffected process gas of 50^{o}C depressed the process gas temperature by only 1^{o}C a distance 1.5 mm from the probe tip. The thermal influence of the probe itself would tend to be a small and constant effect, producing no significant disturbance on the sampling procedure. The remaining aerodynamic and chemical reaction errors were represented as positional errors in the assumed sampling point.

Specifying a point upstream of the probe tip where there is little disturbance the positional error in the assumed sampling part due to aerodynamic effects could be estimated by evaluating the residence time of all the elements which pass into the probe upon sampling. The accuracy of the model did not necessitate work of this complexity and an alternative, less accurate, but still satisfactory strategy was employed; the residence time of elements flowing along the axis of the probe from the point of little disturbance to the probe tip was calculated and taken to represent the mean residence time of all the elements flowing into the capillary. Rosen (1954) showed that the residence time, τ, of the probe axis elements is given by

$$\tau = \frac{r_c}{u_\infty} \int_0^{x/r_c} \frac{\sqrt{\lambda^2+1}}{\alpha'(\sqrt{\lambda^2+1}-\lambda) + \lambda} \, d\lambda \qquad (3.5)$$

where λ is a dummy variable of integration and the value x is related to the fractional flow distortion, f, by

$$\left(\frac{x}{r_c}\right)^2 = \frac{(\alpha'-1)^{2/3}\alpha'^{1/3}}{(2f)^{2/3}} - \alpha' \qquad \alpha' \geq 10 \qquad (3.6)$$

Effective axial error due to chemical reaction in the capillary is theoretically more amenable. The degree of reaction in the probe can be related directly to the distance necessary for the gases in the undisturbed flow field, experiencing nominal reactor operating conditions to travel to achieve the same degree of reaction.

3.14 Simulation Results and Discussion

Two basic sets of simulations were performed at nominal isothermal wall temperatures of 700°C and 800°C. In each set, sampling was simulated from three different axial positions along the centreline within the isothermal region. A constant cooling flowrate of 100 cc/sec (1 atmosphere, 300 K) was used irrespective of the simulated sampling position. These conditions were in fact tested experimentally and close correlation between experimental and predicted capillary flowrates for both simulations added confidence to the results (see Appendix V).

Table 3.4 shows the principal results for the axial sampling errors as predicted by the model compared to typical errors, prevalent in the chromatographic measurement of butane. From measurements discussed in Section 3.5 a typical error of ±4% for the error in butane composition was chosen. The comparison clearly shows the simulated sampling errors are much smaller than the composition error. Furthermore, the aerodynamic axial error acts in an opposite direction to the chemical reaction error leading to an overall error which is smaller than the individual errors. In addition, as sampling is from an isothermal region,

TABLE 3.4

Principal Results From the Gas Sampling Probe Model

Simulation Isothermal Zone Temperature (K)	Simulated Position of the Sampling Probe Tip	Aerodynamic Error (mm)		Reaction Error (mm)	Summation of Sampling Errors (f = 0.05) (mm)	Equivalent Axial Error Due to Chromatographic Measurement (mm)
		f = 0.05	f = 0.01			
973.0	Top of the isothermal gas region*	1.76	2.04	1.32	0.44	7.6
	20 cm below the top	2.01	2.33	0.33	1.68	
	40 cm below the top	2.36	2.73	0.04	2.32	
1073.0	Top of the isothermal gas region	1.69	1.91	1.68	0.01	0.9
	20 cm below the top	1.89	2.19	0.45	1.44	
	40 cm below the top	2.22	2.68	0.06	2.16	

* Assumed to be 50 cm length, situated 62.5 cm from the exit of the reactor

the overall disturbance of the probe would effectively disappear if the overall error remained constant irrespective of the sampling position.

3.15 Experimental Tests on the Sampling Probe

Continuous measurement from the same position in the isothermal region under identical experimental conditions showed that measurements with a cooling medium had a butane/methane ratio ∿2% higher than the ratio obtained without cooling and was further characterised by a marked decrease in the data scatter.

Measurements of heater input against probe position within the reactor showed a sizeable thermal load on heater 5 for a nominal cooling rate of 100 cc/sec. This became important only for sampling in the lower regions of the gas isothermal zone since it suggested that for a cooling flowrate that large, the coolant gas temperature may be significantly below the reactor gas temperature. This would create a decrease in the previously measured value of the temperature. This conclusion was reflected in the axial wall temperature profile which distorted by up to 1 - 2^{o}C in this region. Hence in collection of experimental data, the cooling flowrate was reduced to avoid such distortion. This was the criterion used for setting the coolant flowrate during the experimental runs (see Appendix XI).

3.16 Conclusions on the Sampling Design

The simulations and experimental tests have shown conclusively that representative samples can be withdrawn from the reactor. For this system the sampling errors appear to be much smaller than other inherent errors in the composition measurement, particularly the chromatographic analysis.

Previously, justification for assuming negligible probe sampling errors has centred on varying the sampling rate and observing any trend in the

resulting measurements. One of the uncertainties, inducing lack of confidence in this method, is whether the sample composition is from a point or is the sum of fluxes of the various species passing through the sampled cross-section, since the sampling process alters the original gradients. It is quite probable that even variation in the sampling rate is unable to detect which is more likely to be occurring. Furthermore, there could be no confidence that tests under one set of reactor conditions could be applied to the whole range of sampling positions and reactor conditions used in the experiments.

The principally theoretical approach in this study has shown categorically that the sampling errors are negligible for this probe design and this reactor system.

C H A P T E R 4

ESTIMATION OF THE GLOBAL RATE CONSTANT

4.1 Introduction

The primary objective of kinetically modelling the isothermal laminar flow region was to estimate the rate constant for the overall homogeneous disappearance of butane during the pyrolysis. In this Chapter, a study of the available models for estimation of rate constants in isothermal laminar flow reactors is made. The two principal models, the Radial Dispersion Model (RDM) and the Plug Flow Model (PFM) are compared to show under what conditions estimates of the rate constants from both models are comparable.

4.2 Modelling the Isothermal Gas Region

A number of models are used when interpreting data from isothermal laminar flow reactors. These range from simple one-dimensional models to more complex models incorporating the analysis in two dimensions. A simple model can only be applied, however, if the effects which complicate the mathematical modelling have been minimised by careful design of the reactor. In the limiting ideal situation, experimentally collected kinetic data would not be influenced by the experimental apparatus, being free from critical factors such as heat and mass transfer effects and/or heterogeneous effects which occur at and near the reactor wall.

4.3 The Radial Dispersion Model (RDM)

The parabolic velocity profile characteristic of laminar flow creates a residence time distribution for fluid elements passing through the reactor. Since the flow should be streamlined, no mixing should occur in the radial

direction and strictly, only mass transfer by diffusion can provide effects necessary to counterbalance the concentration gradient set up by the residence time distribution. The resulting radial gradient will be governed by the balance between the speed of reaction and the effectiveness of the diffusive properties of the reacting mixture.

Under conditions of steady state, axial symmetry and convective flow in the axial direction and assuming negligible axial dispersion, the differential equation for a first-order homogeneous chemical reaction in dimensionless form is given by

$$-(1-R^{*2})\frac{\partial C^*}{\partial Z^*} + \omega\left[\frac{\partial^2 C^*}{\partial R^{*2}} + \frac{1}{R^*}\frac{\partial C^*}{\partial R^*}\right] - \beta C^* = 0 \qquad (4.1)$$

where: $R^* = \frac{R}{R_o}$

$C^* = \frac{C}{C_o}$

$Z^* = \frac{Z}{L}$

$\beta = \frac{kL}{v_o}$

$\omega = \frac{D_r L}{R_o^2 v_o} = \alpha\beta$ where $\alpha = \frac{D_r}{kR_o^2}$

Boundary Conditions

$$\frac{\partial C^*}{\partial R^*} = 0 \qquad R^* = 0,\ 1 \qquad Z^* > 0$$

$$C^* = 1 \qquad 0 \leq R^* \leq 1 \qquad Z^* = 0$$

The velocity, v(R) has been replaced by the analytical solution for laminar flow. No readily available solution can be determined for equation (4.1). Lauwerier (1959) reduced the system to an eigenvalue problem determining an orthogonal set of eigenfunctions. The simplicity and directness of a numerical solution outweighs any advantage of this type of analytical representation and equation (4.1) is normally solved numerically.

4.4 The Axial Dispersion Model

The axial dispersion model is a step down in complexity from the radial dispersion model. The one-dimensional approach replaces the superimposed radial dispersion by an effective axial dispersion and for a first-order homogeneous reaction is expressed by

$$\frac{1}{Pe}\frac{d^2C^*}{dZ^{*2}} - \frac{dC^*}{dZ^*} - \beta C^* = 0 \qquad (4.2)$$

where: $Pe = \frac{\bar{v}L}{D_A}$

Boundary Conditions (Danckwerts, 1953)

$$1 = C^*(0) - \frac{1}{Pe}\frac{dC^*}{dZ^*} \qquad Z^* = 0$$

$$0 = \frac{\partial C^*}{\partial Z^*} \qquad Z^* = 1$$

Taylor (1953) first proposed this model for non-reactive systems and many workers (e.g. Vignes and Trambouze, 1962; Wan and Ziegler, 1970; Nigam and Nigam, 1980) have studied the applicability of using the axial dispersion idea to model laminar flow reactor systems. If necessary care is taken the axial dispersion model can be used to represent the two-dimensional RDM with a reasonable degree of accuracy.

4.5 The Plug Flow Model

This, of course, is the simplest one-dimensional model in common use for characterising isothermal laminar flow reactors. The total absence of radial concentration and temperature profiles implies each reacting element of fluid undergoes the same conditions whilst passing through the reactor, even with an imposed radial velocity profile. Both the axial dispersion and plug flow models are deliberate approximations to conditions in the reactor, in an attempt to reduce the complexity of the modelling. For both models, a bulk axial concentration, C_B, is used to

represent any variation of concentration in the radial direction, given in dimensionless form by

$$C_B = 4 \int_0^1 R^* (1 - R^{*2}) C^* dR^* \qquad (4.3)$$

In addition, the residence time of the reacting fluid elements is taken as the mean value for flow with a parabolic velocity profile, giving a mean axial velocity one half of the centreline velocity. Under this assumption the analytical solution for plug flow with a reaction $A \rightarrow nB$ for a laminar flow reactor is given as

$$\frac{n+\delta'}{1+\delta'} \ln \left\{ \frac{1-\phi_{f2}}{1-\phi_{f1}} \right\} + \frac{(n-1)}{(1+\delta')} (\phi_{f1} - \phi_{f2}) = -2\beta Z^* \qquad (4.4)$$

where: δ' = dilution ratio at $Z^* = 0$ $= \left. \dfrac{\text{Inert Flow (moles/sec)}}{\text{Reactant Flow (moles/sec)}} \right|_{Z^* = 0}$

In this study, δ' is of the order 10 and equation (4.4) simplifies to

$$C_B = \frac{1-\phi_{f2}}{1-\phi_{f1}} = e^{-2\beta Z^*} \qquad (4.5)$$

Any error in this simplification will give a constant bias in the pre-exponential factor for the rate constant but should not affect evaluation of the activation energy.

4.6 Rate Constant Estimation

A typical set of data from the experimental system will consist of a set of gas compositions as a function of axial position measured at the centreline over an isothermal region of the reactor.

When there are no radial concentration gradients the data can be conveniently analysed by the straightforward treatment for an isothermal plug flow reactor using equation (4.5).

However, the radial composition will generally vary because of the distribution of residence times. The size of this variation will depend on

the relative restoring effect created by the dispersive nature of the reactant against the disruptive effect created by the speed at which the reaction proceeds.

In the cases where this effect is noticeable, it would be more accurate to use the RDM. Clearly, though, if the dispersive properties of the reacting components are so great that the radial gradients tend to zero, the more convenient use of the plug flow model would facilitate the estimation of the rate constant. To justify this simplification it is vital to determine the error introduced by such an operation.

Previously, justification for plug flow has come by comparing the axial bulk concentration profiles which are produced for limiting values of $\alpha = \omega/\beta$, where ω is the dimensionless radial diffusivity and β, the dimensionless first-order homogeneous Damköhler number, both defined in equation (4.1). Cleland and Wilhelm (1956), in particular, have compared the plug flow profile where $\alpha \to \infty$, to the numerical solution to equation (4.1) for values of $\alpha \neq \infty$. In conclusion they stated that the bulk concentration profiles differ appreciably only when β becomes large or alternatively, when α is low, and set a criterion for acceptable use of plug flow as

$$\omega = \alpha\beta > 1 \qquad (4.6)$$

Equation (4.6) carried the implicit assumption that β remained low enough such that the criterion did not fail, although no limit for β was suggested.

More recently, Chandrasekharan and Calderbank (1980) used a similar approach to simplify the model from two dimensions to one dimension for rate constant estimation from an isothermal tube-wall-catalytic reactor with laminar flow. Common with both examples is the idea that justifica-

tion for model reduction can be derived from comparison of concentration profiles from the two models under review.

Although useful for design purposes, this approach is not adequate for the inverse problem of parameter estimation. No account is taken of estimate sensitivity to data corrupted with noise inherent in measurement from any experimental system. The more correct procedure is to compare estimation capabilities, particularly for the dimensionless rate constant β, of both plug flow and the RDM from the same experimental data.

4.7 Simulation of Composition Data

In order to justify use of plug flow to estimate the rate constant, an analysis has been performed, characterising the reactor behaviour with the RDM.

In a typical system, data analysis is corrupted by three main sources of error:

(a) Measurement error;

(b) Process error;

(c) Model error.

Measurement error was assumed larger than the other sources and accordingly, simulated data was generated by substitution of fixed values of α and β into equation (4.1) which was solved numerically using the implicit Crank-Nicholson finite difference method. Solution to the finite difference equations was achieved by Thomas's Method (e.g. Roach, 1972), a special form of Gaussian Elimination (see Appendix VI).

Addition of a normally distributed random number, ξ, to the centreline data points provided pseudo-experimental data, similar to that reported by Beshty (1978) from fixed axial points along the reactor centreline.

The discussion in Chapter 3 on composition measurement error (see Section 3.5) suggests that the assumption of little process noise is reasonable. Negligible drift as determined by the autocovariance function (see Fig. 3.4) suggested little low frequency process noise and analysis on the accuracy of point compositions revealed a limited degree of higher frequency process noise, even more so because the composition variation encompassed both sampling and measurement uncertainties as well as those due to process noise. Zero model error implies the RDM describes deterministically the conditions in the isothermal region, assuming zero process noise. This is unlikely to be totally true since the dispersion coefficient will change at different points in the reactor due to such intrinsic factors as variation in reactant concentration.

Application of random noise to the first data point merits discussion. In a typical kinetic experiment, the composition of the feed is known with much greater accuracy than that at other points within the reactor, and hence should not be subjected to perturbation by noise. However, in flow reactors for pyrolysis mechanisms, significant amounts of reaction may occur in the preheat section of the reactor, upstream of the isothermal zone. Hence the composition at the first data point is known with no more accuracy than all the other points and must therefore be treated likewise.

4.8 Parameter Re-estimation

For data obtained from a single simulated experimental run, in which the overall reaction was assumed to be first-order, three approaches were used to estimate the unknown rate constant, incorporated in β:

(i) The parameter, ω, is calculated *a priori* by equating the radial diffusivity to the molecular diffusivity. The rate constant, β, can then

be found by non-linear least squares regression techniques using the RDM with this value of ω substituted into the model.

(ii) Alternatively, it can be assumed the radial diffusivity is infinitely larger than the reaction effect and thus assumed that $\alpha \to \infty$, equivalent to perfect radial mixing. Then the parameter, β, can be estimated from the data using the plug flow model, either by linear or non-linear regression.

(iii) A third approach is to simultaneously estimate α and β using the RDM as regression model. This method provides an idea of the degree of correlation between simultaneous estimates of α and β. Of course, for a linear model and noise which is Gaussian with zero mean,

$$E(\hat{\alpha}) = \alpha_s$$
$$E(\hat{\beta}) = \beta_s \qquad (4.7)$$

where s denotes values substituted to produce the simulated data and

E is the expectation operator.

By definition, the dimensionless concentration is unity at $Z^* = 0$. Accordingly, in order to ensure that the uncertainty in this first point had some influence on the estimated profile, a third parameter γ was introduced into the simulation model

$$C_s^* = \gamma C_s \qquad (4.8)$$

where: C_s is the point concentration predicted from the RDM

C_s^* is the point concentration used in the regression of the simulated data.

By scaling all the predicted point concentrations as in equation (4.8) the simulated dimensionless concentration was now not necessarily unity at $Z^* = 0$.

Standard linear and non-linear regression techniques are a familar tool for parameter estimation in time invariant processes and will not be described. A summary of the methods used in this study is given in Appendix VII but a more extensive coverage can be found elsewhere (e.g. Himmelblau, 1970).

Normally for analytically-represented models the minimisation procedure requires the solution of a set of equations given by $\partial S/\partial a_j = 0$ where S represents the sum of squares of deviations between simulated and pseudo-experimental points and a_j represents the j^{th} parameter in the model. As no simple analytical representation was possible, minimisation of S for the non-linear regression in (i) and (ii) was carried out by the algorithm developed by M.J.D. Powell (1964).

4.9 Confidence Regions for Simultaneous Estimation

Predicted concentrations at the various axial positions from the RDM are clearly non-linear functions of α and β, and require use, therefore, of non-linear statistics for the determination of confidence regions and variance for the estimates.

Evaluation of simultaneous parameter estimate confidence regions of a system defined by non-linear statistics is cumbersome and difficult (e.g. Draper and Smith, 1966). An exact confidence contour for either a linear or non-linear regression model is defined by $S(b^*)$ = constant, where b^* denotes estimates of the vector set of parameters b in the model. The value of this $S(b^*)$ is related to a specific probability level, x', by the equation (e.g. Draper and Smith, 1966)

$$S(b^*) = S(\hat{b})\{1 + \frac{p}{N-p} F(p, N-p, 1-x')\} \qquad (4.9)$$

where: $\hat{b}$ is the best estimates of b

p is the number of model parameters

N is the number of experimental data points

F is the Fishers F-distribution

Since the correct distribution properties of the estimates in the general non-linear case are unknown, it is impossible to attribute a specific probability level to a chosen $S(b^*)$. Although the parameters are no longer normally distributed and the error variance estimate of the model is no longer unbiased with respect to the true variance, an estimate of the approximate probability level can be obtained from equation (4.9).

The $S(b^*)$ contour can be examined by selecting a grid network in the parameter subspace and evaluating S at each grid point. Construction of the contour can then be achieved by interpolation around local grid points. For this system, these calculations proved time-consuming and were carried out for only a few cases. A linear statistics approximation was used for the remaining simulations.

4.10 Linear Approximation to the Confidence Regions

In a linear system the variance-covariance matrix of parameter estimates, $V(\hat{b})$, and the error variance, σ^2, are related by

$$V(\hat{b}) = (X^TX)^{-1}\sigma^2 \qquad (4.10)$$

where X^TX is the information matrix (Davies and Goldsmith, 1970).

In reality, σ^2 is not known, although it was defined for the purposes of simulating the experimental data. In equation (4.10), therefore, it is replaced by the sample variance, s_o^2, based on the N-P degrees of freedom.

$$V(b) = (X^TX)^{-1}s_o^2 \qquad (4.11)$$

The $100(1-x')\%$ confidence region for the parameters b is given by the hyper-elliptical boundary

$$(b-\hat{b})^T(X^TX)(b-\hat{b}) = ps_0^2F(p, N-p, 1-x') \qquad (4.12)$$

Substituting equation (4.11) into equation (4.12)

$$(b-\hat{b})^TV^{-1}(b-\hat{b}) = pF(p, N-p, 1-x') \qquad (4.13)$$

For the RDM $\hat{b}$ represents the parameter set $(\hat{\alpha}, \hat{\beta}, \hat{\gamma})^T$. What is required is the projection of the ellipsoid given by equation (4.13) onto the α-β plane. This will give information on the correlation characteristics between simultaneous estimates of α and β. This can be achieved by partitioning the variance covariance matrix, V, and inverting the partition V_p for correlation between α and β and replacing V^{-1} in equation (4.13) by this new matrix V_p^{-1} (Schweppe, 1973)

$$b = (\alpha, \beta \,\vdots\, \gamma)^T \quad , \quad V = \left[\begin{array}{cc:c} v_{\alpha\alpha} & v_{\alpha\beta} & v_{\alpha\gamma} \\ v_{\beta\alpha} & v_{\beta\beta} & v_{\beta\gamma} \\ \hdashline v_{\gamma\alpha} & v_{\gamma\beta} & v_{\gamma\gamma} \end{array}\right] \quad v_{ij} = v_{ji} \qquad (4.14)$$

$$b_p = (\alpha, \beta)^T \quad , \quad V_p = \begin{bmatrix} v_{\alpha\alpha} & v_{\alpha\beta} \\ v_{\beta\alpha} & v_{\beta\beta} \end{bmatrix}$$

Thus the linear confidence ellipse is given by

$$(b_p-\hat{b}_p)^TV_p^{-1}(b_p-\hat{b}_p) = pF(p, N-p, 1-x') \qquad (4.15)$$

Hence an ellipse can be constructed quickly and conveniently if there is available knowledge of the variance-covariance matrix of the parameter estimates. A chi-squared test indicated that to obtain a reasonable estimate of effective parameter variances a data set of at least 50 simulated runs was required. In applying this idea for the RDM to construct approximate linear confidence regions, the distribution of the parameter estimates are assumed normal, consistent with a linear model,

rather than the true unknown distribution created by the non-linearity of the model. The greater the similarity between the two sets of distributions, the greater would be the accuracy of the approximation.

In the cases where the non-linear calculations were performed, the linear contours were compared with the non-linear contours. In this way some idea of the accuracy of the approximation was obtained.

4.11 Simulation Results and Discussion

In the generation of the pseudo-experimental data the error variance, σ^2, used in the random number generator depicted two hypothetical situations. In the first, it was assumed σ^2 was independent of the simulated value of the dimensionless concentration, thus making system errors normal with zero mean and fixed variance, σ^2. In the second instance, the variance, σ_R^2, was made proportional to the value of the simulated concentration being perturbed. As the statistical analysis arbitrarily assumed a constant variance, this served to test the robustness of the regression technique when this assumption was violated. The pseudo-experimental data was assumed to be thirteen axial composition measurements, perturbed with noise characterised as above.

Figure 4.1a and 4.1b illustrate the approximate contours for 95% confidence limits for estimation of the parameters α and β from two random sets of simulated data, obtained by solution to the RDM with $\alpha = 0.45$, $\beta = 0.85$, $\sigma = 0.01$. Both Figures depict the ellipsoidal approximation to the region using linear statistics and the non-linear asymmetrical approximation for the contour with an approximate confidence limit of 95%.

A summary of other linear correlation studies is presented in Table 4.1. Figures 4.1 and 4.2 correspond to run 1.

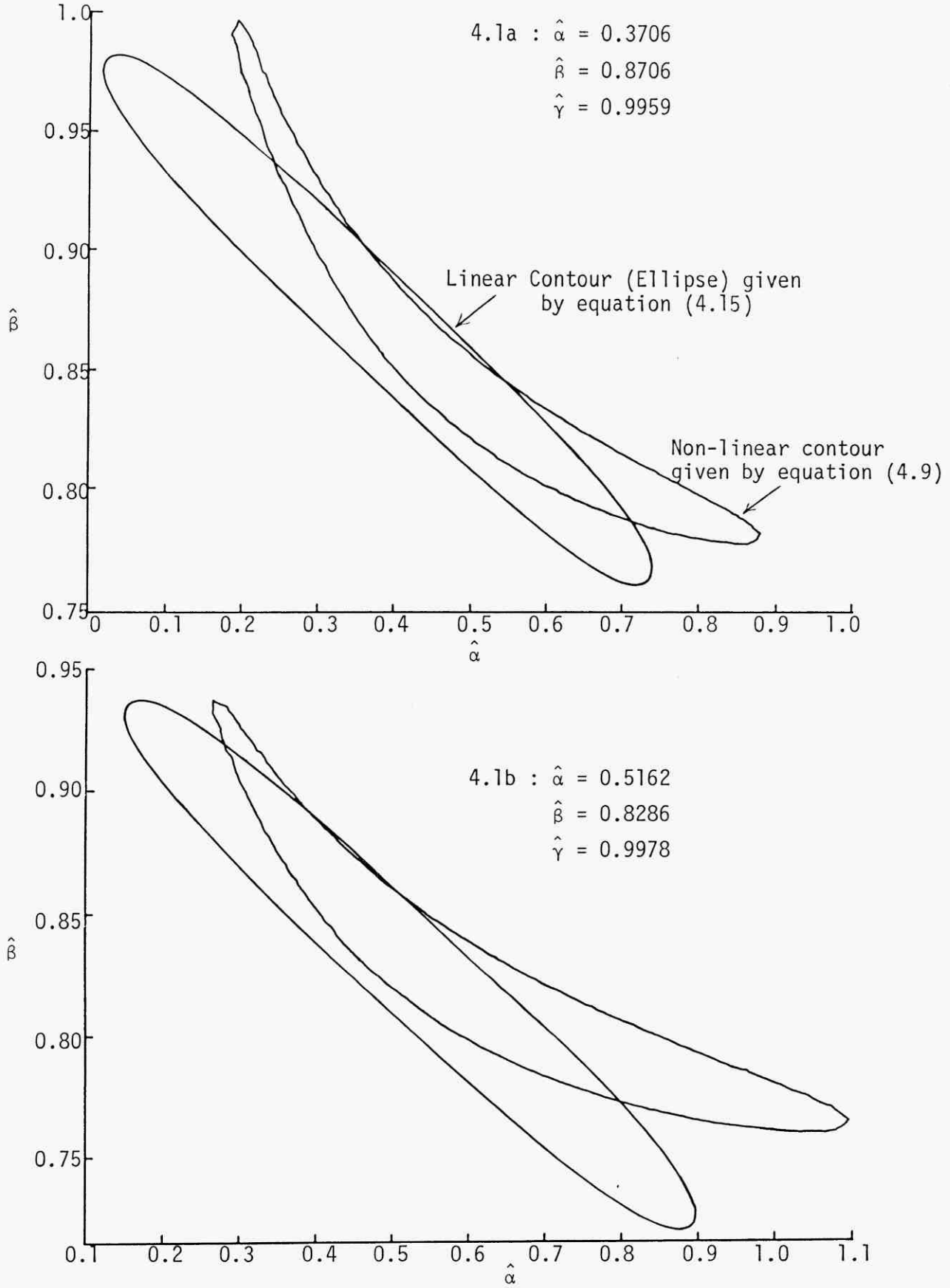

Fig. 4.1 Approximate Linear and Non-linear 95% Confidence Regions for Two Random Sets of Data for the Simulation Set $\alpha = 0.45$, $\beta = 0.85$, $\gamma = 1.0$, $\sigma = 0.01$ (For further reference, see Appendix VIII)

TABLE 4.1

Linear Elliptical Approximations for the 95% Confidence Regions for the Simultaneous Estimation of α and β Using the RDM

Simulation Run No.	σ, σ_R	Simulation α	Simulation β	Mean of $\hat{\alpha}$	Mean of $\hat{\beta}$	SIZE OF LINEAR ELLIPSE		Angle of Inclination of Major Axis to Horizontal [1]
						Semi-Major Axis	Semi-Minor Axis	
1	0.01	0.45	0.85	0.4558	0.8556	0.396	0.045	15.5^{o}
2	0.01	1.5	0.85	1.8881	0.8505	3.450	0.043	0.7^{o}
3	0.033C*	0.45	0.85	0.4914	0.8862	1.113	0.274	14.4^{o}
4	0.033C*	1.5	0.85	1.4937	0.8693	4.192	0.075	0.9^{o}
5	0.01	0.45	2.0	0.4556	2.0138	0.476	0.066	28.5^{o}
6	0.01	1.5	2.0	1.5526	2.0081	2.322	0.009	2.6^{o}
7	0.033C*	0.45	2.0	0.5233	2.0226	1.328	0.190	10.9^{o}
8	0.01C*	0.45	0.25	0.6346	0.2507	1.724	0.070	3.5^{o}
9	0.01C*	1.5	0.25	1.6119	0.2564	2.539	0.064	1.2^{o}

[1] Negative correlation, abscissa axis α, ordinate axis β

The results show that both α and β can, in fact, be observed from measurement of centreline data alone (see Appendix VIII). This is because the radial diffusivity distorts the centreline axial concentration profile from that which would otherwise have been of exponential form. The purpose of this study, however, was solely the determination of the rate constant, β, whereas the estimated value of α is irrelevant. Thus the information desired is the effect estimation of α has on the simultaneous estimation of β, that is, to what extent they might be correlated.

From Figs. 4.1a and 4.1b it appears that the use of linear statistics maintains the overall properties of the non-linear plots, in particular, the inclination of the contour to the horizontal axis, whilst still preserving a reasonably conservative estimate of its size. With this in mind, the simulations were extended for a β range 0.25 - 2.0, constituting small and large rate constants and an α range 0 - 1.5, the range of major interest. Table 4.1 demonstrates clearly that at a value of α = 1.5, inclination of the ellipse is approximately 1^{o} and there is virtually no correlation between estimates of α and estimates of β. Indeed, the value of α appears immaterial and would become totally unobservable in the limit $\alpha \to \infty$. At a value of 0.45 the inclination no longer remains negligible and there is an obvious negative correlation between the two estimates. Even at these values of α the angle of inclination is less than 20^{o} for most of the simulations considered. It is interesting that this angle of inclination does not significantly vary throughout the considered range of β.

The results from the simulations to simultaneously estimate α and β using the RDM are indicative of what might be expected for a general set of experimental data with a general number of experimental points and value

of the error variance. In a linear model the expected values of the model parameters would not depend on either the error variance or the number of the experimental data points, providing of course, that the number of degrees of freedom ≥ 0. What would change would be the variance, or spread, of the parameter estimates as dictated by equation (4.10). Obviously the smaller the error variance and the larger the number of experimental points, the better would be the accuracy of the resulting estimates.

In a non-linear model, this is not quite the situation. The asymmetry of the conditional non-linear parameter probability density function will mean that both the expected value as well as the variance of the estimates will change if the error variance or number of experimental points is altered. Since no information is available about the distribution of the non-linear parameter estimates, however, the simulations have tacitly assumed that the distribution can be approximated as Gaussian and the validity of the assumption has been verified by a comparison between the linear and approximate non-linear confidence regions for estimates of α and β in Figs. 4.1a and 4.1b. This approach also assumes, therefore, that the expected values of the parameter estimates do not significantly vary when the error variance or number of experimental points is changed. Although no simulations with a change in the number of experimental points was performed, some simulations were performed where not only was the error variance increased, but also weighted to the simulated experimental point concentrations as in runs 3, 4 and 7. The results clearly indicate that the expected values of the parameter estimates α and β are not noticeably different from those obtained with similar simulations using a smaller, constant error variance, runs 1, 2 and 5.

Because of the low correlation between estimates of α and β, the estimation of β might be carried out using a predetermined value of the radial diffusivity by equating it to the molecular diffusivity or even a value which tends to infinity. Figures 4.2a and 4.2b show the estimation using an a priori value of ω, estimated from data on molecular diffusion coefficients which could be subject to some considerable error. The plots show that the β estimation can be sensitive to the assumed value of ω, even at large α when correlation between α and β becomes negligibly small. Specifically, the greatest sensitivity occurs in the range where the a priori value of ω is lower than the true value, that used in simulating the data.

A desirable simplification in the estimation procedure is to assume the plug flow model where α and hence $\omega \to \infty$, even when it might be known that the radial mixing is incomplete. Figure 4.3 shows the characteristics of the error associated with such an operation when the real value of α is not infinite. It is clear from Fig. 4.3 that errors in estimating β using plug flow decrease rapidly as α increases from 0, significantly more so for the much-used simplification using linear regression than for the strictly more correct non-linear regression.

At the limits $\alpha = 0$ and $\alpha = \infty$ the prevailing conditions in the reactor for the centreline are plug flow. At $\alpha = \infty$ plug flow exists with a mean velocity, $v_0/2$, whilst at $\alpha = 0$, in the completely segregated case, conditions can be assumed to be plug flow with a velocity, v_0, since the fluid elements flowing along the centreline do not interfere with any other elements flowing through the reactor. Figure 4.3 shows that the bias of the mean created by using linear statistics at these values of α is negligible. The increase in variance of the estimates is due to the non-linearity characteristics of the logarithm function which adds

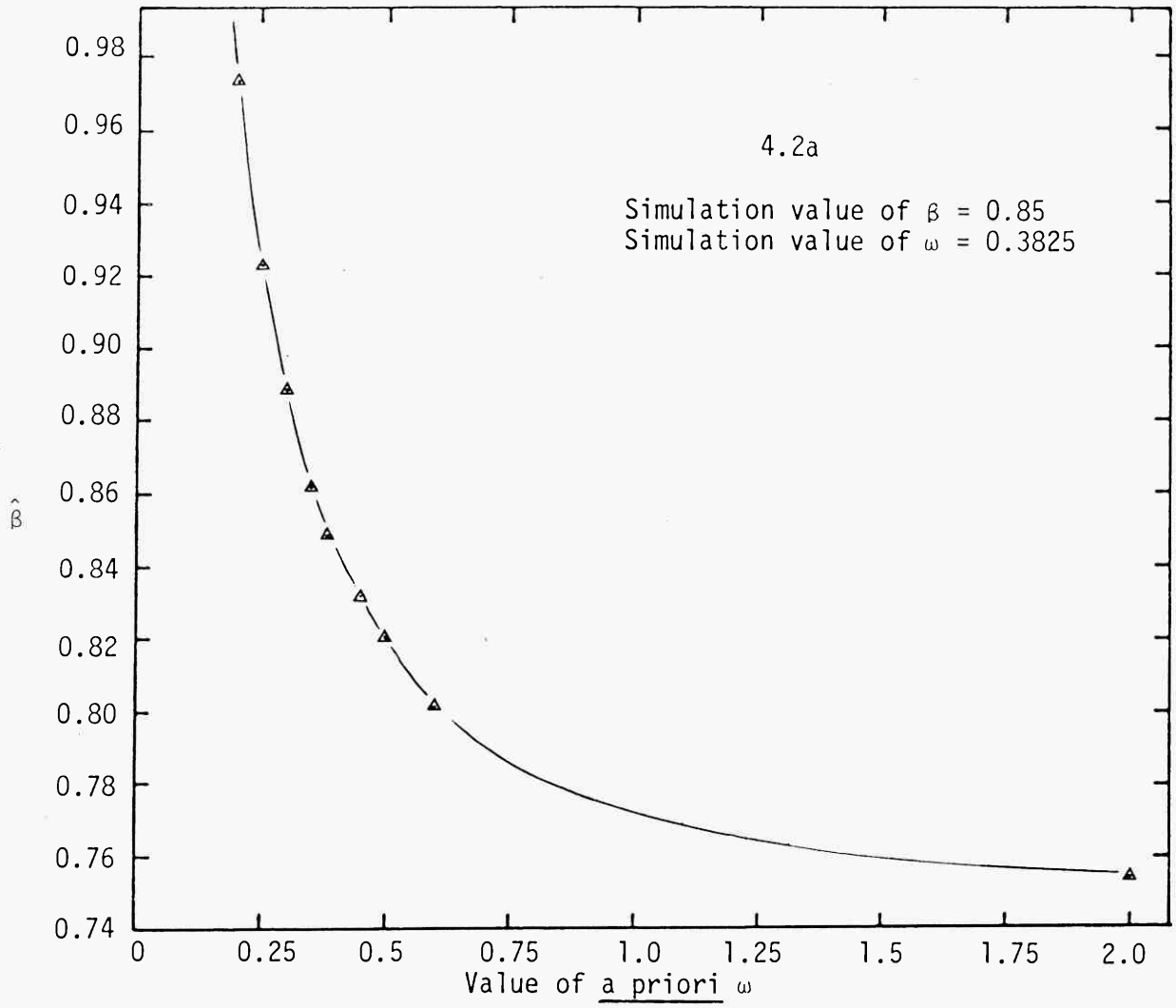

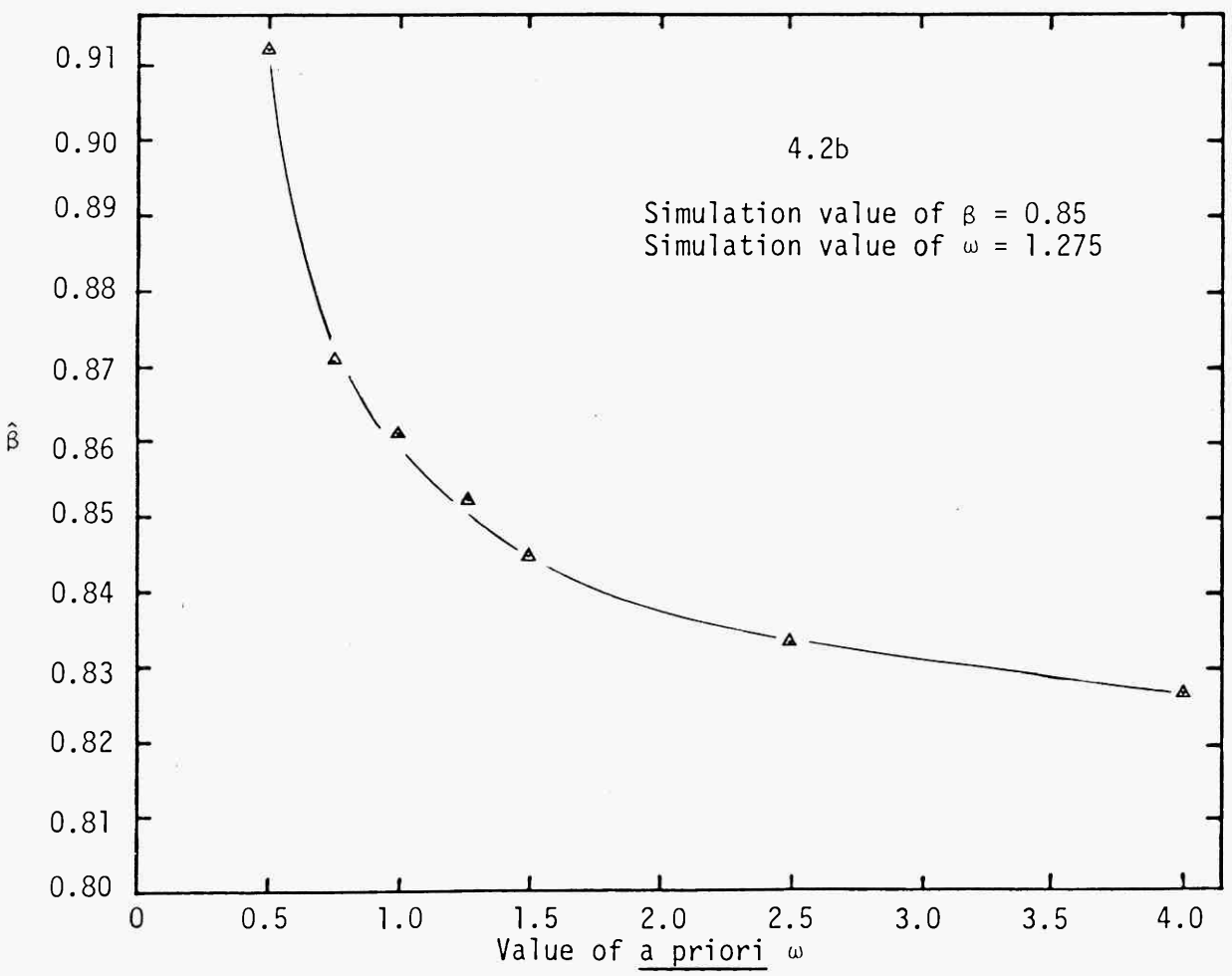

Fig. 4.2 Estimation of β (σ=0.01) using the RDM with an a priori value of ω

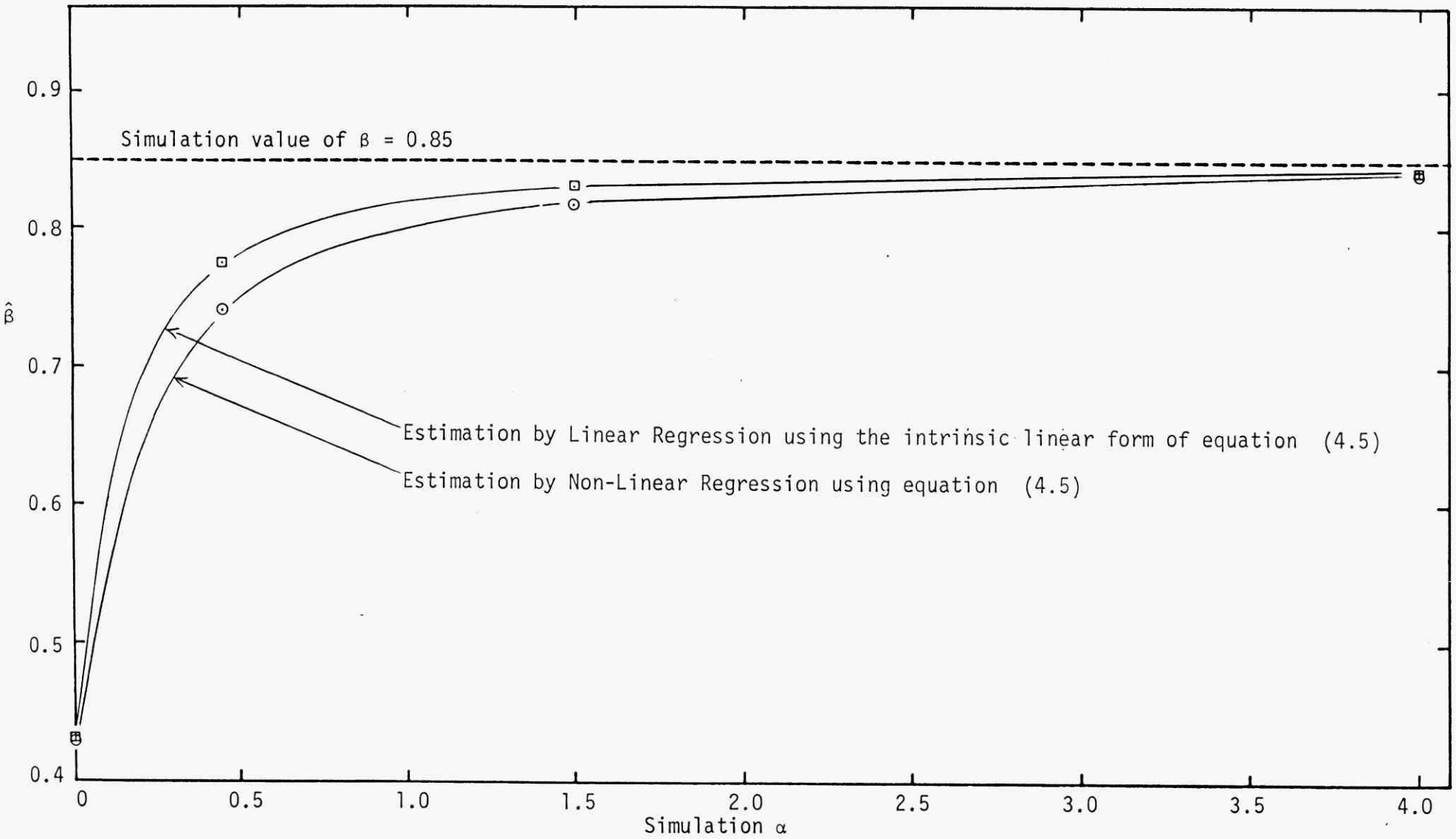

Fig. 4.3 Estimation of β (σ=0.01) using the PFM, assuming $\alpha \to \infty$

far greater weighting to the concentration points which approach 0. Between these two extremities a clear bias can be detected for the linear regression estimates over the strictly correct estimates determined by non-linear regression.

Simulations where the wrong model was applied to the pseudo-experimental data to estimate the rate constant, such as the RDM with an a priori radial diffusivity or the plug flow model when the radial mixing was not infinite, will lead to a bias parameter estimate distribution, because the experimental error noise no longer has zero mean around the best model fit. In these instances also, the expected values as well as the variance of the β estimates will also be conditional upon the size of the error variance. For example, the curves in Figs. 4.2a, 4.2b and 4.3 belong to a whole family of curves which are conditional upon the size of the error variance. Apart from performing a complete series of simulations in which the error variance or number of experimental points are varied, there is no straightforward way of determining the spread of these curves. Nevertheless, the simulations serve well to qualify the trends which occur if the rate constant is estimated using an incorrect model.

An interesting fact to note is that Fig. 4.3 represents the locus of the asymptotes as α and hence $\omega \to \infty$, of the estimates of β with an a priori value of ω such as in Fig. 4.2a and Fig. 4.2b. Thus the asymptote of the curve in Fig. 4.2a, where the true value of α is 0.45, is given by $\beta = 0.7402$ as shown in Fig. 4.3. It shows that estimation of rate constants using the radial dispersion model with an a priori value of ω is not significantly better than estimates from assuming plug flow. Indeed, if the calculated radial diffusivity is markedly lower than the true value, the estimates of β from the plug flow model may even be more accurate.

Estimates of the third parameter, γ, introduced to reduce the bias of the simulation model on the first experimental point varied little about its value used when simulating the data and appeared to have little effect on the α and β estimates.

4.12 Conclusions

From the simulations, several important factors have been determined. Centreline measurements in a laminar flow reactor can lead to accurate estimates of homogeneous first-order rate constants with or without accurate prior knowledge of the radial diffusivity. A negative correlation between estimates of α and β becomes appreciable only for very small values of $\alpha \sim 0.5$. At $\alpha = 1.5$, all the simulations revealed very little correlation with an angle of inclination to the horizontal for the linear confidence regions generally less than 1^{o}. This indicates that as α approaches large values it becomes progressively more and more unobservable from centreline data alone and in the limit $\alpha \to \infty$ becomes totally unobservable. Only at these low values when $\alpha < 0.5$ can both α and β be well estimated from the centreline data.

In addition, the rate constants derived from the RDM using a priori data for the radial diffusivity were comparable with those obtained by assuming the plug flow model. Only when this value is very accurately determined or when the flow tends to be segregated ($\alpha = 0$) does the use of the RDM become considerably more accurate and hence advantageous.

C H A P T E R 5

MODELLING TECHNIQUES FOR THE PYROLYSIS MECHANISM

5.1 Introduction

It has already been shown under what conditions within the reactor, a plug flow approximation can conveniently be used for estimating the global rate constant for the homogeneous decomposition of butane. When studying the product distributions, it is also important to have some idea of how much the residence time distribution is affecting the radial profiles for the product component concentrations. The radical mechanism which contains N molecular or radical species in an ideal plug flow tubular reactor has governing ordinary differential equations

$$\frac{dF}{dz} = A_r S_c r = f(F, Q, A_r, K') \qquad (5.1)$$

where: S_c is a N x N' stoichiometric coefficient matrix

F is a N x 1 vector of species flow

K' is a N' x 1 vector of rate constants

r is a N' x 1 vector of rate expressions

A_r is the cross-sectional area of the reactor

N' is the Number of free radical rate expressions in the model

Q is the volumetric flowrate through the reactor

Z is the axial distance

Boundary Conditions - @ Z = 0 F = F_0 (known)

Evidence that no radial product concentration profiles exist must be presented before the model given by equation (5.1) can be utilised for data from the isothermal laminar flow reactor. Theoretically, this is

difficult to justify. Much of the burden must be produced experimentally. Qualitatively the factors determining whether significant radial concentration profiles are present remain unchanged from those discussed for the disappearance of butane. In this instance, however, the components are being produced but the ratio of the radial dispersion properties counterbalancing the kinetic effect still remains the determining factor. Wakeham and Slater (1973) have shown that methane, ethane and propane all have higher binary diffusion coefficients than butane for diffusion through nitrogen in the range 300 - 700 K. In addition, it is unlikely that the stoichiometric coefficient, or selectivity, of any of the product species exceeds that for butane in the global stoichiometric representation of the pyrolysis;

$$a_1 C_4H_{10} \rightarrow a_2 CH_4 + a_3 C_2H_6 + a_4 C_2H_4 + \ldots$$

In effect this means that the butane is disappearing more quickly than the rate at which any of the products is being formed. If, for sake of simplicity, radial diffusivity is equated to the molecular diffusivity, the smoothing properties for the product species would appear at least as great as for butane.

In addition, extensive testing by Beshty (1978) under similar conditions to that in this study, showed radial product concentrations to be almost non-existent in the isothermal section of the reactor developed for propane pyrolysis. Similar measurement for butane reconfirmed his results. Figure 5.1 shows typical variation for the butane/methane ratio and butane/propylene ratios in the radial direction at a nominal wall temperature of 720^{o}C.

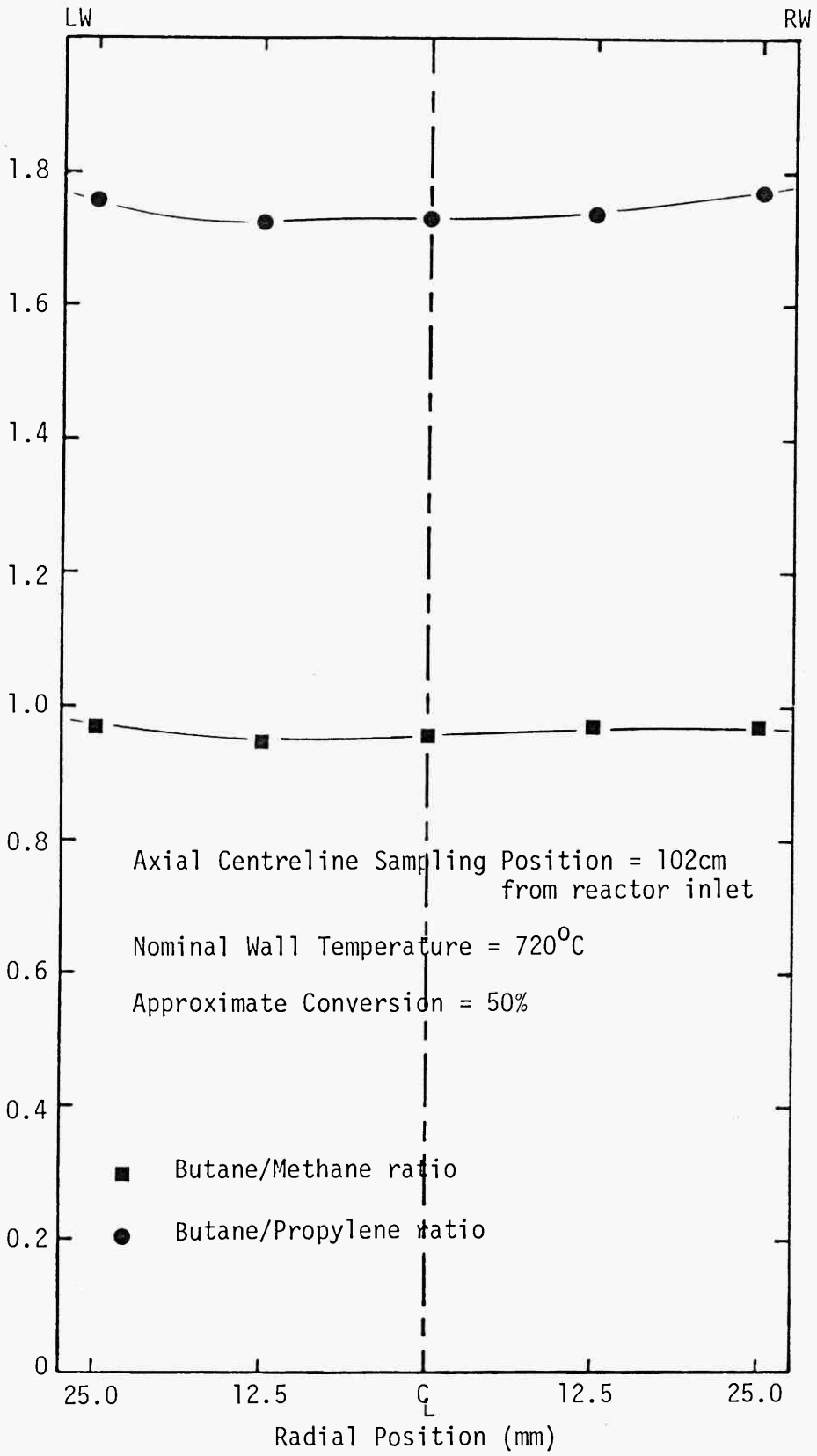

Fig. 5.1 Typical Radial Composition Ratio Profiles

5.2 The Rôle of the Radical Species

Reactions accounting for the butane pyrolysis comprise processes of initiation, radical decomposition, chain transfer, radical addition to non-radical species and radical radical termination. For the case of butane, radicals are initially generated by cleavage of the C-C bond of the butane molecules via two parallel initiation steps

$$C_4H_{10} \rightarrow 1 - C_3H_7^{\cdot} + CH_3^{\cdot}$$

$$C_4H_{10} \rightarrow C_2H_5^{\cdot} + C_2H_5^{\cdot}$$

Even in the most unfavourable case the C-C cleavage will be at least ten times faster than C-H breakage up to temperatures as high as 1500 K (Bradley, 1974). Generation of new, different radicals is then accomplished by continuous reaction between more butane molecules and the radical species produced from the initiation. As new species develop they too enter into all types of reaction and, in this manner, the diverging tree of reactions and species can continue indefinitely. This rapidly gives rise to an exponentially increasing number of possibilities. When the initial pyrolysing mixture consists of a number of hydrocarbons, radical initiation proceeds in a similar way. Unsaturated hydrocarbons particularly of low carbon number, such as ethylene, tend to be more stable and less likely to partake in the initiation procedure because of the strength of the carbon double bond. Nevertheless, they readily become involved in radical addition reactions because of the high reactivity of the radical species.

One of the problems with progressing in such a way is the need to terminate the reaction set at a point when the mechanism does not present a mathematical problem of seemingly insurmountable proportions. As a

result, many simplified mechanisms have been proposed which were developed principally to contain those radical reactions which most governed the overall rate of pyrolysis and the product distribution. A danger of this approach is the uncertainty of knowing for each circumstance when experiment and prediction fall into agreement, whether all the significant reactions have been included or whether it is merely a coincidence. The status of many radical reactions is becoming increasingly more apparent and the influence of many have been confirmed with little doubt. In spite of this, to date an overall mechanism for butane pyrolysis which encompasses secondary, as well as primary, reactions still remains lacking. This is important because secondary reactions are known to be present at conversions as low as 10% (Purnell and Quinn, 1962). The awareness of the major radical species which play a significant rôle in the butane pyrolysis is more well established from the vast amount of work which has been performed in the past.

Many of the important radicals which appear to dominate butane pyrolysis can be illustrated by analysing a typical simplified mechanism, that proposed by Powers and Corcoran (1974) which was used to model the explicit effects of the primary and secondary butyl radicals and of secondary reactions. The rate equations and the rate data which was used in their analysis are presented in Table 5.1. The mechanism indicates the radicals which most actively participate in controlling the product composition, apart from the hydrogen atom, $H^{\cdot}$, appear to be predominantly the following alkyl radicals: the methyl radical $CH_3^{\cdot}$, the propyl radical $1\text{-}C_3H_7^{\cdot}$, the ethyl radical, $C_2H_5^{\cdot}$ and the two isomeric butyl radicals, $1\text{-}C_4H_9^{\cdot}$ and $2\text{-}C_4H_9^{\cdot}$. Expression 23, in fact, couples together the two isomeric radicals $1\text{-}C_3H_7^{\cdot}$ and $2\text{-}C_3H_7^{\cdot}$ as both radicals can be formed through the same reaction path.

TABLE 5.1

Free Radical Mechanism Proposed by Powers and Corcoran (1974) for the Pyrolysis of Butane

Reaction Number	Elementary Reaction Step	Pre-exponential factor, A sec^{-1} or $litre.mole^{-1}\ sec^{-1}$	Activation Energy (kcal/mole)
1	$C_4H_{10} \rightarrow C_2H_5^{\cdot} + C_2H_5^{\cdot}$	5.0 E15	81.0
2	$C_4H_{10} \rightarrow CH_3^{\cdot} + C_3H_7^{\cdot}$	5.0 E15	85.0
3	$C_2H_5^{\cdot} + C_4H_{10} \rightarrow 2 - C_4H_9^{\cdot} + C_2H_6$	3.0 E10	20.1
4	$C_2H_5^{\cdot} + C_4H_{10} \rightarrow 1 - C_4H_9^{\cdot} + C_2H_6$	9.0 E10	22.8
5	$CH_3^{\cdot} + C_4H_{10} \rightarrow 2 - C_4H_9^{\cdot} + CH_4$	5.0 E10	18.2
6	$CH_3^{\cdot} + C_4H_{10} \rightarrow 1 - C_4H_9^{\cdot} + CH_4$	1.0 E11	20.9
7	$C_2H_5^{\cdot} \rightarrow C_2H_4 + H^{\cdot}$	1.7 E13	40.5
8	$H^{\cdot} + C_4H_{10} \rightarrow 2 - C_4H_9^{\cdot} + H_2$	1.0 E12	14.0
9	$H^{\cdot} + C_4H_{10} \rightarrow 1 - C_4H_9^{\cdot} + H_2$	1.3 E12	16.7
10	$C_3H_7^{\cdot} \rightarrow C_3H_6 + H^{\cdot}$	2.6 E14	37.8
11	$C_3H_7^{\cdot} \rightarrow C_2H_4 + CH_3^{\cdot}$	2.0 E13	28.0
12	$1 - C_4H_9^{\cdot} \rightarrow C_2H_4 + C_2H_5^{\cdot}$	2.0 E13	24.0
13	$1 - C_4H_9^{\cdot} \rightarrow 1 - C_4H_8 + H^{\cdot}$	2.6 E14	38.0
14	$2 - C_4H_9^{\cdot} \rightarrow C_3H_6 + CH_3^{\cdot}$	2.0 E13	26.0
15	$2 - C_4H_9^{\cdot} \rightarrow 2 - C_4H_8 + H^{\cdot}$	2.6 E14	37.5
16	$C_2H_5^{\cdot} + C_2H_5^{\cdot} \rightarrow C_4H_{10}$	1.6 E 9	0.
17	$C_2H_5^{\cdot} + C_2H_5^{\cdot} \rightarrow C_2H_6 + C_2H_4$	2.5 E 8	0.
18	$CH_3^{\cdot} + CH_3^{\cdot} \rightarrow C_2H_6$	2.0 E 9	0.
19	$H^{\cdot} + C_2H_4 \rightarrow C_2H_5^{\cdot}$	1.0 E10	0.5
20	$C_2H_5^{\cdot} + C_2H_4 \rightarrow 1 - C_4H_9^{\cdot}$	5.0 E 6	2.0
21	$CH_3^{\cdot} + C_2H_4 \rightarrow C_3H_7^{\cdot}$	1.0 E 7	2.0
22	$CH_3^{\cdot} + C_3H_6 \rightarrow 2 - C_4H_9^{\cdot}$	1.0 E 7	2.0
23	$H^{\cdot} + C_3H_6 \rightarrow C_3H_7^{\cdot}$	6.0 E 9	0.5
24	$CH_3^{\cdot} + C_2H_5^{\cdot} \rightarrow C_3H_8$	2.0 E 9	0.

The absence of two radical terminations merits a little discussion

$$H^{\cdot} + H^{\cdot} \rightarrow H_2$$

$$CH_3^{\cdot} + H^{\cdot} \rightarrow CH_4$$

One might expect both these reactions to be necessary additions to any mechanism since both hydrogen and methane are extremely stable products. However, one of the factors which limits the type of radicals undergoing recombination is the so-called third body restriction (Steacie, 1954). By conservation of momentum the molecule which is formed instantaneously after its formation still possesses the necessary energy for dissociation. Normally this is redistributed among the internal degrees of freedom of the molecule which subsequently achieves stability. However, in the case of the $H^{\cdot}$ and $CH_3^{\cdot}$ radicals there are not enough degrees of freedom available and only the unlikely simultaneous termolecular collision with another molecule which can carry away some of the translational energy, will lead to hydrogen and methane being formed in this way.

At higher temperatures the presence of larger alkyl radicals would be limited because of their tendency to decompose to smaller radicals which are thermally more stable though chemically more reactive. For instance, consider the typical radical reaction

$$2 - C_5H_{11}^{\cdot} \underset{K_2}{\overset{K_1}{\rightleftharpoons}} C_2H_5^{\cdot} + C_3H_6$$

Using rate data from the reference data set compiled by Allara and Shaw (1980), even at temperatures as low as 800 K, the ratio of the two rate constants K_1/K_2 is 160, and at 1000 K is as high as 2400. Clearly, although many radicals larger than $C_4H_9^{\cdot}$ will be present in the pyrolysing mixture, their concentrations will be noticeably lower than the smaller radicals, e.g. $CH_3^{\cdot}$ or $C_2H_5^{\cdot}$.

Edelson and Allara (1980) have shown that the reactions which appear to have the greatest influence on the butane pyrolysis are a combination of initiation, abstraction, decomposition and recombination. Certainly no single type of radical reaction appears to dominate. Apart from initiation reactions 1 and 2 (see Table 5.1) the most sensitive reactions to the available rate data are those which contain $CH_3^{\cdot}$ and $C_2H_5^{\cdot}$ radicals. These include the abstraction reactions 3 and 6, the decomposition reaction 7 and the recombination reaction 24. Reactions 8, 9 and 11 involving $H^{\cdot}$ and $1\text{-}C_3H_7^{\cdot}$ radicals also gave a pronounced influence on the product distribution.

The importance of the butyl radicals was suggested by Powers and Corcoran and the major pathway for their generation is through participation of the butane molecules in abstraction reaction such as 3, 5 and 8. Leathard and Purnell (1970) have indicated that the $2\text{-}C_4H_9^{\cdot}$ decomposes via reaction 14 yielding propylene and $CH_3^{\cdot}$ radicals and that the $1\text{-}C_4H_9^{\cdot}$ decomposes to ethylene and $C_2H_5^{\cdot}$ radicals via reaction 12. Accordingly, Sundaram et al. (1978a) conclude one of the major reactions in butane pyrolysis is the isomerisation reaction

$$1 - C_4H_9^{\cdot} \rightarrow 2 - C_4H_9^{\cdot}$$

The influence of allylic reactions particularly in termination reactions has also been observed. In several notably important studies including that by Powers and Corcoran, allylic radicals have not been considered in the butane termination reaction set (Purnell and Quinn, 1962; Sagert and Laidler, 1963; Large et al., 1972). The major allylic radicals present are $C_3H_5^{\cdot}$ and $C_4H_7^{\cdot}$ and are generated mainly by alkyl radical attack on the higher olefins in an abstraction reaction

$$1 - C_4H_8 + C_2H_5^{\cdot} \rightarrow \underset{\substack{\text{methylallyl} \\ \text{radical}}}{C_4H_7^{\cdot}} + C_2H_6$$

This type of reaction correlates well with the observed inhibitory effect created by propylene caused by disappearance of alkyl radicals to accommodate generation of allyl radicals

$$C_3H_6 + C_2H_5^{\cdot} \rightarrow C_3H_5^{\cdot} + C_2H_6$$

$$C_3H_6 + CH_3^{\cdot} \rightarrow C_3H_5^{\cdot} + CH_4$$

$$C_3H_6 + H^{\cdot} \rightarrow C_3H_5^{\cdot} + H_2$$

Termination of the allylic radicals with alkyl radicals results in formation of olefins other than ethylene and propylene. In fact, this is one of the important pathways to formation of the butenes, e.g.

$$CH_3^{\cdot} + C_3H_5^{\cdot} \rightarrow 1 - C_4H_8$$

Not surprisingly, termination reactions are known to be extremely fast, since both reactants are radicals. However, the extremely low radical concentrations make the overall rate of production of the products very small compared to the rates of production caused by abstraction and decomposition. Apart from alkyl/allylic termination there are no other major pathways to butene formation and this explains why the butenes are only minor products in butane pyrolysis. The mechanism by Powers and Corcoran suggests that butenes can form by decomposition of the butyl radical species. The high activation energies associated with these reactions, however, indicate that they only become significant at high temperatures.

In the later stages of the reaction at higher conversions >80%, the C_5^+ yield constituting heavy molecular components with a carbon number of five or over, becomes of noticeable proportion. Froment et al. (1977) estimated a 7% wt/wt contribution for the heavy component yields at a

conversion of 90%. This is a direct result of the stability of the high hydrogen / carbon ratio molecules such as hydrogen and methane which increase the carbon/hydrogen ratio of the residual reacting mixture. This leads to formation of molecules with large carbon/hydrogen ratios such as aromatics and cyclic olefins. The process at this stage of the pyrolysis, however, is not well understood, and no attempt will be made to elucidate further on the possible kinetics.

5.3 Mathematical Solution to the Radical Mechanism

Three common approaches are used to model the pyrolysis of hydrocarbons in a tubular plug flow reactor:

(i) Direct integration of the model given by equation (5.1).

(ii) Using the steady-state approximation (SSA) to solve the model given by equation (5.1).

(iii) The pseudo-molecular reaction scheme where the direct presence of the radicals is eliminated.

All the methods are discussed in further detail in the literature survey, Chapter 2. The pseudo-molecular reaction scheme was devised principally to overcome the mathematical difficulties associated with (i) and (ii). The ever-increasing availability of more powerful computers are, however, eliminating the original barriers which evoked this approach and hence it was not considered during the data modelling. For an ideal plug flow reactor, integration of the differential equations directly as proposed in (i) is the correct procedure. In the past, however, the SSA has been used because of its mathematical simplicity compared to direct integration. Surprisingly, there is little in literature on attempts to quantify the errors introduced by imposing such an assumption on the radical mechanistics. In some cases (e.g. Illés and Szalai, 1979) the SSA has been

used without any discussion on its validity whatsoever.

Assigning numerical values to all the rate constants and providing an initial flow vector defines equation (5.1) as an initial value problem in non-linear ordinary differential equations. Almost invariably, analytic solutions are not available for these problems but numerical solutions have been extensively studied. Instabilities, however, arise in the usual numerical treatment of these problems because of the stability regions for the classical methods of integration. Instability can be described as a growth of error which is a result of the step size being so large that the numerical formulae no longer give reasonable approximations to the true solution. Stability for a typical numerical formula is characterised by a domain in the complex plane of the product $h'\lambda$ where h' is the step-size of integration and λ are the eigenvalues of the Jacobian given by

$$J = \frac{\partial f_i}{\partial F_j} \qquad i, j = 1, 2 \ldots N \tag{5.2}$$

As a result of the quickly decaying terms associated with the radical species, some of the eigenvalues of J are very large and this limits the value of h' which can be used to ensure the product $h'\lambda$ remains within the stable region. Classical integration formulae such as Runge-Kutta have stability domains which are so restrictive that excessively small values of h' must be taken to maintain a stable solution. Normally, the stability domains of the classical methods are no problem when the problem is more well-posed with a smaller range in value of the eigenvalues. In these situations the step length is limited by the local accuracy of the approximation, rather than the maintenance of stability. A system of differential equations which have large eigenvalues associated with its Jacobian such as this system is termed "stiff" principally because of the apparent reluctance to move forward in the integration.

The most common approach of overcoming this stability restriction is the linear multistep "Backward Differentiation Formulae" (BDF) proposed by Curtiss and Hirschfelder (1952), developed and implemented by Gear (1971) and which have the form

$$\sum_{i=0}^{p'} \alpha_i F^j_{n-i} = h' \beta_o f_j(F_n) \qquad j = 1, 2 \ldots N \qquad (5.3)$$

where: α_i, β_o are known constants

F^j_{n-i} are point solutions for component j at step intervals n, n-1 ... n-p'

p' is the order of the BDF

h' is the step length

Since the solution being sought is F^j_n (j = 1, 2 ... N) equation (5.3) is implicit and is solved iteratively, normally by Newton's method. The advantage of this approach is the large domain of stability. The BDF of orders up to 4 have a stable domain which encircles almost the whole of the left-hand complex plane. Thus the step size, h', can be increased whilst still ensuring the stability of terms involving the large eigenvalues. Now step size and accuracy are not limited by the fast decaying terms but by the slow decaying terms.

The implementation by Gear is a BDF variable step, variable order code. After k + 1 steps at order k a change in step and/or order is always considered. The criterion which determines the order is that one which gives the largest step within the required accuracy, although this is weighted in favour of the lower order formulae because they demand less computer time. At the starting point to the solution the order is 1, given by the Backward Euler Formulae since there is no available information for use of higher orders.

The alternative use of the SSA is mathematically more straightforward and requires less programming and computing time. This approximation is based on the occurrence of steady or near-steady states in which the rate of change of the radical species is given as a small difference between two fast processes, creating and destroying the species through chemical reaction. Then it is assumed the differential terms are zero and the differential equations for the radical species are replaced by algebraic expressions. Since the fast decaying eigenvalues of the original Jacobian were associated with the radical species, the stiffness is removed from the integration of the remaining differential equations for the molecular species and simultaneous solution of the algebraic equations for the radical species.

Normally these algebraic equations are non-linear and must be solved iteratively. In the past, the non-linear set has been solved using Newton's method. This makes use of the local linear approximation to the non-linear equations by expanding the function vector using a Taylor's series

$$p_k = -J^{-1}(x_k)g(x_k)$$
$$x_{k+1} = x_k + p_k \qquad (5.4)$$

where: x represents the independent variable vector (N_r x 1)

g represents the function vector (N_r x 1)

N_r is the number of radical species

The sequence x_0, x_1, x_2 ... x_k, x_{k+1} converges to a solution $\hat{x}$, providing the initial starting point x_0 is sufficiently close to the solution. Difficulty has been encountered for its use for estimating the concentrations of the radical species in the algebraic equations created by the SSA (Snow, 1966). A modified Newton's method is that proposed by

Broyden (1965) and is one of a family referred to as quasi-Newton methods. Broyden's approach replaces the Jacobian by an approximation which is required to satisfy the Secant rule

$$q_i = B_{i+1}\, p_i \tag{5.5}$$

where: q_i is the change in function value between the $i+1^{th}$ and i^{th} iteration.

The matrix B_{i+1} is the approximated updated Jacobian, defined so that the change in g predicted by B_{i+1} in the direction t_i orthogonal to p_i is the same as would be predicted by B_i, thus

$$B_{i+1}\, t_i = B_i t_i \quad , \quad t_i^T p_i = 0 \tag{5.6}$$

Combined with equation (5.5) this uniquely defines the updated approximation

$$B_{i+1} = B_i + \frac{(q_i - B_i p_i) p_i^T}{p_i^T p_i} \tag{5.7}$$

Normally this is stored as the inverse because the update equation is of the form

$$p_i = - B_i^{-1} g_i \tag{5.8}$$

This approach has the advantage that although B_i changes from step to step, not as many evaluations are necessary as with Newton's approach, where the Jacobian must be updated every step.

5.4 Modelling the Isothermal Data

Irrespective of the method to solve the integration, there are basically two approaches of employing the model described by equation (5.1) for data collected from this specific reactor:

(i) To integrate from the start of the reactor, whilst imposing a temperature profile on the integration up to the point when the isothermal

region is assumed to commence. The experimental data could then be compared with the component trajectories obtained by integrating within the isothermal region at the defined isothermal temperature. Initial conditions, F_0, would then be given by the feed to the reactor. It became apparent that this approach could be fraught with serious error and deviation from assumed experimental conditions. Notably, in the preheat region of the reactor, the assumption of plug flow is violated on one important count. This is the region where the radial conditions, most importantly the temperature profile, are being established and in the early stages of preheat will certainly not approximate plug flow. Moreover, the imposition of the temperature profile introduces further error since the profile has inherent with its measurement, a certain degree of uncertainty.

(ii) Alternatively, integration could proceed from the start of the isothermal region using the experimentally obtained data at the start of the region as the initial conditions for the model. In this way, whatever is happening upstream of the isothermal region is being totally ignored during the modelling. Thus the combination of the varying radial velocity profile and the residence time in the preheat region have produced a product distribution given by the measured composition at the start of the isothermal region. This, of course, is entirely feasible since the rate expressions characterising the pyrolysis radical mechanism comprise a whole spectrum of different activation energies. An error is introduced with the initial conditions when the radical concentrations at the start of the isothermal zone could not be measured and would tacitly be assumed zero, or even the steady-state concentrations, calculated by substituting the molecular species into the algebraic equations developed from the proposed radical mechanism.

Data from the reactor system could then be compared with the model predictions through the isothermal length of the reactor.

5.5 Analysis of the Integration Techniques

The preliminary investigation described above suggested that use of approach (ii) might prove more accurate for modelling the data. To substantiate this proposal, the free radical model proposed by Powers and Corcoran was employed to assess the effects of a poorly-determined non-isothermal preheat zone and to assess the sensitivity of the integration solution to unknown initial radical concentrations.

The resulting differential equations from the assumed model were integrated directly using Gear's Algorithm and secondly, assuming the validity of the SSA. Integration using the SSA was achieved by the Kutta-Merson variable step size method whilst the non-linear equations for the radical concentrations were solved by scaling the equations and using Broyden's method at every integration point to solve the scaled equations. The results of the simulations using this simple model helped determine the approach by which any larger, more sophisticated radical scheme might be utilised when modelling the isothermal data.

5.6 Discussion of Simulation Results

The results in Table 5.2 show for this simple model that under isothermal conditions, integration by using the SSA generates a solution very similar to that as obtained using the Gear's Algorithm. Indeed, in most cases, the percentage deviations were well below 0.5% for both molecular and radical species. These findings are in direct contrast to suppositions made by Sundaram and Froment (1978a). In a later communication which compared the advantages and disadvantages of using SSA (1978b) it appears that they used a non-standard formula for the SSA and did not

TABLE 5.2

Major Component Yields (moles/100 moles butane feed) From Isothermal Integration Using Gear's Method and the SSA for the Free Radical Model Given in Table 5.1

	900 K, $\phi \sim 4.8\%$		1000 K, $\phi \sim 54.0\%$		1100 K, $\phi \sim 84.0\%$	
	Gear's Method	SSA	Gear's Method	SSA	Gear's Method	SSA
C_2H_4	1.83	1.84	29.96	29.97	61.62	61.62
C_3H_6	3.13	3.15	29.98	29.99	38.08	38.08
H_2	0.273	0.274	5.33	5.34	15.03	15.03
CH_4	3.19	3.21	37.14	37.16	68.21	68.21

consider application of the SSA as used in these simulations.

Since the analytical equations for the radical species did not contain many non-linear terms, the solution was determined without undue difficulty. In a larger model, the non-linearity of the radical equations increases somewhat and obtaining a solution could prove more difficult, although theoretically, the problem still remains straightforward.

The remaining simulations were performed under conditions which closely approximated those obtained during the collection of the experimental data, to represent the situation where low and high conversions were achieved respectively. Gear's method was used to integrate equation (5.1) from the start of the reactor, under isothermal conditions and then with an imposed non-isothermal profile up to the isothermal region. Comparison of the product distribution from the two solutions amply demonstrated the sensitivity of the integrated solution to an imposed non-isothermal temperature profile. This indicates that method (i) introduces extraneous errors into the solution which could distort the accuracy of the proposed kinetic model. Figures 5.2 and 5.3, Tables 5.3 and 5.4, show the significant discrepancies between major products for both the low conversion and high conversion simulations, (see Appendix IX).

An interesting observation appeared to be the constant off-set between product yields once the isothermal region had been reached. In addition, integration with the same temperature profile as that imposed on the high conversion simulation using the SSA once again produced no significant change in the product distribution predicted using Gear's method.

Simulation was also carried out to test the sensitivity of integration using Gear's method to the initial conditions for the radical species at the start of the isothermal region. This is important since, in

TABLE 5.3 AND TABLE 5.4

Major Component Yields (moles/100 moles butane feed) at ϕ_s = Simulated Conversion of the Entrance of the Isothermal Region (Temperature, T_g) for the Integration of the Free Radical Model Given in Table 5.1

Table 5.3 - Low Conversion Simulation: $\phi_s = 25.2$; $T_g = 939.3$ K

	Gear's method with an imposed linear temperature profile*	Gear's method under isothermal conditions, T_g	% Difference
C_2H_4	14.51	15.41	5.8
C_3H_6	14.94	14.76	-1.2
H_2	3.25	4.25	23.5
CH_4	18.77	18.41	-2.0
C_2H_6	3.17	2.53	-25.3

Table 5.4 - High Conversion Simulation: $\phi_s = 45.0$; $T_g = 970.0$ K

	Gear's method with an imposed linear temperature profile**	Gear's method under isothermal conditions, T_g	SSA with an imposed linear temperature profile**
C_2H_4	28.39	30.72	28.44
C_3H_6	24.62	24.05	24.60
H_2	5.10	7.60	5.11
CH_4	34.48	33.46	34.48
C_2H_6	5.33	3.82	5.32

* $T = 875.0 + 2.55\phi \qquad \phi \leq \phi_s$

$T = T_g = 939.3 \text{ K} \qquad \phi > \phi_s$

** $T = 975.0 + 2.111\phi \qquad \phi \leq \phi_s$

$T = T_g = 970.0 \qquad \phi > \phi_s$

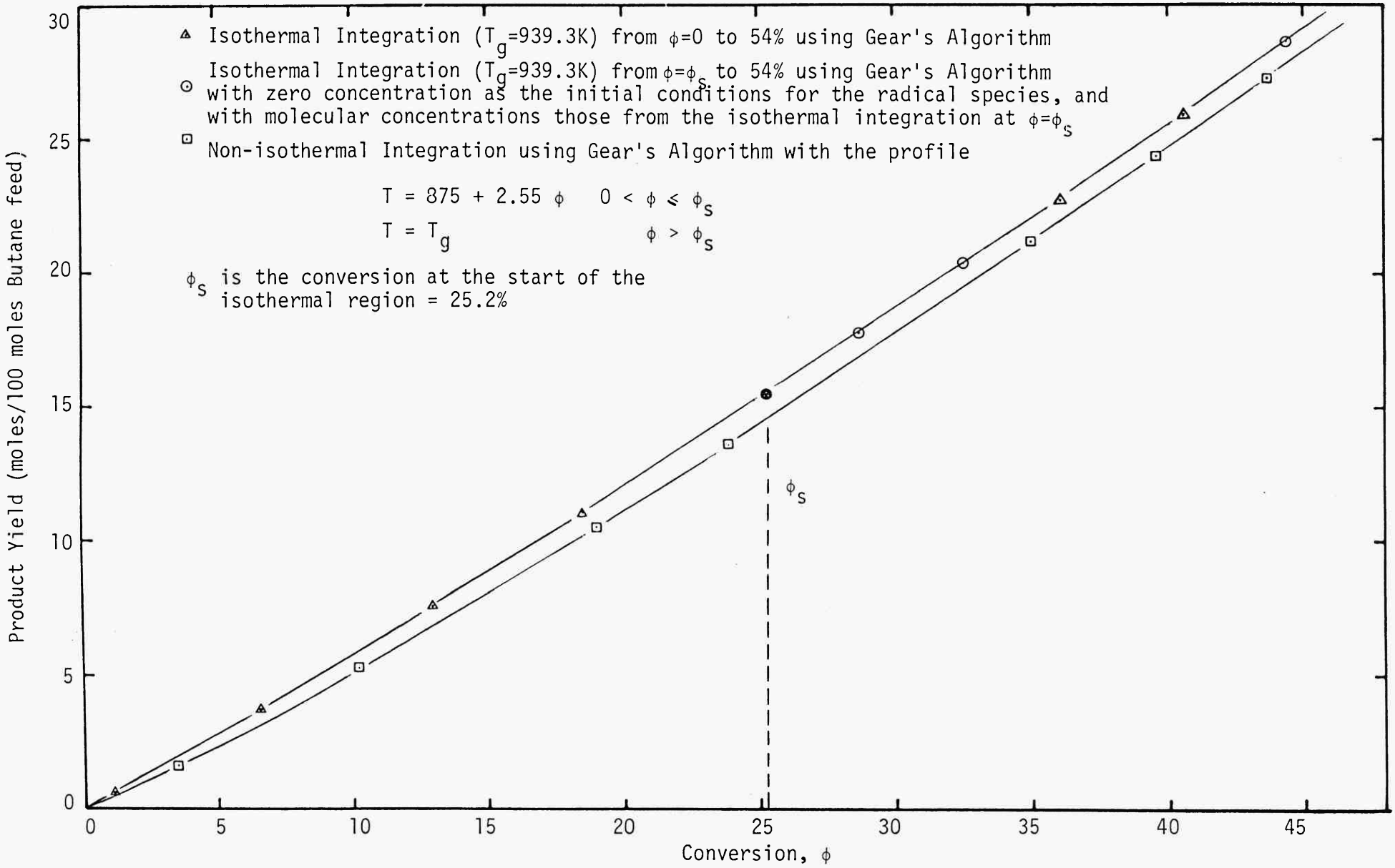

Fig. 5.2 Typical molecular yield (Ethylene) for the Low Conversion Simulations

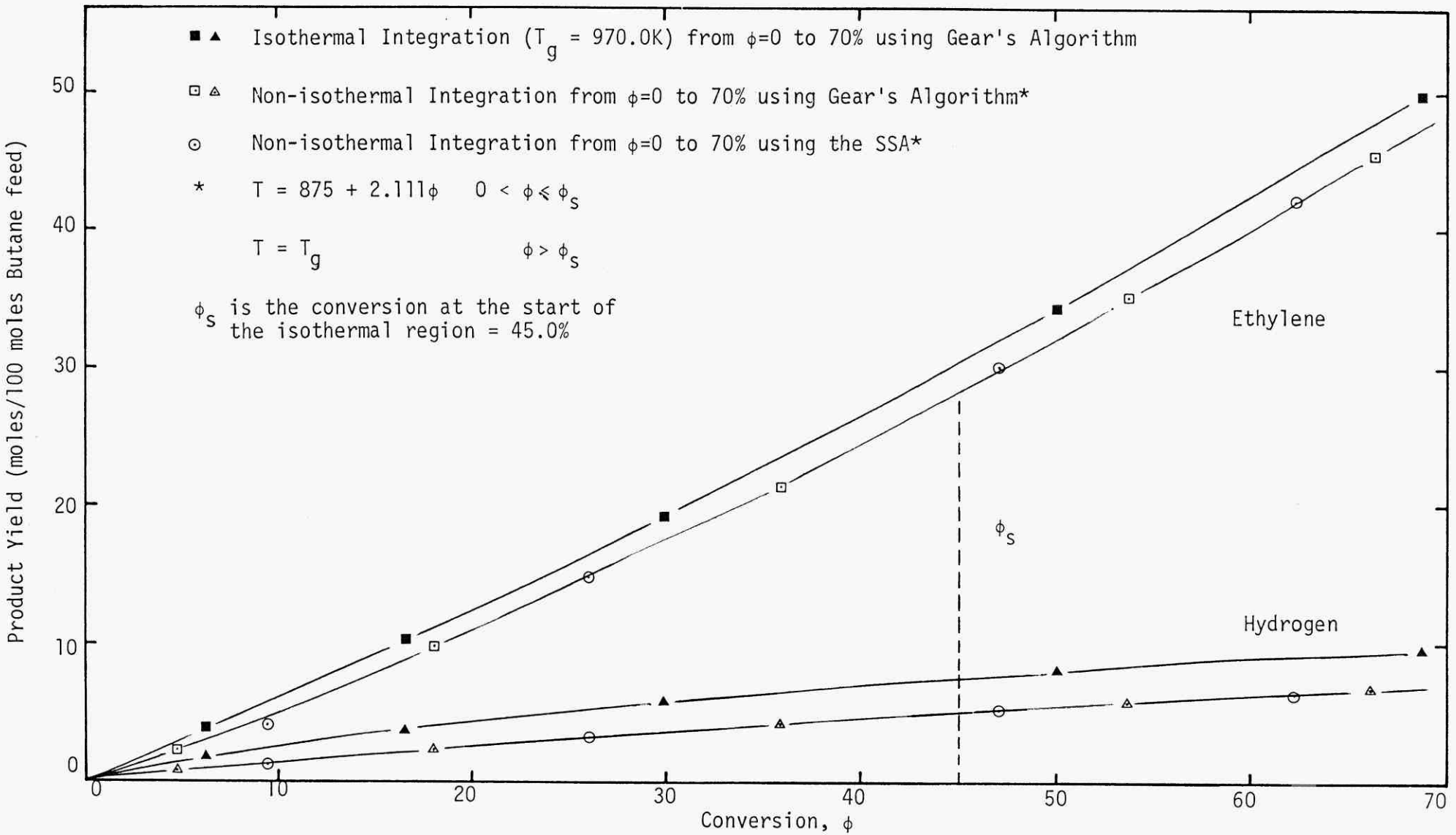

Fig. 5.3 Typical molecular yields (Ethylene and Hydrogen) for the High Conversion Simulations

reality, the radical concentrations are unknown at this point and would be assumed zero if integration was to commence there. Simulated molecular compositions were extracted from isothermal integration using Gear's method and used as pseudo-experimentally obtained data. The resulting integration using Gear's method at the same isothermal temperature showed that the radical concentrations were very quickly reestablished with no noticeable alteration to all the species, radical and molecular, throughout the whole of the isothermal region, e.g. see Fig. 5.2. In this respect, using the steady-state radical concentrations for initial conditions as generated from applying the SSA on the proposed mechanism would prove unnecessary. No simulations were carried out using this simplification because of the rapidity with which the radical concentrations were re-established.

5.7 Conclusions

Several conclusions can be drawn from the simulations. Of the two methods suggested to model the pyrolysis free radical mechanism, the idea of integrating from the start of the isothermal region with initial conditions of zero concentration for the radical species plus experimental values for the molecular species appears to stand out as the more accurate. In this instance, the accuracy of the radical scheme would be reflected in the predicted trajectories compared to the experimental trajectories of primarily the major components produced by the pyrolysis. The advantage of using this approach is that it removes one of the extraneous factors, the temperature profile, which could distort the accuracy of the radical scheme. In non-isothermal experiments, the imposed temperature profile must be measured experimentally - with a notable degree of error. The simulations have indicated a possible high sensitivity of the integrated yields to errors of this kind. In

a recent review by Froment on industrial crackers (1981), the need for accurate instrumentation particularly for temperature is underlined if accurate modelling is to be achieved.

The comparisons made between use of the SSA as a substitute for the mathematical complexities of integrating directly the model equations have shown favourable results for its use in terms of its accuracy. Certainly for the 24-equation model used in the simulations the two methods gave very comparable results, even when a mild temperature gradient was introduced into the integration. In addition, the programming and computing time would be reduced considerably. However, with the advent of modern computers this is becoming less and less of a problem. Under more severe conditions, for instance a larger radical scheme or a larger temperature profile, the SSA may, however, break down. For instance, Bowen et al. (1963) have shown that over large time intervals the SSA may become unstable, even though stable during the incipient integration.

5.8 Evaluation for a Proposed Radical Mechanism

Discrepancies between a proposed model and accurately measured experimental data may be apparent because of four significant factors:

(i) The fundamental rate data is inaccurate.

(ii) The proposed kinetic model may be wrong.

(iii) There is significant lack of evidence in justifying a mathematical simplification, for instance, the SSA.

(iv) There is lack of justification for using a simple mathematical model for experimental data which has been collected under conditions which warrant use of a more complicated mathematical approach.

Fundamental to any mechanism suggested for the kinetics of the butane pyrolysis is the belief that the best experimental and theoretical values available in literature for rate data concerning the fundamental reactions should be used. In the past, some authors (e.g. Sundaram and Froment, 1978a) have adjusted the rate data to ensure a reasonable fit between experimental and predicted product distributions. This has only led to increase the confusion prevalent in reported literature as to which rate data are the most correct for the individual rate expressions.

Even if measurements of all species including the radicals were available, many multiple sets of rate data could still be generated to conveniently fit reported experimental data to predicted results. It is vital to realise that this procedure presents itself as no more than a mathematical curve-fitting exercise with no real fundamental purpose at all. There is, however, no doubt that much of the available rate data is poorly known. Allara and Shaw (1980) purport errors for initiation rate constants to be as high as a factor of 10 and for radical decomposition, rate constant uncertainty is up to within about a factor of 30. Nevertheless, fitting experimental data merely confuses and delays more fundamental attempts to establish exactly what is occurring during pyrolysis. While acknowledging that the erroneous rate data plays a rôle in simulation discrepancies, more emphasis should be placed on ensuring consistent experimental technique and on changing or altering the proposed kinetic model. Indeed, this has been the approach by Edelson and Allara (1980) who have developed a model using rate data determined by theoretical and experimental techniques specifically designed for the study of the individual radical processes. In addition, the kinetic model they developed was generated by considering all pos-

sible reactions to occur and then eliminating those reactions which did not influence the product distribution.

The radical scheme which they developed for butane was used to model some of the data obtained in this study. Originally, the complete model comprised some 500 reactions which further reduced to 98 involving some 37 chemical species by consideration of the relative flux contributions from each reaction. Arrhenius parameters extracted from the recent collective data reference for free radical reactions by Allara and Shaw (1980) were used. The model and appropriate rate data are given in Table 5.5.

The proposed model was integrated using Gear's Algorithm rather than the SSA. Although the simulations have suggested the SSA might be as accurate, the correct procedure is by integrating equation (5.1) as it stands. Moreover, as a result of the simulations, integration was commenced from the start of the experimentally determined isothermal region where the molecular species' concentrations were those compositions measured experimentally and the radical species had initial concentrations assumed zero. This approach was used in favour of integrating from the reactor entrance, principally because of the possibilities of bias in the model predictions due to a poorly superimposed temperature profile.

TABLE 5.5

Free Radical Mechanism Proposed by Edelson and Allara (1980) for the Pyrolysis of Butane

Reaction Number	Elementary Reaction Step	$K = Ae^{-E/RT}$ sec^{-1} or $litre.mole^{-1}$ sec^{-1} $\log_{10}A$	E (kcal/mole)
	Initiation		
1	$C_3H_8 \rightarrow CH_3^{\cdot} + C_2H_5^{\cdot}$	16.9	85.1
2	$1 - C_4H_8 \rightarrow CH_3^{\cdot} + C_3H_5^{\cdot}$	16.1	73.4
3	$1 - C_5H_{10} \rightarrow C_2H_5^{\cdot} + C_3H_5^{\cdot}$	16.0	71.4
4	$1 - C_6H_{12} \rightarrow 1 - C_3H_7^{\cdot} + C_3H_5^{\cdot}$	16.4	71.1
5	$(C_3H_5)_2 \rightarrow C_3H_5^{\cdot} + C_3H_5^{\cdot}$	14.4	59.4
6	1,5 heptadiene $\rightarrow C_3H_5^{\cdot} + C_4H_7^{\cdot}$	15.7	58.7
7	$C_4H_{10} \rightarrow CH_3^{\cdot} + 1 - C_3H_7^{\cdot}$	17.5	85.7
8	$C_4H_{10} \rightarrow C_2H_5^{\cdot} + C_2H_5^{\cdot}$	16.4	82.1
	Hydrogen Transfer		
9	$H_2 + CH_3^{\cdot} \rightarrow H^{\cdot} + CH_4$	9.2	11.3
10	$H_2 + C_3H_5^{\cdot} \rightarrow H^{\cdot} + C_3H_6$	10.5	19.7
11	$C_3H_8 + H^{\cdot} \rightarrow 1 - C_3H_7^{\cdot} + H_2$	11.1	9.7
12	$C_3H_8 + CH_3^{\cdot} \rightarrow 1 - C_3H_7^{\cdot} + CH_4$	9.0	11.5
13	$C_3H_8 + C_2H_5^{\cdot} \rightarrow 1 - C_3H_7^{\cdot} + C_2H_6$	8.5	12.3
14	$C_3H_8 + 2 - C_3H_7^{\cdot} \rightarrow 1 - C_3H_7^{\cdot} + C_3H_8$	8.0	12.9
15	$C_3H_8 + 1 - C_3H_7^{\cdot} \rightarrow 2 - C_3H_7^{\cdot} + C_3H_8$	7.7	10.4
16	$C_3H_8 + C_3H_5^{\cdot} \rightarrow 1 - C_3H_7^{\cdot} + C_3H_6$	8.9	20.5
17	$C_3H_6 + H^{\cdot} \rightarrow C_3H_5^{\cdot} + H_2$	11.0	3.5
18	$C_3H_8 + H^{\cdot} \rightarrow 2 - C_3H_7^{\cdot} + H_2$	10.8	7.7
19	$C_3H_8 + CH_3^{\cdot} \rightarrow 2 - C_3H_7^{\cdot} + CH_4$	8.8	10.5
20	$C_3H_8 + C_2H_5^{\cdot} \rightarrow 2 - C_3H_7^{\cdot} + C_2H_6$	7.7	10.4
21	$C_3H_8 + C_3H_5^{\cdot} \rightarrow 2 - C_3H_7^{\cdot} + C_3H_6$	8.3	16.1
22	$H_2 + C_2H_5^{\cdot} \rightarrow H^{\cdot} + C_2H_6$	9.6	14.0

TABLE 5.5 (contd.)

Reaction Number	Elementary Reaction Step	$K = Ae^{-E/RT}$ sec^{-1} or $litre.mole^{-1}$ sec^{-1} $\log_{10}A$	E (kcal/mole)
23	$C_2H_6 + CH_3^{\cdot} \rightarrow C_2H_5^{\cdot} + CH_4$	8.8	11.6
24	$C_4H_{10} + H^{\cdot} \rightarrow 1 - C_4H_9^{\cdot} + H_2$	11.1	9.7
25	$C_4H_{10} + CH_3^{\cdot} \rightarrow 1 - C_4H_9^{\cdot} + CH_4$	8.6	11.4
26	$C_4H_{10} + C_2H_5^{\cdot} \rightarrow 1 - C_4H_9^{\cdot} + C_2H_6$	8.5	12.3
27	$C_4H_{10} + C_3H_5^{\cdot} \rightarrow 1 - C_4H_9^{\cdot} + C_3H_6$	8.9	20.5
28	$C_3H_6 + CH_3^{\cdot} \rightarrow C_3H_5^{\cdot} + CH_4$	8.2	8.8
29	$C_3H_6 + C_2H_5^{\cdot} \rightarrow C_3H_5^{\cdot} + C_2H_6$	8.0	9.8
30	$C_4H_{10} + H^{\cdot} \rightarrow 2 - C_4H_9^{\cdot} + H_2$	11.1	7.7
31	$C_4H_{10} + CH_3^{\cdot} \rightarrow 2 - C_4H_9^{\cdot} + CH_4$	8.6	9.6
32	$C_4H_{10} + C_2H_5^{\cdot} \rightarrow 2 - C_4H_9^{\cdot} + C_2H_6$	8.0	10.4
33	$C_4H_{10} + C_3H_5^{\cdot} \rightarrow 2 - C_4H_9^{\cdot} + C_3H_6$	8.5	16.4
	Decomposition		
34	$C_2H_5^{\cdot} \rightarrow H^{\cdot} + C_2H_4$	13.6	40.5
35	$1 - C_3H_7^{\cdot} \rightarrow CH_3^{\cdot} + C_2H_4$	13.1	32.5
36	$1 - C_3H_7^{\cdot} \rightarrow H^{\cdot} + C_3H_6$	13.2	38.6
37	$2 - C_3H_7^{\cdot} \rightarrow H^{\cdot} + C_3H_6$	13.9	40.4
38	$2 - C_4H_9^{\cdot} \rightarrow CH_3^{\cdot} + C_3H_6$	14.3	33.2
39	2 - methyl - 1 - propyl$^{\cdot} \rightarrow CH_3^{\cdot} + C_3H_6$	14.0	32.8
40	3 - methyl - 1 - butyl$^{\cdot} \rightarrow 2 - C_3H_7^{\cdot} + C_2H_4$	12.6	26.2
41	4 - methyl - 2 - pentyl$^{\cdot} \rightarrow 2 - C_3H_7^{\cdot} + C_3H_6$	13.4	28.2
42	$1 - C_4H_9^{\cdot} \rightarrow C_2H_5^{\cdot} + C_2H_4$	13.4	28.8
43	$1 - C_5H_{11}^{\cdot} \rightarrow 1 - C_3H_7^{\cdot} + C_2H_4$	13.5	28.4
44	$2 - C_5H_{11}^{\cdot} \rightarrow C_2H_5^{\cdot} + C_3H_6$	12.7	29.1
45	2 - methyl - 1 - butyl$^{\cdot} \rightarrow C_2H_5^{\cdot} + C_3H_6$	13.1	29.5

TABLE 5.5 (contd.)

Reaction Number	Elementary Reaction Step	$K = Ae^{-E/RT}$ sec^{-1} or litre.mole^{-1} sec^{-1} $\log_{10}A$	E (kcal/mole)
	Addition		
46	$H^{\cdot} + C_2H_4 \rightarrow C_2H_5^{\cdot}$	10.6	2.6
47	$H^{\cdot} + C_3H_6 \rightarrow 2 - C_3H_7^{\cdot}$	9.9	1.2
48	$H^{\cdot} + C_3H_6 \rightarrow 1 - C_3H_7^{\cdot}$	9.9	2.9
49	$CH_3^{\cdot} + C_2H_4 \rightarrow 1 - C_3H_7^{\cdot}$	8.1	7.7
50	$CH_3^{\cdot} + C_3H_6 \rightarrow 2 - C_4H_9^{\cdot}$	8.5	7.4
51	$CH_3^{\cdot} + C_3H_6 \rightarrow$ 2 - methyl - 1 - propyl$^{\cdot}$	8.5	9.1
52	$C_2H_5^{\cdot} + C_2H_4 \rightarrow 1 - C_4H_9^{\cdot}$	7.8	7.6
53	$C_2H_5^{\cdot} + C_3H_6 \rightarrow 2 - C_5H_{11}^{\cdot}$	7.6	7.5
54	$1 - C_3H_7^{\cdot} + C_3H_6 \rightarrow 2 - C_6H_{13}^{\cdot}$	7.8	7.0
55	$2 - C_3H_7^{\cdot} + C_2H_4 \rightarrow$ 3 - methyl - 1 - butyl$^{\cdot}$	7.6	6.9
56	$2 - C_3H_7^{\cdot} + C_3H_6 \rightarrow$ 4 - methyl - 2 - pentyl$^{\cdot}$	7.6	6.9
57	$C_2H_5^{\cdot} + C_3H_6 \rightarrow$ 2 - methyl - 1 - butyl$^{\cdot}$	7.6	9.2
	Isomerization		
58	$1 - C_5H_{11}^{\cdot} \rightarrow 2 - C_5H_{11}^{\cdot}$	11.0	20.0
59	$2 - C_5H_{11}^{\cdot} \rightarrow 1 - C_5H_{11}^{\cdot}$	11.1	23.4
60	$1 - C_6H_{13}^{\cdot} \rightarrow 2 - C_6H_{13}^{\cdot}$	9.2	11.1
61	$2 - C_6H_{13}^{\cdot} \rightarrow 1 - C_6H_{13}^{\cdot}$	9.3	14.5
	Termination - Recombination		
62	$H^{\cdot} + 2 - C_3H_7^{\cdot} \rightarrow C_3H_8$	11.0	0.
63	$CH_3^{\cdot} + CH_3^{\cdot} \rightarrow C_2H_6$	10.4	0.
64	$CH_3^{\cdot} + 1 - C_3H_7^{\cdot} \rightarrow C_4H_{10}$	10.3	0.
65	$CH_3^{\cdot} + 2 - C_3H_7^{\cdot} \rightarrow$ 2 - methyl propane	10.2	0.
66	$CH_3^{\cdot} + C_3H_5^{\cdot} \rightarrow 1 - C_4H_8$	10.3	0.
67	$C_2H_5^{\cdot} + 2 - C_3H_7^{\cdot} \rightarrow$ 2 - methyl butane	9.9	0.

TABLE 5.5 (Contd.)

Reaction Number	Elementary Reaction Step	$K = Ae^{-E/RT}$ sec^{-1} or litre.mole^{-1} sec^{-1} $\log_{10}A$	E (kcal/mole)
68	$C_2H_5^{\cdot} + C_3H_5^{\cdot} \rightarrow 1 - C_5H_{10}$	10.0	0.
69	$1 - C_3H_7^{\cdot} + 2 - C_3H_7^{\cdot} \rightarrow$ 2 - methyl pentane	9.9	0.
70	$1 - C_3H_7^{\cdot} + C_3H_5^{\cdot} \rightarrow 1 - C_6H_{12}$	10.0	0.
71	$2 - C_3H_7^{\cdot} + 2 - C_3H_7^{\cdot} \rightarrow$ "product"	9.5	0.
72	$2 - C_3H_7^{\cdot} + C_3H_5^{\cdot} \rightarrow$ "product"	10.0	0.
73	$C_3H_5^{\cdot} + C_3H_5^{\cdot} \rightarrow (C_3H_5)_2$	9.8	0.
74	$C_3H_5^{\cdot} + C_4H_7^{\cdot} \rightarrow$ 1, 5 heptadiene	10.1	0.
75	$CH_3^{\cdot} + C_2H_5^{\cdot} \rightarrow C_3H_8$	10.3	0.
76	$CH_3^{\cdot} + C_4H_7^{\cdot} \rightarrow 2 - C_5H_{10}$	10.4	0.
77	$C_2H_5^{\cdot} + C_2H_5^{\cdot} \rightarrow C_4H_{10}$	9.6	0.
78	$C_2H_5^{\cdot} + C_4H_7^{\cdot} \rightarrow 2 - C_6H_{12}$	10.0	0.
	Termination - Disproportionation		
79	$H^{\cdot} + 2 - C_3H_7^{\cdot} \rightarrow C_3H_6 + H_2$	10.7	0.
80	$CH_3^{\cdot} + 1 - C_3H_7^{\cdot} \rightarrow C_3H_6 + CH_4$	9.1	0.
81	$CH_3^{\cdot} + 2 - C_3H_7^{\cdot} \rightarrow C_3H_6 + CH_4$	9.4	0.
82	$CH_3^{\cdot} + C_4H_7^{\cdot} \rightarrow C_4H_6 + CH_4$	9.9	0.
83	$C_2H_5^{\cdot} + 2 - C_3H_7^{\cdot} \rightarrow C_3H_6 + C_2H_6$	9.2	0.
84	$1 - C_3H_7^{\cdot} + 2 - C_3H_7^{\cdot} \rightarrow C_3H_6 + C_3H_8$	9.2	0.
85	$2 - C_3H_7^{\cdot} + 2 - C_3H_7^{\cdot} \rightarrow C_3H_6 + C_3H_8$	9.3	0.
86	$2 - C_3H_7^{\cdot} + C_4H_7^{\cdot} \rightarrow C_4H_6 + C_3H_8$	9.7	0.
87	$C_3H_5^{\cdot} + C_4H_7^{\cdot} \rightarrow C_4H_6 + C_3H_6$	9.8	0.
88	$C_3H_5^{\cdot} + C_2H_5^{\cdot} \rightarrow C_2H_4 + C_3H_6$	9.1	0.
89	$C_3H_5^{\cdot} + 1 - C_3H_7^{\cdot} \rightarrow C_3H_6 + C_3H_6$	9.0	0.
90	$C_3H_5^{\cdot} + 2 - C_3H_7^{\cdot} \rightarrow C_3H_6 + C_3H_6$	9.0	0.

TABLE 5.5 (contd.)

Reaction Number	Elementary Reaction Step	$K = Ae^{-E/RT}$ sec^{-1} or $litre.mole^{-1}$ sec^{-1} $\log_{10}A$	E (kcal/mole)
91	$C_2H_5^{\cdot} + 2 - C_3H_7^{\cdot} \rightarrow C_3H_8 + C_2H_4$	9.1	0.
92	$1 - C_3H_7^{\cdot} + 2 - C_3H_7^{\cdot} \rightarrow C_3H_8 + C_2H_4$	9.1	0.
93	$CH_3^{\cdot} + C_2H_5^{\cdot} \rightarrow C_2H_4 + CH_4$	8.9	0.
94	$C_2H_5^{\cdot} + C_2H_5^{\cdot} \rightarrow C_2H_4 + C_2H_6$	8.7	0.
95	$C_2H_5^{\cdot} + 2 - C_4H_9^{\cdot} \rightarrow 2 - C_4H_8 + C_2H_6$	9.2	0.
96	$C_2H_5^{\cdot} + C_4H_7^{\cdot} \rightarrow C_4H_6 + C_2H_6$	9.6	0.
97	$C_2H_5^{\cdot} + 2 - C_4H_9^{\cdot} \rightarrow C_4H_{10} + C_2H_4$	8.9	0.
98	$C_2H_5^{\cdot} + C_4H_7^{\cdot} \rightarrow C_2H_4 + 2 - C_4H_8$	9.0	0.

CHAPTER 6

EXPERIMENTAL RESULTS

6.1 Introduction

Under experimentally verified isothermal conditions within a section of the reactor raw experimental data were collected from different axial positions along the centreline of the reactor within the isothermal region. In each run the temperature profiles both axially and radially were measured before and after the collection of the composition data. A typical set of data therefore for each run consisted of product compositions and reactant conversion collected under isothermal conditions for a range of different residence times corresponding to the different axial points where a measurement was taken.

Three different experimental operating conditions led to three separate sets of raw data. The first set, set A (Runs 4 - 10 inc.) consisted of data collected in the isothermal gas range 920 - 990 K at a reactor pressure of 7 psig, with a nominal feed of 10% molar concentration of butane in inert nitrogen. Throughout the experimental runs the Reynolds number was held constant ($\sim$ 80) and continuous monitoring of the axial wall temperature profile, the feed flowrate and reactor pressure ensured that the experimental conditions did not drift during the collection of the data, which covered a time interval of 7 - 8 hours. A similar set of data, set B (Runs 11 - 19 inc.) was collected in the same isothermal gas temperature range with a nominal feed concentration of 5% molar butane in inert nitrogen but with an identical overall feed flowrate to the reactor. Thus the Reynolds number remained unchanged from that of the first set and any change in the experimentally collected data would be a direct consequence of changing the feed composition. Since the global

kinetics were analysed assuming first order characteristics for the butane disappearance, this served as an independent check for justifying such an assumption.

The final set of data, set C (Runs 20 - 27 inc.) were collected under a Reynolds number approximately twice that of the first two sets, with a nominal feed concentration equal to the first set. Although no S/V investigation was performed in this study the result of doubling the flowrate will aid mass transfer to the reactor wall and any heterogeneous contribution to the assumed homogeneous reaction kinetics should be reflected in the analysis of the resulting data. The increase in feed flowrate to cause such a change in the Reynolds number, demanded the use of extra preheating facilities since the design of the reactor was principally for operation at lower flowrates. Without the preheat no adequate isothermal zone, specifically in the radial direction, was attainable. Pretreating the premixed feed gases to approximately 350^{o}C before introducing it to the reactor led to an isothermal space suitably large enough from which to extract a reasonable set of data.

Originally it was intended to extend the temperature range for set C but at higher temperatures the conversion of butane reached such high proportions that this was not possible due to excessive formation of liquid products and carbon build-up. Information on the feed to the reactor, subsequent evaluation of overall material balances and the probe sampling conditions used during the experiments is located in Appendix X.

The experimental data and subsequent analyses are presented here in four sections. Typical measured axial centreline gas temperature profiles for each set of experimental conditions are illustrated in Section 6.2, together with typical plots of the major product yields through the isothermal gas space. Graphical representations of the composition data

collected during the experiments are presented in Section 6.3. These take the form of yield/conversion and selectivity/conversion plots and in this way Sections 6.2 and 6.3 encompass the presentation of typical conditions and composition data as collected from the experimental runs.

Section 6.4 deals principally with analysis of this information in the determination of the global characteristics for the butane pyrolysis; in particular estimation of the apparent rate constants and thus pre-exponential factor and activation energy. Typical plots of rate constant estimation assuming plug flow and first order characteristics, using unweighted linear least squares regression, are presented for different experimental runs from each of the three sets of data. The Arrhenius plots for estimation of the activation energy and pre-exponential factor are also included. Rate constants were also estimated using the radial dispersion model and this tended to justify the simpler approach by which the global parameters were estimated.

Section 6.5 presents the attempts to model the product distributions using the fundamental kinetic mechanism proposed by Allara and Edelson (1980) and described earlier in Chapter 5, Section 5.8.

6.2 Axial Centreline Gas Temperature Profiles

Confirmation of the ability to establish an isothermal region is presented in Figs. 6.1 - 6.5. Plotted on the same reactor profiles are some of the yields for the major products propylene, methane, hydrogen and ethylene and conversion of the parent hydrocarbon, butane. Full details of the axial wall and measured gas temperature profiles are located in Appendix XI. The profiles in Figs. 6.1 - 6.5 show clearly that an isothermal axial profile region was obtained approximately 30 - 36 cm of length for experimental runs in set A and set B (Figs. 6.1 - 6.4) when the average Reynolds

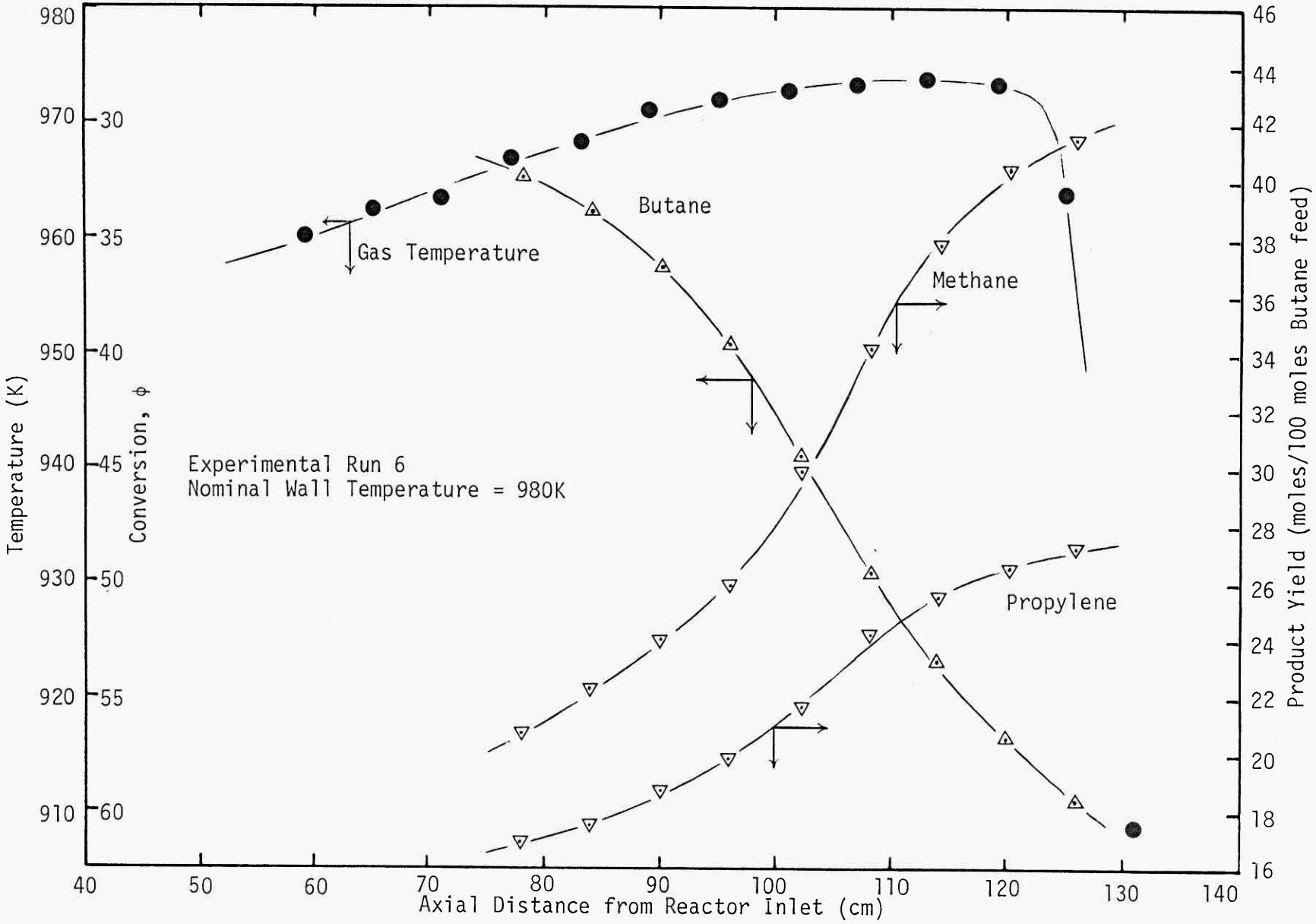

Fig. 6.1 Measured Axial Gas Temperature and Composition Profiles - Set A

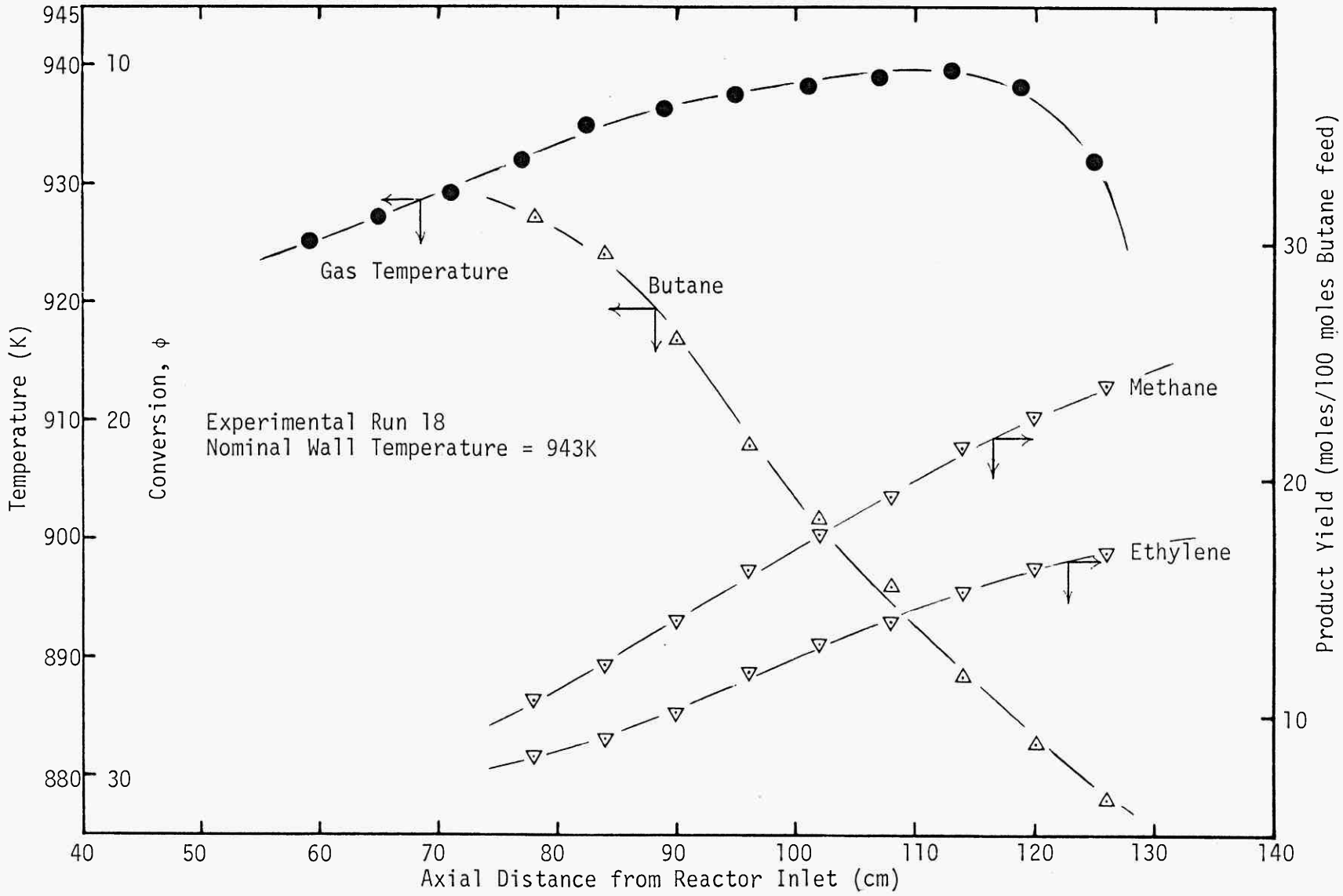

Fig. 6.2 Measured Axial Gas Temperature and Composition Profiles - Set B

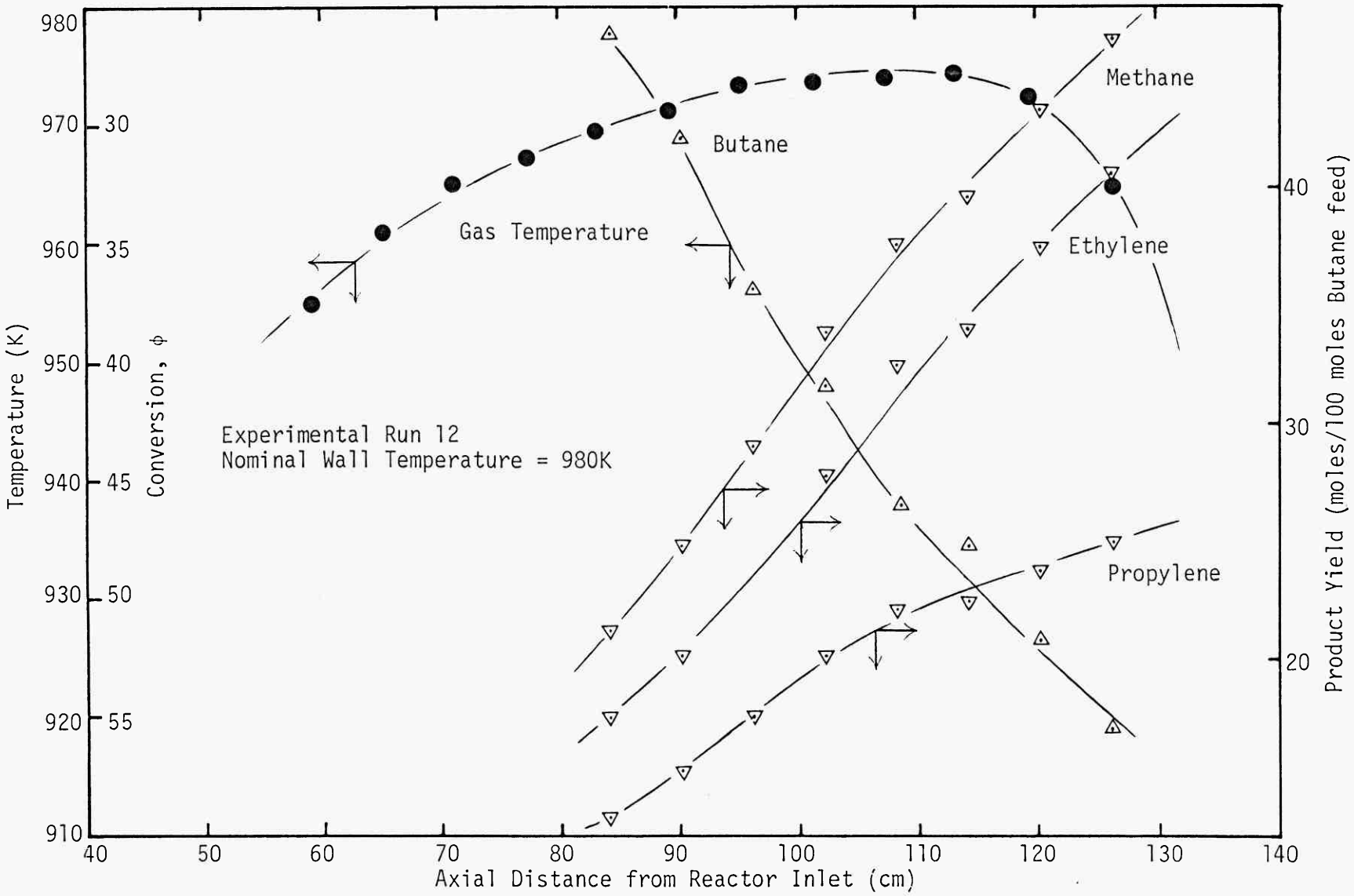

Fig. 6.3 Measured Axial Gas Temperature and Composition Profiles - Set B

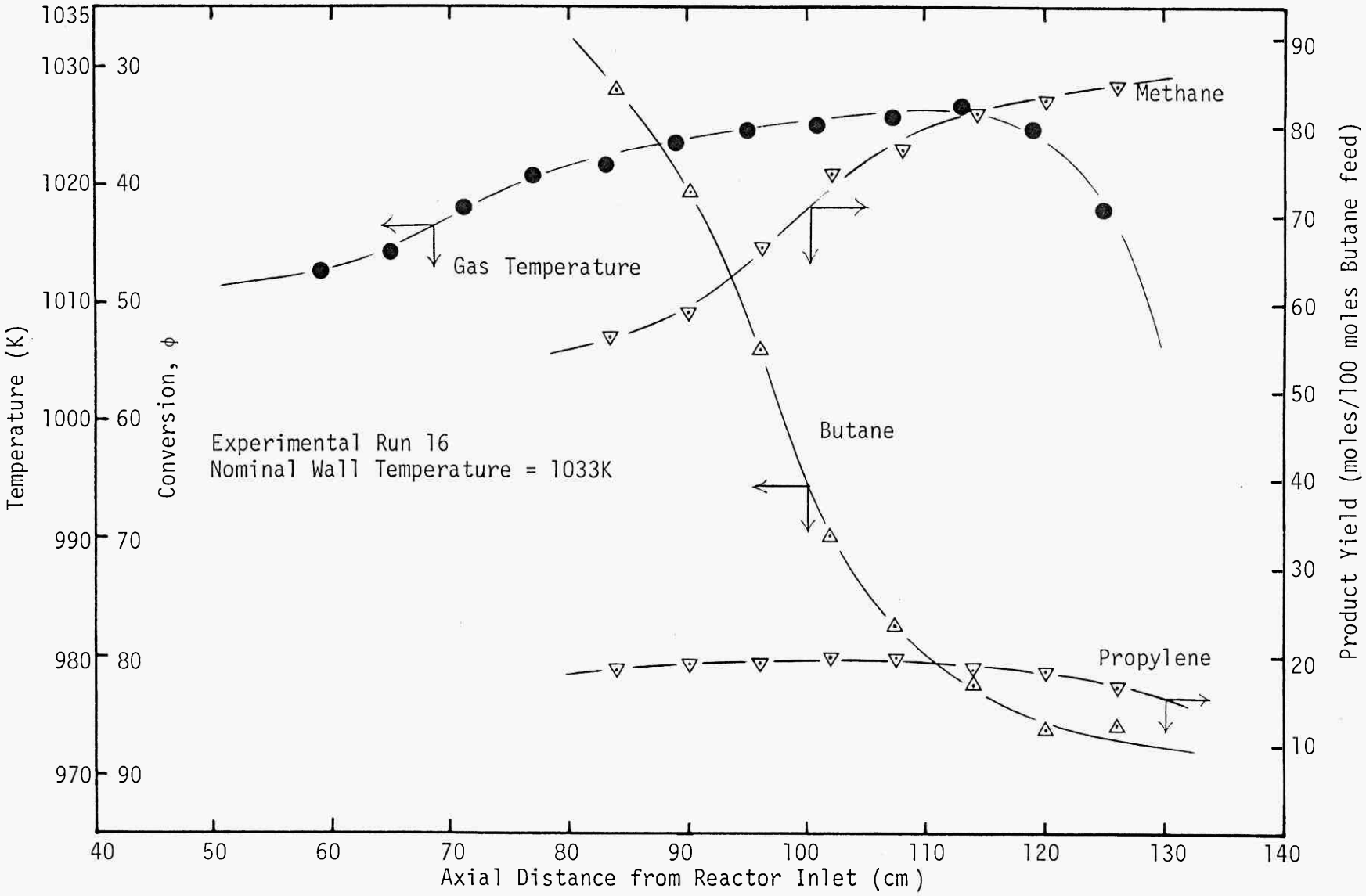

Fig. 6.4 Measured Axial Gas Temperature and Composition Profiles - Set B

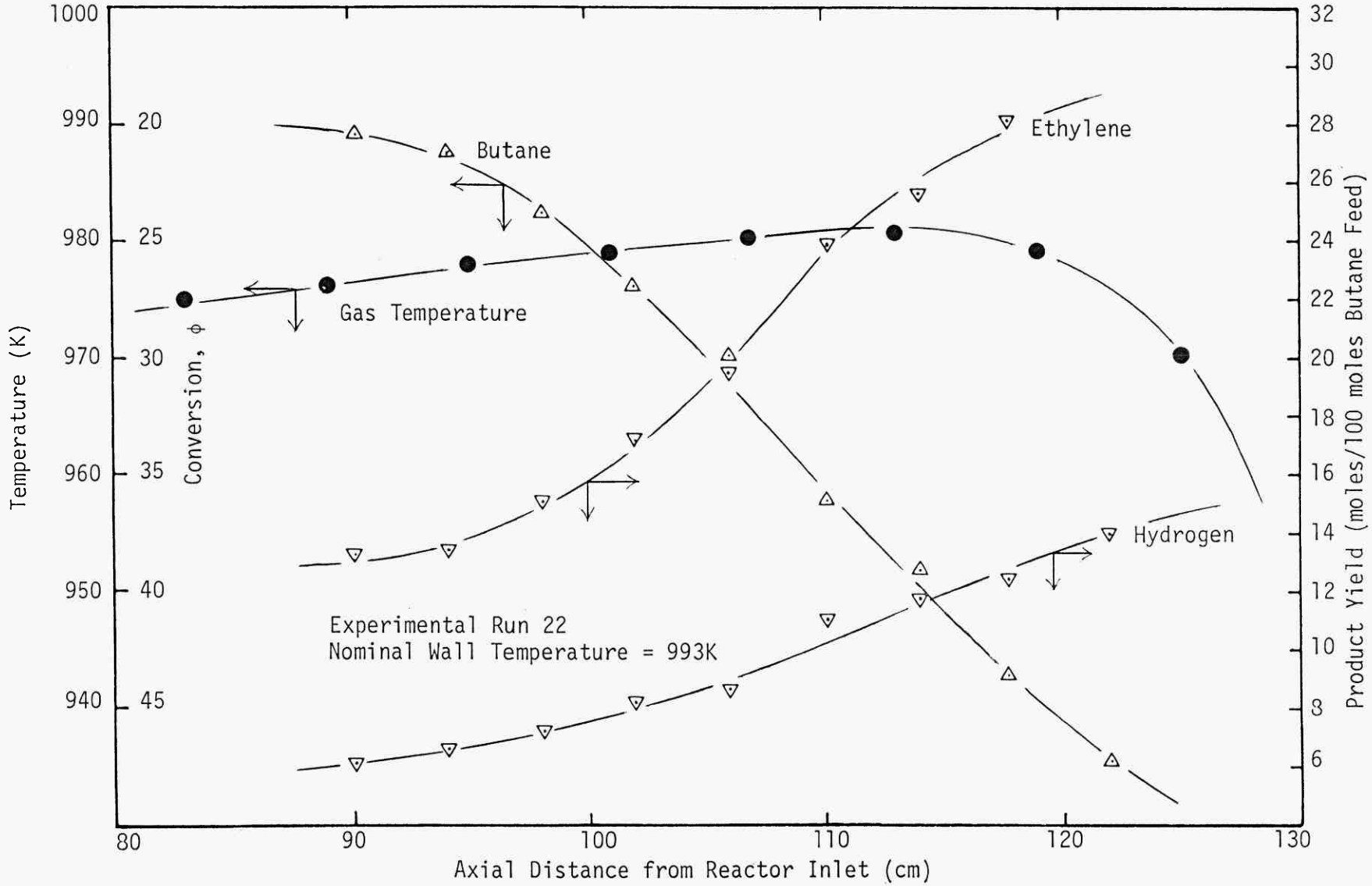

Fig. 6.5 Measured Axial Gas Temperature and Composition Profiles - Set C

number was ∿80, whereas a shorter region, 20 - 24 cm. long, was obtained in set C (Fig. 6.5) where a higher Reynolds number was used ∿ 160, during each run. This increase in Reynolds number was achieved by increasing the mass velocity through the reactor and accounts for the reduction in size of the isothermal section. This occurred despite the fact that the feed gases were preheated up to a temperature of ∿ 350°C before tangential introduction into the reactor. As previously mentioned in Chapter 3, Section 3.3, the variation of temperature through the isothermal region, measured axially and radially was generally less than 3°C and local variation was measured to be within 1°C during a typical run.

An average of all the gas temperatures recorded in the isothermal region was used to typify the thermal conditions and this value was used in equation (3.1) to enable correction of the thermocouple temperature due to correction and radiation heat transfer effects at the thermocouple tip which raise the recorded value higher than its true value. Average corrected temperature differences between gas and wall for set A and set B were of the order 20°C and in set C average differences were larger, ∿ 50°C (Corrected temperatures are tabulated and discussed in Appendix IV.)

6.3 Product Distributions

One of the advantages of this experimental approach is the vast amount of reliable data which is available from a small number of experimental runs. The great variety of products obtained from the pyrolysis is indicative of the complexity of the radical reaction mechanism which is taking place. Product yields for all the major components and measured minor components are presented solely as a function of the conversion in Figs. 6.6 - 6.11. The composition data in full is located in tabular form in Appendix XII. The yield data has been collected from

individual runs under varying conditions of residence time and reaction temperature. If the product distribution depended on the conversion only the yield plots would be characterised by smooth continuous functions with a spread of points determined by experimental measurement errors. Then the conversion/yield characteristics would be independent of the combination of residence time, reaction temperature, reactor pressure and any other factors which might affect the pyrolysis.

For the limitations of the data collected it appears that there is a reasonable correlation between yields of the same product from separate runs upto conversions of 30 - 40%. The certainty of this observation becomes doubtful when the isothermal reaction temperature is high because only a fraction of the composition data collected during these runs was in this nominal conversion range. From these runs therefore little information about the early stages of the reaction could be collected.

Above a conversion of ∿50% a spread of points for the propylene yield can clearly be observed in Figure 6.7 which indicates that at higher conversions, the product distribution and yield are not solely a function of the conversion of the product distribution data. This spread of yield points is also apparent for hydrogen in Fig. 6.9 and to a lesser extent for ethane and ethylene in Figs. 6.8 and 6.10 respectively. The methane yield in Fig. 6.6 remains relatively stable irrespective of the reaction temperature at which the yield data was collected. This reflects the stable structure of methane which at these temperatures becomes a terminal product and thus does not partake in any secondary reactions. If it is proposed that the spread of the yield data is as a result of the effect of subsequent secondary reactions then the idea that even at high temperatures the yield is only a function of conversion upto ∿30% becomes

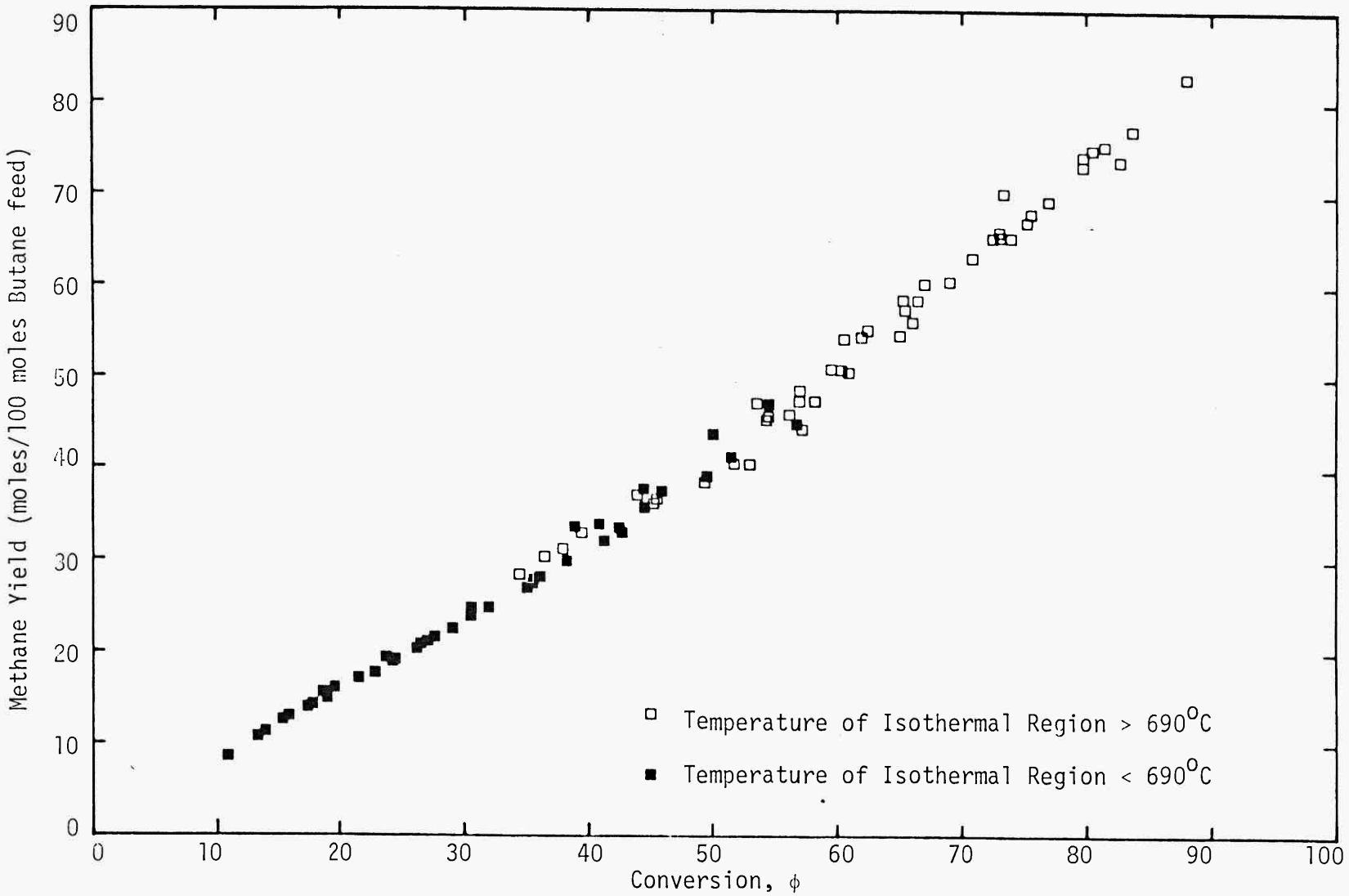

Fig. 6.6 Methane Yield vs. Conversion

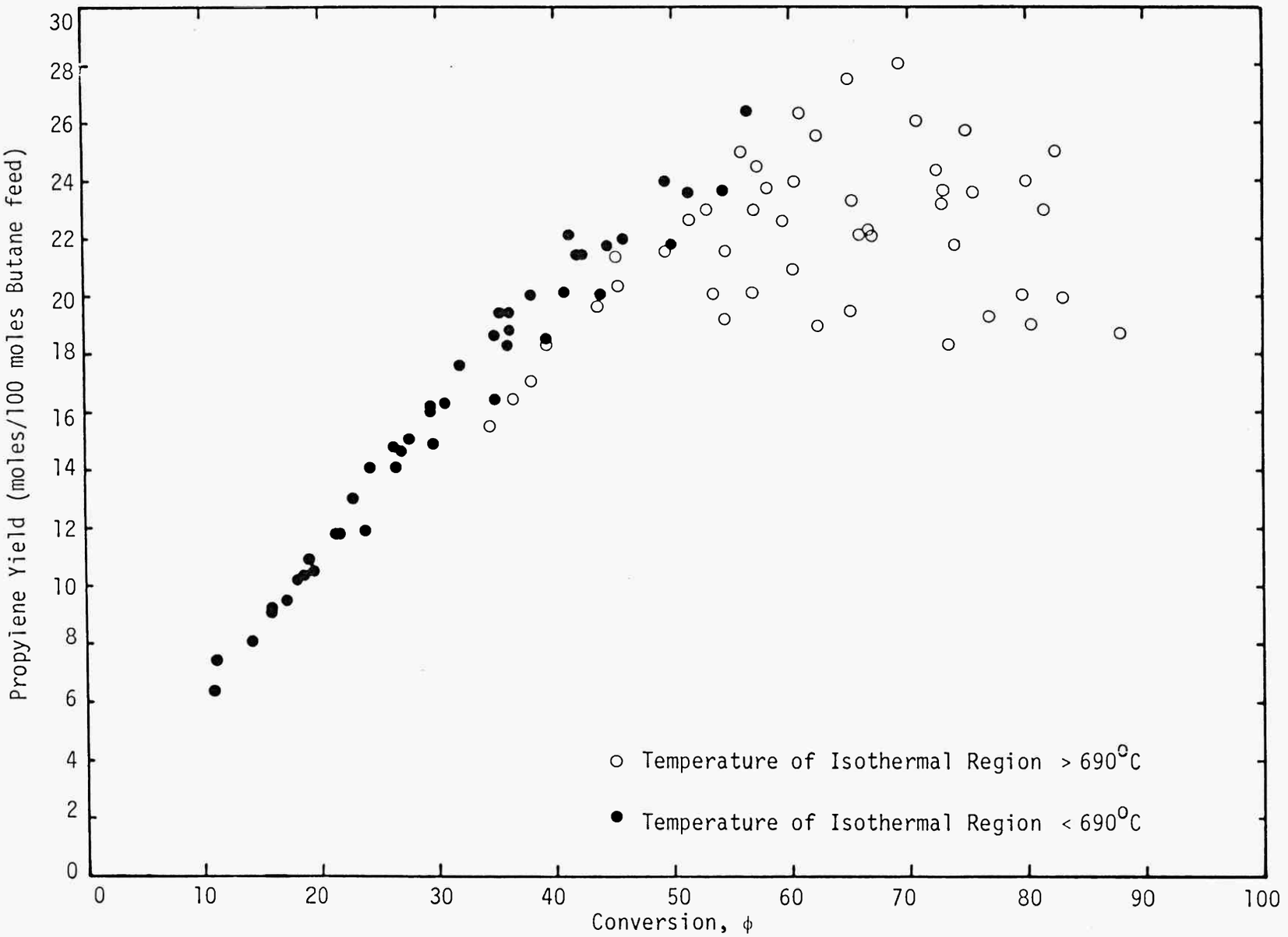

Fig. 6.7 Propylene Yield vs. Conversion

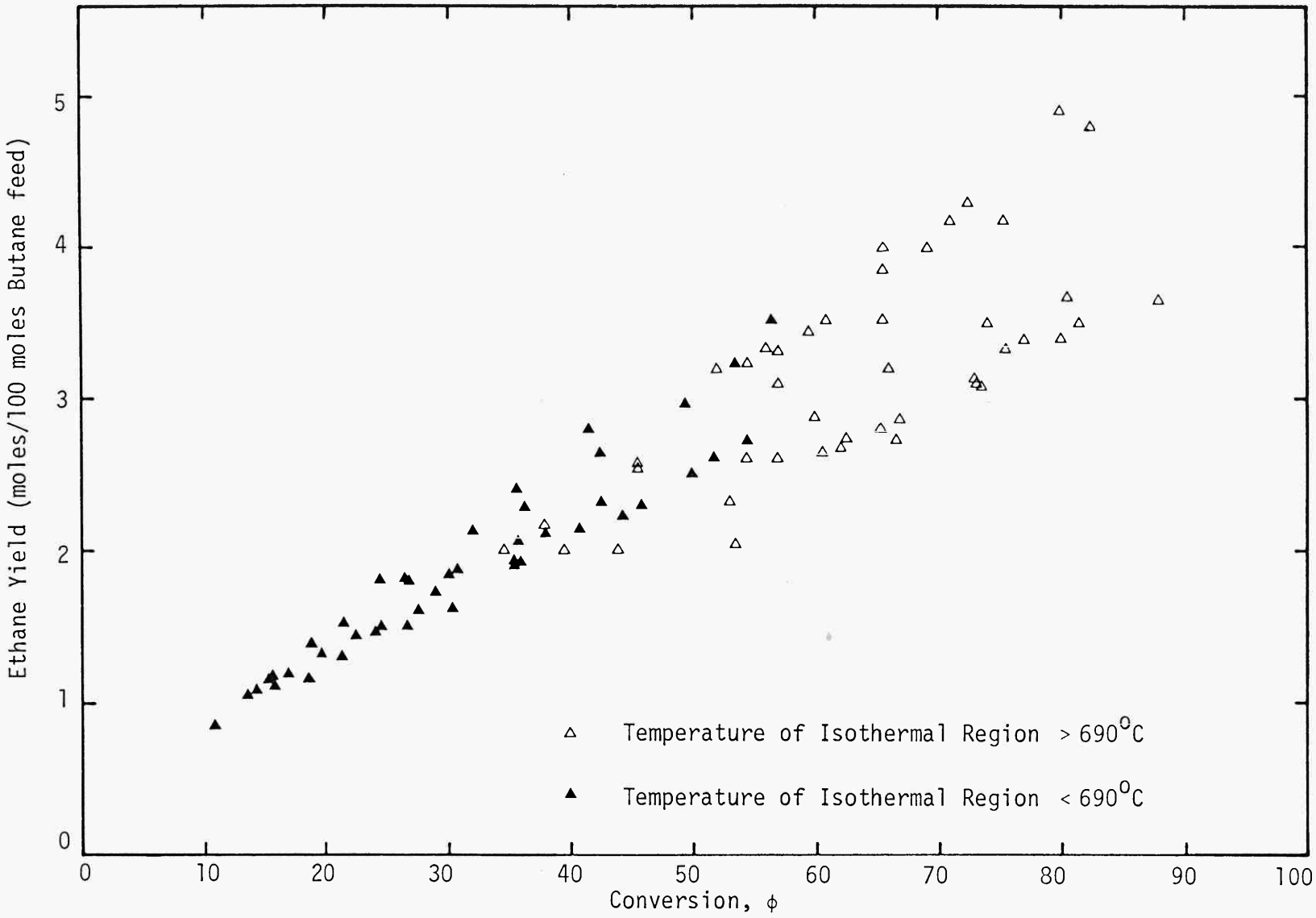

Fig. 6.8 Ethane Yield vs. Conversion

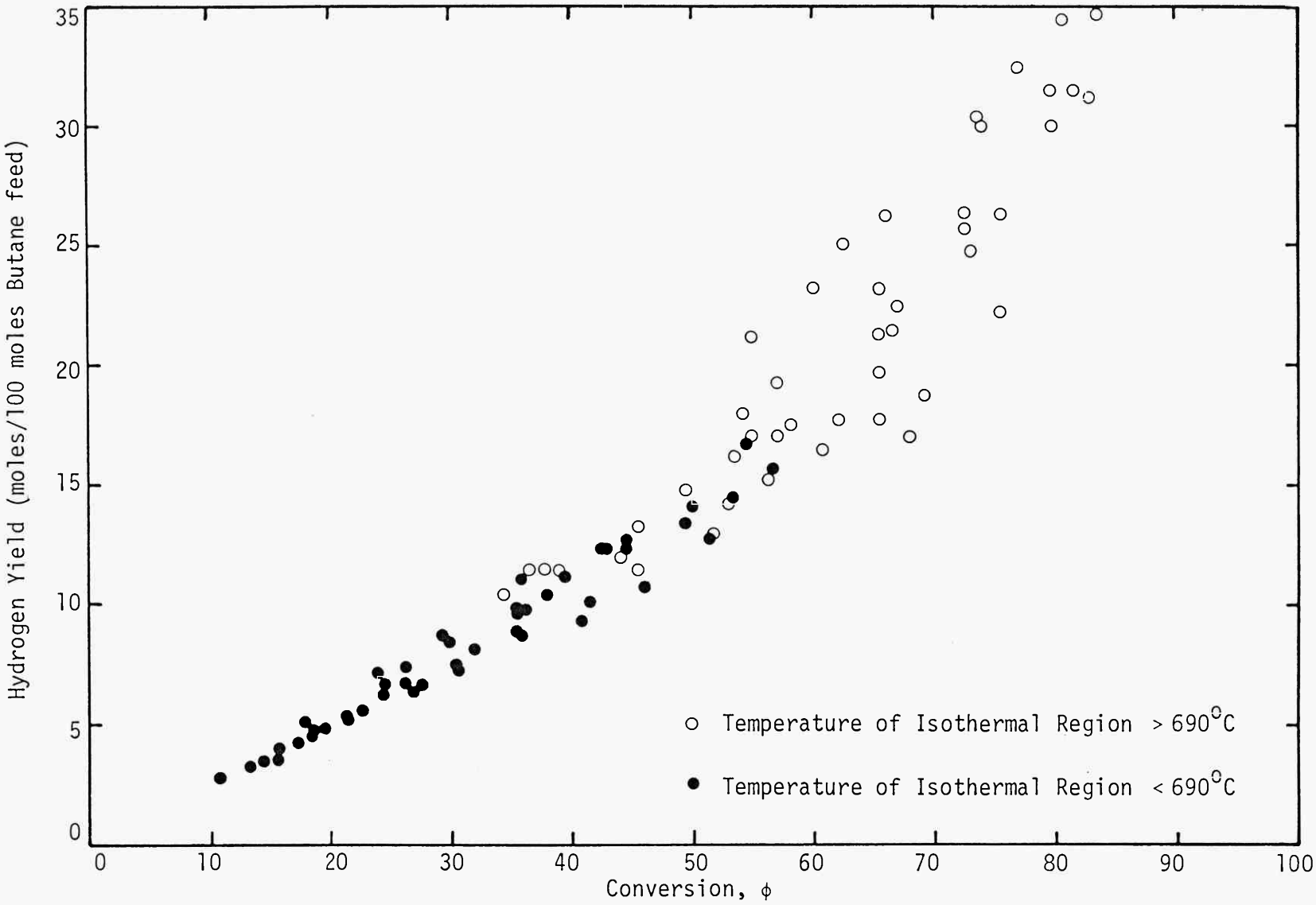

Fig. 6.9 Hydrogen Yield vs. Conversion

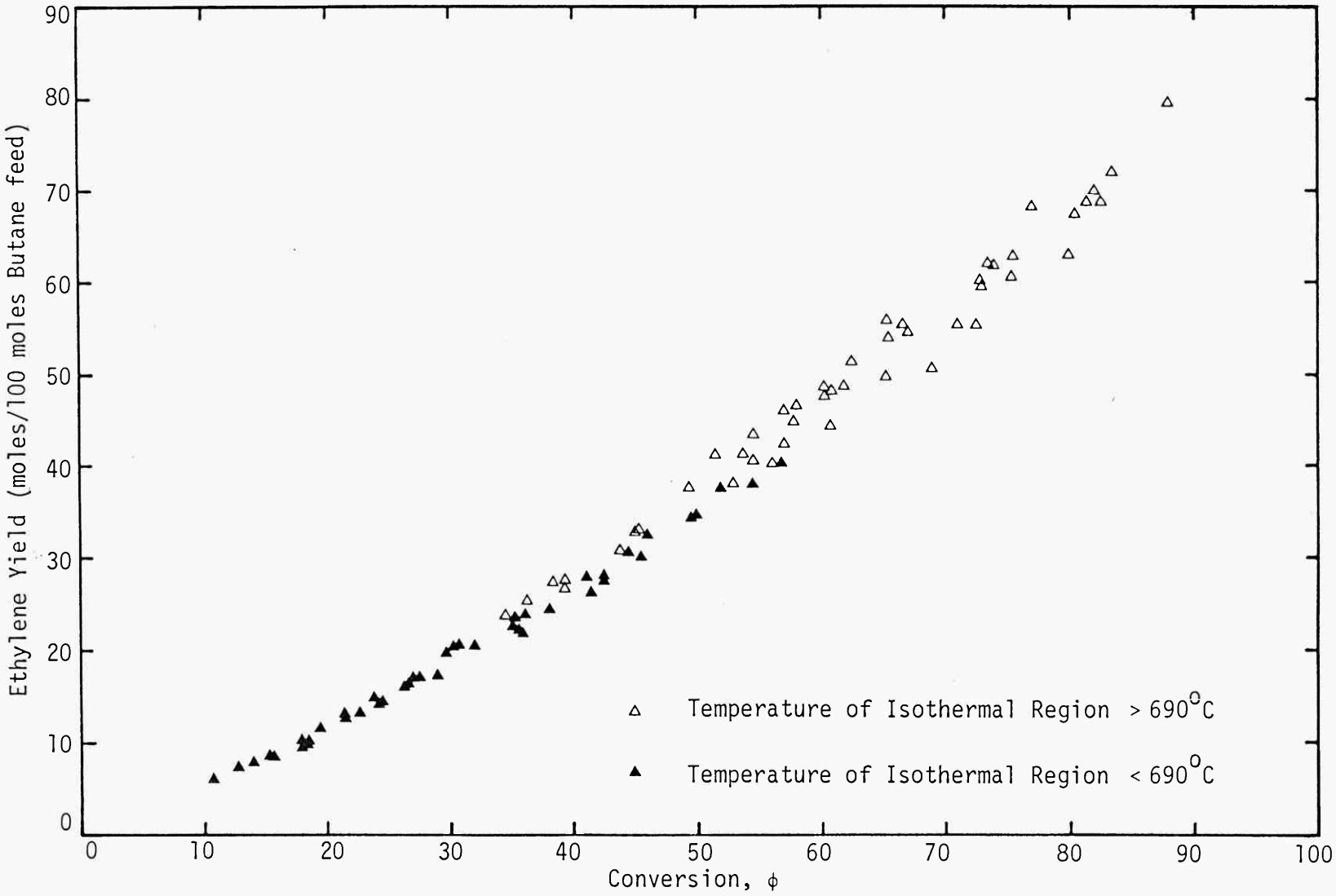

Fig. 6.10 Ethylene Yield vs. Conversion

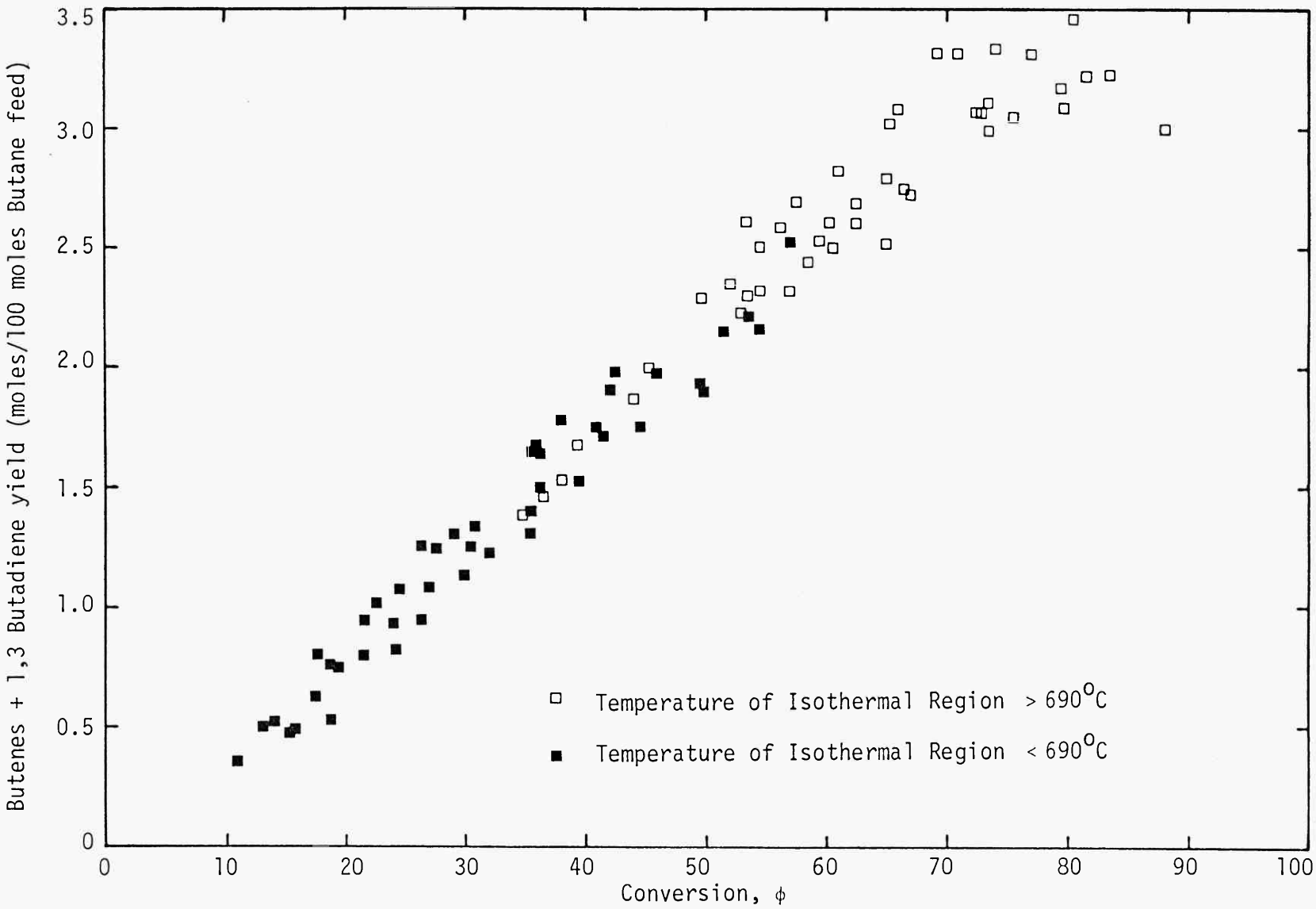

Fig. 6.11 Butenes + 1,3 Butadiene Yield vs. Conversion

more sound.

In order to obtain an idea of the effect of temperature on the distribution at higher conversions the yield data is divided into two classes; low temperature data when the calculated isothermal temperature during the experimental run was below 690^{o}C and high temperature data when the temperature was above this. From this division of data some characteristics of the yield spread became abundantly more clear. Yields for propylene and to a lesser extent ethane are favoured by lower reaction temperatures whilst ethylene yields increase at higher temperatures. The variation of hydrogen with temperature and conversion in Fig. 6.9 is not understood. Hydrogen is a stable terminal product and would be expected to have a yield plot similar in stability to the methane plot, Fig. 6.6. Although the scatter of points does not appear to have any direct correlation with temperature or conversion, slightly higher yields appear to have been achieved from the runs in set C. The implications of this are discussed further in Chapter 7, Section 7.4.

Figure 6.11 gives a cumulative yield plot for 1-butene, cis-2-butene, trans-2-butene and 1,3 butadiene. 1-butene was seen to go through a maximum at about 70% conversion and probably suffers from the same inhibition reactions as propylene due to attack by alkyl radicals, see Chapter 5, Section 5.2. Selectivity towards 1,3 butadiene increased noticeably at very high conversions, > 80%. Propane was also detected in small traces which varied little with change in experimental conditions.

To complement the yield plots the selectivity of the major products, principally the olefins, are presented in Figs. 6.12, 6.13 and 6.14 upto conversions $\sim$ 50%. No new information could be obtained by plotting above this range since the product yields no longer remain a sole function of conversion. Initial selectivities for ethylene and propylene are esti-

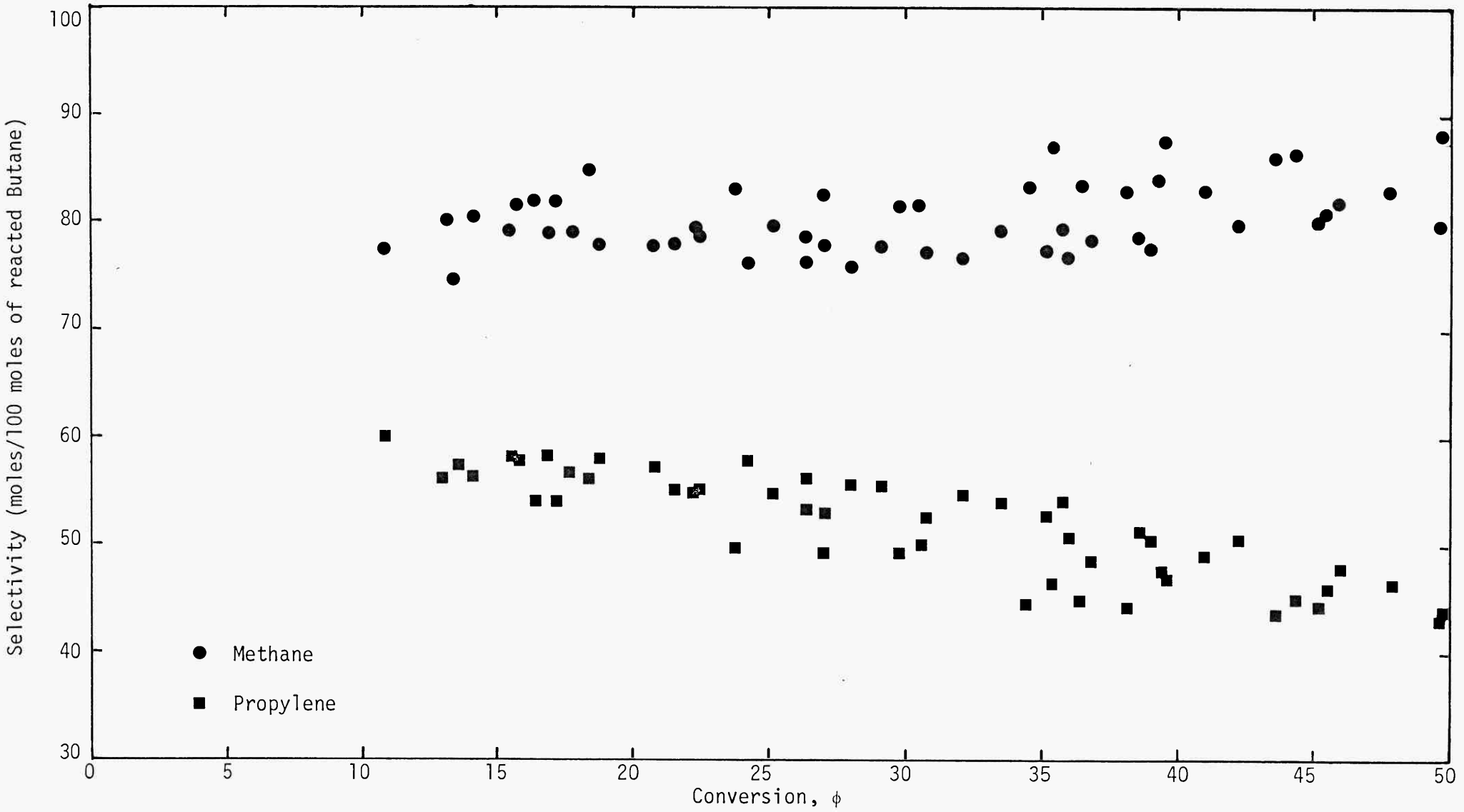

Fig. 6.12 Selectivity for Methane and Propylene

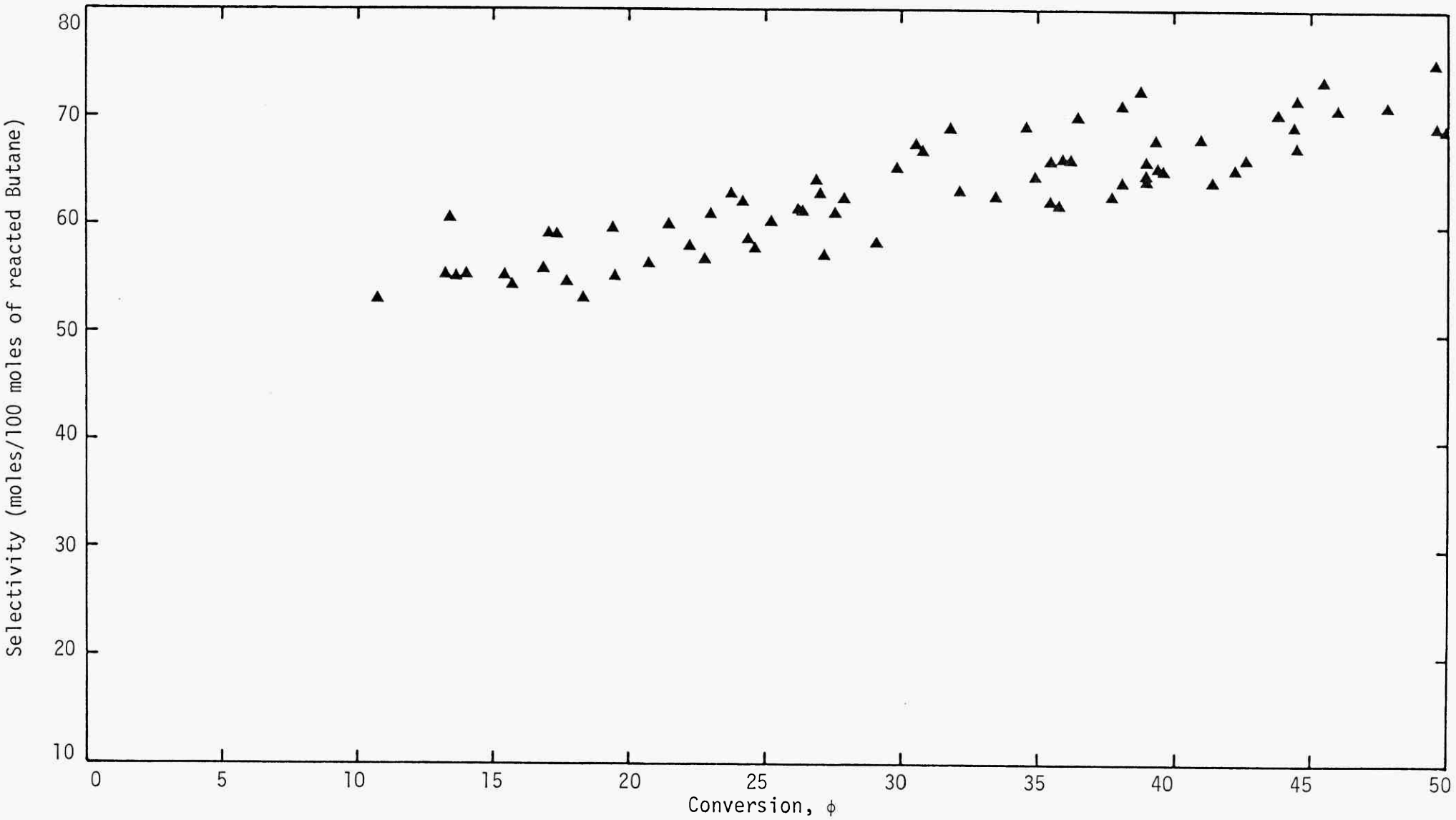

Fig. 6.13 Ethylene Selectivity

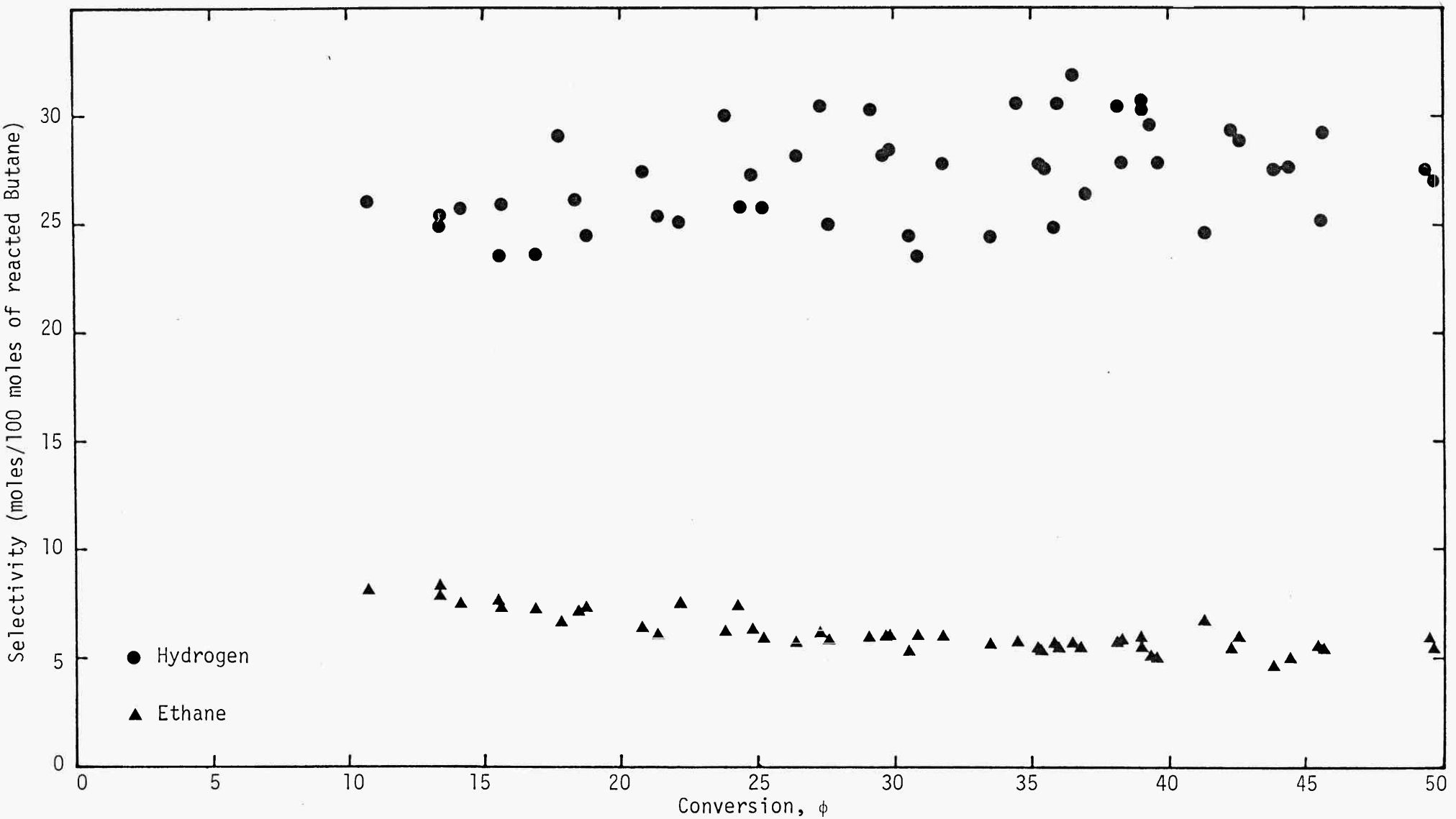

Fig. 6.14 Selectivity for Ethane and Hydrogen

mated to be approximately 45 - 50% and 60 - 65% respectively. The implication of this are discussed further in Chapter 7, Section 7.1.

6.4 Evaluation of the Global Parameters

Calculation of the rate constant from each individual run as presented in Figs. 6.15, 6.16 and 6.17 was based upon the assumption that radial mixing was sufficiently rapid to make the behaviour of the experimental laminar flow reactor equivalent to one with plug flow. This was checked experimentally and Fig. 5.1 in Chapter 5 demonstrates the typical profiles obtained within the isothermal region. Because measurements were available within the reactor space and not only at the effluent, it was computationally straightforward to find a unique value of the rate constant by linear or non-linear least squares. The plots typified by Figs. 6.15, 6.16 and 6.17 indicate that the isothermal gas region stretches slightly further than the centreline gas temperature measurements have suggested. In most instances the composition points downstream of the isothermal gas region do not deviate away from the regression line passing through the composition points located within the isothermal region. This suggests, but does not confirm, that conductivity effects away from the thermocouple probe tip may become significant when measuring this close to the exit, due to the large thermal gradients which exist in this vicinity .

The slight curvature observed in the plot for run 25 in Fig. 6.17 is indicative that the axial temperature gradients within the isothermal region for runs in set C may have been larger than for sets A and B. This is perfectly conceivable because the temperature difference between the gas and wall is considerably larger than in the first two sets. However the measurements taken of gas temperature revealed no discernible difference between the variation of temperature within the isothermal regions between the three sets. For further comment see Appendix IV.

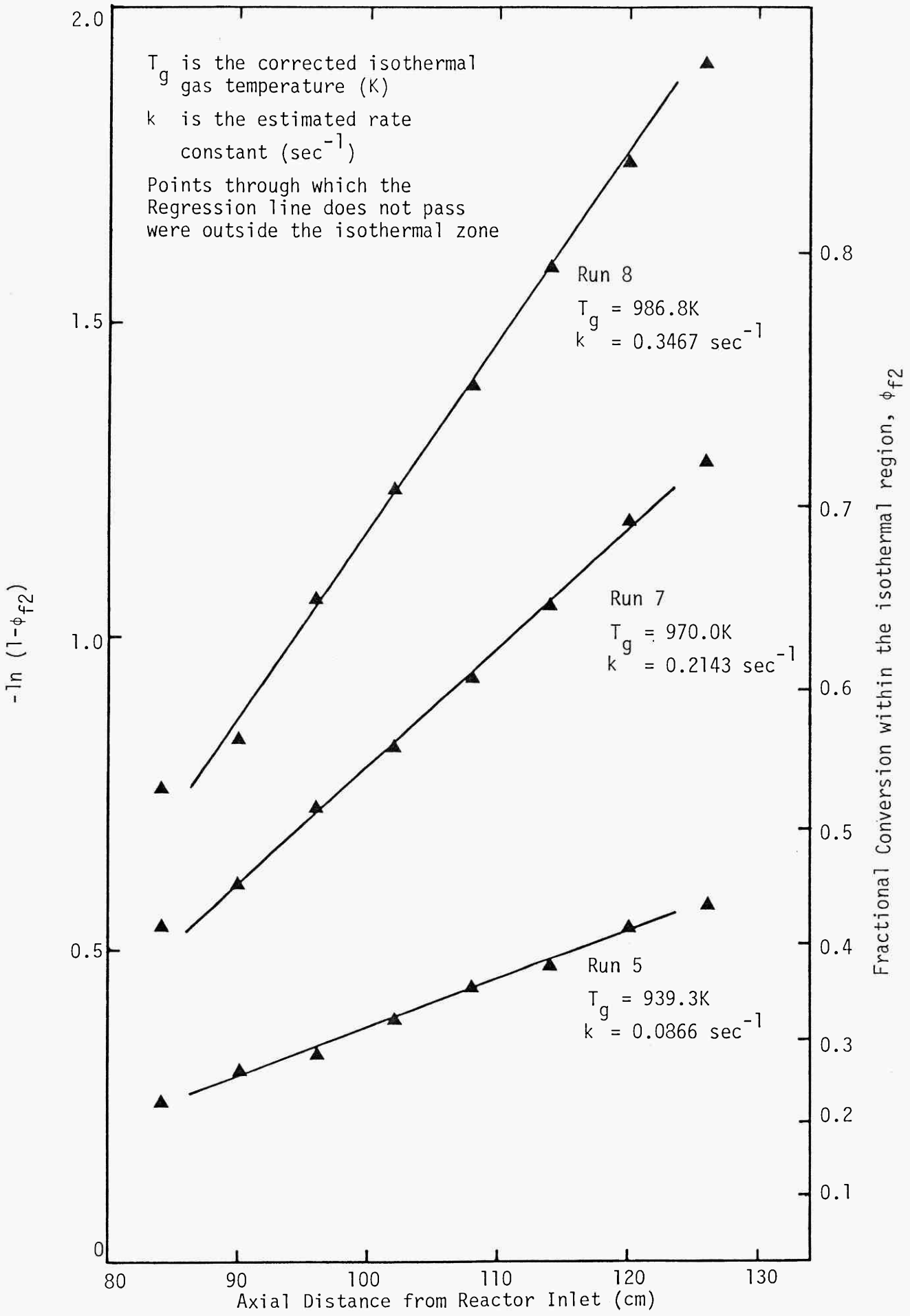

Fig. 6.15 Unweighted Linear Least Squares Estimation of the Rate Constant - Experimental Set A

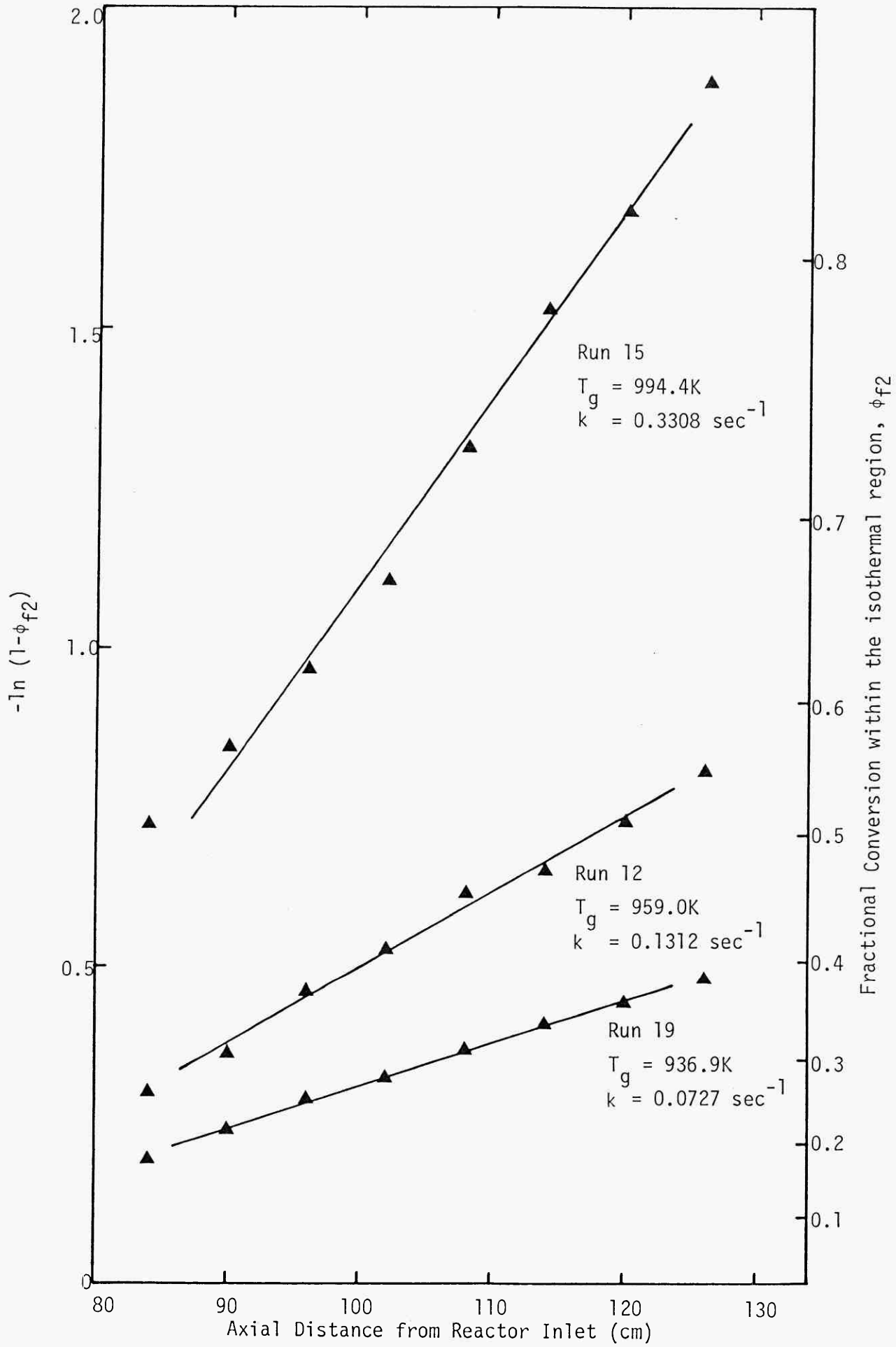

Fig. 6.16 Unweighted Linear Least Squares Estimation of the Rate Constant - Experimental Set B

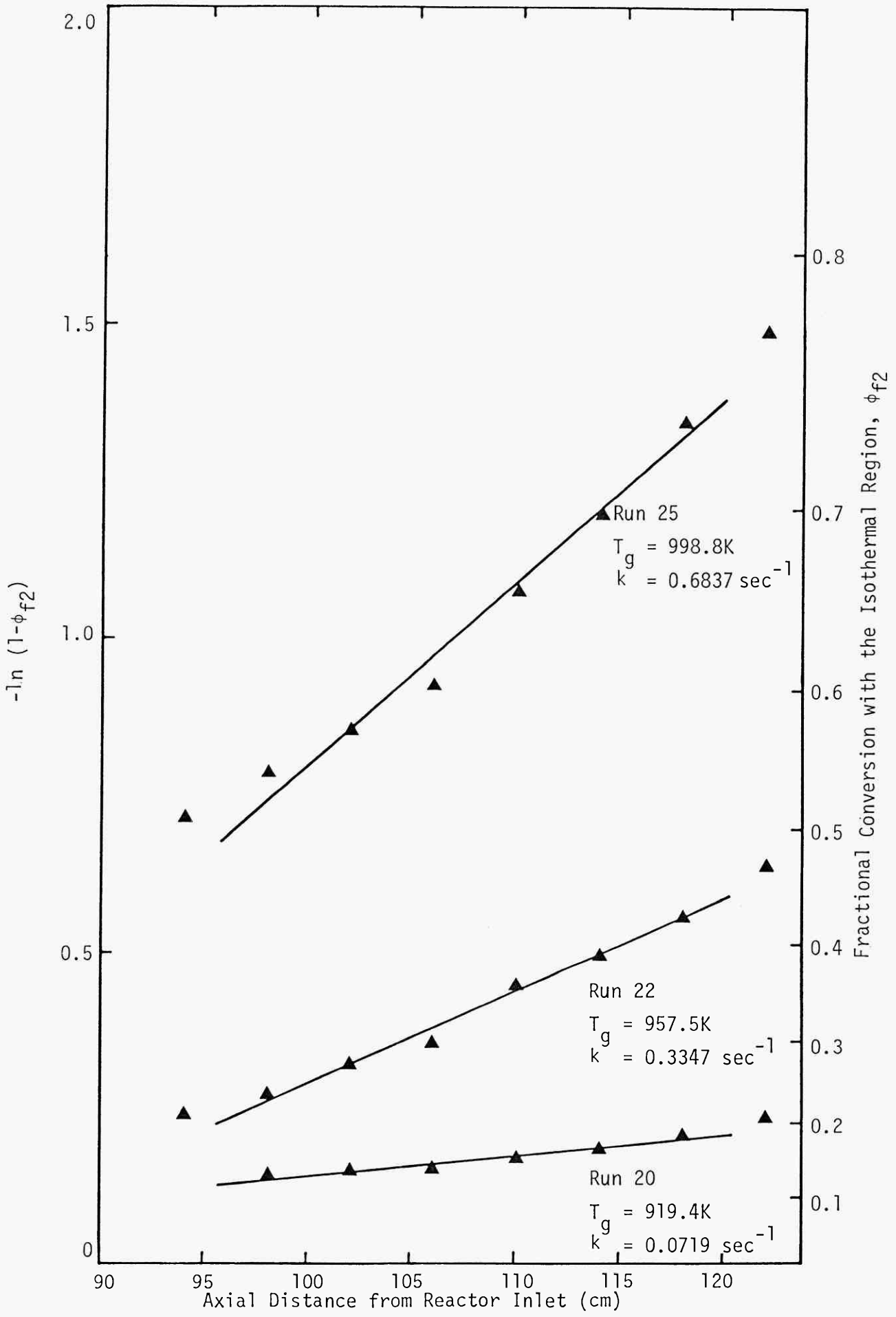

Fig. 6.17 Unweighted Linear Least Squares Estimation of the Rate Constant - Experimental Set C

The validity of the plug flow approximation was tested in several ways. The most direct approach was the simultaneous estimation of both the rate constant and the radial mixing parameter from the data, using the radial dispersion model, as described in Chapter 4. Alternatively it could be assumed that molecular diffusion was the only means by which radial dispersion was occurring and thus the radial dispersion coefficient was equated to the radial molecular diffusion coefficient. Wakeham and Slater (1973) developed an equation which was used to estimate the diffusion coeffient for butane in nitrogen

$$\ln(Dm) = -11.513 + 1.61 \ln(T) \qquad (6.1)$$

where: T is the temperature (K)

Dm is the diffusion coefficient (cm^2/sec)

Although primarily applicable in the temperature range 300 - 700 K Wakeham (1981) estimates errors to be no greater than 10 - 15% for extrapolation to the temperature range used in this study. Using this a priori value of the dispersion coefficient led to an estimation of only the rate constant with the radial dispersion model. Lastly the rate constant was estimated assuming the validity of the plug flow model using linear and non-linear regression. Results for all three different approaches are summarised in Table 6.1.

The simultaneous estimates of the rate constant and the radial dispersion coefficient seem to be divided into two types of results. In some cases, the simultaneous estimate of the dispersion coefficient, presented as the parameter α , see Chapter 4, Section 4.3, is very large and not surprisingly the estimate of the rate constant incorporated in the parameter β tallies well with estimates using plug flow. In the second instance the value of α is small enough that an effect on the simultaneous estimate of β is observed, which as a result deviates from the plug flow estimate. This agrees with the simulations in Chapter 4 which predicted

TABLE 6.1

Summary of Results for Estimation of α and β
From the Experimental Data

Run Number	β_1	α_1	β_2	α_2	β_3	K_3 (sec^{-1})	β_4
4	0.0931	3.10	0.1122	1.062	0.0841	0.0610	0.0837
5	0.1246	3.28	0.1559	0.765	0.1164	0.0866	0.1155
6	0.2138	2.31	0.2732	0.442	0.2011	0.1524	0.1997
7	0.2799	146.5	0.3859	0.318	0.2817	0.2143	0.2797
8	0.4589	3735.5	0.6520	0.191	0.4500	0.3467	0.4590
9	0.4721	0.78	0.5959	0.206	0.4251	0.3313	0.4167
11	0.2103	1.03	0.2553	0.391	0.1795	0.1658	0.1765
12	0.1805	21419.1	0.2407	0.516	0.1776	0.1312	0.1805
13	0.2617	1779.0	0.3534	0.354	0.2473	0.1850	0.2618
14	0.3326	23727.4	0.4892	0.207	0.3250	0.3101	0.3326
15	0.5334	0.3583	0.5921	0.216	0.4351	0.3308	0.4177
16	0.5856	224.2	0.8499	0.151	0.5477	0.4233	0.5855
17	0.1164	948.5	0.1520	0.813	0.1164	0.0847	0.1165
18	0.0734	13814.0	0.0965	1.268	0.0720	0.0520	0.0734
19	0.1010	29123.0	0.1335	0.921	0.1007	0.0727	0.1010
20	0.0435	2.81	0.0583	0.667	0.0327	0.0719	0.0324
21	0.0827	1.70	0.1146	0.345	0.0648	0.1453	0.0638
22	0.1629	1.77	0.2596	0.154	0.1462	0.3347	0.1448
23	0.2696	0.49	0.3586	0.112	0.2116	0.4969	0.1979
25	0.3634	0.41	0.4946	0.083	0.2868	0.6837	0.2735
26	0.3323	14494.0	0.6156	0.054	0.3299	0.9956	0.3322

1 Simultaneous estimation of α and β using the RDM.

2 Estimation of β using the RDM using an a priori value of α, calculated using equation (6.1).

3 Estimation of β using the PFM with linear regression, by assuming $\alpha \to \infty$.

4 Estimation of β using the PFM with non-linear regression, by assuming $\alpha \to \infty$.

a correlation between estimates of α and β in the range where α was noticeably small. The second set of results where an a priori value of the dispersion coefficient is substituted into the regression model also exhibits this same effect, where the estimates of β differ significantly from those of plug flow, directly as a result of the low values of α. The implications of this disparity are discussed in Chapter 7, Section 7.2.

The rate constants obtained from the plug flow model were used to estimate the Arrhenius parameters of the global kinetics for the rate of butane decomposition. A comparison between the non-linear plug flow regression estimates and the linear plug flow estimates revealed little difference and for convenience the linear estimates were used to generate the activation energy and pre-exponential factor.

The weighted linear regression plots for the calculation of the Arrhenius parameters from the three data sets are shown in Figs. 6.18, 6.19 and 6.20. The weights for the linear regression were determined from the estimated variances of each estimated rate constant. These Arrhenius parameters were also evaluated by non-linear regression using the inverse of these variances as appropriate weights. The known high correlation between the pre-exponential factor and activation energy warranted a reparametization

$$k = A' e^{-\frac{E}{R_u}\left(\frac{1}{T} - \frac{1}{T^*}\right)}$$

$$A' = A e^{-E/RT^*} \qquad (6.2)$$

where T* is the average temperature for the rate constant data used in the regression. The results from the non-linear regression are presented alongside the linear regression estimates for comparison. Error bounds for the linear regression estimates were straightforward to calculate

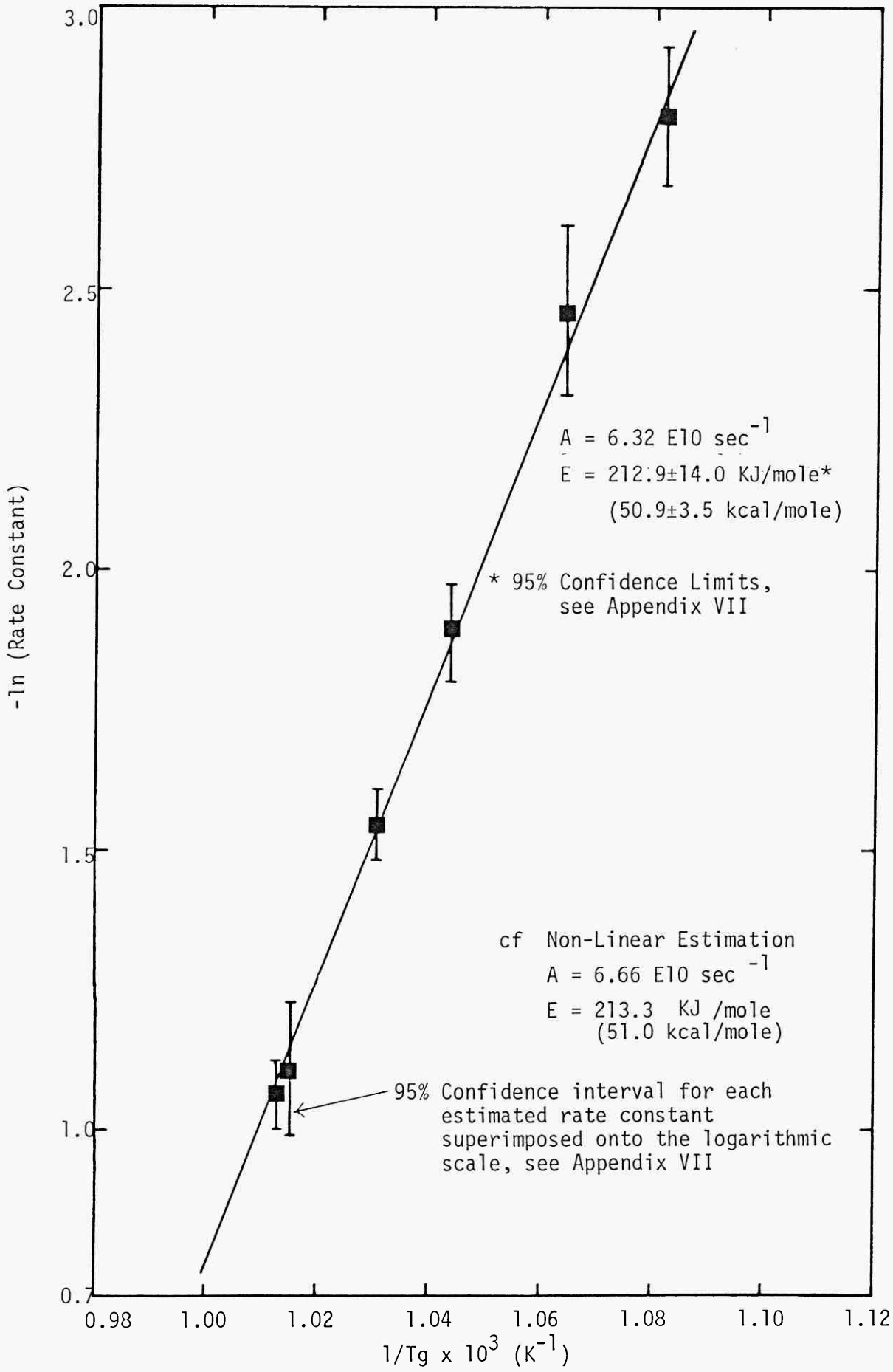

Fig. 6.18 Arrhenius Plot for Experimental Set A

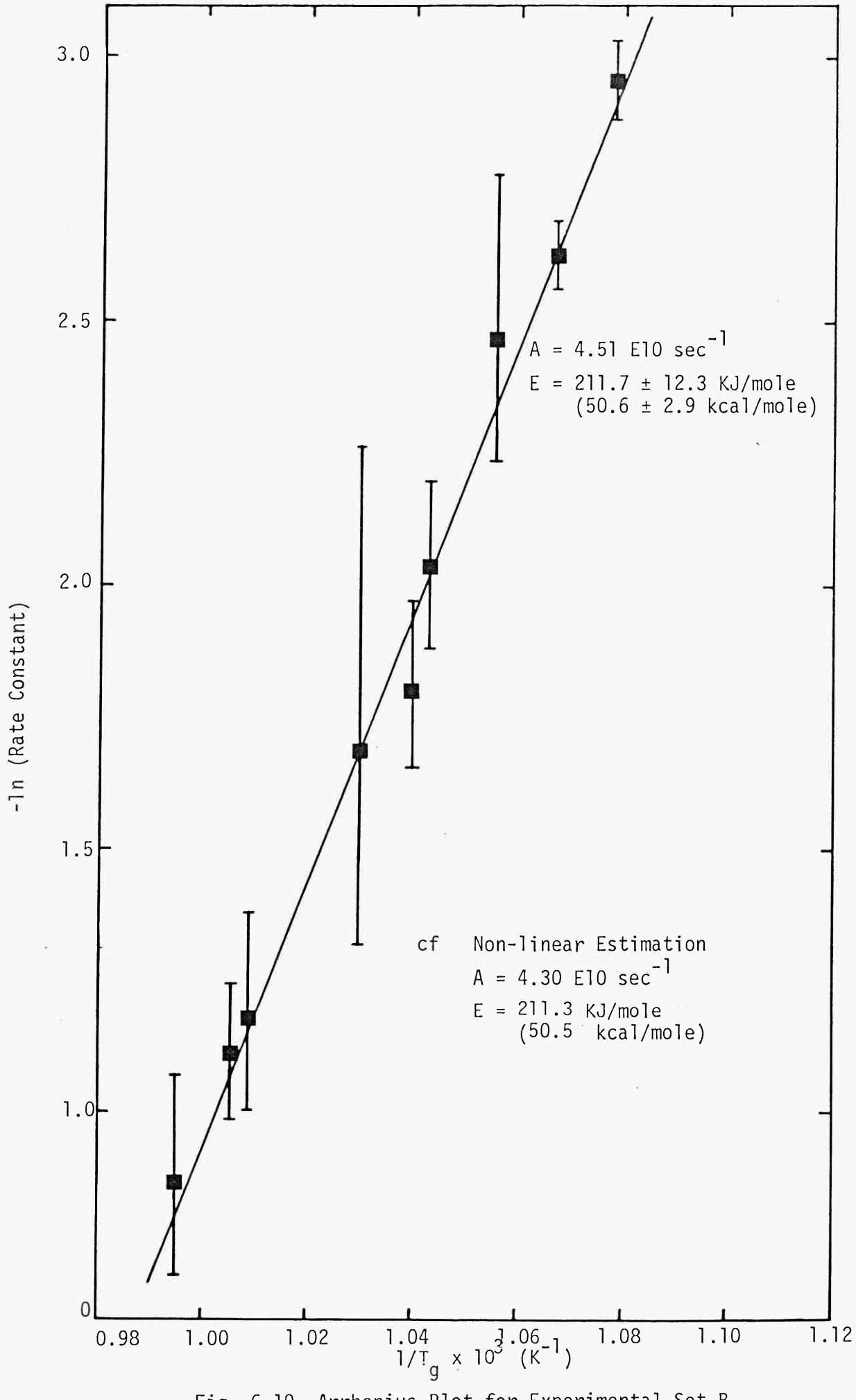

Fig. 6.19 Arrhenius Plot for Experimental Set B

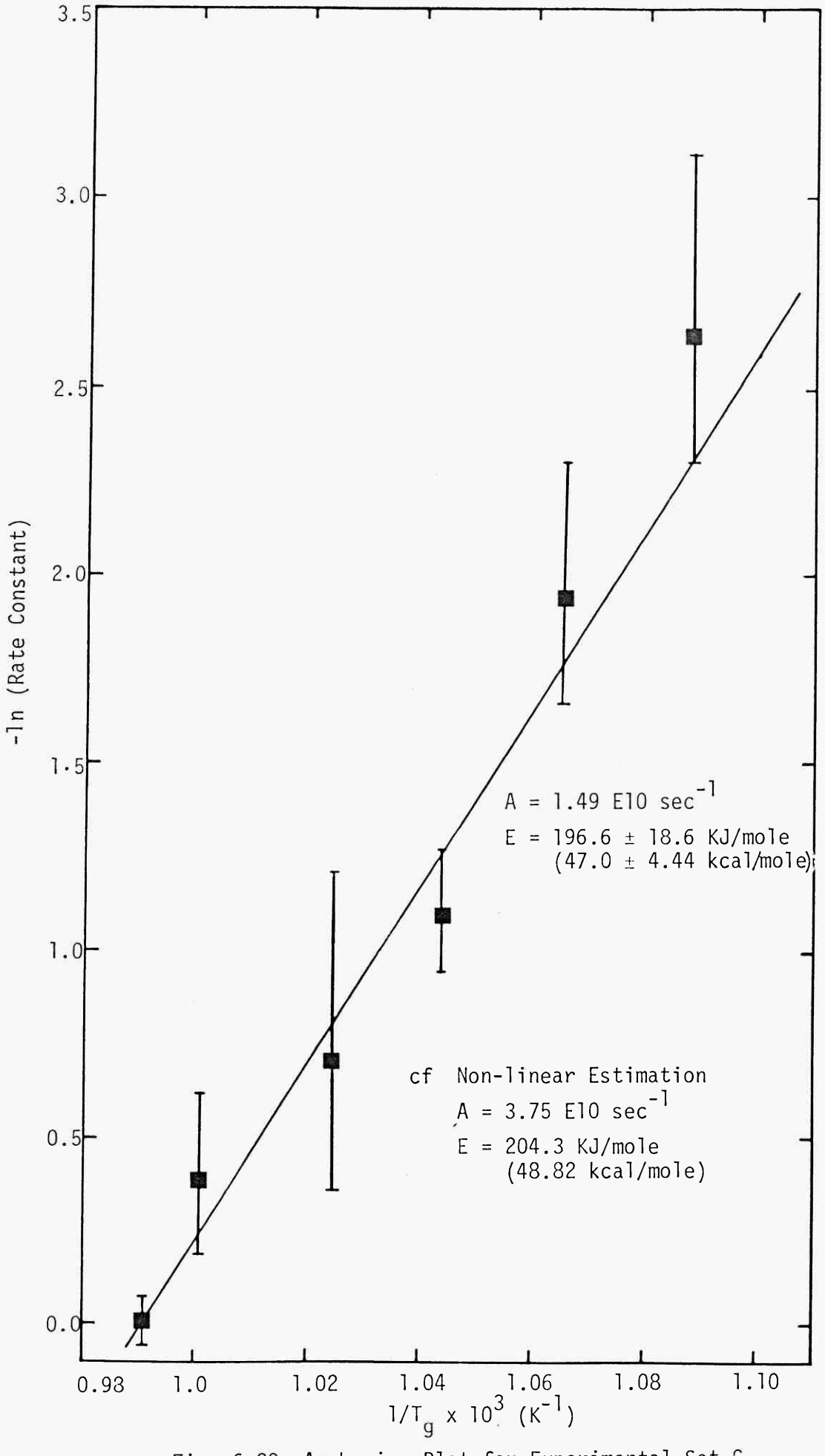

Fig. 6.20 Arrhenius Plot for Experimental Set C

and the method is described in Appendix VII. This is not the case for the non-linear regression and a procedure similar to that described in Chapter 4, Section 4.9 would need to be adopted.

The procedure revealed similar activation energies for Runs A and B but a slightly lower value with set C. The rate constants for the runs in set C were however predominantly higher than those in set A and set B and the implications of these findings are discussed in Chapter 7, Section 7.3.

6.5 Kinetic Modelling of the Product Distribution

The kinetic model proposed by Edelson and Allara (1980) and discussed in Chapter 5, Section 5.8, was used to predict experimental product yields from two experimental runs in set A , run 5 (Tg = 939.3 K) and run 7 (Tg = 970.0 K). The differential equations for this model, generalised by equation (5.1) were integrated using Gear's method from the entrance of the experimentally determined isothermal region in each run, using the measured molecular yields as initial conditions for the model. The radical concentrations were assumed zero but were very quickly established in the early stages of the integration. The simulations discussed in Chapter 5 suggested that little error would be incurred by such a procedure and Fig. 6.21 confirms this for run 5.

Figure 6.22 shows the prediction of the pyrolysis rate as a function of the calculated axial position along the reactor for run 5. Clearly the overall rate of butane disappearance is well below that obtained experimentally. This was observed for both the simulations and with both cases the observed rate was approximately double that predicted. Figures 6.23 and 6.24 present the predicted product yields as a function of conversion and there is a good fit for both the simulations. A slight discrepancy is observed for the product yield of methane which is lower than that measured.

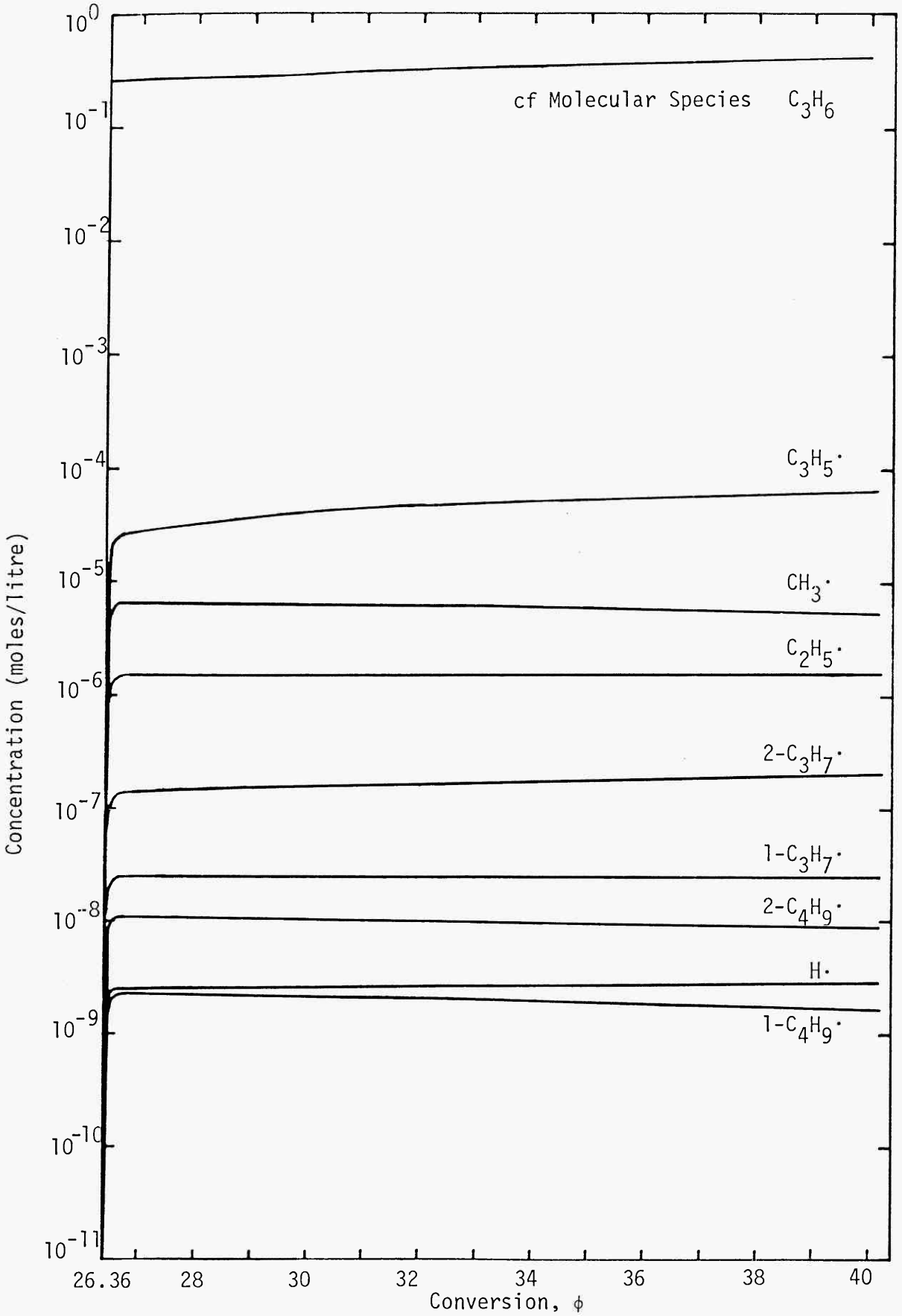

Fig. 6.21 Predict Radical Concentrations for Conditions in Experimental Run 5 (Rate Data of Allara and Shaw)

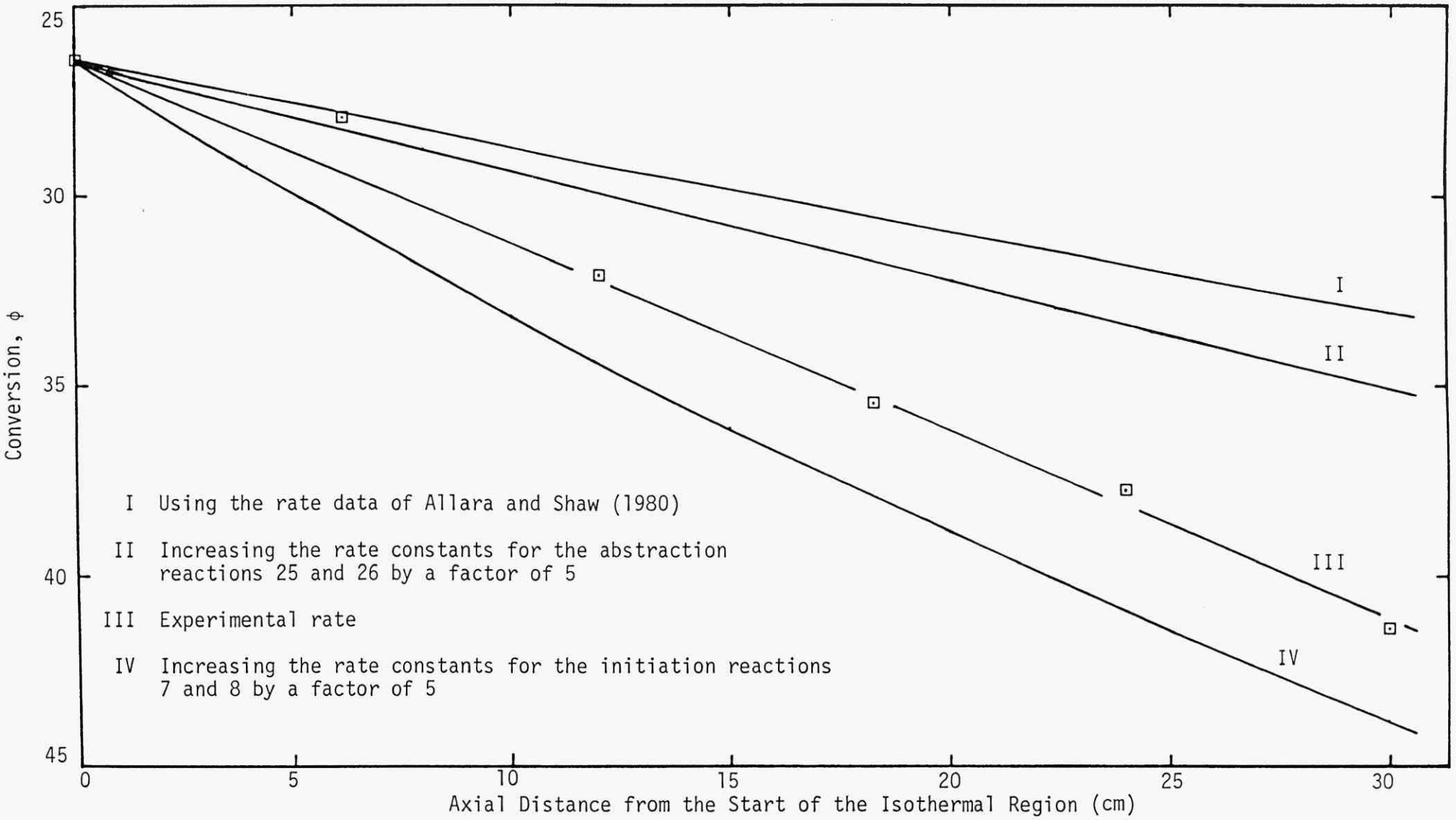

Fig. 6.22 Predicted Butane Decomposition Rate using the Model of Edelson and Allara, (1980), Experimental Run 5 (Tg = 939.3K)

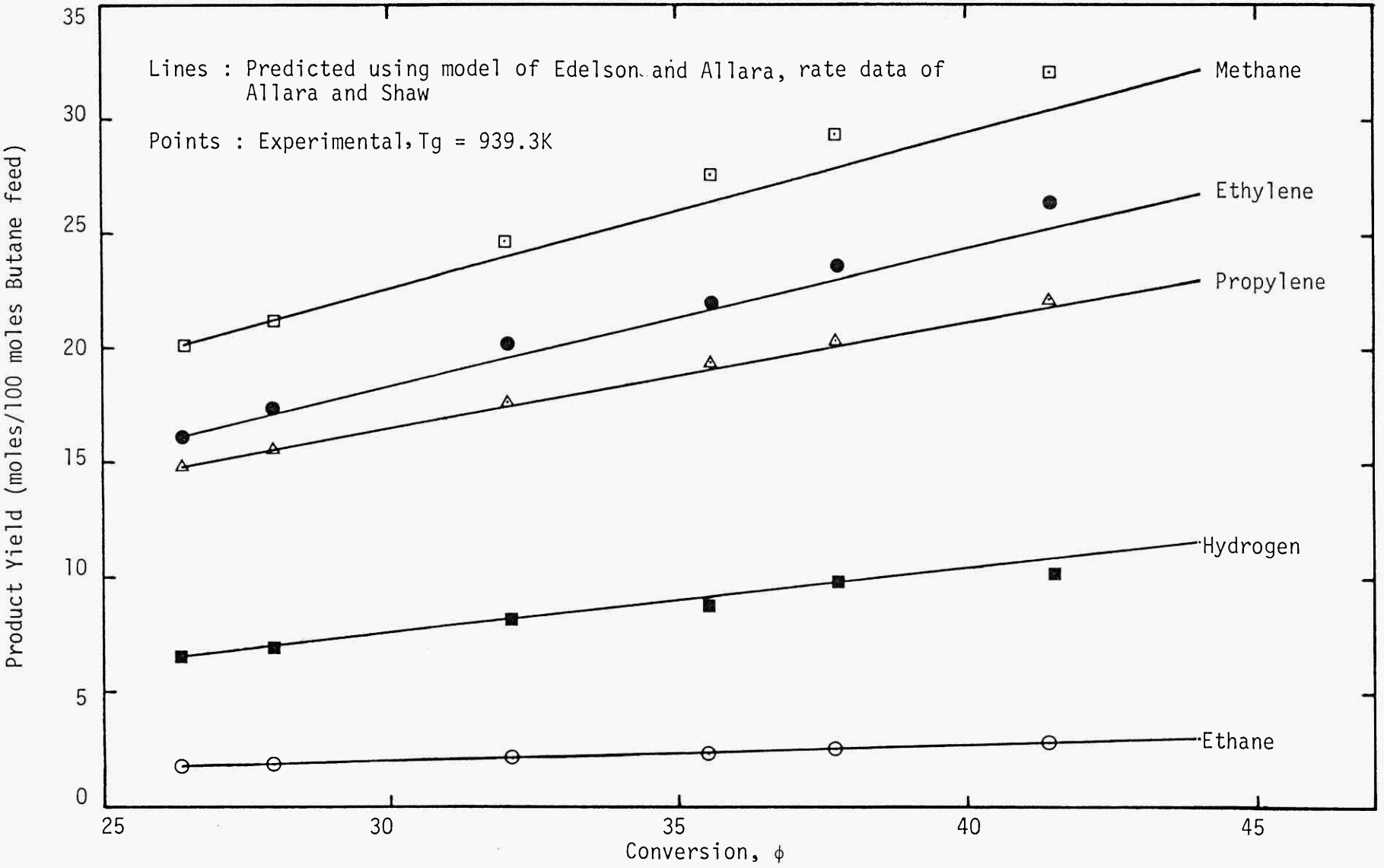

Fig. 6.23 Product Distribution vs. Conversion for Experimental Run 5

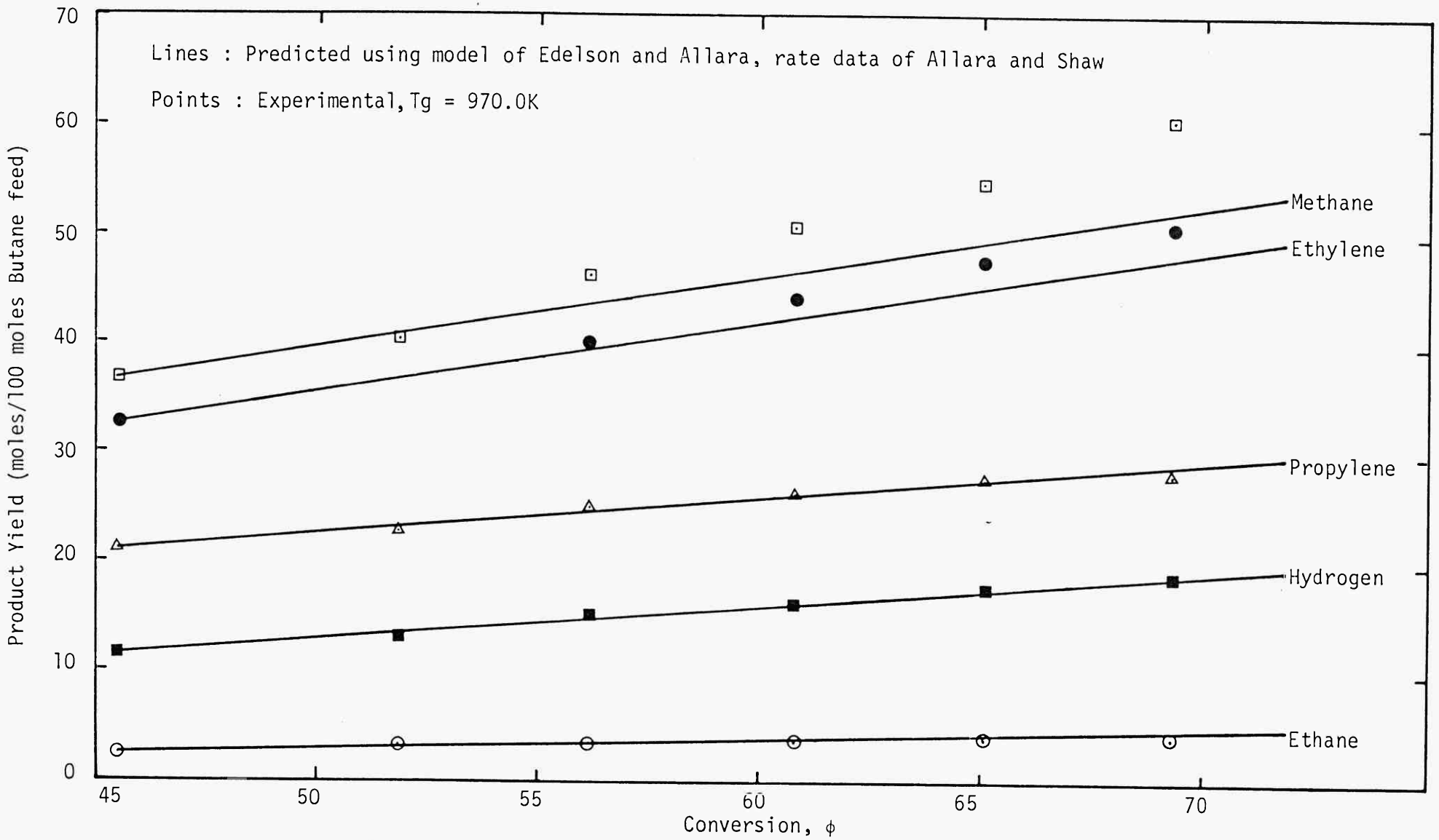

Fig. 6.24 Product Distribution vs. Conversion for Experimental Run 7

Two further simulations were performed principally to observe the effect probable errors in the rate data might have on both the simulated product distribution and the simulated decomposition rate of butane. A sensitivity analysis by Edelson and Allara (1980) indicated that the expressions whose rate data had most influence were:

	Expression No. (see Table 5.5)
$C_4H_{10} \rightarrow CH_3\cdot + 1\text{-}C_3H_7\cdot$	7
$C_4H_{10} \rightarrow 2C_2H_5\cdot$	8
$C_4H_{10} + CH_3\cdot \rightarrow 1\text{-}C_4H_9\cdot + CH_4$	25
$C_4H_{10} + C_2H_5\cdot \rightarrow 1\text{-}C_4H_9\cdot + C_2H_6$	26

Under experimental conditions pertaining to run 5 an increase in the rate data by a factor of 5 for the two initiation steps 7 and 8 produced little change in the product distribution, presented in Fig. 6.25, but revealed a marked increase in the decomposition rate as illustrated in Fig. 6.22. An increase in the rate data by the same magnitude for the two abstraction reactions 25 and 26 resulted in an effect quite opposite to that for change in the initiation rate data. More effect was produced with the product distribution, see Fig. 6.26, than the decomposition rate presented also on Fig. 6.22. In both simulations the change in rate data was well within the bounds of recognised uncertainty (Allara and Shaw, 1980) and this is discussed in greater detail in Chapter 7, Section 7.4.

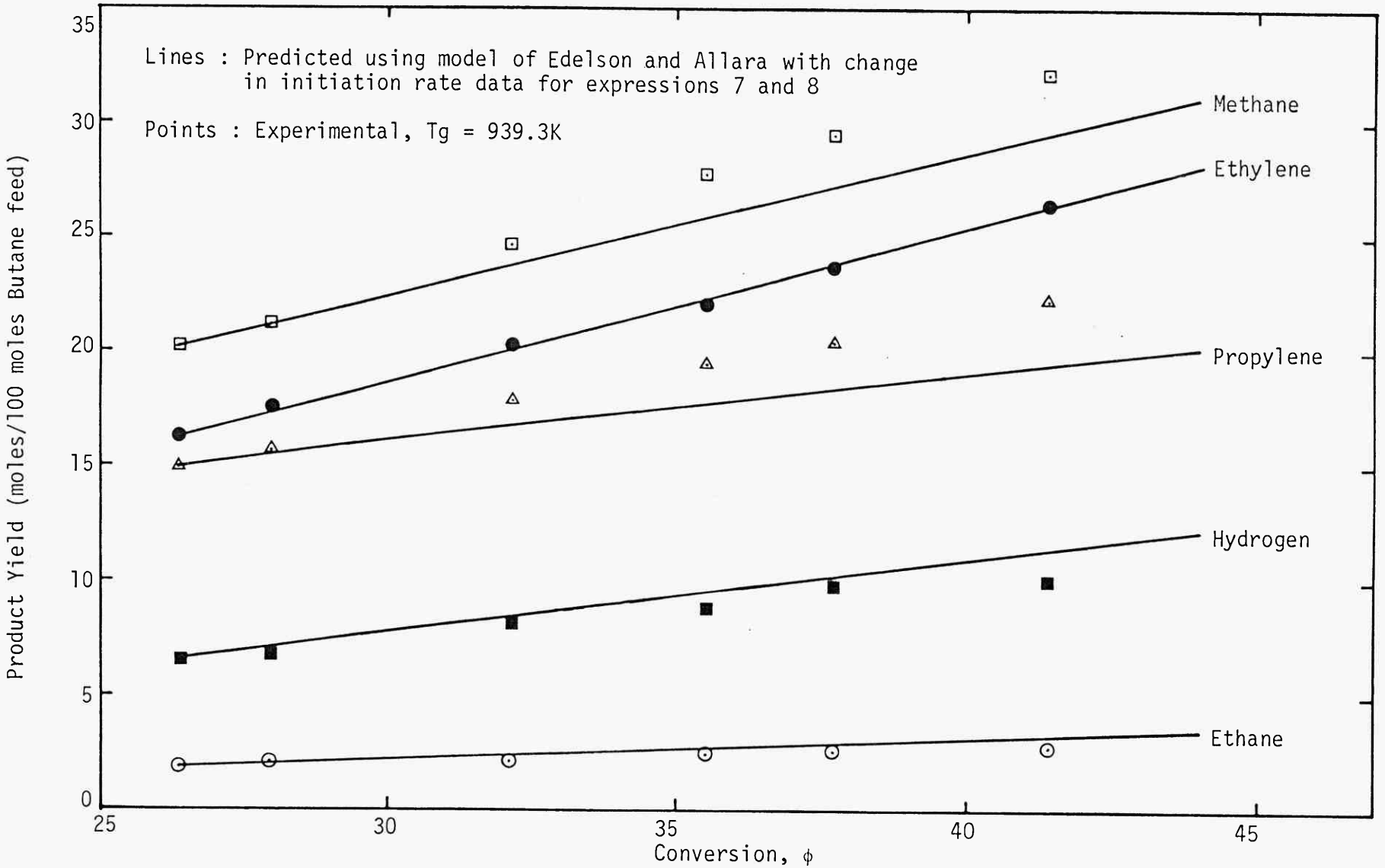

Fig. 6.25 Product Distribution vs. Conversion for Experimental Run 5

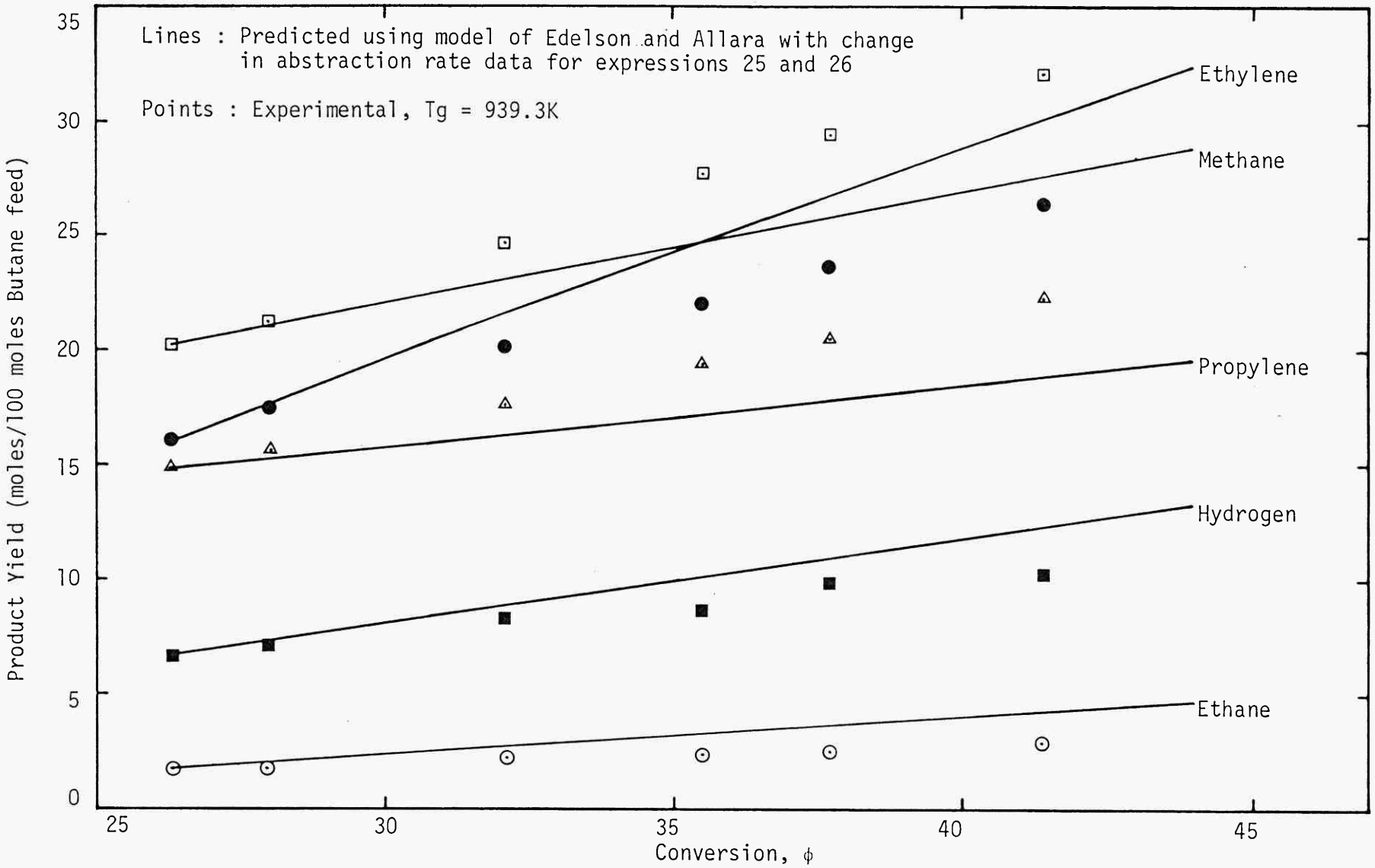

Fig. 6.26 Product Distribution vs. Conversion for Experimental Run 5

CHAPTER 7

DISCUSSION OF EXPERIMENTAL RESULTS

The major objective of this work has been to establish an experimental technique which adds credibility to the reliability of the data for the pyrolysis of butane. In addition it has been noted that it is vital to rigorously test and justify the application of any mathematical model to evaluate the kinetic information obtained from the experiments. The great care and detail taken to obtain reliable data would prove meaningless without such an operation. By proceeding in this manner there can be more confidence in the accuracy of the kinetic parameters and this leads to a more objective and worthwhile discussion on discrepancies between values reported from this study and values reported in previous literature.

7.1 Comparison of Product Distribution with Previous Literature

There have been a number of studies on the product distribution in the pyrolysis of butane. The low temperatures used in many studies meant investigation in the 0 - 20% conversion range. Froment et al (1977) studied butane pyrolysis in a pilot plant reactor in the temperature range 650 - 850^{o}C and determined that the product distribution was a function of conversion, total pressure, temperature and the partial pressure of butane. On plotting the product yields against conversion the influence of temperature was found to be negligible in the range investigated. With methane the yield appeared to be independent of both temperature and butane partial pressure and this agrees with the findings in this study. A contrast is apparent between Froment's data and that reported here regarding the influence of temperature on the product distribution. Pacey and Purnell (1972b), Hill (1977), Sandler and Chung (1961) and Illés and Szalai (1979) all report the propylene yield is sensitive to temperature.

They agree with this study that in the temperature range studied lower temperatures favour propylene production and conversely that higher temperatures favour production of ethylene. This is consistent with the idea that lower olefins are more thermally stable than higher olefins. Higher olefins are reported to decompose into lower olefins and produce other secondary products such as 1,3 butadiene.

Yields for hydrogen and ethane are similar to those previously reported (e.g. Sandler and Chung, 1961; Sundaram and Froment, 1978a). Quantitatively it is difficult to compare product yields since the distribution depends to some extent on the catalytic activity of the reactor material, the S/V ratio of the reactor, reactor pressure and on the temperature range used in each study. Most of the minor products detected have been reported in previous literature. It is generally accepted that they account for no more than 3 - 4% mole/mole of the product distribution upto moderately high conversions. This was also determined in this study, see Fig. 6.11. Sundaram and Froment (1978a), Purnell and Quinn (1962) and Sandler and Chung (1961) have all detected minor products similar to those detected in this study. Sundaram and Froment (1978a) in addition measured small quantities of acetylene and Purnell and Quinn (1962) measured small quantities of 1-pentane both of which were not measured. Very small traces of what is believed to be methylacetylene detected in this study have not been reported in previous literature.

It has been common in the past to represent the primary reactions by a stoichiometric molecular reaction scheme from which the initial selectivity at zero conversion for the primary products can be estimated. Steacie and Puddington (1938) found the reaction products could be represented as

$$C_4H_{10} \rightarrow {}^2/_3\ CH_4 + {}^2/_3\ C_3H_6 + {}^1/_3\ C_2H_4 + {}^1/_3\ C_2H_6$$

More recently Sandler and Chung (1961) proposed the following

$$0.62\ (C_4H_{10} \rightarrow CH_4 + C_3H_6)$$

$$0.25\ (C_4H_{10} \rightarrow C_2H_4 + C_2H_6)$$

$$0.06\ (C_4H_{10} \rightarrow 2C_2H_4 + H_2)$$

$$0.07\ (C_4H_{10} \rightarrow C_4H_8 + H_2)$$

This scheme seemed to account for the reported observation that ethylene yields were normally considerably higher than those for ethane.

Since the lowest conversion data from this study is approximately 10% any extrapolation to zero conversion might incur a considerable degree of error.

Figure 6.12 indicates initial selectivities for methane and propylene of approximately 70 - 75% and 60 - 65% respectively. Sandler and Chung's reaction scheme predicts a value of 62% for both products. Initial selectivity for ethylene appears to be higher with a value $\sim$ 50% compared to the predicted value of 37%. Similar discrepancies are noted for hydrogen and ethane selectivity. Clearly this stoichiometric relationship does not fit well with the experimental data collected in this study. Even accounting for the inaccuracies incurred by extrapolation this indicates that a stoichiometric relationship of this relative simplicity is not complex enough to efficiently describe the primary product distribution of the pyrolysis.

7.2 Generation of the Rate Constants from the Isothermal Data

Having experimentally verified the data from each experimental run as isothermal, calculation of the global rate constant for the butane

decomposition was achieved in three different ways as discussed and presented in Chapter 6, Section 6.4.

The simultaneous estimates of the rate constant incorporated in the parameter β and radial dispersion coefficient incorporated in the parameter α, see Chapter 4, Section 4.3, appear to be of two distinct varieties. Some runs are characterised by large estimates of α and estimates of β which correspond closely to estimates from the same data using the plug flow model. In other cases the estimates are characterised by low values of α and accordingly the estimates of β significantly deviate from the plug flow estimates. Superficially this might be explained by suggesting that the simultaneous estimate of α truly reflects the experimental conditions within the reactor. If this is the situation then there are some runs where factors other than molecular diffusion are contributing to the efficiency of radial mixing whilst in others this contribution is completely lacking and the molecular diffusion dominates. This seems unlikely since if this were true some correlation would be expected between the a priori estimate and the simultaneous estimate of α. This does not appear to be the case. Furthermore, there is no logical, physical explanation why these runs should be particularly different from those runs where large values of the simultaneous estimate of α were obtained.

A second, alternative suggestion appears more logical and consistent. Providing sufficient experimental data points are available any non-uniformity in the distribution of experimental errors around the correct model will become sufficiently uncorrelated that a good fit to the experimental data will be procurable with model parameter estimates which closely reflect the correct values. Furthermore, decrease in the data error variance decreases the parameter estimate variance (e.g. for

a linear system see equation (4.10)) and the estimates become progressively more accurate and less sensitive to any non-uniformity in the experimental error distribution around the model fit.

In the situation, however, where a poor distribution of errors around the true model is coupled with an excessively large error variance, biased estimates of the model parameters will be generated from the model fit. This seems to explain the random variation of the simultaneous estimation of the α and β parameters with the RDM. As discussed in Chapter 3, Section 3.4, the long elution times for the measurement of the product components meant only a limited number of experimental points could be taken from within the reactor during each typical run. Normally this number was limited to nine, of which six were situated within the isothermal region. With only six points there is a finite probability that biased estimates will be obtained if the experimental error distribution around the correct model is poor and the error variance is not small enough to minimise the consequences of this poor distribution. In these instances, since the radial dispersion model has more adjustable parameters than the plug flow model, the fit to the data will tend to be closer with a smaller estimated error variance. However, the model fitting generates parameter estimates which are not indicative of the true solution and in these instances these values must be considered having no fundamental importance.

The decrease in adjustable model parameters with the plug flow model restricts the mobility of the plug flow model to accurately fit the data and in this respect a more accurate estimate of the rate constant should ultimately be obtained.

It seems therefore that although satisfactory estimates of the rate

constants have been attained the number of available experimental points during some runs was too small to minimise the effect of the apparent correlation created by the errors incurred during the experimental measurement.

From the runs where there is little correlation the estimates of the rate constant are similar from both the simultaneous estimation and the plug flow estimation. Moreover, the estimated radial dispersion coefficient is much larger than the a priori values which suggests some supplementary radial mixing is occurring besides diffusion; this is probably the result of natural convection currents superimposed onto the forced convection. Mixed convection occurs primarily for laminar flow and depends upon the relative magnitude of the Reynolds number, Prandtl number and Grashof number. The increased heat and mass transfer is a result of bouyancy forces present in the flowing gas due to local temperature and density variation.

Eckert and Diagula (1954) studied mixed convection in a tubular pipe with its axis parallel to the direction of gravitational acceleration and developed some equations which bounded conditions when free convection is significant. Typical Reynolds numbers and Grashof numbers for this system indicate that free convection is occurring within the reactor, see Appendix XIII. The effect of this additional convection is to increase heat and mass transport both radially and axially within the bulk of the gas and would explain the large estimates of α. Since the radial dispersion coefficient is not simply the molecular diffusivity the one dimensional axial dispersion model might give estimates of the rate constant as accurate as the radial dispersion model for experiments in this reactor under conditions similar to these.

Attempts were also made to globally model the rate of generation of the products from the decomposition. Previous contributions include that by Powers and Corcoran (1974) who determined that the orders of reaction with respect to butane for the various products were not equal and varied from 1.15 to 1.67. If as a first approximation first order is assumed then the initial rates of production for each product is given by the rate of butane disappearance times each product fractional selectivity. If the fractional selectivity remains unchanged as the reaction proceeds under isothermal conditions then the first order approximation holds well. A preliminary investigation using data from this reactor shows that at low conversions this is an acceptable approximation. The limited data however near zero conversion limits the value of such an analysis from this study.

7.3 Comparison of the Arrhenius Parameters with Previous Literature

The global Arrhenius parameters from this study for the kinetics of the butane decomposition fall towards the lower end of a range of values previously reported in literature. To facilitate a comparison between reported values and values estimated in this study, Table 7.1 was constructed which summarises all the important contributions previously made towards analysis of the butane global kinetics. Included in the table for each contribution there is a concise discription of the reactor, reactor material and other important features which prove relevant during the subsequent discussion.

The whole range of parameters in Table 7.1 illustrate effectively the confusion in literature regarding the characteristics of the global kinetics. The studies have been over a wide range of temperature, 450 - 900^{o}C, and have been carried out in both static and flow reactors. In both types of reactor, reactor material of known catalytic activity

TABLE 7.1

Summary of Previous Work on the Global Kinetics of Butane Pyrolysis

Reference	Reactor Details	Temperature Range (°C)	Conversion Range	S/V ratio cm^{-1}	Assumed Order of Reaction	Activation Energy (Kcal/mole)	Pre-exponential Factor (sec^{-1} or litre $mole^{-1}$ sec^{-1})	Other Comments
Pease and Durgan (1930)	Continuous glass flow	625-650	0-35	-	1	65.0	-	First order rate constant falls as conversion increases Heterogeneous contribution thought <1% of the total reaction.
Paul and Marek (1934)	Continuous flow reactor, copper and fused silica	530-625	0-9	12.8	1	73.9	3.16×10^{17}	No heterogeneous contribution observed
Steacie and Puddington (1938)	Static Quartz	513-572	0-50	-	1	58.70	5.13×10^{12}	Product composition not a function of temperature and pressure over studied range First order constants fall off as reaction proceeds
King, Sandler and Chung (1959)	Continuous flow vycor, stainless steel, chromium iron	650-850	0-90	-	1	40.0	1.0×10^{9}	

TABLE 7.1 (cont/d...)

Reference	Reactor Details	Temperature Range (°C)	Conversion Range	S/V ratio cm^{-1}	Assumed Order of Reaction	Activation Energy (Kcal/mole)	Pre-exponential Factor (sec^{-1} or litre $mole^{-1}$ sec^{-1})	Other Comments
Sandler and Chung (1961)	Continuous flow, vycor glass	700-900	0-90	-	1	45.60	9.55×10^{9}	Most runs in annular reactor space. Use of novel reactor design to improve mixing. Other experiments included runs with a silica reactor, annular porcelain reactor
Kupparman and Larson (1962)	Static reactor Material unknown	480-570			1	52.5	1.7×10^{10}	
Wang et al (1963)	Continuous flow, quartz reactor, internal diameter = 1 inch	460-560	0-10	~1.6	1	54.6	3.34×10^{12}	Axial length of reactor adjustable
					2	56.8	2.55×10^{14}	Sampling at the exit, radially also. Reynolds number ~2000
Sagert and Laidler (1963)	Static quartz	520-590	0-15	~3	$^{3}/_{2}$	59.9	3.24×10^{15}	Experiments included 11.6 fold increase in S/V ratio

TABLE 7.1 (cont/d...)

Reference	Reactor Details	Temperature Range (°C)	Conversion Range	S/V ratio cm^{-1}	Assumed Order of Reaction	Activation Energy (Kcal/mole)	Pre-exponential Factor (sec^{-1} or litre $mole^{-1}$ sec^{-1})	Other Comments
Illés (1969)	Continuous flow quartz, internal diameter, 8mm length 110cm	600-820	0-100	2.0	1	52.2	6.4×10^{11}	Atmospheric pressure sampling at exit of reactor Average Re ~200 Rate constant inhibited by products in the form $K = K_o - \beta\phi$ for 1st order kinetics
Froment et al (1977)	Continuous flow nickel chromium alloy (Sandrik/ Sanicro31), internal diameter = 10 mm length 21.75 metres	650-850	0-100	4.0	1	i. 49.090 ii. 48.720 iii. 49.210 iv. 50.450	i. 7.3×10^{10} ii. 6.7×10^{10} iii. 7.1×10^{10} iv. 1.4×10^{11}	Initial partial pressure butane variation i. 1.2 atm. ii. 0.8 atm. iii. 1.4 atm. iv. 1.0 atm. Steam dilution ratio also varied. Equivalent reactor volume concept used. Reynolds number 4,500 - 7,000
THIS STUDY	Continuous flow Inconel 600 reactor, internal diameter 5.25cm, length 180cm	650-715	7-85	0.8	1	50.87	6.32×10^{10}	SET A Reynolds number ~80
		645-735	14-85	0.8	1	50.60	4.51×10^{10}	SET B Reynolds number ~80
		645-740	10-83	0.8	1	47.00	1.49×10^{10}	SET C Reynolds number ~160

and reactor material of known limited catalytic activity have both been used. The use of catalytically active reactor materials gives rise to the possibility of heterogeneous reactions at the reactor surface in addition to the homogeneous reaction occurring within the reactor. In spite of the proven catalytic nature of many of the reactor materials used, previous workers have failed to assess fully the influence of possible interactions with the reactor wall, generally assuming the reaction to be fully homogeneous. A preliminary inspection reveals that in general the activation energies from the quartz reactors are higher than those from stainless steel reactors. Moreover, the general lack of reported radial and axial composition and temperature measurements within the reactor call for discussion on the possibility of heat and mass transfer limitations which might have existed with many of the previously report studies.

The reactor material used in this study was Inconel, comprising approximately 76% w/w nickel, 1% w/w manganese, 15% w/w chromium and 8% w/w iron. The activity of nickel and iron has been clearly demonstrated by Crynes and Albright (1969) for propane pyrolysis in the range 600 - 750^{o}C. They determined that nickel reactors were effective in promoting secondary reactions, especially if pretreated with steam. The effect of chromium has been studied by King, Sandler and Chung (1959) who determined that carbon was not deposited on stainless steel surfaces which had been chromium plated. Furthermore, they noticed that there was a substantial improvement in the ethylene selectivity. Cambron and Bayley (1933) found that 18/8 Cr-Ni stainless steel was unsuitable for pyrolysis of the lower paraffins due to excessive carbon formation but claimed nickel free alloys containing over 20% w/w chromium were satisfactory.

The situation becomes more complex if the catalytic activity of the reactor surface is such that carbon is deposited since carbon coatings are known to be highly reactive (e.g. Purnell and Quinn, 1961; Volkan and April, 1977). In this event the rôle of the surface may actually alter depending on the time of reactor operation. Beshty (1978) recently discovered that catalytically reactive atoms from the surface can actually diffuse through the carbon to regain contact with the reacting mixture. Clearly the reactor in this study can influence the butane decomposition through heterogenous reactions with the surface.

Since the main objective is to determine intrinsic chemical parameters it is important to ensure that the process is not restricted by heat or mass transfer limitation rather than the chemical kinetics which are characterised by these chemical parameters. The possible effects of heat transfer limitations were confidently excluded after taking direct gas and wall temperatures under all the conditions from which the kinetic data was extracted. A boundary layer must exist near the reactor wall because the gas temperature is lower than the wall temperature. The lack of temperature gradients measured both radially and axially showed, however, that the reaction was not limited by heat transfer within the bulk of the gas but by the chemical kinetics of the decomposition reaction. Since the pyrolysis reaction is endothermic this condition would be more difficult to achieve for undiluted systems unless radial heat transport was very rapid, such as in turbulent flow.

It is conceivable that the change in Reynolds number in the runs for set C might alter this condition to the point where heat transfer limitations might become more important, since the temperature difference between the gas and wall is higher than for the runs in set A and set B.

Extensive measurements disclosed that within the bulk of the gas the temperature still remained isothermal and that the majority of the temperature drop must therefore still be across a thin boundary layer near the wall. The rate constants were then computed from the corrected temperatures due to convection and radiation between the thermocouple probe, the process gas and the reactor wall. In this way any heat transfer effects became of secondary importance.

Confidently dismissing any possible heat transfer limitations as being secondary indicates that the primary reason for any change in the observed kinetics will be change in mass transfer limitations between the bulk gas and the reactor wall surface. Then at the reactor wall the rate of heterogenous reaction will equal the mass transfer rate of reactant from the bulk gas through the boundary layer to the wall.

Experimental runs in set A and set B were achieved with approximately identical Reynolds number. Then any mass transfer through the boundary layer which determines the heterogeneous contribution to the reaction kinetics remains constant and its effect is minimised. Consequently the kinetics of the homogeneous reaction will be more closely reflected in the overall kinetics which are observed. The study in both sets covered a wide range of conversion 7 - 85% and a similar gas temperature range 650 - 730^{o}C. In addition the data were analysed assuming an order of 1 which was independently checked by a change in feed composition between the two sets. The results revealed an almost identical activation energy of 50.7 kcal/mol (212 KJ/mole) but pre-exponential factors which differed by $\sim$ 30%, see Table 7.1. The reason for the difference in pre-exponential factor is not entirely known but may be caused in part by a constant bias detected in the measuring instrument used to

monitor the axial wall temperature profile in the runs in set A. For further comment, see Appendix IV.

Experimental runs in set C were devised to confirm the suspicion that the heterogeneous contribution is significantly large that it will affect the overall observed kinetics. Runs in set C were identical to runs in set A in every aspect except that the mass velocity was approximately doubled. Since the reactor geometry was unchanged the net effect was doubling of the Reynolds number. The results from set C gave rate constants approximately twice as large as in the first two sets at the same reaction temperature. Although the heat transfer effects have been shown as secondary the larger corrected temperature difference recorded between the wall and the gas for runs in set C makes the calculated gas temperature more sensitive to errors in the parameters in equation (3.1) than for set A and set B. This is important because substantial errors in the emissivity and heat transfer coefficient are most likely. This would generate the effect of moving the Arrhenius plot illustrated in Fig. 6.21 for set C closer to those for sets A and B and would thus tend to alleviate the observed difference in apparent rate constants calculated from runs in set C. Under typical thermal conditions reported in each data set the calculated gas temperature for runs in set C are approximately 3 times more sensitive to parameter errors in equation (3.1) than for set A and set B. The calculations described in Appendix IV show, however, that this effect is unlikely to account for more than 25% of the discrepancy between the observed rate constants from set C and the first two sets.

The majority of this increase might therefore be related to increased mass transfer to the wall. Although the factors affecting the radial concentration within the reactor are complex this general trend is

predicted by general boundary layer theory for mass transfer in laminar flow. The Sherwood number based on the axial distance from the reactor inlet (Z) is given by

$$Sh_Z = \frac{K_m Z}{D_m} = (\text{Constant})\ Sc^{1/3}\ Re_Z^{1/2} \qquad (7.1)$$

where D_m is the molecular diffusion coeffient. Thus the local mass transfer coefficient, K_m, is greater at higher mass velocity, as observed in this study. The developing velocity and temperature profiles upstream of the isothermal region, coupled with such complications as natural convection effects and homogeneous reaction prevent a rigorous application of the boundary layer theory. Nevertheless if the General Film Theory is assumed the boundary layer thickness is given by

$$\delta = \frac{D_m}{K_m} \qquad (7.2)$$

which suggests a decrease in the mass transfer boundary layer thickness with an increase in the Reynold's number.

The increased mass transfer associated with this increases the heterogeneous contribution which accordingly increases the overall rate of reaction. However, the diffusive process to the wall is complicated by the thermal boundary layer through which the reacting fluid elements must travel before encountering the wall. The supplementary reaction occurring due to the higher temperatures will subsequently increase the mass transfer boundary concentration gradient, which will enhance apparent diffusion of reactant away from the bulk gas. The larger thermal gradients for the runs in set C result in this effect being more substantial for these runs than those in sets A and B, and accordingly part of the increase in the rate of reaction is associated with a homo-

geneous contribution and cannot be attributed solely to heterogeneous effects. The slight decrease in the overall activation energy compared to the values from set A and set B is not inconsistent with the idea of an increased heterogeneous contribution since the activation energy associated with the wall activity is most likely lower than the activation energy characterising the homogeneous contribution. However, because it was more difficult to maintain an isothermal region for these runs the uncertainty in the estimated rate constants is higher than in sets A and B. A statistical analysis indicated that the activation energies from all three experimental sets were not statistically different from each other at a significance level of 5% (see Appendix VII).

The experimental preparation made in this study has restricted the possible extraneous factors which have generated a spectrum of global parameters as previously reported and presented in Table 7.1. Activation energies vary from 40 Kcal/mole to 73.9 Kcal/mole and pre-exponential factors from 10^9 sec^{-1} to as high as 3.16×10^{17} sec^{-1}. The results for this study are in good agreement with that by Froment et al (1977) and Kupparman and Larson (1962). Correlation with the results of Froment et al are improved further since their study was carried out in a nickel chromium alloy reactor and a temperature range similar to those in this study. Of all the previous studies made on butane pyrolysis these pilot scale studies are most likely to approximate the assumption of plug flow when no radial temperature or composition profiles exist. This is because the average Reynolds number was $\sim$ 6000 which is approaching the region when fully turbulent conditions are achieved. Even so their use of the equivalent reactor volume concept because of the steep axial temperature gradients experienced cannot add credibility to their results.

Most of the other studies are characterised by use of static and continuous flow reactors almost invariably fabricated from quartz or glass. Some catalytic activity by quartz has been observed. Voevodsky (1959) and Laidler et al (1962) both observed a reduction in the reaction rate for propane pyrolysis in static quartz reactors when the S/V ratio was increased in the temperature range 580 - 650°C. Sagert and Laidler (1963) observed a decrease in the rate for butane pyrolysis in a static quartz reactor in the range 520 - 590°C. A significant heterogeneous influence from the nickel chromium reactors will restrict the compatability of comparing data from the work with that from the quartz reactors. If the decomposition could be shown to be almost totally homogeneous with little heterogeneous contribution irrespective of the reactor material then any discrepancy between results from this work and from previous work in quartz reactors could be related to variation in experimental technique and theoretical analysis.

The results from this work however indicate that heterogeneous contributions from nickel chromium reactors can influence the overall observed kinetics within the temperature range studied. This disagrees with Pratt and Rogers (1979) and with earlier work (e.g. Pease, 1928; Frey and Smith, 1928) who discovered the reaction appeared first order and homogeneous with no effect on the kinetics from variation in the reactor S/V ratio or change in the reactor material. King, Sandler and Chung (1959) discovered that surfaces containing nickel and iron promoted undesirable secondary reaction products under high temperature and long residence time conditions. In any event, the consequences of the observed increase in apparent rate constant when the flow rate was increased in set C prohibits a direct comparison between results from

this study and those from the quartz reactor studies.

Results from the static quartz reactor studies gave similar activation energies but a difference of $\sim$ 1000 between the pre-exponential factors. Steacie and Puddington (1938) reported an order of 1 and a rate constant which fell off as reaction proceeded. Sagert and Laidler (1963) observed an order of $^3/_2$ with no fall off during reaction. The discrepancy in noted order may account for the observed fall off in the apparent rate constant. Studies with continuous flow quartz reactors generally give activation energies lower than with the static reactors but still higher than the values determined in this study. Illés (1969) reports a value similar to that determined here but noted the rate constant fell off due to proposed inhibition from the reaction products. The method of data collection was from the reactor exit only which required subsequent changes in the throughput to obtain a full set of kinetic data. Flow conditions in the reactor were such that the average Reynold's number was $\sim$ 200, clearly in the laminar flow regime.

The reported higher activation energies with the continuous flow and static quartz reactors is probably due to the heterogeneous effects of the reactor surface. Increase in the S/V ratio with quartz as reactor material seems to decrease the rate of decomposition of butane, indicating an increase in overall activation energy is to be expected. In this study the heterogeneous effect appears to increase the overall decomposition rate which would have a lower overall activation energy associated with it. Clearly the catalytic effects between the two materials is quite different. Sagert and Laidler (1963) suggest that the quartz activity is present because of the effects on the homogeneous

radical chain reactions created by termination and initiation of radicals occurring at the reactor wall, and its effect would diminish and become less important at higher temperatures than those used in their study, 520 - 590^{o}C. Nickel containing reactors are said to aid in promoting secondary reactions although probably the catalytic activity is not restricted to these reactions alone.

In general it is difficult to analyse the factors which might resolve the variation in the reported order and activation energy. Too frequently insufficient information is reported in many studies on how steps were taken to ensure that the experimental data was not taken from a system restricted by heat and/or mass transfer limitations, rather than from the chemical kinetics of the reaction. Furthermore, the illustrated catalytic activity of some reactor materials, particularly those containing nickel and iron e.g. 18/8 stainless steel or Inconel, coupled with the possibility of heat and/or mass transfer limitations can quite adequately describe the variation of the reported global kinetic parameters for the decomposition of butane.

7.4 Kinetic Modelling of the Product Distribution

The homogeneous free radical mechanism proposed by Edelson and Allara (1980) and the rate data coupled by Allara and Shaw (1980) were used to predict experimental product yields from two experimental runs and results are presented in Chapter 6, Section 6.5.

In consideration of the limitations imposed on the model, the simulations which were performed appear to fit the experimental data quite adequately. Although predicted rates of butane disappearance were considerably below that observed experimentally, predicted product distributions appeared to fit well with the experimental data for both the simulations performed.

The experimental data illustrated in Chapter 6, Section 6.2 clearly show that at conversions higher than ∿ 40% the product distribution could no longer be described as a function of conversion alone but that additional variables such as temperature played a leading rôle. One of the factors which could also alter the product distribution is of course the heterogeneous contribution to the butane pyrolysis, and normally this would be reflected in two ways:

(i) The product distribution from the runs in set C should vary from that obtained in set A and set B;

(ii) The homogeneous model, used to predict the product distribution should not fit consistently well with all the experimental product distributions from all the experimental runs.

A slight tendency was observed in the product distribution for set C when compared to the first two sets. Principally, hydrogen and ethylene yields appeared slightly higher and propylene yields slightly lower for set C when compared to the other data sets, under similar conversion and temperature ranges. This would be consistent with the idea in literature that the heterogeneous contribution aids secondary reactions particularly molecular processes such as dehydrogenation. However the indirect way by which the heterogeneous contribution was measured does not provide conclusive evidence that the product distribution is dependent upon the degree of heterogeneous contribution. Only a series of experiments which considerably vary the S/V ratio of the reactor geometry, under isothermal conditions, will help resolve the issue either way. Moreover, the limited number of simulations performed for predicting the product distribution using the homogeneous model adds nothing to

supplement the statement that the product distribution is significantly altered by variation in the heterogeneous effect of the wall.

It is evident, however, that the heterogeneous effect does alter the overall rate of reaction from the experimental runs in set C. It is quite probable that the discrepancy between the predicted and observed rates of butane disappearance in the simulations may be in part due to the lack of heterogeneous contribution to the simulation model. It may also, in part, be due to inaccurate rate data, which is discussed later in this section.

There are several important features of the radical model which should not be overlooked. The model uses rate data collected at temperatures substantially lower than the temperature range used to collect the experimental data being simulated. In spite of the apparent lack of heterogeneous contribution this does indicate the impressive way in which the state of knowledge about the rate data is improving. However since the model was developed and refined for prediction of experimental rates and product distribution at low temperaturers there is a possibility that equations which are not important at low temperatures but which become more important at higher temperatures may have been omitted from the model. For example the isomerisation of the butyl radicals

$$1\text{-}C_4H_9\cdot \rightarrow 2\text{-}C_4H_9\cdot$$

is not included. Sundaram et al (1978a) conclude this is a major reaction at high temperatures since each radical decomposes to generate different major products, see Chapter 5, Section 5.2.

An additional inconsistency in the model equations is the notable absence of any independent reactions which generate the $C_4H_7\cdot$ methylallyl radical.

This radical dominates the production of 1,3 butadiene and the isomeric cis- and trans-2-butenes which are present especially in the latter stages of the reaction. This radical was not generated and hence no change in these product yields were observed in the model predictions. This explains why there is no plot for the predicted product cumulative yield versus that experimentally obtained.

In this study no rigorous calculations were carried out on the sensitivity of the predicted yields to variation in the available rate data. It is difficult to extract any sound information about any individual reaction or reaction set from the overall model simulation without an analysis of this kind. The main conclusions must be limited to the obvious that product distributions agree well with the data from this study although the predicted overall decomposition rate of butane is markedly below the observed rate.

Edelson and Allara (1980) performed a sensitivity analysis using the same model but for data collected in a lower temperature range. This provides a useful procedure to help pinpoint elements of the mechanism which might require further study.

Under the conditions studied in their analysis the initiation and abstraction reactions

$$CH_3\cdot + C_4H_{10} \rightarrow 1\text{-}C_4H_9\cdot + CH_4$$

$$C_2H_5\cdot + C_4H_{10} \rightarrow 1\text{-}C_4H_9\cdot + C_2H_6$$

$$C_4H_{10} \rightarrow C_2H_5\cdot + C_2H_5\cdot$$

$$C_4H_{10} \rightarrow CH_3\cdot + 1\text{-}C_3H_7\cdot$$

have the largest effect on the accuracy of the computed rate for the

given rate data. According to Allara and Shaw (1980) at the temperatures in this study the errors for the abstraction and initiation rate constants are about a factor of 10. Quantitatively it is easy to see why the initiation reactions have such a large influence on the rate of butane decomposition. The initiation reactions that generate the radicals are much slower than those reactions which follow. Thus if the initial reaction rate is effectively accelerated or retarded a large change in the overall rate would be expected. This is the process which occurs during sensitisation which provides an additional source of radicals and inhibition which removes radicals that are initially formed. Since the initiation rate data for butane is not accurately known this could part explain the predicted low decomposition rate. It is worth noting that a change in the product composition might be expected if a change in the initiation rate is made, since the concentrations of the radicals are fixed by the rates at which initiation and termination occur. A typical simulation was carried out to test the sensitivity of the decomposition rate to the accuracy of the initiation rate data by arbitrarily increasing rate of initiation by a factor of 5, within the bounds of accuracy for contemporary rate data. The result on the overall decomposition rate is illustrated in Fig. 6.22 and demonstrates that the predicted rate can easily be adjusted to accurately fit the measured decomposition rate. The idea of the simulation was not this, however, but to illustrate that the observed decomposition rate was within the error bounds of the initiation rate data. The product distribution did not alter appreciably apart from the propylene yield which was lower than previously predicted, see Fig. 6.25.

Compared to the rate of decomposition of butane via abstraction reactions the rate of butane decomposition by initiation is small. The initiation

reactions control the overall rate of disappearance by altering the concentration of the available radicals which partake in the abstraction reactions. The major abstraction reactions which involve butane molecules and which therefore determine the overall rate and subsequent product distribution are the reactions with the alkyl radicals. There is surprisingly little good experimental data on abstraction reactions (Allara and Shaw, 1980) and accuracy is estimated to be about a factor of 10. A simulation was also performed in which the rate constants for the two abstraction reactions

$$CH_3\cdot + C_4H_{10} \rightarrow 1\text{-}C_4H_9\cdot + CH_4$$

$$C_2H_5\cdot + C_4H_{10} \rightarrow 1\text{-}C_4H_9\cdot + C_2H_6$$

were also arbitrarily increased by a factor of 5. An increase of approximately 25% was observed in the overall decomposition rate but most influence appeared to be on the product distribution which altered quite significantly, see Fig. 6.26. This demonstrates quite effectively the sensitivity of the product distribution to variation in the available rate data which still lies within the recognised bounds of acceptable accuracy.

The kinetics which control the overall rate of disappearance and the subsequent product distribution are obviously very complex. Even if predicted product distributions do not fit well with the experimental data, this does not verify that the heterogeneous contribution affects the product distribution because the simulations have clearly shown the sensitivity of the distribution to variation, within the estimated bounds of accuracy, of the model rate data. Indeed the limited simulations on the product distribution so far suggest that the product distribution is not greatly affected by the presence of any heterogeneous

reaction, although the argument is always suspect because of the possible use of inaccurate rate data in the model.

An experimental approach which could add credence to the idea that the product distribution is affected by heterogeneous reaction is to vary substantially the S/V ratio of the reactor under identical isothermal conditions, having initially demonstrated the lack of heat transfer limitations throughout the experiments. In this way, variation of the product distribution in the same conversion range will be principally as a result of the heterogeneous contribution to the kinetics and not due to other contributory factors such as temperature. Alternatively, the heterogeneous contribution can be effectively removed by using a reactor tube wall which is known to exhibit a limited catalytic activity, such as quartz.

CHAPTER 8

CONCLUSIONS

The work presented in this study has demonstrated the feasibility of obtaining accurate experimental data for the pyrolysis of butane under well defined and consistent experimental conditions. Experiments were performed such as to minimise the effects of radial heat and mass transfer limitations and non-isothermal axial gas temperature profiles; these effects tend to obscure the kinetic evaluation of the subsequent data collected. Accordingly, at constant flowrates and using a set of probes inserted through the base of the reactor, experimental data were obtained for butane conversion and product composition as a function of residence time through a measured isothermal gas zone, situated in the lower section of the reactor space. Extensive measurement of temperature within the reactor space ensured that the process limiting the pyrolysis reaction was the chemical kinetics rather than any extraneous complications created by a poor experimental procedure. A thermocouple probe showed the existence of an isothermal gas region $\sim$ 30cm length where the measured gas temperature in both axial and radial directions varied by less than $4^{o}C$. This confirmed that within the bulk of the process gas stream the rate of the pyrolysis reaction was not influenced by heat transfer limitations and that the majority of the radial temperature drop between the wall and gas was through a thin boundary layer situated at the wall surface. Furthermore, the isothermal reaction zone removed all uncertainty associated with kinetic analysis of non-isothermal data.

A detailed design of the gas sampling probe revealed the sampling procedure along the centreline of the isothermal region could remove samples representative of well determined point locations in the undisturbed unsampled process stream. Sample elements were removed from the reactor

down an inner capillary around which a coolant stream of nitrogen flowed. Major contributors to sampling error, which was represented as an uncertainty in the axial sampling point, were the aerodynamic disturbance upstream of the probe tip and insufficient quenching of the sampled gas.

Thermal influences were considered and shown to be insignificant. Consequently it was established that each major disturbance created axial uncertainties in opposing directions and a mathematical model developed for the probe indicated that the individual errors, as well as the overall error were much smaller than other uncertainties in the measuring process, most pertinently the Gas Chromatographic measurement.

A problem with using an isothermal laminar flow reactor is the existence of radial concentration profiles, whose magnitude will depend to a large extent on the degree of segregation and dispersion in the radial direction. Experimental measurements indicated extremely flat radial concentration profiles which suggested the possibility of using a plug flow model for the isothermal zone despite the presence of the radial velocity profile. To justify this approach experimental data from the isothermal gas region were simulated using the radial dispersion model with superimposed noise to represent measurement error for a specified number of centreline sampling points. The simulations showed that estimates of the global rate constant for a pseudo first order reaction using a plug flow model were very similar to estimates obtained by attempting to remodel the isothermal region with radial dispersion.

For each set of actual experimental data collected from the reactor, the global rate constant was estimated using the radial dispersion and both linear and non-linear forms of the plug flow model. The Arrhenius

parameters obtained for the overall global expression for each set of experimental operating conditions are presented in Table 8.1

TABLE 8.1

Summary of Results for the Global Kinetics of Butane Pyrolysis from this Study

Set	Temperature Range (°C)	Conversion Range	Reynolds Number	Order of Reaction	$K=Ae^{-E/RT}$ $A(sec^{-1})$	$E(KJ/mole)\pm 2S'_0$
A	650-715	6-80	80	1	6.32×10^{10}	212.9±14.0
B	655-735	14-85	80	1	4.51×10^{10}	211.7±12.3
C	645-740	10-80	160	1	1.49×10^{10}	196.6±18.6

Thus it was shown that the overall kinetics could be well fitted by a pseudo first order rate expression with a constant activation energy over the entire conversion range studied. Activation energies from all three experimental sets were shown to be statistically identical at a significance level of 5%. The result that the overall kinetics appears first order upto the conversions studied may appear surprising principally because of the observed inhibition properties of some of the pyrolysis products, particularly propylene. Experimentally however the propylene peaks at a conversion as high as 75% which correlates well with the results determined here that the inhibitive effect does not exhibit itself as a major influence on the overall reaction at least upto conversions of 70%

Apparent rate constants from experimental set C were approximately twice

those from sets A and B; this effect may have resulted from a combination of influences; a more pronounced homogeneous contribution to the reaction near the wall due to the larger temperature drop through the thermal boundary layer; and an increased heterogeneous contribution due to a decrease in the mass transfer boundary layer thickness with a subsequent increase in the mass transfer rate to the catalytic wall. In addition, at the higher gas velocities a measurement uncertainty was introduced by the larger parametric sensitivity for calculating the corrected isothermal gas temperature due to radiative effects from the reactor wall, raising the measured gas temperature above its true value.

The contribution caused by the catalytic wall effects indicates the overall reaction is mixed homogeneous-heterogeneous which emphasises the special care which is necessary in carrying out experimental work for such systems. The argument for a heterogeneous influence is strengthened further by the consistently higher activation energies reported in the literature for studies in tubular flow and static reactors fabricated from material of little or no catalytic activity. The indirect method by which the heterogeneous contribution was attained in this study makes a quantitative judgement of its significance rather difficult and further studies should include more direct methods of achieving the same effect. This might include insertion of annuli through the reactor base to afford experiments with varying S/V ratios for the reactor or replacement of the reactor tube by one fabricated from material of different catalytic activity.

The product distribution obtained in this study agrees with most work previously accomplished on butane pyrolysis, specifically that high temperatures favour production of ethylene whilst conversely propylene

and ethane production are favoured by lower temperatures. A homogeneous free radical model, proposed by Edelson and Allara (1980) for pyrolysis of butane in the temperature range 400 - 530°C and comprising 98 elementary rate steps and 37 molecular and radical species was used to predict the product distribution for two experimental runs performed under conditions in set A. The rate data used for the model were from the reference set compiled by Allara and Shaw (1980) and are based consistently on fundamental experimental data, thermochemistry, theory and structural analogy independent from any pyrolysis data. Integration of the model was achieved using Gear's method for "stiff" systems and the predicted distribution agreed very well with the experimentally observed distribution as a function of butane conversion. However the predicted decomposition rate of butane was considerably lower than the observed rate.

A further set of simulations showed that the observed and predicted decomposition rates could be well matched by adjustment of the initiation rate data, yet remain within the currently recognised bounds of uncertainty for the rate data as indicated by Allara and Shaw.

Furthermore this change in rate data did not significantly alter the predicted product distribution which remained consistent with the experimental distribution. Clearly, providing sufficient care and preparation is made, a complex model for the mechanistic pyrolysis kinetics such as that by Edelson and Allara, based on a fundamental approach coupled with a rate data set independently constructed from the experimental data can lead to close agreement between predicted and experimental results.

APPENDICES

A P P E N D I X I

SENSITIVITY COEFFICIENTS FOR THE COMPOSITION ANALYTICAL SYSTEM

The sensitivity coefficients for each component under the relevant chromatographic conditions were obtained on the basis of peak heights using a series of gas mixtures from flowrate addition. Mixture compositions were chosen to reflect the same composition range expected for measurements from the reactor. Each component was added to the bulk gas stream using an independent rotameter, calibrated using a bubble gas flow meter. The composition of each standard mixture was then calculated assuming Dalton's Law and that the partial pressures were directly proportional to the individual flowrates. Internal standards were used in each mixture and these were given arbitrary sensitivity coefficients of 1. Thus the sensitivity coefficient of a general component was that measure of its sensitivity relative to the sensitivity of the internal standard. Typically, then, a standard mixture would contain an internal standard, the component whose sensitivity coefficient was to be evaluated and nitrogen to make the gas mixture composition similar to that expected from the reactor during the experiments.

In each calibration the sensitivity coefficient was evaluated 5 times under identical standard compositions and the average used in the subsequent analysis of the measurement information from the experimental runs.

Column + Chromatographic Detector	Component	Sensitivity Coefficient
Chromosorb 102	C_3H_6	1.00
Mesh Size 80/100	C_2H_6	3.00
+ FID	C_2H_4	3.56
17% Sebaconitrile	C_3H_6	0.91
/Chromosorb PAW 70/80	trans-2-C_4H_8	0.74
+ FID	cis-2-C_4H_8	0.67
	1-C_4H_8	0.79
	C_3H_8	0.98
	CH_4	0.47
	1,3 C_4H_6	0.58
	C_2H_2	0.72
	C_4H_{10}	1.00
Porapak Q	C_4H_{10}	1.00
+ TCD	N_2	3.27
(Feed Measurement)		
Porapak Q	H_2	6.6
+ TCD	CH_4	1.0
(Hydrogen Measurement)		
Porapak Q	N_2	1.67
+ TCD	CH_4	1.0
(Measurement of C/N ratio)		

A P P E N D I X I I

INTERPRETATION OF THE CHROMATOGRAPHIC MEASUREMENTS

Normally there are two ways of evaluating the conversion for composition measurements from the reactor.

(1) Continuous measurement of nitrogen, where for an arbitrary point in the reactor, the fractional conversion ϕ_f, assuming no volume expansion within the reactor because of the high dilution, is given as

$$\phi_f = \frac{y_{bo} - y_b}{y_{bo}} \qquad (II.1)$$

where: y_{bo} is the calculated mole fraction of butane in the reactor feed

y_b is the mole fraction of butane at the arbitrary point in the reactor

As a result of the large dilution factor both y_{bo} and y_b will be of small magnitude and thus this method may be subject to large inherent errors because of the subtraction between two relatively small numbers.

(2) Since the chromatographic system was incapable of measuring nitrogen at each point the conversion was calculated on a nitrogen free basis. A typical set of sensitivity adjusted component heights h_1', h_2' ... h_n' accordingly leads to mole fractions y_1, y_2 ... y_n for the n components measured. Let the reaction occurring within the reactor be represented as

$$a_1C_4H_{10} \rightarrow a_2X_2 + a_3X_3 + \cdots a_{n-1}X_{n-1} + a_nX_n$$

where X_i is a typical product, e.g. CH_4, C_2H_6 ... etc., and then for an axial point, z, in the reactor, the mole fraction of butane on a nitrogen free basis y_1 is given as

$$y_1 = \frac{N_b}{N_t} = \frac{N_{bo} + a_1\xi}{N_{bo} + \xi \sum_{i=1}^{n} a_i(z)} \qquad \text{(II.2)}$$

where: N_t is the total molar flowrate of butane and the products

N_b is the flowrate of the butane

ξ is the extent of reaction

On rearranging equation (II.2)

$$\xi = \frac{N_{bo}(1 - y_1)}{y_1 \sum_{i=1}^{n} a_i - a_1} \qquad \text{(II.3)}$$

By definition the fractional conversion is related to the extent of reaction as

$$\phi_f = \frac{\xi}{N_{bo}} \qquad \text{(II.4)}$$

whence from equations (II.3) and (II.4)

$$\phi_f = \frac{1 - y_1}{y_1 \sum_{i=1}^{n} a_i - a_1} \qquad \text{(II.5)}$$

Evaluation of $\sum_{i=1}^{n} a_i$

For a n - 1 product component composition, if a_1 is forced to be -1, the unknown coefficients are a_2, a_3 ... a_n if the fractional conversion is to be evaluated using equation (II.5). In this instance, the a_i are equivalent to the fractional selectivity defined as

$$a_i = \frac{\text{Number of moles of component i generated}}{\text{One mole of butane reacted}}$$

From the general definition of extent of reaction

$$\frac{y_i}{y_j} = \frac{N_i}{N_t} \cdot \frac{N_t}{N_j} = \frac{N_{io} + a_i\xi}{N_{jo} + a_j\xi} \qquad i,j = 1, 2, 3 \ldots n \qquad \text{(II.6)}$$

Since $N_{ko} = 0$, $k = 2, 3 \ldots n$, then

$$\frac{y_i}{y_j} = \frac{a_i}{a_j} \qquad i,j = 2, 3, 4 \ldots n \qquad \text{(II.7)}$$

This constitutes n-2 independent equations since no information is gained when i = j. An elemental balance on the overall representation of the reaction gives

$$\text{Carbon balance:} \qquad 4 = \sum_{i=2}^{n} a_i \, c_i \qquad \text{(II.8)}$$

$$\text{Hydrogen balance:} \qquad 10 = \sum_{i=2}^{n} a_i \, h_i \qquad \text{(II.9)}$$

where h_i, c_i are the number of hydrogen and carbon atoms of product component X_i. Either equation (II.8) or equation (II.9) can be used to provide the last independent equation necessary to evaluate the stoichiometric coefficients a_2, a_3 ... a_n. Since the equations are not independent of each other, the residual equation is fully defined and, in fact, can be used to assess the accuracy of the calculation of a_i since both sides of the equation should of course exactly balance. For further comment on this, see Appendix X.

In the evaluation of the fractional conversion equation (II.9) was used to ensure the hydrogen measurement had some influence on the final results. By substitution of a_i ($i \neq j$) using equation (II.7) into equation (II.9)

$$a_j = \frac{10 y_j}{\sum_{i=2}^{n} y_i \, h_i} \qquad j = 2, 3 \ldots n \qquad \text{(II.10)}$$

Thus, substitution of $\sum_{i=2}^{n} a_i$ into equation (II.5) generates the conversion for this measured set of mole fractions.

In the determination of the products there are two principal factors which will give errors in the value of the calculated fractional conversion. Firstly, the accuracy of the measurements and this has been discussed in Chapter 3, Section 3.5, and found to be satisfactorily small. Secondly, an error will be introduced if there exists some components

which have not been detected or could not be measured, e.g. 1-pentane, acetylene, C_5+ products.

TABLE II.1

	Actually Determined	Assuming 2% mole/mole of products was unmeasured benzene
Fractional Conversion, ϕ_f	0.295	0.306
$\sum_{i=2}^{n} a_i$	2.260	2.228
Residual Carbon balance using equation (II.8)	-1.8%	+7%

Table II.1 shows the difference in the calculated value for ϕ_f for a typical composition measurement assuming 2% of the products was unmeasured benzene. This indicates that only at high conversions (> 80%) when high C/H ratio components are formed will a significant error in the conversion be evident. Most runs in this study were performed with $\phi_f < 0.8$.

Determination of Product Yields

Product yield p_i is defined as

$$p_i = \frac{\text{number of moles of product i formed}}{\text{100 moles of reactant feed}}$$

thus

$$p_i = 100 \frac{N_i}{N_{bo}} \qquad \text{(II.11)}$$

Selectivity, s_i, is defined as

$$s_i = \frac{\text{number of moles of product i formed}}{\text{100 moles of reactant reacted}}$$

thus

$$s_i = 100 \frac{N_i}{N_{bo} - N_b} \qquad \text{(II.12)}$$

Using the definition of the fractional conversion

$$p_i = \phi_f s_i = \phi a_i \qquad \text{(II.13)}$$

where $\phi = 100\ \phi_f$

A P P E N D I X I I I

SENSITIVITY OF THE COMPOSITION MEASUREMENTS

One of the problems with the analytical system was the limited number of measurements which could be taken during each experimental run. This provoked an accuracy analysis on the six major components which is discussed in Chapter 3, Section 3.5. This was accomplished by a series of peak height ratio measurements, the statistics of which are presented in Table III.1. It was assumed that the statistics could be applied to any measurement data by converting the standard deviations to a variation about the mean. Similar statistics were measured for the butane/nitrogen feed ratio for conditions as used during the experimental runs in Sets A, B and C, and when an additional 5 metres of premixing was available before the gas entered the reactor. This served to check that fluctuations in the feed composition were not due to poor premixing of the two feed components. A set of measurements were also taken on the effects of using nitrogen cooling in the probe during sampling and the statistics of these measurements are also given in Table III.1.

The Autocovariance Function

The most important property of the sampling sequence is whiteness or independence between samples at different time instances. Tests for correlation are normally based on the autocorrelation function or the autovariance function a_k for time lags k = 1, 2, 3 ... n.

$$a_k = E\{(m_i - \bar{m})(m_{i-k} - \bar{m})^T\} \qquad \text{(III.1)}$$

where: $\bar{m}$ is $E(m_i)$

E is the expectation operator

m_i is a measurement at k = i

If the sampling sequence exhibits whiteness then a_k is zero at every point except time k. If correlation is experienced then a_k is not zero at points other than k but decays away to zero as the sequence tends to ∞. The rate of decay indicates the degree of correlation which exists in the sequence. If the function decays away quickly then little correlation is present. Often a_k is estimated as

$$\hat{a}_k = \frac{1}{N} \sum_{i=k}^{N} (m_i - \hat{\bar{m}})(m_{i-k} - \hat{\bar{m}})^T \qquad \text{(III.2)}$$

where $\hat{\bar{m}}$ is the sample mean and $\hat{a}_k$ can be shown to be an unbiased and consistent estimate of a_k.

Autocovariance functions for the nitrogen/butane ratio of the feed stream to the reactor and the butane/methane ratio at a typical point in the reactor were calculated. Measurements for each ratio were taken at time intervals of 10 minutes over a typical experimentation period of ~6 hours, and the autocovariance functions are illustrated in Chapter 3, Figs. 3.4a and 3.4b. The calculations show that the nitrogen/butane noise is virtually uncorrelated although there appears to be a little, although satisfactorily small correlation for the butane/methane. This may be as a consequence of the limited number of samples taken which may not be totally representative of the overall sequence.

TABLE III.1

Composition Error Analysis - Ratio Statistics[1]

Measurement Ratio	Mean Value	Standard Deviation
C_4H_{10}/C_3H_6	5.318	0.1401
CH_4/C_3H_6	1.216	0.0261
C_2H_4/C_3H_6	2.024	0.0204
C_2H_6/C_3H_6	0.1852	0.0054
H_2/CH_4	0.3772	0.0071
N_2/C_4H_{10} (feed)	14.104	0.4128
N_2/C_4H_{10} with additional 5 m mixing	15.573	0.4006
C_4H_{10}/CH_4 - probe no cooling	6.96	0.3448
C_4H_{10}/CH_4 - probe cooling rate 100 cc/sec (1 atm, 300 K)	7.16	0.2283

[1] Wall temperature = 700°C, Sampling Position = 102 cm from reactor inlet.

A P P E N D I X I V

MEASUREMENT OF THE GAS TEMPERATURE

Spatial gas temperatures within the reactor were measured using a chromel-alumel thermocouple probe, 3 mm diameter, and inconel sheath. Local variation during each experimental run was shown to be of the order 1^{o}C and a typical temperature-time history for the centreline axial measured gas temperature profile is given in Table IV.1. Radial temperature measurements were also taken at each axial point and local variation was also of the same order. The average radial temperature profile did not differ from the axial point measurements within the isothermal region by more than 1 - 2^{o}C. A typical profile is illustrated in Chapter 3, Section 3.8.

TABLE IV.1

Temperature-Time History for Centreline Axial Measured Gas Temperatures
Nominal Wall Temperature = 710^{o}C

Axial distance from reactor inlet (cm)	Time of experimental run (hr)						
	Start	1.0	2.0	3.0	4.0	5.0	6.0
59.0	957.0	958.0	958.5	958.5	958.5	956.5	958.5
65.0	964.0	965.0	965.5	965.5	966.0	965.0	965.0
71.0	964.0	966.0	966.0	966.0	965.5	965.0	965.5
77.0	965.0	966.0	966.5	966.5	965.0	966.0	966.0
83.0	967.5	967.5	967.5	967.0	967.5	967.5	967.5
89.0	969.5	969.5	970.0	970.5	970.5	970.0	970.0
95.0	970.0	970.5	971.0	971.5	971.5	972.0	971.5
101.0	970.5	971.0	971.5	971.5	971.5	971.0	971.0
107.0	973.0	973.0	973.5	972.5	972.5	973.5	973.0
113.0	973.5	974.0	974.5	974.0	973.0	974.0	973.0
119.0	971.0	972.0	972.0	971.5	971.0	971.5	971.5
125.0	962.0	963.0	963.5	963.0	963.0	962.5	963.0

Evaluation of the Gas Temperature Correction Equation

The recorded temperature of the gas by the thermocouple probe was higher than the true gas temperature because of radiation effects from the wall. Approximating the tip to be hemispherical and performing a simple energy balance on the hemispherical section

$$A_h\dot{q}_1 = A_h\dot{q}_2 + A_m\dot{q}_3 + A_t\dot{q}_4 + A_i\dot{q}_5 \qquad \text{(IV.1)}$$

where: A_h is the surface area of the hemispherical section (m^2)

A_i is the cross-sectional area of the mineral insulant (m^2)

A_m is the cross-sectional area of the inconel sheath (m^2)

A_t is the cross-sectional area of the thermocouple wires (m^2)

$\dot{q}_1$ is the rate of radiation which falls onto the hemispherical section (W/m^2)

$\dot{q}_2$ is the rate of convection heat loss from the hemispherical section to the process gas (W/m^2)

$\dot{q}_3$ is the conductive heat loss from the tip along the inconel sheath (W/m^2)

$\dot{q}_4$ is the conductive heat loss from the tip along the thermocouple wires (W/m^2)

$\dot{q}_5$ is the conductive heat loss from the tip through the mineral insulant (W/m^2)

Since the heat capacity of the probe is small, and the exterior is fabricated from a material of good thermal conductivity, it is reasonable to assume that at and near the probe tip the temperature is uniform and there is no conduction of energy away from the tip. Thus equation (IV.1) reduces to

$$\dot{q}_1 = \dot{q}_2 \qquad \text{(IV.2)}$$

Consider a sphere of area A_s ($= 2A_h$) situated within the reactor space. Since a sphere distributes radiation uniformly

$$F_{sw} = 1 - \frac{2\omega_1}{4\pi} \qquad (IV.3)$$

where: F_{sw} is the radiation view factor (for radiation from the sphere) to the reactor wall

ω_1 is the solid angle of the reactor exit and entrance relative to the sphere

Normally, the solid angles for the reactor exit and entrance will differ, depending on the position of the sphere within the reactor. For a reactor cross-sectional area A_r and diameter, d,

$$\omega_1 \sim \frac{A_r}{4\pi L^2} = \frac{\pi d^2}{4\pi L^2 . 4} = \frac{1}{16(L/d)^2} \qquad (IV.4)$$

where L is the distance of the sphere from the exit or entrance. Thus, substituting equation (IV.4) into equation (IV.3)

$$F_{sw} = 1 - \frac{1}{32\pi(L/d)^2} \qquad (IV.5)$$

In the worst instance $L/d \sim 2$, thus $F_{sw} \sim 1$ is a good approximation, equivalent to a sphere situated within a reactor of infinite length. Using the reciprocity theorem for view factors

$$A_w F_{ws} = A_s \qquad (IV.6)$$

where A_w is the total surface area of the reactor. The radiation falling on the sphere is then given by

$$A_s \dot{q}_1 = A_w F_{ws} \varepsilon_w \sigma_c T_w^4 - A_s \varepsilon_s \sigma_c T_s^4 \qquad (IV.7)$$

Substituting for $A_w F_{ws}$ using equation (IV.6)

$$\dot{q}_1 = \sigma_c(\varepsilon_w T_w^4 - \varepsilon_s T_s^4) \qquad \text{(IV.8)}$$

Since both the probe and the wall surface are fabricated from the same material and both will undergo similar transformations due to such factors as carbon laydown, $\varepsilon_w \sim \varepsilon_s \sim \varepsilon$ and

$$\dot{q}_1 = \sigma_c \varepsilon(T_w^4 - T_s^4) \qquad \text{(IV.9)}$$

Substituting for the convective heat loss, equation (IV.2) then becomes

$$\sigma_c \varepsilon(T_w^4 - T_s^4) = h(T_s - T_g)$$

$$\text{or} \qquad T_g = T_s - \frac{\sigma_c \varepsilon}{h}(T_w^4 - T_s^4) \qquad \text{(IV.10)}$$

where: T_g is the true gas temperature (K)

h is the heat transfer coefficient between the process gas and the thermocouple tip (W/m^2 K)

The heat transfer coefficient, h, was estimated by a correlation for flow around a sphere

$$\frac{hd_t}{K} = Nu = 2.0 + 1.3Pr^{0.15} + 0.66Re^{0.5}Pr^{0.33} \qquad \text{(IV.11)}$$

$$1 < Re = \frac{\rho v_o d_t}{\mu} < 10^4$$

where: d_t is the diameter of the thermocouple probe tip

Beek and Muttzall (1975) state that the heat transfer coefficient, h, is determined mainly by the conditions on the streamline side of the body and should therefore be a reasonable approximation for a hemisphere. Using the averaged gas temperature as recorded by the thermocouple probe and the average wall temperature within the isothermal region, the corrected gas temperature was calculated using equation

TABLE IV.2

Evaluation of the Gas Temperature

Run Number	Wall Temperature (K)	Thermocouple Temperature (K)	h*	Re**	Corrected Gas Temperature (K)
4	939.5	934.0	90.1	8.9	923.8
5	960.0	953.0	91.2	8.8	939.3
6	980.5	972.5	92.1	8.7	957.1
7	1000.0	990.5	92.8	8.5	970.0
8	1019.5	1009.5	93.6	8.4	986.8
9	1020.0	1009.5	93.9	8.5	985.7
11	980.0	974.0	91.7	8.5	961.6
12	980.5	973.5	91.7	8.5	959.0
13	993.0	986.0	92.3	8.4	971.0
14	1013.5	1006.5	93.3	8.3	990.8
15	1019.0	1011.5	93.4	8.2	994.4
16	1033.5	1025.0	94.1	8.2	1005.0
17	963.5	958.0	90.9	8.6	947.1
18	943.5	938.0	89.9	8.6	927.6
19	953.0	947.5	90.4	8.6	939.9
20	954.0	941.0	104.2	17.8	919.4
21	974.0	961.0	105.3	17.6	938.2
22	993.0	980.5	106.3	17.4	957.5
23	1014.0	1001.0	107.5	17.3	975.8
25	1053.0	103.5	109.1	16.7	998.3
26	1073.5	1053.5	110.1	16.5	1009.0

* Heat transfer coefficient (W/m^2 K)

** Reynolds Number based on thermocouple probe diameter

(IV.10) and is presented in Table IV.2 for all the experimental runs. The physical property data bank for the heat transfer coefficient is identical to that in the probe sampling model which is discussed in Appendix V. Corrected gas temperatures for run 10, run 24 and run 27 were not calculated principally because they were not used in estimation of the global rate constant for the disappearnce of butane. Run 10 was terminated after ∿4 hours because the gas sampling probe became blocked with carbon on the inner capillary wall. Run 27 was performed at a conversion range (76 - 92%) considered too high to be useful in the rate constant estimation and was accompanied by production of liquid products. Run 24 inexplicably gave meaningless and random composition data and was therefore not used.

Sensitivity of the Gas Temperature Correction

One of the problems associated with equation (IV.10) is the sensitivity of the calculated gas temperature to the accuracy of the parameters of the equation, the emissivity, ε, and the heat transfer coefficient, h. Most importantly, the sensitivity is dependent on the difference between the wall temperature and the measured gas temperature using the thermocouple probe. The larger difference for set C indicates that the calculated gas temperature is more sensitive to parameter errors than for set A and set B. Furthermore, the result of these errors could reduce the difference between the calculated rates of decomposition under similar conditions between set C and the first two sets. Hence it is vital to show that the observed discrepancy between the rate constants is not because of errors involved with the estimated gas temperature, rather than the heterogeneous contribution. As an approximation from equation (IV.10)

$$\Delta T_g \approx \left(\frac{\partial T_g}{\partial C_1}\right)_{T_s,T_w} \Delta C_1 + \left(\frac{\partial T_g}{\partial T_s}\right)_{C_1,T_w} \Delta T_s + \left(\frac{\partial T_g}{\partial T_w}\right)_{C_1,T_s} \Delta T_w \qquad \text{(IV.12)}$$

where: $C_1 = \frac{\varepsilon}{h}$. Further simplifying by assuming T_w, $T_s \sim$ constant

$$\Delta T_g \sim -\Delta C_1 \sigma_c (T_w^4 - T_s^4) \qquad \text{(IV.13)}$$

As an example, let $T_w = 720^oC$, then $T_{s_1} \sim 713^oC$ and $T_{s_2} \sim 707^oC$ where the subscript 1 denotes the experimental sets A and B and subscript 2 denotes experimental set C.

TABLE IV.3

$\frac{\Delta C_1}{C_1}$	ΔT_{g_1} (^oC)	ΔT_{g_2} (^oC)	$\Delta T_{g_1} - \Delta T_{g_2}$ (^oC)
±0.25	±3.4	±6.3	±2.9
±0.50	±6.8	±12.6	±5.8
±0.75	±10.2	±18.9	±8.7
±1.0	±13.6	±25.2	±11.6

If the error of the parameter C_1 is negative the effect is to bring together the two calculated gas temperatures by the amount $\Delta T_{g_1} - \Delta T_{g_2}$. Conversely, if the error is positive, the effect is to increase the difference between the two gas temperatures by the amount $\Delta T_{g_1} - \Delta T_{g_2}$. The emissivity used in the calculations was chosen to be 0.9, on the basis that the surface of both the reactor and the probe was coated with carbon which was thick enough to become the effective emittor of the radiation. However, there is a significant difference between the emissivity of inconel ($\sim$ 0.6) and that of carbon which means an error in the simulated emissivity may be as great as 50%. There is no doubt that significant errors in the calculated heat transfer coefficient exist but it is difficult to specify exactly what they might be. Tentatively suggesting an error of 50% in the simulated value gives $\Delta C_1/C_1$ a value of 0.33. From Table IV.3 the maximum change in the temperature difference from an error in the parameter C_1 of this size

is likely to be no larger than $\sim 5^{o}C$. Note that this assumes an equal percentage error for each set of experimental conditions which may not be a satisfactory assumption to make. At $720^{o}C$, assuming an activation energy of 50 kcal/mole this error would constitute no more than ~20% of the difference between the observed rate constants between set C and sets A and B. Variation in wall temperature in other experimental runs do not create changes considerably larger than that detected in this example which indicates that the majority of the increase in the rate constant for runs in set C is more likely to be due to heterogeneous effects rather than changes in the thermal conditions in the reactor.

In the parameter analysis it was assumed that both T_w and T_s were constant and accurately determined. If this assumption is relaxed, then possible errors in the corrected gas temperature due to measurement errors assuming $C_1 \sim$ constant can be approximated as

$$\Delta T_g \approx \Delta T_s \left(1 + \frac{4\sigma_c \varepsilon}{h} T_s^3\right) - \frac{4\sigma_c \varepsilon}{h} T_w^3 \Delta T_w \qquad \text{(IV.14)}$$

For most runs, the thermocouple temperature, T_s, varied through the assumed isothermal region by an average of $3^{o}C$. Equation (IV.3) shows that the procedure to evaluate the corrected gas temperature amplifies this variation so that the true gas temperature will vary by a quantity greater than $3^{o}C$, possibly to such an extent as to make the assumption of isothermality rather tenuous. Substituting a value of $\Delta T_s = 1.5^{o}C$, $\Delta T_w \sim 0$ into equation (IV.14) gives typical values of $\Delta T_g \sim 4.0^{o}C$ which shows that the true gas temperature variation through the isothermal region may be as large as $8 - 9^{o}C$. However, the amplification factor is sensitive to the value of C_1 which is subject to possible large errors. Specifically, the emissivity is more likely to be smaller rather than larger than the simulated value of 0.9 and would consequently reduce

the range of the true gas temperature within the isothermal region.

Since the measured temperature variation is monotonically progressive from the start of the isothermal region, some sort of curvature might be expected in the conversion data points as represented in Figs. 6.15, 6.16 and 6.17 in Chapter 6, a result of the progressive increase in the value of the rate constant. This was not observed in all the runs in experimental set A and set B. Curvature trends were, however, detected in the runs in set C which accordingly led to rate constants of larger uncertainty than for the first two sets. Nevertheless, a satisfactory set of Arrhenius parameters were still calculated for set C.

In experimental set A axial wall temperatures were measured using a Ngl 6400 D.V.M., and axial centreline gas temperatures using a Datron 1051 D.V.M. For sets B and C both the axial wall temperatures and axial centreline gas temperatures were measured using the Datron 1059 D.V.M. Apart from the nominal change in feed concentration between sets A and B, this changeover in the D.V.M. monitoring the axial wall temperatures was the only other alteration which could possibly explain the apparent difference in the pre-exponential factor. A calibration test on both the Ngl 6400 and the Datron 1051 revealed that in the temperature range 950 - 1050 K, the Ngl 6400 had a negative drift of approximately 20 μV ($\sim 2^{o}$C for a Pt/Pt 13% Rh thermocouple) whilst the Datron 1059 showed negligible drift. Introducing this error in equation (IV.14), assuming $C_1, T_s \sim$ constant and T_w = 1000 K gives ΔT_g = -4.2 K which for an activation energy of 212 KJ/mole (50.7 kcal/mole) would lead to a decrease in the rate constant of about 10%. Thus the discrepancy between rate constants from runs in set A and set B could well be reconciled to this poor calibration of the Ngl 6400, which is situated on the experimental apparatus; even more so because the difference

in the rate constants is regular and systematic, consistent with the bias which would be present because of the inaccurate calibration.

In future experiments, it is recommended that the thermocouple probe is constructed with a Pt/Pt 13% Rh thermocouple and that both wall and gas temperature measurements are measured with the same D.V.M. in the same voltage range such that calibration errors would become secondary and not seriously affect the measurements which are taken.

A P P E N D I X V

THE GAS SAMPLING PROBE MODEL

Preliminary Investigation

According to Shapiro (1954) frictional effects are very important at high Mach numbers. Typically for a friction factor of only 0.0025 and for an initial Mach number of 3 (after exiting from the divergent portion of the converging-diverging nozzle) the shock wave transmission back to subsonic flow occurs only 52 pipe diameters downstream of the initial point. In the present probe design, typical values of the friction factor are larger ($\sim$ 0.01) and L/D ratios are of the order 1000. This shows that the idea of aerodynamic quenching is not feasible for a probe of this material and dimension.

In addition, an energy balance around the nozzle shows

$$H_o' + \tfrac{1}{2}u_o^2 = H' + \tfrac{1}{2}u^2 \qquad (V.1)$$

where: H_o' is the enthalpy per unit mass upstream of the nozzle

u_o is the velocity upstream of the nozzle = u_∞

H' is the enthalpy per unit mass downstream of the nozzle, in the capillary

u is the velocity downstream of the nozzle, in the capillary

Rearranging equation (V.1), assuming $C_p \neq f$ (temperature)

$$C_pT_o + \tfrac{1}{2}u_o^2 = C_pT_x + \tfrac{1}{2}u_x^2$$

thus

$$T_o - T_x = \frac{u_x^2 - u_o^2}{2C_p} \qquad (V.2)$$

For subsonic flow, e.g. $u_x \sim 40$ m/sec (determined by conditions downstream of the nozzle and the pressure in the reactor), even when critical conditions are obtained in the throat of the nozzle $T_o - T_x \sim 0.8^oC$. Clearly, use of subsonic flow in the capillary alone, without a cooling medium will lead to insufficient quenching of the sample. The only advantage with using velocities of this size is the resulting very small residence time within the probe. This is balanced by the pressure drop through the capillary due to too small a capillary diameter against an excessive aerodynamic disturbance due to too large a capillary diameter Typical velocities in the gas cooled probe were of the order ~8 m/sec, with a pressure drop through the probe ~1.5 m of length, of approximately 0.5 bar.

Development of the Gas Sampling Model

A series of energy, mass and momentum balances on the probe gave the following equations.

Energy

$$\frac{dT_1}{d\ell} = \frac{-u_1\, du_1}{C_p\, d\ell} + \frac{h_{02}\,\pi\, d_3 A_1 (T_1 - T_2)}{G_1\, C_p} + \frac{h_{03}\,\pi\, d_1 A_c (T_1 - T_c)}{G_1\, C_p}$$

$$\frac{dT_2}{d\ell} = \frac{-u_2\, du_2}{C_p\, d\ell} + \frac{h_{01}\,\pi\, d_5 A_2 (T_p - T_2)}{G_2\, C_p} + \frac{h_{02}\,\pi\, d_3 A_1 (T_1 - T_2)}{G_2\, C_p}$$

$$\frac{dT_c}{d\ell} = \frac{-u_c\, du_c}{C_p\, d\ell} + \frac{h_{03}\,\pi\, d_1 A_c (T_1 - T_c)}{G_c\, C_p} + \frac{R_b(\Delta H_R)}{G_c\, C_p}$$

Momentum

$$\frac{dP_1}{d\ell} = \frac{G_1^2 C_f\, \pi (d_2 + d_3)}{2\rho_1\, A_1} - G_1 \frac{du_1}{d\ell} \qquad (V.3)$$

$$\frac{dP_2}{d\ell} = \frac{-G_2^2 C_f\, \pi (d_4 + d_5)}{2\rho_2\, A_2} - G_2 \frac{du_2}{d\ell}$$

$$\frac{dP_c}{d\ell} = \frac{-2C_f G_c^2}{\rho_c d_1} - G_c \frac{du_2}{d\ell}$$

Mass

$$\frac{dF_c}{d\ell} = R_b A_c = - K_b C_b A_c$$

Boundary conditions: @ $\ell = 0$ (Probe Tip) $T_1 = T_2$

$$P_1 = P_2$$

@ $\ell = L_p$ (Probe End) $P_c = P_2 = 1$ atmosphere

$$T_1 = 300 \text{ K}$$

Equations (V.3) constitute a coupled two-point boundary value problem. The equations can be solved either from the probe end or probe tip. Integration can continue from the probe end if G_1 (or G_2) is set and initial values for G_c, P_1 and T_2 are given. The solution to the model is obtained by simultaneous manipulation of G_c, P_1 and T_2 such that the integrated solution at the probe tip complies with the constraints there. Alternatively, integration can be carried out from the probe tip if T_1 (or T_2) is set and initial values for P_1, G_c and G_1 (or G_2) are given or G_1 (or G_2) is set and initial values for P_1, G_c and T_1 (or T_2) are given. Once again, the model solution is obtained by simultaneous iteration of P_1, G_c and G_1 (or P_1, G_c and T_1) until the integrated solution at the probe end agrees with the boundary conditions imposed there. A computer program was attempted for the latter approach (with P_1, G_c and G_1 as free variables) but at no time was a successful solution obtained. As a result of the complexity of the probe model a series of assumptions were made which decoupled the equations so that iteration could be achieved by sequential manipulation of each of the three variables, and the resulting equations are given in Chapter 3,

Section 3.12. In this way, each of the boundary conditions were effectively decoupled such that each subset could be satisfied sequentially by iteration of just one of the free variables. An attempt was made to set G_1 and use T_1 (or T_2) as the additional free variable, but this proved more unstable than the former approach and was therefore not used.

Simplifications Used in the Gas Sampling Model

In deriving the resulting controlling equations for the gas sampling model given in Chapter 3, Section 3.12, a number of simplifications were made justifiable using an overall magnitude analysis.

Assumption 1

$$u \frac{du}{d\ell} << C_p \frac{dT}{d\ell}$$

$$0\left\{\frac{8 \times 4}{1.4}\right\} << 0\left\{\frac{1000 \times 500}{1.4}\right\}$$

$$0(10) << 0(10^5)$$

Assumption 2

$$G \frac{du}{d\ell} << \frac{dP}{d\ell}$$

$$0\left\{\frac{50 \times 4}{1.4}\right\} << 0\left\{\frac{0.5 \times 10^5}{1.4}\right\}$$

$$0(10^2) << 0(10^4)$$

Assumption 3

$$\frac{R_b(\Delta H_R)^*}{G_c C_p} << \frac{dT_c}{d\ell}$$

$$0\left\{\frac{2 \times 100{,}000}{50{,}000}\right\} << 0\left\{\frac{500}{1.4}\right\}$$

$$0(1) << 0(10^2)$$

* ΔH_R has been approximated to the heat of reaction for propane as calculated by Beshty (1978).

Assumption 4

$$\frac{h_{03}\,\pi\,d_1 A_1 (T_1 - T_c)}{G_1\,C_p} \ll \frac{h_{02}\,\pi\,d_3 A_1 (T_1 - T_2)}{G_1\,C_p}$$

$$0\{120 \times 0.0006 \times 10\} \ll 0\{90 \times 0.0027 \times 100\}$$

$$0(1) \ll 0(10)$$

Assumption 5

The probe outer wall temperature was assumed to be equivalent to the nominal reactor wall temperature.

$$T_p = T_w \qquad \text{isothermal region} \qquad \ell \leq \ell_1$$

$$T_p = T_w - \frac{(T_p - T_e)(\ell - \ell_1)}{0.625} \qquad \text{linear region down to exit of reactor} \qquad \ell_2 \geq \ell > \ell_1 \quad \text{(V.4)}$$

$$T_p = T_e - \frac{(T_e - T_a)(\ell - (\ell_1 + 0.625))}{L_p - (\ell_1 + \ell_2)} \qquad \text{linear region from exit of reactor to end of probe} \qquad L_p \geq \ell > \ell_2$$

where: ℓ_1 is the distance (m) that the probe is situated within the isothermal region (simulation input)

ℓ_2 is the distance (m) between the end of the isothermal region and reactor exit $\sim$ 0.625 m

L_p is the probe length $\sim$ 1.4 m

T_a is ambient temperature $\sim$ 300 K

T_e is the temperature at the reactor exit, measured $\sim$ 323 K

T_p is the probe wall temperature (K)

T_w is the reactor wall temperature (K)

Undoubtedly, assumption 5 is a gross simplification of the real conditions and in reality, T_p is more likely to be considerably lower than T_w. In this respect, the simulated profile serves to illustrate the

simplicity of the model compared to the complexity which in reality exists. This higher value for T_p was chosen so as to subject the fluid elements passing down the capillary to conditions more severe than they are likely to encounter. Even under these conditions the simulations revealed a negligible degree of reaction within the capillary when a coolant was being employed.

Databank of Physical Property Used in the Sampling Model

Physical properties of nitrogen were used throughout the simulations since the large dilution ratios used in the experimental runs meant only ∿10% mole/mole of the reacting mixture was not nitrogen.

Property	Source	Equation
Thermal conductivity, K (W/mK)	International Critical Tables (Vol. 5) (1929)	$K = K_{273} \frac{387}{T+114} \left\{\frac{T}{273}\right\}^{3/2}$ $K_{273} = 2.28 \times 10^{-2}$ W/mK, T in K ("Sutherland's Equation")
Friction factor, C_f	Kay and Nedderman (1974)	$0 < R_e < 1190 \quad C_f = \frac{16}{R_e}$ $1190 < R_e < 10^5 \quad C_f = 0.079\ R_e^{-\frac{1}{4}}$ ("Blasius Law")
Density, ρ (kg/m^3)	-	$P = \rho \acute{R} T$ ("Perfect Gas Law")
Viscosity, μ (Ns/m^2)	Perry (1963)	$\mu(T_2) = \frac{\mu(T_1) f(T_2)}{f(T_1)}$ $f = 1.058\ T_{re}^{0.645} - \frac{0.261}{(1.9\ T_{re})^{0.9 \log_{10}}} (1.9\ T_{re})$ where $T_{re} = \frac{T}{T_c}$ and T_c = critical temperature of nitrogen = 126 K reference point: $T_1 = 300$ K, $f(T_1) = 1.7442$, $\mu_1 = 17.875 \times 10^{-6}$ (Ns/m^2)

Rate constant for first order disappearance of butane, k_b (sec^{-1})	Sandler and Chung (1961)	$k_b = 9.55 \times 10^9 \, e^{-190790./RT}$

Determination of the Thermal Influence

One of the factors which could affect probe sampling characteristics is the thermal effect created by the probe and by the cooling on the temperature and velocity profiles upstream and in the close vicinity of the probe tip. Consider the following simplified model:

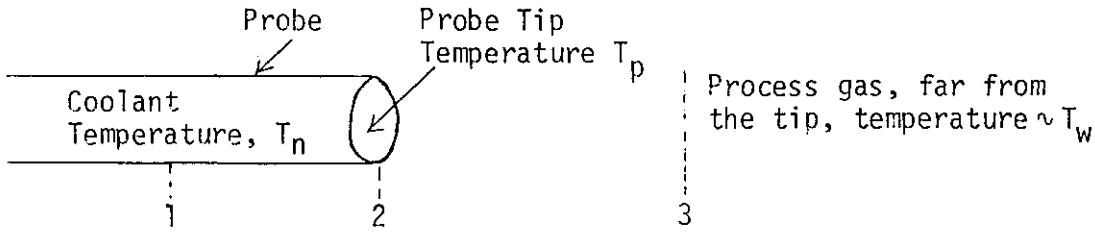

An energy balance on an elemental section between points 2 and 3 reduces to

$$- \rho v_o C_p \frac{dT}{d\ell} + \frac{K d^2T}{d\ell^2} = 0 \qquad (V.5)$$

Boundary conditions

$$@ \ \ell = 0 \qquad T = T_p$$

$$@ \ \ell = \infty \qquad T = T_w$$

Substituting for $\frac{dT}{d\ell} = C'$ and twice integrating the solution directly, after insertion of the boundary conditions, the solution to equation (V.5) becomes

$$T(\ell) = T_w + (T_p - T_w)e^{-\Omega\ell} \qquad (V.6)$$

where

$$\Omega = \frac{\rho v_o C_p}{K}$$

At $\ell = 0$ an energy balance between either side of point 2 reveals

$$\left.\frac{-K dT}{d\ell}\right|_{\ell=0} = h(T_p - T_n) = \Omega K(T_w - T_p) \qquad (V.7)$$

Typical values for $\Omega \sim 1650$, $K \sim 0.07$ and assuming the heat transfer coefficient between the probe tip and coolant nitrogen flow can be approximated by equation (3.3) in Chapter 3 with D, the diameter of the probe

$$41(T_p - T_n) \approx 115(T_p - T_w) \qquad (V.8)$$

Example

Let $T_w = 973$ K

$T_n = 923$ K

From equation (V.8) $T_p = 960$ K and the temperature of the gas just 1 K below T_w at a distance ~1.6 mm from the probe tip using equation (V.6). The much simplified analysis above indicates that the cooling effects of nitrogen are propagated upstream of the probe tip so badly that its thermal effect can be neglected. Although the quality of the calculated heat transfer coefficient, h, is poor the damping quality of the exponential function suggests its value will not much affect the trend reported in the analysis. For instance, an error of 100% for h increases the length upstream where the temperature difference is 1 K between the process gas at that point and that infinitely far from the probe to 1.85 mm, a negligible increase. Moreover, the stagnant regions of coolant which are likely to be set up around the tip will most likely make h lower than that used in the analysis which strengthens further the arguments that the thermal effects are small. It is worth noting that the pre-cooling of the gas elements before entering the probe and the drop in the probe tip temperature are not taken into account in the simulations. In reality, however, the probe tip temperature will be governed by more factors than assumed in the analysis and the gas elements which enter the probe are unlikely to be cooled to the extent

suggested since the boundary condition at $\ell = 0$ used to solve equation (V.5) is not strictly correct.

Aerodynamic and Chemical Reaction Error

Chemical reaction error is defined as the distance required to travel under reactor conditions to achieve the same degree of reaction as that which occurred during the sampling procedure. The controlling equation is given by

$$\frac{dF_c}{d\ell} = - k_b C_c A_r = Q \frac{dC_c}{d\ell} \qquad (V.9)$$

Boundary conditions: @ $\ell = 0$ $F_c = F_{c0}$

@ $\ell = \ell'$ $F_c = F_{c1}$

where $F_{c0} - F_{c1}$ is the quantity of reaction which occurred in the capillary as predicted by the simulation and thus the chemical reaction error is the quantity, ℓ'. Integrating equation (V.9) between F_{c0} and F_{c1}

$$\ell' = \frac{\bar{v}}{k_b} \ln \left\{ \frac{F_{c0}}{F_{c1}} \right\} \qquad (V.10)$$

where $\bar{v}$ is the mean velocity in the reactor. One effect, clearly present yet not considered, is the heterogeneous reaction occurring at the capillary wall which would enhance the amount of reaction and thus increase the estimated reaction error. If the majority of the reaction is considered homogeneous, this would not be a serious error. In fact, the simulations indicate that the reaction error is reasonably small under most sampling conditions in the reactor.

In the model, estimation of the aerodynamic error has been simplified principally because of the otherwise complex procedure to evaluate the relative axial error. The correct analysis is to measure the residence time of all the elements being withdrawn and by weighting the distribution by flow proportion, evaluate the mean residence time and thus

estimate accurately how much faster the gases are moving than if there had been no sampling taking place. The calculation is tedious and numerically complicated, requiring knowledge of the stream function, ψ which must first be obtained from the velocity potential, ϕ. In brief, the method entails numerically integrating along each streamline into the probe to determine the residence time of the elements flowing directly adjacent to it. Evaluation of the last streamline to enter the probe could be determined by knowledge of the sampling rate, determined by conditions downstream of the probe tip.

The alternative strategy, discussed in Chapter 3, Section 3.13, is to assume the residence time of centreline axis elements is equivalent to the required weighted mean. The error was evaluated for two values of the fractional flow, f (see Chapter 3, Section 3.9) to ensure that the value converged quickley as $f \to 0$, equivalent to an infinite distance from the probe. Having evaluated each error the sampling error, incorporating all the component errors can be compared to a typical expected measurement error taken to be ±4% relative of the butane concentration, evaluated using equation (V.10).

Principal Simulation Model Results

Two basic simulations were performed at nominal wall temperatures of 700°C and 800°C. The idea of maintaining a constant overall sampling error could be achieved by changing the coolant flowrate as the probe traversed the isothermal region in the simulations. The inaccuracy of heat transfer data, physical property data, outer wall temperature profile and characterisations of the individual disturbances did not warrant such confidence and a constant coolant flow of 100 cc/sec (1 atmosphere, 300 K) was chosen throughout the simulations. Table V.1 shows the predicted capillary flowrates at 700°C and 800°C against the

experimentally observed flowrates under identical conditions. Table V.2 shows typical temperature and pressure profiles along the probe length for a typical set of conditions used in the simulations.

TABLE V.1

Axial position of Probe Tip From Reactor Entrance (cm)	Predicted* Flowrate (cc/sec)	Observed* Flowrate (cc/sec)	Calculated Temperature Difference Between Coolant Nitrogen and Process Gas at the Probe Tip (°C)
		700°C	
64.1	1.34	1.33	15
74.1	-	1.45	-
84.1	1.72	1.58	43
94.1	-	1.78	-
104.1	2.31	2.05	120
114.1	-	2.50	-
		800°C	
64.1	1.16	1.12	15
74.1	-	1.25	-
84.1	1.51	1.41	44
94.1	-	1.62	-
104.1	2.08	1.88	122
114.1	-	2.25	-

* 1 atm, 300 K.

TABLE V.2

Reactor pressure = 7 psig = 1.483 bar a

Reactor temperature = 700°C = 973 K

Position of probe tip = 0.345 m from the base of the isothermal region

Coolant flowrate (1 atm, 300 K) = 100 cm^3/sec

Capillary flowrate (1 atm, 300 K) = 1.78 cm^3/sec

Distance from Probe Tip (m)	T_1 (K)	T_2 (K)	T_c (K)	P_1 (bar)	P_2 (bar)	P_c (bar)
0	930.0	930.0	973.0	1.421	1.421	1.483
0.01	929.7	939.1	942.6	1.423	1.416	1.476
0.02	929.8	945.8	933.5	1.425	1.411	1.470
0.03	927.6	950.7	930.3	1.427	1.407	1.463
0.05	924.3	956.8	926.7	1.431	1.398	1.450
0.10	911.7	961.0	915.7	1.441	1.375	1.418
0.15	894.6	959.6	900.0	1.451	1.351	1.385
0.20	872.6	956.3	879.4	1.460	1.327	1.355
0.30	809.3	946.3	820.9	1.477	1.277	1.291
0.40	714.3	907.8	730.4	1.492	1.228	1.235
0.60	518.4	713.1	533.9	1.514	1.143	1.153
0.80	377.7	523.0	388.9	1.529	1.086	1.101
1.00	314.9	352.9	318.1	1.540	1.052	1.068
1.20	303.9	314.2	304.6	1.550	1.032	1.041
Probe End, 1.39	300.0	303.8	300.4	1.558	1.014	1.014

A P P E N D I X V I

NUMERICAL SOLUTION TO THE RADIAL DISPERSION MODEL

If the velocity profile is described by Poiseuille's equation, axial diffusion is negligible compared with radial diffusion, there is no expansion on reaction and the reaction is first order, the governing partial differential equation for the Radial Dispersion Model is given as

$$-(1 - R^{*2}) \frac{\partial C^*}{\partial Z^*} + \omega \left\{ \frac{\partial^2 C^*}{\partial R^{*2}} + \frac{1}{R^*} \frac{\partial C^*}{\partial R^*} \right\} - \beta C^* = 0 \qquad \text{(VI.1)}$$

Boundary conditions

$$\frac{\partial C^*}{\partial R^*} = 0 \qquad R^* = 0, 1 \qquad Z^* > 0$$

$$C^* = 1 \qquad Z^* = 0 \qquad 0 \leqslant R^* \leqslant 1$$

Normally equation (VI.1) is solved numerically. The finite different method is one of the commonest methods to numerically solve sets of partial differential equations. The basic operations are performed on a grid of selected points within a known defined boundary. A multi-dimensional Taylor series expansion enables an approximation to be developed for all the derivatives of each independent variable averaged or centred at one or a set of points on the grid. Pointwise or explicit methods of solution are forms where the solution depends on points previously known or calculated. The problems of stability for explicit methods are overcome by representing the derivatives and terms in the differential equations by a finite difference form evaluated at an advanced set of points where the values of each independent variable are unknown. Now the problem becomes implicit since a set of algebraic equations are derived which must be solved simultaneously for each row

of unknown grid points. A typical implicit formula, for instance, would be

$$\frac{\partial C^*}{\partial R^*} \approx \theta \left.\frac{\partial C^*}{\partial R^*}\right|_{i,j} + (1-\theta) \left.\frac{\partial C^*}{\partial R^*}\right|_{i,j+1} \qquad 0 \leq \theta \leq 1 \qquad \text{(VI.2)}$$

where the point solutions being sought are $C^*_{i,j+1}$ $i = 1, 2, 3 \ldots$. It can be shown that when $\theta \geq \frac{1}{2}$ the method is always stable. Solution to the equation when $\theta = \frac{1}{2}$ is known as the Crank-Nicholson method and was the method employed by Cleland and Wilhelm (1956) and was used in this study for the solution to the RDM.

To reduce the number of numerical calculations and to remain in accordance with the procedure by Cleland and Wilhelm, equation (VI.1) was divided throughout by β, producing a new dimensionless parameter $\lambda = \beta Z^*$ which generates the equation

$$-(1-R^{*2}) \frac{\partial C^*}{\partial \lambda} + \alpha \left[\frac{\partial^2 C^*}{\partial R^{*2}} + \frac{1}{R^*} \frac{\partial C^*}{\partial R^*}\right] - C^* = 0 \qquad \text{(VI.3)}$$

Boundary conditions

$$\frac{\partial C^*}{\partial R^*} = 0 \qquad R^* = 0, 1 \qquad \lambda > 0$$

$$C^* = 1 \qquad \lambda = 0 \qquad 0 \leq R^* \leq 1$$

The Crank-Nicholson finite difference approximations to each term in the equation are well described in the paper by Cleland and Wilhelm and are not derived here. At the reactor centreline the term $1/R^* \, \partial C^*/\partial R^*$ is indeterminate and L'hôpital's rule reveals

$$\lim_{R^* \to 0} \frac{1}{R^*} \frac{\partial C^*}{\partial R^*} = \lim_{R^* \to 0} \frac{\partial^2 C^*}{\partial R^*} = \left.\frac{\partial^2 C^*}{\partial R^2}\right|_{R^*=0}$$

Thus equation (VI.3) becomes

$$-\frac{\partial C^*}{\partial \lambda} + 2\alpha \frac{\partial^2 C^*}{\partial R^{*2}} - C^* = 0 \qquad R^* = 0 \qquad \text{(VI.4)}$$

Equation (VI.4) now determines the centreline concentration whilst satisfying both the original equation and the centreline boundary condition. Averaging the Taylor's series expansion of equation (VI.4) about the (1, k) and (1, k+1)th grid points, where (x, y) denotes radial and axial directions respectively, gives the finite difference approximation. In addition, an extra relationship is given by

$$C^*_{j-1,k} = C^*_{j+1,k} = C^*_{2,k} \qquad k > 0 \qquad \text{(VI.5)}$$

and the final expression for the centreline is given as

$$\frac{C^*_{1,k+1} - C^*_{1,k}}{\Delta\lambda} = \frac{2\alpha}{\Delta R^{*2}} \{C^*_{2,k+1} - C^*_{1,k+1} + C^*_{2,k} - C^*_{1,k}\} - \frac{\{C^*_{1,k+1} + C^*_{1,k}\}}{2} \qquad \text{(VI.6)}$$

where $\Delta\lambda$ and ΔR^* are the axial and radial grid space sizings respectively. At the reactor wall equation (VI.3) reduces to

$$\alpha \frac{\partial^2 C^*}{\partial R^{*2}} - C^* = 0 \qquad R^* = 1 \qquad \text{(VI.7)}$$

Furthermore, by imposing $\partial C^*/\partial R^* = 0$ on the expansion of C^* the second-order derivative is approximated by

$$\left.\frac{\partial^2 C^*}{\partial R^{*2}}\right|_{R^*=1} = \frac{2}{\Delta R^{*2}} \{C^*_{j'} - C^*_{j'+1}\} \qquad \text{(VI.8)}$$

where j' is the penultimate radial position before the wall. Averaging of equation (VI.7) using the approximation given by equation (VI.8) about the (j'+1, k) and (j'+1, k+1)th grid points yields the Crank-Nicholson finite difference approximation for the reactor wall

$$\frac{1}{\Delta R^{*2}} \{C^*_{j',k+1} - C^*_{j'+1,k+1} + C^*_{j'+1,k}\} - \tfrac{1}{2}\{C^*_{j'+1,k} + C^*_{j'+1,k+1}\} = 0 \qquad \text{(VI.9)}$$

Inspection of the equations show that the N unknown concentrations, $C^*_{j,k+1}$, at N radial points on the $(k+1)^{th}$ axial plane are given by the N linear equations

$$\tilde{A}\, C_{k+1} = \tilde{b} \qquad \text{(VI.10)}$$

where: C_{k+1} is a N x 1 vector of the unknowns $(C^*_{1,k+1}, C^*_{2,k+1} \cdots C^*_{N,k+1})^T$

$\tilde{b}$ is a N x 1 vector of known functions, principally linear combinations of $C^*_{j,k}$

$\tilde{A}$ is a N x N matrix with known elements.

The matrix $\tilde{A}$ is tridiagonal and solution to equation (VI.10) is obtained using Thomas's Method. Roache (1972) gives a concise and accurate explanation of how the method works. Radial concentration solution points are quickly and easily obtained for the $(k+1)^{th}$ axial station and this process can be repeated, in the typical marching style of parabolic partial differential equations.

Accuracy of the Finite Difference Approximations

The Thomas Method categorises a typical interior point in equation (VI.10) as

$$- R_j\, C^*_{j+1} + S_j\, C^*_j - T_j\, C^*_{j-1} = b_j \qquad \text{(VI.11)}$$

where R_j, S_j and T_j represent elements in the $\tilde{A}$ matrix and the axial station subscript has been dropped for convenience. To keep the size of round-off error to low proportions it is sufficient that

$$R_j < 0,\ S_j < 0,\ T_j < 0$$

$$S_j > R_j + T_j \qquad j = 2, \ldots N-1 \qquad \text{(VI.12)}$$

The corresponding formulae for S_j, R_j and T_j in the radial dispersion model indicate categorically that the system is well conditioned.

$$R_j = \frac{\alpha}{2\Delta R^{*2}} + \frac{\alpha}{4R_j^{*}\Delta R^{*}}$$

$$S_j = \frac{(1-R_j^{*2})}{\Delta\lambda} + 0.5 + \frac{\alpha}{\Delta R^{*2}} \qquad \text{(VI.13)}$$

$$T_j = \frac{\alpha}{2\Delta R^{*2}} - \frac{\alpha}{4R_j^{*}\Delta R^{*}}$$

To further test the efficiency and accuracy of the Thomas Method a solution to equation (VI.10) was also obtained by the General Gaussian Elimination Technique. Since $\tilde{A}$ was non-singular for the general case, the solution so obtained was unique since rank $\tilde{A}$ = N.

Both algorithms given the same input data gave exact concentrations to an accuracy $>10^{-9}$, far greater than the accuracy due to the finite difference approximation to equation (VI.3). Comparison of computer time revealed that the Thomas method was an order of magnitude faster which concluded that the Thomas Method provided the quickest and most efficient way of solving the RDM.

An analysis on the accuracy of the concentration profile derived from the finite difference method was also carried out. Leading error terms in the Taylor series approximations to the differential equation are summarised in Table VI.1

TABLE VI.1

General formula	$-\frac{\alpha\, O(\Delta R_j^{*2})(1-R_j^{*})}{R_j^{*}} - (1-R_j^{*2})O(\Delta\lambda)$
Reactor centreline formula	$-2\alpha\, O(\Delta R_j^{*2})$
Wall boundary condition	$+\alpha\, O(\Delta R^{*})$

For a typical concentration point, chosen in the reactor, variation of radial accuracy from 10 to 30 stations created a change in the concentration of less than 0.1%. Variation of axial accuracy from 0 to 5 axial stations between specified axial reactor positions produced a change of less than 0.2%. With respect to the computer time required for each run 15 radial stations were chosen and the equations were solved at 2 axial stations between each specified reactor position.

A P P E N D I X V I I

SUMMARY OF REGRESSION TECHNIQUES

Estimation of the rate constants both in the simulations in Chapter 4 and for the experimental data, and estimation of the global Arrhenius parameters all required use of linear and non-linear regression techniques. A brief introduction of the methods used are given here but a more detailed description can be found, for instance, in Draper and Smith (1966).

The model for estimation of the rate constant assuming plug flow is given by equation (4.5)

$$\frac{1 - \phi_{f2}}{1 - \phi_{f1}} = e^{-2\beta Z^*} + \varepsilon_i \qquad \text{(VII.1)}$$

and the model for the Arrhenius parameters by

$$k = Ae^{-E/RT} + \varepsilon_i \qquad \text{(VII.2)}$$

where ε_i denotes the general model error. Both models given by equations (VII.1) and (VII.2) are non-linear in the parameters β, A and E and thus non-linear regression techniques should be used to estimate them. Since both are intrinsically linear, however, very often they are reduced to linear models and linear regression is used to estimate the parameters

$$\ln(1 - \phi_{f2}) = -2\beta Z^* + \text{constant} + \varepsilon_i \qquad \text{(VII.3)}$$

$$\ln k = \ln A - \frac{E}{RT} + \varepsilon_i \qquad \text{(VII.4)}$$

When plug flow was assumed, estimation of the rate constants from the

experimental data was achieved using unweighted linear least squares, since no prior information was available about the confidence with which each point was known. For a general linear model

$$y_i = b_o + b_i x_{1i} + b_2 x_{2i} + \ldots b_{(p-1)} x_{(p-1)i} + \varepsilon_i \quad \text{(VII.5)}$$

where: y_i is the i^{th} measurement of the dependent variable

x_{ji} is the i^{th} measurement or set point for the independent variable x_j

ε_i is the unknown error associated with the measurement

The best estimates of the parameters b_o, b_1 ... b_{p-1} denoted by the vector $\hat{b}$ are obtained by minimising the sum of squares of the residuals between measured values and predicted values of y_i

$$S = (y - Xb)^T(y - Xb) \quad \text{(VII.6)}$$

and the estimates are given by

$$\hat{b} = [X^T X]^{-1} X^T y \quad \text{(VII.7)}$$

where: X is the n x p matrix (rank X ≥ p) of the independent measurements 1, X_{1i}, X_{2i} ... $X_{(p-1)i}$

n is the number of independent measurements

y is the N x 1 vector of measurements, y_i

Furthermore, the covariance matrix of $\hat{b}$ can be developed as

$$V(\hat{b}) = (X^T X)^{-1} \sigma^2 \quad \text{(VII.8)}$$

The quantity σ^2 represents the variance of the residuals between experimental measurement and predicted values for the dependent variable y and is thus approximated by s_o^2 given by

$$s_o^2 = \frac{S}{n - p} \qquad \text{(VII.9)}$$

where n-p is the number of degrees of freedom for the regression fit and shows that p degrees of freedom have been lost because there are p linear restrictions on the values of the residuals $y_i - \hat{y}$. This is because the parameter set $\hat{b}$ has been estimated from the data. This procedure was used for evaluation of the rate constants using the model given by equation (VII.3). Using equations (VII.8) and (VII.9) a 95% confidence range for each rate constant was established as

$$E(k) \approx \hat{k} \pm t_{0.025,n-2} s_o' = \hat{k} \pm t_{0.025,n-2} \frac{s_o}{\sum_{i=1}^{n} (Z_i - \bar{Z})^2} \qquad \text{(VII.10)}$$

where: s_o' is the estimated variance of the rate constant from eqn. (VII.8)

t is the Students t-test

Z is the axial distance from the start of the isothermal region

A similar approach was used in the evaluation of the global Arrhenius parameters. As equation (VII.10) provided some <u>a priori</u> information on the estimates of the dependent variables (the rate constants), weighted linear regression was used where the weights were based upon the inverse of the estimated variances of the rate constants ($1/s_o'^2$). Using the linear model given by equation (VII.4) the dependent variable for the linear regression is the logarithm of the rate constant. Approximate variances, v_i, for the logarithm of the i^{th} rate constant, k_i, were estimated as

$$v_i^{\frac{1}{2}} = \tfrac{1}{2} \ln \left\{ \frac{k_i + s_{oi}'}{k_i - s_{oi}'} \right\} \qquad \text{(VII.11)}$$

$$w_i = \frac{1}{v_i}$$

where w_i was the weighting for point i in the linear regression. The weighted regression estimates can easily be shown to be given by

$$\hat{b} = (X^T W X)^{-1} X^T W y \qquad W = \text{diag}(w_i) \tag{VII.12}$$

and the covariance of the estimates

$$V(\hat{b}) = (X^T W X)^{-1} \tag{VII.13}$$

The results from use of this procedure are given in Chapter 6, Section 6.4 where the confidence limits for the activation energy and pre-exponential factor were estimated using the Students t-test with n-2 degrees of freedom. The value of these estimated confidence ranges is rather limited, because of the poor confidence with which the variances of the logarithm of the rate constants were known. Even the estimates of the variances of the rate constants were not known with any high accuracy. Nevertheless, the analysis does serve to put approximate bounds on the parameter estimates by which some idea of their accuracy can be obtained.

Results from experimental set C gave a slightly lower activation energy than the first two sets, A and B, (see Chapter 7, Table 7.1). This difference may be apparent primarily because it actually reflects a change in the fundamental kinetics of the pyrolysis or because of the greater uncertainty with which the data was collected during set C.

Let $\hat{b}_1$ = estimated slope from the Arrhenius plot for the runs in set B
= 25461.3 K

$\hat{b}_2$ = estimated slope from the Arrhenius plot for the runs in set C
= 23641.9 K.

Proposing a two-tailed significance test $H_o : b_1 = b_2$ then

$$E(\hat{b}_1 - \hat{b}_2) = E(\hat{b}_1) - E(\hat{b}_2) = 0 \tag{VII.14}$$

$$\text{var}(\hat{b}_1 - \hat{b}_2) = \text{var}(\hat{b}_1) + \text{var}(\hat{b}_2) \approx s^2_{\hat{b}_1} + s^2_{\hat{b}_2} = 282904.3 + 648721.0 \tag{VII.15}$$

where $s^2_{\hat{b}_1}$ and $s^2_{\hat{b}_2}$ are estimated variances of $\hat{b}_1$ and $\hat{b}_2$ using equation

(VII.13) with estimates for the elements in the matrix W given by equation (VII.11). Assuming H_0 is correct then $b_1 - b_2$ is normally distributed with variance $var(\hat{b}_1) + var(\hat{b}_2)$ and the t-statistic can now be formed as

$$T = \frac{\hat{b}_1 - \hat{b}_2}{\sqrt{s^{\hat{}2}_{b_1} + s^{\hat{}2}_{b_2}}} \sim 1.88 \qquad \text{(VII.16)}$$

with $(n_1-2) + (n_2-2)$ degrees of freedom, where n_i is the number of experimental points for estimate $\hat{b}_i$. At a significance level of 5% ($x' = 0.025$), for 11 degrees of freedom, $t \sim 2.201$. Since the rejection zone for the hypothesis $H_0 : b_1 = b_2$ is $t < T$, the values $\hat{b}_1$ and $\hat{b}_2$ are not statistically different at a significance level of 5%.

Alternatively, the models given by equations (VII.1) and (VII.2) could be used to estimate the model parameters by non-linear regression. An exact analogous approach to linear regression is used except that the equations generated from the operation of evaluating $\partial S / \partial b$ are non-linear and must be solved iteratively. This was done for estimation of both the rate constants and the Arrhenius parameters using Broyden's Algorithm to solve the non-linear equations. The high correlation between estimates of the activation energy and the pre-exponential factor demanded a reparametization of the pre-exponential factor given by equation (6.2) in Chapter 6.

In the situation where the rate constant was estimated using the RDM, no analytical form of the model was available and parameter estimates were generated using an algorithm based on Powell's Method (1964) which minimised the objective function given by S . Of course, the process would be totally acceptable for parameter estimation using a model with a known analytical form such as the Arrhenius model, equation (VII.2), or the PFM, equation (VII.1), and would give identical values as that obtained by solving the analytical equations given by $\partial S / \partial b = 0$.

Residual Sum of Squares for the Non-Linear Estimation of α and β

Run Number	Number of Points	Simultaneous Estimation of α and β Using the RDM	Estimation of β Using the RDM With an a priori value of α	Estimation of β Using the Non-linear PFM (see eqn. VII.1)
4	6	9.055 E-5	9.918 E-5	1.290 E-4
5	6	1.850 E-4	3.402 E-4	3.887 E-4
6	6	1.009 E-4	5.228 E-4	4.083 E-4
7	6	2.366 E-4	1.082 E-3	2.343 E-4
8	6	7.382 E-4	4.728 E-3	7.065 E-4
9	6	7.402 E-4	1.415 E-3	2.250 E-3
11	5	1.951 E-5	5.416 E-5	4.794 E-4
12	6	7.649 E-4	2.404 E-3	7.540 E-4
13	6	8.096 E-3	1.259 E-2	8.088 E-3
14	5	1.188 E-3	3.649 E-3	1.168 E-3
15	6	3.840 E-4	4.724 E-3	2.772 E-3
16	6	4.130 E-3	1.068 E-2	4.115 E-3
17	6	1.084 E-3	2.311 E-3	1.074 E-3
18	6	4.333 E-5	2.271 E-4	4.229 E-5
19	6	5.705 E-5	4.200 E-4	5.524 E-5
20	6	9.120 E-5	1.638 E-4	2.236 E-4
21	6	1.801 E-4	3.814 E-4	5.451 E-4
22	6	3.503 E-4	5.332 E-4	6.666 E-4
23	6	3.737 E-3	5.881 E-3	7.579 E-3
25	6	9.440 E-4	2.480 E-3	3.817 E-3
26	5	1.733 E-4	4.282 E-4	1.684 E-4

A P P E N D I X V I I I

SIMULATED ESTIMATION OF THE GLOBAL RATE CONSTANT

Non-linear plots of the confidence regions for the α-β plane in the simulations in Chapter 4, Section 4.11 are governed by equation (4.9)

$$S(b) = S(\hat{b}) \{1 + \frac{p}{N-p} F(p, N-p, 1-x')\} \qquad \text{(VIII.1)}$$

Substituting values for p (= 3), N (= 13) and F (= 3.71) used in the simulations, an approximate 95% confidence interval is given as

$$S(b) = 2.113\, S(\hat{b}) \qquad \text{(VIII.2)}$$

These are the non-linear contours which are constructed in Fig. 4.1a and 4.1b, where S(b) was determined in each simulation using an available contouring package. Each linear approximation of the non-linear contour was developed from estimates of the covariance matrix for the parameter estimates on the basis of 50 simulations for each set of simulated conditions of α and β. Reasonable estimates for the covariance matrix elements were difficult to judge since there is no analytic equivalent for the information matrix X^TX in equation (4.10). The simulation set size, 50, was guestimated from a chi-squared test with N-3 degrees of freedom (Mandel, 1964) to estimate the "true" variance of α, β and γ assuming their sample distributions were Gaussian, when in reality, they are not because of the non-linearity of the RDM. The validity of using only 50 simulations was, however, reconciled by the close proximity between the non-linear contour and the linear approximation, illustrated in Figs. 4.1a and 4.1b.

Observability of the RDM Parameters

One of the problems with sampling from the centreline only is to ensure that all the parameters in the model are observable from these measurements alone. This will be true providing each parameter has an independent influence on the centreline profile; in this way, each parameter can be estimated from the noisy centreline measurements. In the limit of infinite radial mixing the parameter α becomes totally unobservable since its value has no effect on the estimated simulation centreline profile.

For a linear time invariant deterministic model, the problem of observability is trivial

$$y = Hb \qquad \text{(VIII.3)}$$

where: H is a N' x N matrix of known elements

b is a N x 1 parameter vector

y is a N' x 1 measurement vector

The parameter states b are observable from the measurement vector y providing

$$\text{rank } H \geq N \qquad \text{(VIII.4)}$$

According to Aoki (1967), a stochastic representation of the given model where measurements with noisy statistics are introduced is observable if the deterministic model is observable.

For non-linear models, there is no straightforward way to obtain whether the parameters are totally observable from the measurement data. Several simulations were performed to ensure that the deterministic representation of the RDM did have observable parameters, which uniquely defined the model and the results are given in Table VIII.1.

TABLE VIII.1

True parameters $\alpha = 0.45$

$\beta = 0.85$

$\gamma = 1.00$

Initial conditions			Number of function evaluations using Powell's Algorithm	Residual sum of squares
α	β	γ		
1.0	1.2	1.1	271	0.74 E-15
0.1	1.2	1.1	229	0.31 E-15
0.1	0.6	0.9	194	0.19 E-14
1.0	0.6	1.2	264	0.82 E-18
0.1	0.2	0.7	NO SOLUTION OBTAINED	

In each simulation where a solution was obtained, the true parameter set was re-obtained with effectively a zero residual sum of squares (in fact, a finite value must be obtained depending on the tolerance set in the algorithm). This demonstrates that the deterministic non-linear RDM is observable and it is tacitly assumed that the same is true for the stochastic non-linear RDM, although this cannot be effectively demonstrated.

Simulation Results

(I) Table VIII.2: Estimated elements of the covariance matrix, V (see Chapter 4, Section 4.10).

(II) Tables VIII.3 and VIII.4: Estimation of β using an *a priori* value of ω.

(III) Table VIII.5: Estimation of β when radial mixing is finite, assuming plug flow.

TABLE VIII.2

Simulation Set			Elements of $V = v_{ij}$					
α	β	σ, σ_R	$v_{\alpha\alpha}$	$v_{\beta\beta}$	$v_{\gamma\gamma}$	$v_{\alpha\beta}$	$v_{\alpha\gamma}$	$v_{\beta\gamma}$
0.45	0.85	0.01	1.309 E-2	1.199 E-3	4.123 E-5	-3.624 E-3	3.187 E-4	-4.929 E-5
1.5	0.85	0.01	1.098	3.134 E-4	9.159 E-5	-1.284 E-2	6.347 E-3	-5.780 E-5
0.45	0.85	0.033 C^*	0.1048	1.324 E-2	3.523 E-4	-2.520 E-2	2.329 E-3	1.390 E-4
1.5	0.85	0.033 C^*	1.578	9.318 E-4	6.164 E-4	-2.582 E-2	1.058 E-2	-3.846 E-5
0.45	2.0	0.01	1.572 E-2	5.0 E-3	2.387 E-5	-8.4 E-3	9.855 E-5	-2.717 E-5
1.5	2.0	0.01	0.4835	1.7 E-3	1.5836 E-5	-2.18 E-2	4.914 E-4	-3.284 E-6
0.45	2.0	0.033 C^*	0.1531	8.784 E-3	8.974 E-4	-2.879 E-2	4.869 E-3	-9.252 E-4
0.45	0.25	0.01 C^*	0.2661	1.453 E-3	4.415 E-5	-1.637 E-2	-6.942 E-4	1.631 E-4
1.5	0.25	0.01 C^*	0.5793	6.651 E-4	4.048 E-5	-1.249 E-2	2.579 E-3	8.862 E-7

TABLE VIII.3

Simulation: $\beta = 0.85$, $\omega = 0.3825$, $\sigma = 0.01$

50 simulations per set

Assumed ω	Mean of β	95% Confidence Interval
0.2000	0.9727	2.52 E-2
0.2500	0.9231	3.04 E-2
0.3000	0.8883	2.69 E-2
0.3500	0.8615	2.27 E-2
0.3825	0.8484	2.33 E-2
0.4500	0.8312	2.02 E-2
0.5000	0.8204	2.48 E-2
0.6000	0.8013	2.30 E-2
2.0000	0.7538	1.89 E-2

TABLE VIII.4

Simulation: $\beta = 0.85$, $\omega = 1.275$, $\sigma = 0.01$

50 simulations per set

Assumed ω	Mean of β	95% Confidence Interval
0.500	0.9119	2.55 E-2
0.750	0.8706	2.03 E-2
1.000	0.8609	2.24 E-2
1.275	0.8520	2.22 E-2
1.500	0.8441	2.25 E-2
1.750	0.8351	1.90 E-2
2.000	0.8391	2.16 E-2
2.500	0.8329	2.24 E-2
4.250	0.8261	2.07 E-2

TABLE VIII.5

Simulation: $\beta = 0.85$, $\sigma = 0.01$

50 simulations per set

Simulation	Linear Regression		Non-Linear Regression	
α	Mean of β	95% Confidence Interval	Mean of β	95% Confidence Interval
0	0.4251	1.89 E-2	0.4247	1.44 E-2
0.45	0.7736	2.67 E-2	0.7402	2.20 E-2
1.5	0.8307	2.60 E-2	0.8174	1.70 E-2
4.0	0.8414	3.07 E-2	0.8406	1.97 E-2

A P P E N D I X I X

PRODUCT DISTRIBUTION SIMULATION USING THE SIMPLE FREE RADICAL MECHANISM

The free radical mechanism proposed by Powers and Corcoran (1974) was used in the simulations in Chapter 5 to indicate an acceptable way by which the larger mechanism proposed by Allara and Edelson (1980) should be used to model the experimentally obtained product distributions. The volume of data generated by these simulations precludes its addition to this Appendix and only the numerical values from the simulations described in Figs. 5.2 and 5.3 in Chapter 5 are included. In all the simulations an error analysis was continuously performed to ensure that the error limits were such that estimated errors in the solution (either the algebraic equations for the radical species, the integration by the Kutta-Merson variable step size method, or the integration by using Gear's Algorithm) were small enough that they did not influence any conclusions drawn from the simulation results.

Data Used in Fig. 5.2

Simulation conditions closely approximate those for experimental run 5 (set A).

Isothermal temperature (T_g) = 939.3 K. Conversion range within the isothermal zone (ϕ_s - ϕ_e) = 25.2 - 42.0.

Table IX.1: Isothermal integration ($T = T_g$) from ϕ = 0 to 54% using Gear's method. As initial conditions, all radical and molecular species flows were zero apart from butane, diluted with inert nitrogen. Ethylene used as a typical molecular yield.

Table IX.2: Isothermal integration ($T = T_g$) from $\phi = \phi_s$ to 54% using Gear's method. As initial conditions the molecular species concentrations were those predicted by integration from $\phi = 0$. The radical species' concentration were assumed zero. Ethylene used as a typcial molecular yield.

Table IX.3: Non-isothermal integration from $\phi = 0$ to 54% with Gear's method using the following imposed temperature profile:

$$T = 875. + 2.55\,\phi \qquad \phi \leq \phi_s$$

$$T = T_g = 939.3\ K \qquad \phi > \phi_s$$

Ethylene was used as a typical molecular yield.

Data Used in Fig. 5.3

Simulation conditions closely approximate those for experimental run 7 (set A).

Isothermal temperature (T_g) = 970.0 K. Conversion range within the isothermal zone (ϕ_s - ϕ_e) = 45.0 - 70.0.

Table IX.4: Isothermal integration ($T = T_g$) from $\phi = 0$ to 70% using Gear's method. As initial conditions, all species' concentration were zero except the butane feed. Ethylene and hydrogen used as typical molecular yields.

Table IX.5: Non-isothermal integration from $\phi = 0$ to 70% using Gear's method with the following imposed temperature profile:

$$T = 875. + 2.111\phi \qquad \phi \leq \phi_s$$

$$T = T_g = 970.0\ K \qquad \phi > \phi_s$$

Ethylene and hydrogen used as typical molecular yields.

Table IX.6: Non-isothermal integration from ϕ = 0 to 70% using the SSA with the same imposed profile as above.

TABLE IX.1

Conversion	Ethylene Yield (100 moles/100 moles feed)
0	0
1.12	0.60
6.56	3.70
12.98	7.56
18.49	11.02
25.24	15.41
31.02	19.28
26.05	22.75
40.49	25.86
47.98	31.24
54.07	35.75

TABLE IX.2

Conversion	Ethylene Yield
25.24	15.41
25.26	15.43
28.75	17.76
32.55	20.33
44.41	28.65
51.15	33.57

TABLE IX.3

Conversion	Ethylene Yield
0	0
3.48	1.68
10.18	5.25
19.03	10.49
23.89	13.60
35.03	21.16
39.61	24.38
43.67	27.28
47.31	29.92
50.57	32.32

TABLE IX.4

Conversion	Ethylene Yield	Hydrogen Yield
0	0	0
6.32	3.73	1.63
16.55	10.27	3.74
24.65	15.78	5.09
29.79	19.41	5.82
39.61	26.59	7.05
50.09	34.61	8.11
57.90	40.85	8.78
63.92	45.81	9.24
68.70	49.85	9.56

TABLE IX.5

Conversion	Ethylene Yield	Hydrogen Yield
0	0	0
4.69	2.30	0.75
11.07	5.72	1.55
18.09	9.81	2.34
29.71	17.28	3.55
35.88	21.58	4.18
44.49	27.99	5.06
53.73	35.28	5.92
60.73	40.99	6.48
66.18	45.58	6.86

TABLE IX.6

Conversion	Ethylene Yield	Hydrogen Yield
0	0	0
2.47	1.18	0.42
7.99	4.03	1.18
18.83	10.26	2.42
26.10	14.87	3.18
37.82	22.99	4.38
47.20	30.10	5.33
55.76	36.92	6.09
62.29	42.30	6.60
67.42	46.64	6.95
71.55	50.22	7.20

A P P E N D I X X

OVERALL MATERIAL BALANCES AND GAS PROBE SAMPLING CONDITIONS

Sampling and Coolant Flowrates

Earlier experiments had revealed that the sampling flowrate did not remain constant when sampling from the same reactor position and tended to fall due to slow continuous build-up of carbon on the inner capillary wall, brought about by heterogeneous reaction occurring at the wall surface. In this respect, the probe model described in Chapter 3, Section 3.12 is erroneous because it fails to account for the heterogeneous reaction and hence ignores this gradual decay in sampling flowrate under the same available pressure drop.

During the experiments, the probe sampling flowrate was held at a value of 1.5 cm^3/sec (1 atm, $\sim$300 K) for all the sampling positions within the reactor. In the situation when the available pressure drop could not produce such a flow, the flow control valve was fully opened. At no time, in all the experiments, did the flowrate drop below 1 cm^3/sec. Maintaining a constant flowrate tends to decrease the aerodynamic error, yet increase the reaction error as sampling progresses down the isothermal region, although the simulations show that apart from the higher zones of the region, the reaction error is almost negligible. The overall effect was to reduce the difference between the two errors and thus aid in maintaining a smaller overall sampling error throughout the whole of the sampling zone, since each individual error is acting in opposite directions, see Chapter 3, Section 3.13.

It was discussed in Chapter 3, Section 3.15, that a coolant flowrate of 100 cc/sec for the sampling procedure was too large for the base section

of the isothermal region. A coolant flowrate that large was well above a value needed to adequately quench the sample, since the sample elements had comparatively little to travel to be withdrawn from the reactor. This was fully reflected in the simulations which predicted an unnecessarily excess temperature difference between the sampled gas elements and the coolant flow, see Appendix V. As a result, the calculated error due to chemical reaction with the probe was of negligible proportions.

Experimentally, the subsequent "heat sink" effect of the probe distorted the axial temperature profile by 1 - 2^{o}C from the profile which existed under similar operating conditions but with no coolant flowing through the probe. This suggests that some sort of thermal effect is occurring within the reactor which could seriously affect the temperature field of the process gas upstream of the sampling point. Table X.1 shows the change in heat input from the five heaters to the reactor as a result of introducing a coolant flowrate for the probe of 100 cc/sec.

TABLE X.1

Axial position of probe tip from reactor entrance (cm)	Heater 1 (W)	Heater 2 (W)	Heater 3 (W)	Heater 4 (W)	Heater 5 (W)
84.1	∿0	∿0	4.0	6.0	14.0
96.1	∿0	∿0	2.0	7.0	12.0
108.1	∿0	∿0	∿0.5	8.5	12.0
120.1	∿0	∿0	∿0	2.0	22.0

Power measurement was made by a bank of semi-conductor thermistors which were calibrated for resistance against power input to each heater.

Quantitatively, it was difficult to select a coolant flowrate which could adequately restrict the amount of chemical reaction within the

probe and yet ensure that no thermal effects around the probe tip would be present. The coolant flowrate was finally chosen so that no distortion whatsoever could be detected in the observed axial temperature throughout the whole sampling time period and range of sampling positions. Typically, flowrates as illustrated in Table X.2 were chosen.

TABLE X.2

Axial position of the probe tip from the reactor entrance (cm)	Coolant flowrate used cm^3/sec (1 atm, 300 K)
84.1	100.0
90.1	80.0
96.1	65.0
102.1	50.0
108.1	40.0
114.1	30.0
120.1	30.0
126.1	30.0

Feed Flow and Composition Measurement and Overall Material Balances

Feed composition was measured prior to experimental gas sampling within the reactor since the chromatographic analysis was limited to measuring either nitrogen or hydrogen. Normally a series of about 15 measurements were taken and the average composition used as the final value. It is worth noting that although feed composition measurement was taken, it did not influence the calculation of either the conversion or the product yields as described in Appendix II. To complement the feed measurement an overall carbon material balance was calculated by measuring the nitrogen/methane ratio at the last experimental sampling point in each

experiment. In addition, the composition analysis in Appendix II afforded another indication of the accuracy of the overall composition measurements by balancing the measured carbon input to that predicted by equation (II.8). A certain degree of correlation is discernible between the two independently measured carbon balances illustrated in Tables X.3, X.4 and X.5. The discrepancy between the amount of carbon in the feed and that measured or predicted at the last experimental point is an indication of the combination of the amount of carbon lay-down on the reactor surface and the amount of hydrocarbon that was not measured or detected during the composition analysis.

TABLE X.3 - Experimental Set A

	Run 4	Run 5	Run 6	Run 7	Run 8	Run 9	Run 10
Feed Flowrate (cm^3/sec, 1 atm. 300 K)							
- Butane	10.7	11.0	11.0	10.6	10.8	11.1	10.7
- Nitrogen	98.4	99.1	99.1	98.4	97.7	98.8	98.0
- Overall	109.1	110.1	110.1	109.0	108.5	109.9	108.7
Feed Composition (%)							
- Butane	9.69	9.86	10.30	9.80	9.93	10.18	11.57
- Nitrogen	90.31	90.14	89.70	90.20	90.07	89.82	88.43
Approximate Reynolds Number in the Isothermal Region	78.6	78.2	77.4	75.8	74.7	75.8	-
Centreline Velocity (cm/sec)	21.8	22.3	22.7	22.8	23.1	23.4	-
Carbon Balance I (%)*	+0.05	-0.93	-2.46	-2.79	-6.86	-7.70	-2.27
Carbon Balance II (%)**	-4.00	-3.96	-3.90	-3.90	-3.73	-3.69	-

* Using equation (II.8) in Appendix II

** From CH_4/N_2 measurement at the last sampling point

TABLE X.4 - Experimental Set B

	Run 11	Run 12	Run 13	Run 14	Run 15	Run 16	Run 17	Run 18	Run 19
Feed Flowrate (cm^3/sec, 1 atm.300 K)									
- Butane	5.20	5.15	5.20	5.20	5.05	5.25	5.15	5.15	5.15
- Nitrogen	101.6	101.9	101.9	101.9	101.2	101.6	101.6	101.2	101.6
- Overall	106.8	107.1	107.1	107.1	106.3	106.9	106.8	106.4	106.8
Feed Composition (%)									
- Butane	4.80	4.94	5.08	5.01	5 13	4.97	4.97	4.84	5.15
- Nitrogen	95.20	95.06	94.92	94.99	94.87	95.03	95.03	95.16	94.85
Approximate Reynolds Number in the Isothermal Region	74.9	75.2	74.4	73.6	72.8	72.8	75.4	76.3	79.9
Centreline Velocity (cm/sec)	22.2	22.2	22.4	22.9	22.8	23.2	21.8	21.3	22.7
Carbon Balance I (%)	-3.71	-1.91	-3.08	-6.08	-7.71	-9.33	-3.05	-2.36	-1.69
Carbon Balance II (%)	+0.47	-4.38	-0.74	-5.83	-1.31	-10.52	-2.02	-	-5.40

TABLE X.5 - Experimental Set C

	Run 20	Run 21	Run 22	Run 23	Run 24	Run 25	Run 26	Run 27
Feed Flowrate (cm^3/sec, 1 atm.300 K)								
- Butane	22.4	21.6	21.4	21.9	22.4	22.2	22.0	21.4
- Nitrogen	199.0	199.8	200.2	201.1	199.8	199.0	199.8	199.8
- Overall	221.4	221.4	221.6	223.0	222.2	221.2	221.8	221.2
Feed Composition (%)								
- Butane	10.04	9.80	9.85	10.12	9.98	10.14	9.68	9.77
- Nitrogen	89.96	90.2	90.15	89.88	90.02	89.86	90.32	90.23
Approximate Reynolds Number in the Isothermal Region	159.5	157.4	155.6	154.8	-	151.2	150.5	-
Centreline Velocity (cm/sec)	43.9	44.8	45.8	47.0	-	47.7	48.3	-
Carbon Balance I (%)	+0.52	-1.04	-1.43	-2.85	-4.57	-8.69	-6.85	-10.60
Carbon Balance II (%)	-5.70	-4.30	-1.21	-3.00	-13.49	-3.46	-7.64	-24.16

A P P E N D I X X I

MEASURED AXIAL WALL AND CENTRELINE GAS TEMPERATURE PROFILES

Axial wall temperature profiles were measured using 14 Pt/Pt 13% Rh uncompensated thermocouples. Five additional thermocouples were used as measurement for the 5 thyristor controllers which regulated the heat input to each furnace heater. Constant monitoring ensured the axial temperature profile remained unchanged throughout the whole time period of each experiment. Variation of the profile was found to be virtually non-existent, certainly less than $1^{o}C$ from the originally determined profile. Wall profiles used for each experimental run in sets A, B and C are given in Tables XI.1, XI.2 and XI.3 respectively.

Axial and radial gas temperatures were measured using a chromel-alumel uncompensated thermocouple probe. Overall measured gas temperature variation was less than $3\text{-}4^{o}C$ in all radial and axial directions throughout the isothermal section. Normally in each experimental run, two axial sets of temperature measurements were made, before and after the gas sampling in the reactor. With each axial set, two radial temperature sets were taken, one near the top, and one near the base of the chosen isothermal region. Radial temperature variation near the top of the isothermal region was consistently only $2\text{-}3^{o}C$ above the centreline measurement and near the base variation was as little as $1^{o}C$.

The difference between the two axial gas temperature profiles was consistent with the local time-gas temperature history measurements illustrated in Appendix IV, Table IV.1, and was less than $1^{o}C$. Averaged measured axial gas temperature profiles for each experimental run in Sets A, B and C are given in Tables XI.4, XI.5 and XI.6 respectively, and corrected gas temperatures for each run are given in Appendix IV.

TABLE XI.1

Axial Wall Temperature Measurements for Experiment Set A (^{o}C)

Distance From Reactor Entrance (cm)	Thermocouple Number	Run 4	Run 5	Run 6	Run 7	Run 8	Run 9	Run 10
25.0	1	185.0	183.0	200.0	202.0	212.0	210.0	192.0
42.0	2	595.5	614.5	638.0	641.0	661.0	651.0	615.0
46.8	3C*	~666.0	~687.0	~707.0	~727.0	~746.0	~746.0	~707.0
52.0	4	694.0	715.0	741.0	748.0	770.0	767.0	734.5
57.2	5	-	-	-	-	-	-	-
62.4	6C	~666.0	~687.0	707.0	~727.0	~746.0	~746.0	~707.0
67.6	7	666.0	687.0	~707.0	727.0	747.0	747.0	707.0
73.3	8	-	-	-	-	-	-	-
79.0	9	665.0	-	-	-	-	-	-
84.8	10C	~666.0	~687.0	~707.0	~727.0	~746.0	~747.0	~707.0
90.6	11	666.0	686.5	706.0	727.0	746.0	747.0	707.0
96.4	12	666.0	687.0	707.0	726.5	746.0	747.0	707.0
102.3	13	665.5	687.0	706.5	725.5	746.0	746.5	705.0
108.2	14C	~666.0	~687.0	~707.0	~727.0	~746.0	~746.0	~707.0
114.0	15	667.0	688.0	707.0	727.5	747.0	748.0	707.5
119.4	16	666.0	687.0	706.0	727.0	747.0	746.5	707.0
124.7	17	667.5	687.0	708.0	727.0	747.5	747.0	707.0
130.0	18C	~640.0	~650.0	~670.0	~690.0	~710.0	~710.0	~670.0
135.3	19	493.5	504.0	523.0	538.0	555.0	548.0	512.0

* C denotes controller input.

TABLE XI.2

Axial Wall Temperature Measurements for Experiment Set B (^{o}C)

Distance From Reactor Entrance (cm)	Thermocouple Number	Run 11	Run 12	Run 13	Run 14	Run 15	Run 16	Run 17	Run 18	Run 19
25.0	1	192.0	185.5	196.5	200.0	199.0	203.0	181.5	179.0	180.0
42.0	2	610.0	603.5	626.5	642.0	641.0	662.0	599.0	582.5	593.5
46.8	3C	~707.0	~707.0	~720.0	~740.0	~746.0	~760.0	~690.0	~670.0	~680.0
52.0	4	732.0	730.0	757.0	776.0	777.0	797.5	723.5	704.5	715.5
57.2	5	-	-	-	-	-	-	-	-	-
62.4	6C	~707.0	~707.0	~720.0	~740.0	~746.0	~760.0	~690.0	~670.0	~680.0
67.6	7	707.0	707.0	720.0	740.0	746.0	760.0	690.0	670.5	680.5
73.3	8	-	-	-	-	-	-	-	-	-
79.0	9	-	-	-	-	-	-	-	-	-
84.8	10C	~707.0	~707.0	~720.0	~740.0	~746.0	~760.0	~690.0	~670.0	~680.0
90.6	11	707.0	707.0	720.0	740.5	745.5	760.0	690.0	670.0	680.0
96.4	12	707.0	707.0	720.5	741.5	746.0	761.0	690.5	671.0	681.0
102.3	13	706.0	706.5	719.0	740.0	745.0	760.0	690.0	670.0	680.0
108.2	14C	~707.0	~707.0	~720.0	~740.0	~746.0	~760.0	~690.0	~670.0	~680.0
114.0	15	707.5	707.5	721.0	741.5	747.0	762.0	692.5	670.0	680.5
119.4	16	707.0	707.5	719.5	740.0	746.0	761.0	691.0	670.0	680.0
124.7	17	707.0	707.5	721.0	740.0	746.0	760.0	690.0	670.0	680.5
130.0	18C	~670.0	~670.0	~685.0	~700.0	~705.0	~720.0	~655.0	~640.0	~650.0
135.3	19	580.0	503.5	522.0	535.5	537.0	550.0	493.5	482.0	487.0

TABLE XI.3

Axial Wall Temperature Measurements for Experiment Set C (^{o}C)

Distance From Reactor Entrance (cm)	Thermocouple Number	Run 20	Run 21	Run 22	Run 23	Run 24	Run 25	Run 26	Run 27
25.0	1	400.0	380.0	400.0	401.0	406.0	396.0	435.0	438.5
42.0	2	605.0	614.5	633.5	651.5	667.5	676.5	707.5	725.0
46.8	3C	~680.0	~700.0	~720.0	~740.0	~760.0	~780.0	~800.0	~820.0
52.0	4	713.5	728.0	759.0	778.0	802.5	821.0	844.5	-
57.2	5	-	-	-	-	-	-	-	-
62.4	6C	~680.0	~700.0	~720.0	~740.0	~760.0	~780.0	~800.0	~820.0
67.6	7	680.5	701.0	720.0	744.0	763.0	780.5	800.5	821.0
73.3	8	-	-	-	-	-	-	-	-
79.0	9	-	-	-	-	-	-	-	-
84.8	10C	~680.0	~700.0	~720.0	~740.0	~760.0	~780.0	~800.0	~820.0
90.6	11	680.5	701.0	720.0	740.5	757.0	780.0	800.5	820.5
96.4	12	681.0	701.0	720.5	741.0	758.0	781.0	801.5	820.5
102.3	13	680.0	700.5	718.0	739.0	756.5	~778.0	798.5	818.5
108.2	14C	~680.0	~700.0	~720.0	~740.0	~760.0	~780.0	~800.0	~820.0
114.0	15	682.0	702.0	722.0	742.5	760.0	781.5	801.0	821.0
119.4	16	681.0	701.0	721.0	741.5	758.0	780.5	800.5	820.0
124.7	17	680.0	700.5	720.5	741.0	756.5	780.0	800.0	820.0
130.0	18C	~650.0	~665.0	~685.0	~705.0	~720.0	~745.0	~765.0	~785.0
135.3	19	498.0	532.5	538.0	555.0	561.0	575.0	-	-

TABLE XI.4

Average Axial Centreline Gas Temperature Measurements for Experiment Set A (^{o}C)

Distance From Reactor Entrance (cm)	Run 4	Run 5	Run 6	Run 7	Run 8	Run 9	Run 10
59.0	644.0	665.0	687.0	705.5	722.5	718.5	678.0
65.0	648.0	667.5	688.5	708.0	727.0	727.0	687.0
71.0	650.5	670.0	691.0	711.0	729.5	730.5	692.0
77.0	653.0	672.0	693.5	712.0	730.5	730.5	691.5
83.0	656.0	676.0	696.0	714.5	734.0	732.0	693.0
89.0	659.0	678.5	698.0	715.5	735.0	734.5	695.0
95.0	660.5	679.5	699.0	716.0	736.0	736.0	696.5
101.0	661.0	680.0	699.5	717.0	736.5	736.5	696.5
107.0	661.5	680.0	700.0	718.0	738.0	737.5	698.0
113.0	662.0	680.5	700.5	718.5	737.5	738.0	698.0
119.0	662.0	681.0	700.5	718.5	737.0	736.0	696.0
125.0	653.0	673.0	693.0	712.5	730.0	730.0	692.0
131.0	593.0	613.0	635.5	650.0	661.6	655.5	633.0

TABLE XI.5

Average Axial Centreline Gas Temperature Measurements for Experiment Set B (^{o}C)

Distance From Reactor Entrance (cm)	Run 11	Run 12	Run 13	Run 14	Run 15	Run 16	Run 17	Run 18	Run 19
59.0	680.5	682.0	700.0	723.0	721.0	739.5	669.5	652.0	663.0
65.0	688.5	688.0	703.0	726.0	728.5	741.0	673.0	654.5	666.5
71.0	693.0	692.0	705.5	726.5	730.0	745.0	675.0	656.5	666.5
77.0	694.0	694.0	708.5	728.5	732.0	747.0	679.0	659.0	668.5
83.0	696.5	696.5	711.0	731.5	735.0	748.5	681.5	662.0	670.5
89.0	698.5	698.5	711.5	732.0	737.0	750.5	683.5	663.5	672.5
95.0	700.0	700.5	712.5	733.5	737.5	751.0	684.5	664.5	674.0
101.0	701.0	701.0	713.5	734.0	738.0	751.5	685.0	665.0	675.0
107.0	701.0	701.0	714.5	734.5	739.5	752.5	685.5	665.5	675.5
113.0	701.5	701.5	714.0	734.0	740.5	753.5	686.5	666.5	675.5
119.0	701.0	699.5	712.0	732.0	739.0	751.5	685.0	665.0	673.5
125.0	695.0	692.0	703.0	726.0	734.0	745.0	680.0	659.0	667.0
131.0	619.5	-	636.0	647.0	653.0	656.0	604.5	592.0	600.0

TABLE XI.6

Average Axial Centreline Gas Temperature Measurements for Experiment Set C (^{o}C)

Distance From Reactor Entrance (cm)	Run 20	Run 21	Run 22	Run 23	Run 24	Run 25	Run 26	Run 27
59.0	655.0	675.0	693.0	714.5	-	749.5	770.5	-
65.0	656.0	676.0	695.0	716.5	-	753.0	770.0	-
71.0	658.0	678.0	696.0	718.5	-	754.0	772.0	-
77.0	660.0	681.5	699.0	720.5	-	754.5	772.5	797.0
83.0	661.5	684.0	702.0	721.0	734.0	755.0	773.5	799.5
89.0	663.5	685.0	703.0	723.0	736.0	756.0	776.5	801.0
95.0	666.5	686.5	705.0	723.5	738.5	759.5	777.0	801.5
101.0	667.5	687.0	706.0	725.5	740.5	761.0	778.5	803.0
107.0	667.5	687.5	707.0	726.5	740.0	762.5	781.0	805.0
113.0	668.0	689.0	708.0	729.0	740.0	763.5	780.5	804.0
119.0	669.0	689.0	706.5	729.5	742.0	762.0	782.5	803.0
125.0	661.0	680.0	697.5	719.0	731.0	753.5	774.0	-
131.0	-	-	640.0	658.0	-	703.5	-	-

A P P E N D I X X I I

COMPOSITION DATA

The composition data as determined from the experimental runs is reported as conversion vs. product yield for all products measured, where the product yield is defined as

$$p_i = \frac{\text{Number of moles of product i formed}}{\text{100 moles of butane feed}}$$

Calculation of such quantities as product selectivity can be directly obtained from the yield data using equation (II.13).

The asterisks located in the axial position from the reactor entrance column denote the region in the reactor which was considered isothermal. Thus the sampling points between these two markers were used in the evaluation of the butane decomposition rate constant and hence Arrhenius parameters. Further information, concerning the axial wall and gas temperature profiles are located in Appendix XI and further information on the feed flowrate and composition and on conditions within the reactor are given in Appendix X.

Experimental Set A ; Run 4 (Corrected Gas Temperature = 923.8 K)

Conversion	Reactor Position (cm)	CH_4	C_3H_8	C_3H_6	C_4H_{10}	$1\text{-}C_4H_8$	Trans-2 $\text{-}C_4H_8$	Cis-2 $\text{-}C_4H_8$	1,3 C_4H_6	C_2H_4	C_2H_6	H_2
6.45	78.1	4.80	.11	4.01	93.55	.10	.06	.03	.02	3.44	.54	1.39
8.04	84.1	6.80	.11	4.49	91.96	.15	.08	.05	.03	4.03	.61	2.20
10.70	90.1*	8.33	.12	6.40	89.30	.17	.09	.06	.04	5.65	.85	2.79
13.43	96.1	10.01	.13	7.70	86.57	.19	.09	.05	.06	8.15	1.13	3.40
15.67	102.1	12.78	.13	9.01	84.33	.23	.10	.07	.07	8.48	1.17	4.08
18.40	108.1	15.61	.15	10.30	81.60	.28	.14	.10	.09	9.77	1.31	4.79
22.19	114.1	16.55	.16	13.24	77.81	.39	.15	.10	.10	12.88	1.67	5.54
24.29	120.1*	18.55	.16	14.11	75.71	.42	.17	.11	.11	14.20	1.81	6.29
26.26	126.1	20.17	.17	15.26	73.74	.47	.17	.12	.12	15.33	1.94	6.60
29.08	132.1	22.17	.18	16.86	70.92	.53	.19	.13	.15	17.16	2.18	7.23
30.51	138.1	22.89	.18	17.05	69.49	.54	.19	.13	.16	19.34	2.37	7.53
		Experimental Set A ; Run 5 (Corrected Gas Temperature = 939.3 K)										
17.60	78.1	13.29	.17	10.15	82.40	.32	.12	.08	.08	10.73	1.23	4.05
22.59	84.1	17.14	.17	12.88	77.41	.42	.15	.10	.12	13.94	1.53	5.42
26.36	90.1*	20.18	.18	14.84	73.64	.51	.16	.12	.16	16.12	1.82	6.61
27.94	96.1	21.18	.19	15.58	72.06	.55	.19	.13	.18	17.42	2.06	6.84
32.11	102.1	24.65	.20	17.61	67.89	.64	.20	.14	.23	20.26	2.15	8.15
35.53	108.1	27.73	.22	19.43	64.47	.72	.22	.16	.29	22.03	2.42	8.85
37.71	114.1	29.41	.22	20.39	62.29	.77	.23	.16	.34	23.62	2.52	9.73
41.38	120.1*	32.16	.24	22.24	58.62	.86	.25	.19	.39	26.39	2.80	10.14
43.65	126.1	34.70	.25	23.06	56.35	.88	.26	.19	.45	27.65	2.98	10.77

Experimental Set A ; Run 6 (Corrected Gas Temperature = 957.1 K)

Conversion	Reactor Position (cm)	CH_4	C_3H_8	C_3H_6	C_4H_{10}	1-C_4H_8	Trans-2 -C_4H_8	Cis-2 -C_4H_8	1,3 C_4H_6	C_2H_4	C_2H_6	H_2
32.09	78.1	24.45	.21	16.91	67.91	.70	.20	.14	.30	20.72	1.95	9.55
33.73	84.1	25.98	.22	17.44	66.27	.69	.20	.14	.29	22.28	2.00	9.93
36.25	90.1*	28.14	.22	18.72	63.75	.78	.21	.15	.36	23.97	2.27	9.81
39.61	96.1	31.79	.24	19.86	60.39	.85	.23	.16	.41	25.92	2.39	11.16
44.58	102.1	35.88	.25	21.73	55.42	.96	.25	.19	.54	29.97	2.48	12.87
49.57	108.1	38.97	.27	24.18	50.43	1.07	.28	.21	.67	34.24	2.98	13.62
53.43	114.1	41.83	.29	25.48	46.57	1.10	.29	.21	.76	37.92	3.25	14.88
56.76	120.1*	44.99	.30	26.53	43.24	1.17	.30	.21	.88	40.46	3.53	15.70
59.46	126.1	48.71	.31	27.25	40.54	1.18	.30	.22	.95	41.46	3.54	17.25

Experimental Set A ; Run 7 (Corrected Gas Temperature = 970.0 K)

36.18	78.1	28.47	.22	17.65	63.82	.81	.21	.15	.45	25.70	2.04	8.63
41.66	84.1	33.73	.25	19.70	58.34	.91	.23	.17	.60	29.35	2.33	10.31
45.52	90.1*	36.71	.26	21.20	54.48	1.01	.25	.18	.67	32.55	2.57	11.53
51.89	96.1	40.16	.28	22.64	48.11	1.08	.26	.19	.82	41.07	3.20	13.00
56.17	102.1	46.20	.30	25.03	43.83	1.17	.27	.20	.97	40.33	3.38	15.26
60.82	108.1	50.68	.32	26.37	39.18	1.22	.29	.21	1.12	44.28	3.54	16.46
65.05	114.1	54.76	.33	27.47	34.95	1.28	.30	.22	1.24	47.64	4.01	17.80
69.33	120.1*	60.51	.35	28.09	30.67	1.27	.31	.22	1.51	50.78	4.01	18.68
72.22	126.1	61.47	.35	28.49	27.78	1.32	.31	.23	1.53	56.90	4.28	19.22

Experimental Set A ; Run 8 (Corrected Gas Temperature = 986.8 K)

Conversion	Reactor Position (cm)	CH_4	C_3H_8	C_3H_6	C_4H_{10}	1-C_4H_8	Trans-2 -C_4H_8	Cis-2 -C_4H_8	1,3 C_4H_6	C_2H_4	C_2H_6	H_2
47.91	78.1	36.62	.28	20.53	52.09	1.02	.25	.18	.41	37.22	2.62	12.90
53.27	84.1	42.40	.29	21.95	46.73	1.07	.26	.19	.99	41.50	2.94	16.64
56.98	90.1*	48.73	.30	22.93	43.02	1.10	.26	.19	1.11	42.33	3.09	17.08
65.53	96.1	55.01	.32	24.85	34.47	1.22	.27	.20	1.33	52.25	3.54	19.46
70.94	102.1	62.85	.35	26.05	29.06	1.25	.28	.21	1.58	54.75	4.18	19.88
75.38	108.1	67.11	.35	25.79	24.62	1.22	.28	.21	1.79	60.51	4.17	22.37
79.61	11.41	71.69	.35	25.51	20.39	1.18	.26	.20	2.00	64.03	4.35	27.38
82.71	120.1*	73.69	.36	25.09	17.29	1.08	.25	.19	2.10	68.12	4.81	31.26
85.20	126.1	77.18	.35	24.02	14.80	.95	.24	.15	2.22	71.57	4.85	33.28

Experimental Set A ; Run 9 (Corrected Gas Temperature = 985.7 K)

49.03	78.1	39.94	.27	20.01	50.97	.94	.25	.19	.82	38.61	2.92	13.10
48.07	84.1	39.05	.26	19.92	51.93	.90	.24	.18	.75	36.46	2.82	15.32
54.43	90.1*	46.11	.28	21.58	45.57	1.01	.25	.19	.89	40.56	3.24	18.04
59.49	96.1	51.16	.30	22.56	40.51	1.04	.27	.19	1.02	44.58	2.45	21.14
65.40	102.1	57.82	.32	23.35	34.60	1.11	.27	.20	1.22	49.53	2.87	23.23
72.46	108.1	65.57	.34	24.34	27.54	1.10	.29	.20	1.49	55.33	4.32	26.64
76.77	114.1	71.14	.35	23.71	23.23	1.03	.27	.19	1.62	59.96	4.56	29.21
79.75	120.1*	73.40	.36	24.00	20.25	1.04	.25	.19	1.69	62.91	2.91	31.87
82.22	126.1	76.06	.36	24.01	17.78	1.01	.24	.19	1.76	65.78	5.01	32.89

Experimental Set A ; Run 10 (Not used for rate constant estimation)

Conversion	Reactor Position (cm)	CH_4	C_3H_8	C_3H_6	C_4H_{10}	1-C_4H_8	Trans-2 -C_4H_8	Cis-2 -C_4H_8	1,3 C_4H_6	C_2H_4	C_2H_6	H_2
22.69	78.1	18.92	.18	11.15	77.31	.37	.24	.20	.14	14.05	1.64	6.37
28.63	84.1	22.33	.20	14.66	71.37	.51	.27	.21	.16	18.78	2.10	7.52
30.64	90.1	25.44	.22	15.03	69.36	.54	.26	.19	.13	19.52	2.18	8.57
35.92	96.1	29.73	.23	17.68	64.08	.64	.28	.22	.29	23.33	2.64	8.84
40.05	102.1	34.29	.26	19.31	59.95	.78	.29	.21	.40	25.56	2.81	9.64
44.24	108.1	36.94	.28	21.39	55.76	.85	.34	.24	.34	28.63	3.31	11.37

Experimental Set B ; Run 11 (Corrected Gas Temperature = 961.6 K)

25.59	78.1	21.75	.18	12.24	74.41	.48	.20	.15	.12	16.70	1.47	7.05
28.21	84.1	23.95	.18	13.25	71.79	.52	.20	.14	.13	18.34	1.51	9.19
27.70	90.1	23.94	.17	13.23	72.30	.52	.21	.14	.14	17.84	1.48	7.68
35.43	96.1*	30.87	.19	16.49	64.57	.69	.22	.17	.23	23.36	1.90	9.65
39.51	102.1	34.63	.21	18.31	60.49	.80	.24	.18	.30	25.66	1.99	11.42
44.44	108.1	38.25	.22	20.11	55.56	.90	.25	.19	.40	30.59	2.22	12.27
50.05	114.1	44.12	.24	21.84	49.95	.98	.26	.20	.47	34.50	2.50	14.33
54.64	120.1*	47.62	.26	23.64	45.36	1.09	.28	.20	.59	37.79	2.72	16.91
58.47	126.1	50.82	.28	24.82	41.53	1.10	.29	.21	.69	42.03	2.95	16.74

Experimental Set B ; Run 12 (Corrected Gas Temperature = 959.0 K)

Conversion	Reactor Position (cm)	CH_4	C_3H_8	C_3H_6	C_4H_{10}	$1\text{-}C_4H_8$	Trans-2 $-C_4H_8$	Cis-2 $-C_4H_8$	1,3 C_4H_6	C_2H_4	C_2H_6	H_2
33.04	78.1	25.77	.19	17.20	66.96	.74	.23	.17	.34	22.27	1.81	7.55
26.17	84.1	21.18	.16	13.15	73.83	.52	.19	.20	.23	17.37	1.39	6.58
30.53	90.1*	24.77	.18	15.27	69.47	.62	.20	.15	.27	20.60	1.58	7.51
36.88	96.1	28.94	.19	17.61	63.12	.74	.23	.16	.35	26.82	1.99	9.76
40.96	102.1	33.83	.22	20.09	59.04	.87	.25	.18	.45	27.85	2.15	9.47
45.96	108.1	37.52	.23	22.08	54.04	.96	.26	.19	.53	32.49	2.30	10.77
47.78	114.1	39.57	.24	22.22	52.22	1.00	.27	.19	.58	33.92	2.37	11.99
51.81	120.1*	42.83	.25	23.68	48.19	1.03	.28	.20	.64	37.54	2.62	13.08
55.59	126.1	46.28	.27	25.05	44.41	1.09	.30	.21	.75	40.37	2.87	14.03

Experimental Set B ; Run 13 (Corrected Gas Temperature = 971.0 K)

39.82	84.1	31.71		17.91	60.18	.79	.23	.17	.51	30.42	2.04	9.96
39.32	90.1*	32.99		18.25	60.68	.79	.23	.17	.50	26.60	2.00	11.60
43.83	96.1	37.42		19.63	56.17	.89	.24	.17	.58	30.74	2.00	12.11
52.99	102.1	45.21		23.15	47.01	1.11	.27	.20	.91	37.99	2.33	14.32
58.30	108.1	27.19		23.77	41.70	1.09	.27	.21	.88	46.42	2.73	17.56
62.17	114.1	51.85		25.48	37.83	1.15	.29	.21	.95	48.59	2.66	17.63
60.57	120.1*	51.56		23.95	39.43	1.08	.27	.20	.95	47.64	2.64	17.21
68.03	126.1	57.61		25.83	31.97	1.15	.28	.21	1.11	55.37	3.01	19.61

Experimental Set B ; Run 14 (Corrected Gas Temperature = 990.8 K)

Conversion	Reactor Position (cm)	CH_4	C_3H_8	C_3H_6	C_4H_{10}	1-C_4H_8	Trans-2 -C_4H_8	Cis-2 -C_4H_8	1,3 C_4H_6	C_2H_4	C_2H_6	H_2
51.43	78.1	42.56	.26	20.93	48.57	1.00	.24	.18	.94	40.66	2.06	14.27
50.63	84.1	46.87	.25	20.24	49.37	1.00	.24	.18	.92	35.10	1.65	15.73
53.62	90.1*	47.22	.24	20.11	46.38	1.00	.22	.16	.88	41.26	2.05	17.59
61.86	96.1	53.48	.26	21.34	38.14	1.06	.22	.17	1.11	51.91	2.65	19.07
66.73	102.1	58.99	.28	22.34	33.27	1.13	.22	.18	1.23	55.38	2.72	21.50
73.04	108.1	65.82	.29	23.75	26.96	1.11	.25	.19	1.53	59.56	3.14	24.93
75.52	114.1*	68.04	.30	23.66	24.48	1.10	.24	.18	1.54	62.76	3.37	26.39
78.70	120.1	70.58	.31	23.82	21.30	1.08	.24	.18	1.64	66.51	3.55	28.60

Experimental Set B ; Run 15 (Corrected Gas Temperature = 994.4 K)

54.54	78.1	46.37	.24	20.03	45.46	1.02	.23	.17	.96	43.31	2.43	18.83
51.56	84.1	44.06	.23	19.09	48.44	.96	.22	.16	.87	40.71	2.32	17.46
57.12	90.1*	49.69	.24	20.11	42.88	1.00	.22	.16	1.00	45.95	2.62	19.26
62.07	96.1	54.69	.26	21.62	37.93	1.12	.23	.18	1.08	50.39	2.75	19.42
66.99	102.1	60.17	.28	22.15	33.01	1.15	.23	.17	1.28	43.38	2.87	22.51
73.28	108.1	65.88	.29	23.19	26.72	1.21	.23	.18	1.49	60.34	3.14	25.95
78.30	114.1	72.38	.29	22.63	21.70	1.09	.22	.17	1.70	65.87	3.32	28.28
81.51	120.1*	75.28	.30	23.02	18.49	1.06	.21	.16	1.79	68.50	3.50	31.61
84.90	126.1	77.38	.29	22.46	15.10	.91	.19	.14	1.76	73.96	3.91	35.17

Experimental Set B ; Run 16 (Corrected Gas Temperature = 1005.0 K)

Conversion	Reactor Position (cm)	CH_4	C_3H_8	C_3H_6	C_4H_{10}	1-C_4H_8	Trans-2 -C_4H_8	Cis-2 -C_4H_8	1,3 C_4H_6	C_2H_4	C_2H_6	H_2
60.94	84.1	56.06	.25	18.83	39.06	.93	.21	.15	1.11	51.27	2.66	18.77
65.33	90.1*	58.90	.25	19.44	34.67	1.00	.20	.15	1.19	56.09	2.79	22.81
71.99	96.1	66.21	.26	19.31	28.01	1.00	.19	.15	1.40	62.77	3.02	27.48
79.88	102.1	74.50	.29	20.04	20.12	.99	.18	.14	1.78	70.87	3.39	30.05
83.70	108.1	77.27	.29	19.85	16.30	.94	.18	.14	1.96	75.23	3.47	34.97
86.20	114.1	81.77	.29	18.83	13.80	.84	.17	.13	1.95	77.36	3.63	37.43
88.07	120.1*	82.96	.28	18.75	11.93	.81	.17	.13	1.95	79.55	3.65	40.40
87.60	126.1	84.64	.26	17.44	12.40	.75	.16	.13	1.89	77.96	3.76	42.12

Experimental Set B ; Run 17 (Corrected Gas Temperature = 947.1 K)

24.26	78.1	18.09	.15	13.28	75.74	.54	.21	.15	.26	15.16	1.46	7.07
25.46	84.1	19.53	.15	13.92	74.54	.55	.22	.17	.30	15.78	1.48	6.70
26.35	90.1*	20.75	.16	14.07	73.65	.55	.22	.16	.32	16.18	1.49	7.42
31.87	96.1	22.83	.15	17.13	68.13	.61	.22	.16	.33	22.01	1.94	8.90
35.18	102.1	27.19	.19	18.59	64.82	.77	.26	.19	.44	22.61	1.90	9.78
38.13	108.1	29.92	.20	19.99	61.87	.84	.27	.20	.49	24.34	2.10	10.43
39.01	114.1	30.64	.19	19.98	60.99	.83	.27	.20	.49	25.08	2.13	11.98
42.28	120.1*	33.66	.20	21.43	57.72	.87	.29	.21	.54	27.42	2.32	12.44
44.12	126.1	35.47	.21	21.90	55.88	.91	.28	.22	.56	28.35	2.36	14.38

Experimental Set B ; Run 18 (Corrected Gas Temperature = 927.6 K)

Conversion	Reactor Position (cm)	CH_4	C_3H_8	C_3H_6	C_4H_{10}	$1\text{-}C_4H_8$	Trans-2 $\text{-}C_4H_8$	Cis-2 $\text{-}C_4H_8$	1,3 C_4H_6	C_2H_4	C_2H_6	H_2
14.32	78.1	10.73	.11	8.23	85.68	.30	.15	.11	.11	8.30	.88	4.03
15.37	84.1	12.11	.12	8.93	84.63	.33	.17	.12	.13	8.02	1.03	4.40
17.78	90.1*	14.03	.12	10.11	82.22	.37	.17	.12	.14	9.72	1.16	5.19
20.74	96.1	16.18	.14	11.85	79.26	.43	.20	.15	.17	11.68	1.30	5.65
22.80	102.1	17.68	.13	13.07	77.20	.46	.21	.15	.20	12.92	1.44	6.30
24.68	108.1	19.23	.13	13.97	75.32	.51	.21	.15	.20	14.22	1.51	6.97
27.28	114.1	21.30	.15	15.26	72.72	.56	.24	.16	.24	15.57	1.68	8.37
29.14	120.1*	22.67	.16	16.20	70.86	.60	.25	.18	.27	16.94	1.72	8.85
30.71	126.1	23.99	.17	16.91	69.29	.62	.26	.19	.31	17.78	1.82	9.75

Experimental Set B; Run 19 (Corrected Gas Temperature = 936.9 K)

17.34	78.1	13.57	.13	9.76	82.66	.37	.17	.12	.18	10.08	1.08	4.28
17.88	84.1	13.94	.13	9.91	82.12	.41	.25	.17	.25	10.55	1.14	3.83
21.41	90.1*	17.02	.13	11.75	78.59	.44	.19	.14	.19	12.86	1.30	5.22
25.21	96.1	20.09	.16	13.82	74.79	.52	.22	.15	.23	15.19	1.47	6.21
27.67	102.1	22.11	.15	15.07	72.33	.57	.22	.16	.28	16.90	1.60	6.64
30.76	108.1	23.73	.16	16.24	69.24	.64	.24	.16	.30	20.51	1.86	7.19
35.53	114.1	26.57	.18	18.05	66.47	.72	.26	.19	.37	20.96	1.86	8.19
35.81	120.1*	28.33	.19	19.37	64.19	.77	.28	.20	.40	22.15	2.06	8.90
38.24	126.1	30.43	.19	20.26	61.76	.79	.29	.21	.46	23.59	2.18	10.67

Experimental Set C ; Run 20 (Corrected Gas Temperature = 919.4 K)

Conversion	Reactor Position (cm)	CH_4	C_3H_8	C_3H_6	C_4H_{10}	$1\text{-}C_4H_8$	Trans-2 $-C_4H_8$	Cis-2 $-C_4H_8$	1,3 C_4H_6	C_2H_4	C_2H_6	H_2
10.65	90.1	8.40	.11	6.08	89.35	.18	.11	.08	.05	5.88	.83	2.73
11.20	94.1	9.16	.10	6.31	88.80	.18	.11	.07	.05	6.88	.87	2.90
13.29	98.1*	10.70	.11	7.53	86.71	.22	.12	.09	.07	7.33	1.05	3.32
13.61	102.1	11.01	.11	7.68	86.39	.23	.13	.09	.07	7.48	1.04	3.52
14.13	106.1	11.45	.11	7.98	85.87	.23	.13	.09	.07	7.80	1.07	3.63
15.45	110.1	12.23	.12	8.96	84.55	.27	.14	.10	.08	8.60	1.19	3.63
16.93	114.1	13.34	.13	9.84	83.07	.31	.15	.10	.09	9.48	1.24	4.00
18.76	118.1*	14.67	.13	10.95	81.24	.35	.17	.12	.11	10.37	1.39	4.61
21.23	122.1	15.87	.16	12.70	78.77	.44	.21	.15	.17	11.97	1.57	4.94

Experimental Set C ; Run 21 (Corrected Gas Temperature = 938.2 K)

13.55	90.1	11.32	.11	7.30	86.45	.21	.12	.09	.07	7.75	.97	3.43
14.84	94.1	12.38	.12	7.96	85.16	.25	.12	.09	.09	8.55	1.03	3.81
17.26	98.1*	14.13	.12	9.32	82.74	.30	.14	.10	.11	10.19	1.18	4.41
17.48	102.1	14.34	.13	9.41	82.52	.30	.13	.09	.12	10.32	12.1	4.43
19.48	106.1	16.19	.13	10.34	80.52	.35	.15	.10	.13	11.61	1.32	4.82
21.54	110.1	16.97	.14	11.88	78.46	.38	.16	.11	.14	13.19	1.48	5.18
24.29	114.1	19.07	.15	13.23	75.71	.47	.18	.13	.18	15.08	1.68	5.83
26.96	118.1*	21.19	.17	14.59	73.04	.51	.21	.14	.22	16.92	1.83	6.35
30.26	122.1	22.66	.18	16.72	69.74	.31	.25	.18	.32	19.15	1.94	6.99

Experimental Set C ; Run 22 (Corrected Gas Temperature = 957.5 K)

Conversion	Reactor Position (cm)	CH_4	C_3H_8	C_3H_6	C_4H_{10}	1-C_4H_8	Trans-2 -C_4H_8	Cis-2 -C_4H_8	1,3 C_4H_6	C_2H_4	C_2H_6	H_2
20.54	90.1	15.99	.14	10.64	79.46	.37	.15	.11	.16	13.25	1.36	6.06
21.31	94.1	17.59	.14	10.62	78.69	.37	.15	.11	.16	13.37	1.33	6.56
23.82	98.1*	19.71	.15	11.88	76.18	.42	.16	.12	.18	15.01	1.46	7.17
26.93	102.1	22.19	.16	13.32	73.07	.48	.18	.13	.21	17.22	1.65	8.20
29.87	106.1	24.33	.17	14.82	70.13	.55	.19	.14	.26	19.49	1.83	8.64
36.04	110.1	27.67	.20	18.35	63.96	.78	.31	.17	.42	23.90	1.92	11.06
38.96	114.1	30.11	.23	19.71	61.04	.83	.25	.19	.53	25.66	2.38	11.81
42.60	118.1*	32.95	.25	21.54	57.40	.92	.28	.21	.60	28.18	2.63	12.42
47.26	122.1	36.36	.29	23.04	52.74	1.01	.32	.23	.74	32.61	2.79	14.05

Experimental Set C ; Run 23 (Corrected Gas Temperature = 975.8 K)

28.79	90.1	23.56	.17	13.29	71.21	.52	.19	.13	.30	19.66	1.65	9.42
31.07	94.1	25.89	.18	14.20	68.93	.55	.19	.13	.32	21.25	1.82	9.66
34.56	98.1*	28.76	.19	15.50	65.44	.63	.20	.15	.38	24.21	1.97	10.62
36.51	102.1	30.40	.20	16.40	63.49	.68	.21	.15	.41	25.21	2.14	11.68
38.17	106.1	31.55	.20	17.05	61.83	.72	.21	.15	.45	27.08	2.17	11.62
45.57	110.1	36.49	.23	20.36	54.43	.94	.25	.18	.66	33.46	2.55	13.34
49.63	114.1	39.26	.26	21.54	50.37	1.01	.26	.19	.77	37.77	2.79	14.74
57.35	118.1*	44.41	.31	24.54	42.65	1.12	.29	.20	1.08	44.79	3.34	17.07
59.47	122.1	47.56	.32	25.13	40.53	1.18	.28	.21	1.06	45.90	3.42	19.44

Experimental Set C ; Run 24 (Not used in rate constant estimation)

Conversion	Reactor Position (cm)	CH_4	C_3H_8	C_3H_6	C_4H_{10}	1-C_4H_8	Trans-2 -C_4H_8	Cis-2 -C_4H_8	1,3 C_4H_6	C_2H_4	C_2H_6	H_2
40.92	90.1	33.03	.22	16.71	59.08	.72	.21	.15	.51	32.98	2.13	11.50
44.50	94.1	36.91	.24	18.12	55.50	.82	.23	.16	.63	33.67	2.34	14.65
51.71	98.1	43.43	.26	19.90	48.29	.96	.24	.17	.88	40.26	2.70	16.92
48.37	102.1	40.05	.26	18.61	51.63	.90	.23	.17	.74	37.93	2.54	16.53
50.47	106.1	42.07	.26	19.48	49.53	.88	.24	.17	.79	39.49	2.62	16.97
56.51	110.1	44.20	.14	21.25	43.49	1.12	.25	.19	1.20	47.72	2.72	19.10
59.32	114.1	48.93	.15	22.29	40.68	1.17	.28	.19	1.15	47.22	3.02	20.73
63.02	118.1	51.91	.15	22.58	36.98	1.17	.27	.19	1.20	50.79	3.34	23.53
70.09	122.1	57.21	.17	23.55	29.91	1.16	.27	.21	1.51	59.41	3.89	27.03

Experimental Set C ; Run 25 (Corrected Gas Temperature = 998.8 K)

47.01	90.1	39.91	.24	17.47	52.99	.87	.21	.15	.69	35.90	2.26	18.54
51.25	94.1	43.12	.26	18.94	48.75	.99	.23	.16	.84	39.55	2.15	20.66
54.47	98.1*	45.58	.27	19.28	45.53	1.01	.22	.17	.90	43.70	2.61	21.37
57.50	102.1	43.99	.26	18.51	42.50	.98	.23	.16	.88	52.17	2.52	21.62
60.24	106.1	50.99	.29	20.91	39.76	1.13	.25	.18	1.05	48.48	2.88	23.22
66.06	110.1	55.99	.32	22.20	33.94	1.17	.26	.19	1.47	53.43	3.19	26.33
70.02	114.1	61.00	.33	22.04	29.98	1.21	.25	.19	1.58	57.13	3.24	28.58
74.05	118.1*	65.25	.31	21.87	25.95	1.18	.25	.18	1.73	61.84	3.50	30.61
77.62	122.1	74.51	.29	20.44	22.38	1.05	.22	.15	1.81	63.45	3.48	31.63

Experimental Set C ; Run 26 (Corrected Gas Temperature = 1009.0 K)

Conversion	Reactor Position (cm)	CH_4	C_3H_8	C_3H_6	C_4H_{10}	$1\text{-}C_4H_8$	Trans-2 $\text{-}C_4H_8$	Cis-2 $\text{-}C_4H_8$	1,3 C_4H_6	C_2H_4	C_2H_6	H_2
58.43	90.1	49.30	.30	19.29	41.57	1.08	.26	.16	1.05	48.45	2.45	23.54
60.82	94.1	50.91	.30	19.53	39.18	1.11	.24	.17	1.10	51.73	2.74	24.21
63.83	98.1	55.31	.31	20.26	36.17	1.13	.24	.18	1.20	52.53	3.02	25.64
62.52	102.1*	55.34	.30	19.12	37.48	1.09	.22	.16	1.26	51.42	2.75	25.34
68.29	106.1	60.96	.31	19.91	31.71	1.19	.23	.17	1.44	57.31	2.98	27.31
73.59	110.1	70.14	.35	18.34	26.21	.96	.19	.13	1.72	61.94	3.09	30.92
77.06	114.1	69.20	.32	19.39	22.94	1.07	.21	.16	1.90	68.27	3.41	32.62
80.68	118.1*	75.01	.32	19.07	19.32	1.07	.20	.16	2.04	70.52	3.66	34.68
83.96	122.1	74.11	.30	17.94	16.04	.90	.19	.15	2.05	81.55	3.86	34.61

Experimental Set C ; Run 27 (Not used in rate constant estimation)

75.85	90.1	67.39	.36	20.73	24.15	1.19	.22	.17	1.66	65.39	3.36	32.02
79.83	94.1	72.58	.36	19.95	20.17	1.14	.23	.17	1.89	71.05	3.37	32.07
83.08	98.1	79.92	.35	19.11	16.92	1.15	.21	.16	2.20	71.24	3.25	35.19
86.07	102.1	81.69	.33	18.20	13.93	.99	.19	.15	2.20	78.43	3.43	35.36
82.64	106.1	73.26	.33	18.45	17.36	1.09	.20	.17	2.08	77.60	3.48	35.78
88.72	110.1	83.72	.33	17.21	11.28	.94	.15	.15	2.38	81.09	3.35	42.28
91.87	114.1	88.12	.29	14.83	8.13	.66	.14	.12	2.50	87.25	3.44	44.93

A P P E N D I X X I I I

MIXED CONVECTION WITHIN THE REACTOR

Normally with forced flow the influences of body forces on flow and heat and mass transfer can be neglected. However, for the low Reynolds number used in this study the influence of free convection combined with forced convection cannot be considered negligible. Although it is of interest to know when body forces are no longer insignificant, the large number of influencing parameters make such an analysis difficult to accomplish. In addition to the Reynolds, Grashof and Prandtl numbers, the geometry of the flow boundaries and the orientation of the flow relative to the gravitational field are also important contributors to influencing the prevailing flow condition. Furthermore, the majority of information in literature characterises conditions in a vertical tubular reactor where the buoyancy effects aid the direction of the forced convection (e.g. Santarelli and Faraboschi, 1973), rather than where the effects act in opposite directions.

Since the largest natural convective effects are near the wall where the velocity approaches zero for laminar systems, separation of the flow from the wall occurs very easily. This instability in the flow system results in turbulent mixing close to the wall which enhances the heat and mass transport above that normally expected for "pure" forced convective systems. As a result, the Nusselt number (and by analogy, the Sherwood number for mass transfer) for the mixed system is larger than the Nusselt number calculated using classical formulae for forced convection in pure laminar flow. The actual amount of enhancement

of heat and mass transfer is, however, difficult to quantify. Incropera and Dewitt (1981) include a review of this work and indicate that the most recent study directly relevant to this problem was that by Brown and Gauvin (1965). They in turn stated that for conditions where the buoyant forces were large enough to alter the heat transfer rate there was no satisfactory equation for predicting the actual size of the enhancement. Incroperra and Dewitt generalise the conditions where mixed convection is present as

$$\frac{Ge}{Re^2} >> 1 \qquad \text{"Pure" free convection}$$

$$\frac{Gr}{Re^2} \sim 1 \qquad \text{Mixed convection} \qquad \text{(XIII.1)}$$

$$\frac{Gr}{Re^2} << 1 \qquad \text{"Pure" forced convection}$$

For conditions typical in this system

$$Gr = \frac{D^3 \rho^2 g' \beta' \Delta T}{\mu^2} = \frac{(0.0525)^3 (0.5)^2 9.81\ 20}{960(35 \times 10^{-6})^2} \sim 6 \times 10^3$$

Thus $Gr/Re^2 \sim 1$, consistent with the generalised limits of mixed convection given in equation (XIII.1). Eckert and Diagula (1954) have developed bounded conditions for which the effects of mixed convection alter the Nusselt number by greater than 10% from that calculated using correlations for pure natural and forced convection as:

$$Re_1 > 0.276\ Gr^{\frac{3}{4}} Pr^{-\frac{1}{4}} \left(\frac{L}{D}\right)^{\frac{1}{4}} \qquad \text{Forced Convection Dominant}$$

$$Re_2 < 0.0306\ Gr^{\frac{3}{4}} Pr^{-\frac{1}{4}} \left(\frac{L}{D}\right)^{\frac{1}{4}} \qquad \text{Free Convection Dominant} \qquad \text{(XIII.2)}$$

$$Re_2 < Re < Re_1 \qquad \text{Mixed Convection Dominant}$$

Substituting for conditions in the reactor yields the bound (Pr $\sim$ 0.7, L/D $\sim$ 20)

$$48 < Re < 432$$

Thus the bounds by Eckert and Diagula provide further evidence that suggests natural convection was assisting in the heat and mass transfer which prevailed during the collection of the experimental data.

N O M E N C L A T U R E

Where appropriate, the equation where the variable is first introduced is located at the end of the symbol definition.

A	Pre-exponential Factor (6.2)
A_1	Cross-Sectional Area (C.S.A.) of Stream 1 in the gas sampling probe (3.4)
A_2	C.S.A. of Stream 2 in the gas sampling probe (3.4)
A_c	C.S.A. of the capillary in the gas sampling probe (3.4).
A_r	C.S.A. of the reactor (5.1)
A_i	C.S.A. of the mineral insulant in the thermocouple probe (IV.1)
A_m	C.S.A. of the thermocouple probe inconel sheath (IV.1)
A_t	C.S.A. of the thermocouple wires in the probe (IV.1)
A_w	Surface area of the reactor (IV.6)
A_h	Surface area of the hemispherical thermocouple probe tip (IV.1)
A_s	$2A_h$ (IV.1)
A'	Reparameterised pre-exponential factor (6.2)
$\tilde{A}$	Tridiagonal matrix (VI.10)
a_i	Stoichiometric coefficient for molecular species i
a_k	Autocovariance function at time lag k (III.1)
b	Vector of parameters (4.9)
b_p	Subset of b (4.14)
$\tilde{b}$	Vector of known functions (VI.10)
C	Concentration (4.1)
C_o	Concentration at the start of the isothermal region (4.1)
C^*	C/C_o, dimensionless (4.1)
C_B	Radial bulk concentration (4.3)
C_s	Simulation dimensionless concentration (4.8)
C_s^*	γC_s (4.8)
C_1	ε/h (IV.12)
C_f	Friction factor (3.4)
C_p	Specific heat capacity (3.3)
c_i	Carbon atom number in a molecule of component i (II.9)
D	Diameter (3.3)
D_r	Radial dispersion coefficient (4.1)
D_A	Axial dispersion coefficient (4.2)

D_m Diffusion coefficient (6.1)

d_1, d_2, d_3, d_4, d_5, d_6 Gas sampling probe dimensions, see Fig. 3.6

d_t Diameter of thermocouple probe (IV.11)

E Activation energy (6.2)

F Fishers F-distribution (4.9)

F Vector of species flow (5.1)

F_c Flowrate of butane in the probe capillary (3.4)

F_{xy} Radiation view factor for radiation from surface x onto surface y (IV.3)

f Fractional flow distortion = u_r/u_∞

G_1 Mass velocity of coolant nitrogen in Stream 1 of the gas sampling probe (3.4)

G_2 Mass velocity of coolant nitrogen in Stream 2 of the gas sampling probe (3.4)

G_c Mass velocity of the sample gas flowing down the probe capillary (3.4)

g Function vector of radical species (5.4)

g' Acceleration due to gravity (XIII.1)

H' Enthalpy per unit mass (V.1)

H Matrix of known elements, used in observability discussion (VIII.3)

ΔH_R Heat of reaction for butane pyrolysis (V.3)

h Heat transfer coefficient (3.1)

h_0 Overall heat transfer coefficient (3.4)

h' Integration step length (5.3)

h_i' Component heights from the chromatographic measurements

h_i Hydrogen atom number in a molecule of component i (II.9)

J Jacobian matrix (5.2)

K_m Mass transfer coefficient (7.1)

K' Vector of rate constants (5.1)

K Thermal conductivity (3.3)

k Rate constant for butane (6.2)

k_b Rate constant for butane used in the gas sampling probe model (3.4)

L_p Probe length (3.4)

ℓ Length (4.1)

L Reactor length or length of an isothermal zone (4.1)

m_i Measurement at time k = i (III.1)

N, n General numbers

N_{bo} Number of moles of butane in the feed to the reactor (II.2)

N_t Overall molar flowrate (N_2 free basis) (II.2)

N_{io} Product i flow in the feed to the reactor (II.6)

P_1 Pressure of coolant nitrogen in Stream 1 of the gas sampling probe (3.4)

P_2 Pressure of coolant nitrogen in Stream 2 of the gas sampling probe (3.4)

P_c Pressure of sample gas in the probe capillary (3.4)

p Number of model parameters (4.9)

p' Order of the BDF implemented by Gear (5.3)

p_i Product yield for component i (II.11)

p_k Step length vector (5.4)

Q Volumetric flowrate (5.1)

q Change in function value g (5.5)

$\dot{q}$ Rate of heat transfer

$\dot{q}_1$, $\dot{q}_2$, $\dot{q}_3$, $\dot{q}_4$, $\dot{q}_5$ See eqn. (IV.1)

R_b Rate of reaction of butane in the gas sampling probe capillary (V.3)

R Radius (4.1)

R_o Radius of the reactor (4.1)

R^* $= R/R_o$, dimensionless (4.1)

R' Gas constant for nitrogen

R_u Universal gas constant (6.2)

r Vector of rate expressions (5.1)

r_c Probe capillary radius (3.2)

S_c Stoichiometric coefficient matrix (5.1)

S Residual sum of squares (4.9)

s_o^2 Sample error variance (4.11)

s_o' Parameter sample variance (VII.10)

s_i Selectivity

T_1 Temperature of coolant nitrogen in Stream 1 of the gas sampling probe (3.4)

T_2 Temperature of coolant nitrogen in Stream 2 of the gas sampling probe (3.4)

T_c Temperature of the gas sample in the probe capillary (3.4)

T_s Measured (thermocouple) gas temperature (3.1)

T_g Corrected gas temperature (3.1)

T_w Reactor wall temperature (3.1)

T^* Average temperature (6.2)

T_e Temperature at the reactor exit (see Assumptions, Appendix V)

T_a Ambient temperature (see Assumptions, Appendix V)

T_p Gas sampling probe outer wall temperature (3.4)

T_n Temperature of coolant nitrogen at the gas sampling probe tip (V.7)

u_1 Velocity of the coolant nitrogen in Stream 1 of the gas sampling probe (3.4)

u_2 Velocity of the coolant nitrogen in Stream 2 of the gas sampling probe (3.4)

u_c Velocity of the gas sample in the probe capillary (3.4)

u_∞ Nominal process gas velocity (3.2)

u_r Radial velocity component caused by sampling

V Variance covariance matrix (4.10)

V_p Partitioned subset of V (4.14)

v_o Centreline velocity (4.1)

$\overline{v}$ Mean velocity (4.2)

W Diagonal matrix of weighting elements (VII.12)

w_i An element of W

X Matrix of independent measurements or set-points (4.10)

x Undetermined distance perpendicular to the gas sampling probe tip (3.6)

x' Specific probability level (4.9)

x_k Independent variable vector (5.4)

y_b Mole fraction of butane (II.1)

y_{bo} y_b for reactor feed (II.1)

y_i Mole fraction for component i (N_2 free basis) (II.2)

y Vector of dependent variables (VII.6)

Z Reactor distance

Z^* Z/L, dimensionless (4.1)

Greek Symbols

α D_r/kR_o^2 (4.1)

α' Sampling rate, $Q/\pi r_c^2 u_\infty$ (3.2)

α_i Known constants (5.3)

β kL/v_o (4.1)

β_o Known constant (5.3)

β' Coefficient of thermal expansion (XIII.1)

γ Scaling parameter (4.8)

δ' Dilution ratio (4.4)

δ Boundary layer thickness (7.2)

ϵ Emissivity (3.1)

λ βZ^* (VI.3)

μ Viscosity

θ Linear partition parameter (VI.2)

ξ Extent of reaction (II.2)

ρ Density (3.4)

σ^2 Error variance (4.10)

σ_c Stefan's constant (3.1)

ϕ_f Fractional conversion (4.4)

ϕ Conversion

ω $D_r L/R_o^2 v_o$ (4.1)

ω_1 Solid angle (IV.3)

Ω $\rho v_o C_p/K$ (V.6)

Dimensionless Numbers

Gr Grashof Number: $\beta' g' \Delta T D^3 \rho^2/\mu^2$

Nu Nusselt Number: hD/K

Pe Peclet Number: $\bar{v}L/D_A$

Pr Prandtl Number: $\mu C_p/K$

Re Reynolds Number: $\rho \bar{v} D/\mu$

Sc Schmidt Number: $\mu/\rho D_m$

Sh Sherwood Number: $K_m D/D_m$

R E F E R E N C E S

Aiken, R.C. and Lapidus, L., AIChE J. 21, 817 (1975).

Albright, L.F., Correspondence, Ind. Eng. Chem. Proc. Des. Dev. 17(3), 377 (1978).

Allara, D.L. and Edelson, D., Int. Jour. Chem. Kin. VII, 479 (1975).

Allara, D.L. and Shaw, R., Jour. Phys. and Chem. Ref. Data 9(3), 523 (1980).

Andrews, A.J. and Pollock, I.W., Ind. Eng. Chem. 51, 125 (1959).

Appleby, W.G., Avery, W.H., Meerbott, W.K. and Sartor, A.F., Jour. Am. Chem. Soc. 75, 1809 (1953).

Batten, J.J., Combus. Sci. and Tech. 1, 365 (1970).

Beek, W. and Muttzall, K.M.K., "Transport Phenomena", New York, Wiley-Interscience, (1975).

Benson, S.W., "Thermochemical Kinetics", New York, Wiley, (1968).

Beshty, B.S., "The Isothermal Pyrolysis of Propane in a Pilot Scale Reactor", PhD Thesis, University of London (1978).

Blakemore, J.E., Barker, J.R. and Corcoran, W.H., Ind. Eng. Chem. Fundam. 12(2), 147 (1973).

Bowen, J.R., Acrivos, A. and Oppenheim, A.K., Chem. Eng. Sci. 18, 177 (1963).

Bradley, D. and Matthews, K.J., Mech. Eng. Sci. 10, 299 (1968).

Bradley, J.N., Proc. Roy. Soc. A337, 199 (1974).

Brown, C.K. and Gauvin, W.H., Can. Jour. Chem. Eng. 43, 306 (1965).

Broyden, C.G., Math. Comp. 19, 577 (1965).

Buekens, A.G. and Froment, G.F., Ind. Eng. Chem. Proc. Des. Dev. 7(3), 435 (1968).

Calderbank, P.H., Chem. Eng. Progr. 50, Symp. Series No. 9, 53 (1964).

Cambron, A., Can. Jour. Res. 7, 646 (1932).

Cambron, A. and Bayley, C.H., Can. Jour. Res. 9, 583 (1933).

Carnahan, B., Luther, H.A. and Wilkes, J.O., "Applied Numerical Methods", New York, Wiley (1969).

Chandrasekharan, K. and Calderbank, P.H., Presented at the Sixth International Symposium on Chemical Reaction Engineering, Nice, France, March 25-27, 1980; see Chem. Eng. Sci. 35, 341 (1980).

Cleland, F.A. and Wilhelm, R.H., AIChE Jour. 2, 489 (1956).

Crynes, B.L. and Albright, L.F., Ind. Eng. Chem. Proc. Des. Dev. 8(1), 25 (1969).

Curtiss, C.F. and Hirschfelder, J.O., Proc. Nat. Acad. Sci. U.S. 38, 235 (1952).

Danckwerts, P.V., Chem. Eng. Sci. 2, 1 (1953).

Davies, O.L. and Goldsmith, P.L., "Statistical Methods in Research and Production", Edinburgh, Oliver and Boyd (1970).

Dente, M., Ranzi, E. and Goosens, A.G., Presented at 12th European Symposium for Computer Applications in Chemical Engineering, Montreux, Switzerland, April 8-11, 1979.

Draper, N.R. and Smith, H., "Applied Regression Analysis", London, Wiley (1966).

Dunkleman, J.J. and Albright, L.F., Am. Chem. Soc. Symp. Series, Editor: R.F. Gould, 241 (1976).

Ebrey, G.O. and Engelder, C.J., Ind. Eng. Chem. 23, 1033 (1931).

Echols, L.S. and Pease, R.N., Jour. Am. Chem. Soc. 58, 1317 (1936).

Eckert, E.R.G. and Diagula, A.J., Trans. Am. Soc. Mech. Eng. 76, 497 (1954).

Edelson, D. and Allara, D.L., AIChE Jour. 19(3), 638 (1973).

Edelson, D. and Allara, D.L., Int. Jour. Chem. Kin. XII, 605 (1980).

Eisenberg, B. and Bliss, H., "Symposium on Recent Kinetic Studies", 59th National Meeting AIChE, Columbus, Ohio, May (1966).

Evering, B.L., Jour. Am. Chem. Soc. 61, 1400 (1939).

Frey, F.E. and Smith, D.F., Ind. Eng. Chem. 20, 948 (1928).

Fristrom, R.M. and Westenberg, A.A., "Flame Structure", New York, McGraw-Hill (1965).

Fritz, K. and Groenig, H., Proc. Int. Symposium on Shock Tube and Shock Wave Research, 11th, 383 (1977).

Froment, G.F., Chem. Eng. Sci. 36, 1271 (1981).

Froment, G.F., Van de Steene, B.O., Vanden Berghe, P.J. and Goosens, A.J., AIChE Jour. 23(1), 93 (1977).

Gear, C.W., Communs. Ass. Comput. Mach. 14, 176 (1971).

Goldfinger, P., Letort, P. and Niclause, M., "Contribution à l'etude de la structure moleculaire", Victor Henri Commemorative Volume, Desoer, Liège, Belgium, 283 (1948).

Hautman, D.J., Santoro, R.J., Dryer, F.L. and Glassman, I., Int. Jour. Chem. Kin. XIII, 149 (1981).

Hepp, H.J. and Frey, F.E., Ind. Eng. Chem. 45(2), 410 (1953).

Herriot, G.E., Eckert, R.E. and Albright, L.F., AIChE Jour. 18, 84 (1972).

Hill, J.C., Presented before the Division of Petroleum Chemistry Inc. Am. Chem. Soc., New Orleans, March 20-25 (1977).

Himmelblau, D.M., "Process Analysis by Statistical Methods", New York, Wiley (1970).

Hougen, O.A. and Watson, K.M., "Chemical Process Principals", Vol. III, New York, Wiley (1947).

Hurd, C.D. and Azorlosa, J.L., Jour. Am. Chem. Soc. 73, 33 (1951).

Hurd, C.D. and Spence, L.K., Jour. Am. Chem. Soc. 51, 3353 (1929).

Illés, V., Acta. Chim. Acad. Sci. Hung. 59(1), 35 (1969).

Illés, V. and Szalai, O., Acta. Chim. Acad. Sci. Hung. 101(3), 267 (1979).

Incropera, F.P. and Dewitt, D.P., "Fundamentals of Heat Transfer", New York, Wiley (1981).

Kay, J.M. and Nedderman, R.M., " Fluid Mechanics and Heat Transfer", Cambridge (1974).

King, R.O., Sandler, S. and Chung, Y.H., Trans. of the Engineering Institute of Canada (EIC) 3(1), 1 (1959).

Kupparman, A. and Larson, J.G., Long Abstracts of Papers presented at the Am. Chem. Soc. Meeting, Washington DC, March 21-24 (1962).

Laidler, K.J., "Chemical Kinetics", New York, McGraw-Hill (1965).

Laidler, K.J., Sagert, N.H. and Wojciechowski, B.W., Parts I and II, Proc. Roy. Soc. A270, 254 (1962).

Laidler, K.J. and Wojciechowski, B.W., Proc. Roy. Soc. A260, 103 (1961).

Large, J., Martin, R. and Niclause, M., Bull. Soc. Chim. Fr. 3, 961 (1972).

Lauwerier, H.A., Appl. Sci. Res. A8, 366 (1959).

Leathard, D.A. and Purnell, J.H., Proc. Roy. Soc. A305, 517 (1968).

Leathard, D.A. and Purnell, J.H., Ann. Rev. Phys. Chem. 21, 197 (1970).

Maizus, Z.K., Markovich, V.G. and Neiman, M.B., Doklady Akad. Nauk. USSR, 66, 1121 (1949).

Mandel, J., "The Statistical Analysis of Experimental Data", New York, Interscience (1964).

Martin, R., Dzierzysnki, M. and Niclause, M., Jour. Chim. Phys. 61, 790 (1964)

Massey, B.S., "Mechanics of Fluids", 2nd edn., London, Van Nostrand Reinhold (1970).

Murata, M. and Saito, S., Jour. Chem. Eng. Japan 8(1), 39 (1975).

Niclause, N., Martin, R. Combes, A., Fusy, J. and Dzierzysnki, M., Ind. Chim. Belge. 32, 674 (1967).

Nigam, K.M. and Nigam, K. .P., Chem. Eng. Sci. 35, 2358 (1980).

Pacey, P.D. and Purnell, J.H., Int. Jour. Chem. Kin. IV, 657 (1972a).

Pacey, P.D. and Purnell, J.H., Ind. Eng. Chem. Fundam. 11(2), 233 (1972b).

Papoulis, A., "Probability, Random Variables and Stochastic Processes", London, McGraw-Hill (1965).

Paul, R.E. and Marek, L.F., Ind. Eng. Chem. 26(4), 454 (1934).

Pease, R.N., Jour. Am. Chem. Soc. 50, 1779 (1928).

Pease, R.N. and Durgan, E.S., Jour. Am. Chem. Soc. 52, 1262 (1930).

Perry, J.H., "Chemical Engineers' Handbook", 4th edn., London, McGraw-Hill (1963).

Poltarak, V.A., Leitus, L. Ya. and Voevodskii, V., Russ. Jour. Phys. Chem. 33, 379 (1959).

Powell, M.J.D., The Comp. Jour. 7, 155 (1964).

Powers, D.R. and Corcoran, W.H., Ind. Eng. Chem. Fundam. 13(4), 351 (1974).

Pratt, G.L. and Rogers, D., Jour. Chem. Soc., Faraday Trans. 1 75(12), 1089 (1979).

Purnell, J.H. and Quinn, C.P., Jour. Chem. Soc. 114, 4128 (1961).

Purnell, J.H. and Quinn, C.P., Proc. Roy. Soc. A270, 267 (1962).

Rice, F.O., Jour. Am. Chem. Soc. 53, 1959 (1931).

Rice, F.O. and Herzfeld, K.F., Jour. Am. Chem. Soc. 56, 284 (1934).

Rice, F.O. and Johnston, W.R., Jour. Am. Chem. Soc. 56, 214 (1934).

Rice, F.O., Johnston, W.R. and Evering, B.L., Jour. Am. Chem. Soc. 54, 3529 (1932).

Rice, F.O. and Polly, O.L., Jour. Chem. Phys. 6, 273 (1938).

Roache, P.J., "Computational Fluid Dynamics", Albuquerque, New Mexico, Hermosa (1972).

Rosen, P., John Hopkins University, Applied Physics Laboratory, Silver Spring, Maryland Report APL/JHU, CF-2248, July 29 (1954).

Sagert, N.H. and Laidler, K.J., Can. Jour. Chem., Pts. I and II, 41, 838 (1963).

Sandler, S. and Chung, Y., Ind. Eng. Chem. 53(5), 391 (1961).

Santarelli, P. and Foraboschi, F.P., The Chem. Eng. Jour. 6, 59 (1973).

Schweppe, F.C., "Uncertain Dynamic Systems", New Jersey, Prentice Hall (1973).

Seinfeld, J.H., Lapidus, L. and Hwang, M., Ind. Eng. Chem. Fundam. 9, 266 (1970).

Sena, M.P. and Kershenbaum, L.S., AIChE Symposium Series No. 147, 71, 111 (1975).

Shah, M.M., Ind. Eng. Chem. 59, 70 (1967).

Shah, R.K. and London, A.L., "Laminar Flow Forced Convection in Ducts: A Source Book for Compact Heat Exchanger Analytical Data", New York, Academic (1978).

Shapiro, A.H., "The Dynamics and Thermodynamics of Compressible Fluid Flow", 2 Vols., New York, Ronald (1953-4).

Snow, R.H., Jour. Phys. Chem. 70(9), 2780 (1966).

Steacie, E.W.R., "Atomic and Free Radical Reactions", 2nd edn., Monograph Series No. 125, 3 Vols., New York, Reinhold (1954).

Steacie, E.W.R. and Folkins, H.O., Can. Jour. Res. B17, 105 (1939).

Steacie, E.W.R. and Puddington, I.E., Can. Jour. Res. B16, 176 (1938).

Stubbs, F.J. and Hinshelwood, C.N., Proc. Roy. Soc. A201, 18 (1950).

Sundaram, K.M. and Froment, G.F., Chem. Eng. Sci., Pts. I and II, 32, 601 (1977).

Sundaram, K.M. and Froment, G.F., Ind. Eng. Chem. Fundam. 17, 174 (1978a).

Sundaram, K.M. and Froment, G.F., Int. Jour. Chem. Kin. X, 1189 (1978b).

Taylor, G.I., Proc. Roy. Soc. A219, 186 (1953).

Torok, J. and Sandler, S., Can. Jour. Chem. 47, 2707 (1969).

Van Damme, P.S., Narayanan, S. and Froment, G.F., AIChE Jour. 21, 1065 (1975).

Vignes, J.P. and Trambouze, P.J., Chem. Eng. Sci. 17, 73 (1962).

Voevodsky, V.V., Trans. Fara. Soc. 55, 65 (1959).

Volkan, A.G. and April, G.C., Ind. Eng. Chem. Proc. Des. Dev. 16(4), 429 (1977).

Wakeham, W.A. and Slater, D.H., J. Phys. B: Atom. Molec. Phys. 6, 886 (1973).

Wakeham, W.A., Personal Communication, (1981).

Wan, C. and Ziegler, E.N., Chem. Eng. Sci. 25, 723 (1970).

Wang, Y.L., Winker, R.G. and Corcoran, W.H., Ind. Eng. Chem. Fundam. 2(3), 161 (1963).

Williams-Gardner, A., Fuel 4, 430 (1925).

Wojciechowski, B.W. and Laidler, K.J., Can. Jour. Chem. 38, 1027 (1960).